Queen Mary University of London

Submitted in partial fulfilment of the requirements of the Degree of Doctor of Philosophy

Isolation methodology is essential to the evaluation of the extracellular vesicle component of the senescence-associated secretory phenotype

Ryan Wallis

Supervisors:
Dr Cleo L. Bishop
Professor David Kelsell

Centre for Cell Biology and Cutaneous Research
The Blizard Institute
Barts and the London School of Medicine and Dentistry
Queen Mary University of London

July 2020

Statement of Originality

I, Ryan Wallis, confirm that the research included within this thesis is my own work or that where it has been carried out in collaboration with, or supported by others, that this is duly acknowledged below and my contribution indicated. Previously published material is also acknowledged below.

I attest that I have exercised reasonable care to ensure that the work is original, and does not to the best of my knowledge break any UK law, infringe any third party's copyright or other Intellectual Property Right, or contain any confidential material.

I accept that the College has the right to use plagiarism detection software to check the electronic version of the thesis.

I confirm that this thesis has not been previously submitted for the award of a degree by this or any other university.

Signature: **Ryan Wallis**

Date: 29.07.2020

Details of collaboration and publications:

Publications

Wallis, R., Mizen, H. and Bishop, C. L. (2020) 'The Bright and Dark Side of Extracellular Vesicles in the Senescence-Associated Secretory Phenotype', *Mechanisms of Ageing and Development*. Elsevier, p. 111263. doi: 10.1016/j.mad.2020.111263. – Review

Collaborations

Mass spectrometry samples was performed through collaboration with Natasa Josipovic and Argyris Papantonis (Institute of Pathology, Göttingen) via the CECAD proteomic facility (University of Cologne).

Experiments using the human mammary fibroblast model of senescence reversal were performed though supervision of Regenerative Medicine MSc student, Kishan vara

Acknowledgments

This project was funded by the Professor Derek Willoughby Foundation and The Medical College of Saint Bartholomew's Hospital Trust.

In the first instance, I would like to thank my supervisor, Cleo Bishop, for her unparalleled support, dedication and constancy throughout my PhD. From preparing for my panel interview, through extension proposals and global pandemics, you have been an indefatigable presence and it has been a pleasure to be a part of your lab.

I would also like to thank the members of the Bishop group, past and present, who have made the lab such a fantastic place to work. Maddi and Deb for showing me the ropes, Stef and Hannah for always being there, and Beth and Meg for putting up with me generally. My special thanks to Elly, for being the first person I would turn to if anything went wrong, your patience, encouragement and advice were invaluable.

I would also like to thank the other PhD students in CBCR for keeping things light, both in and out of work. In particular Florence, Kasia, Eleri and Rosie, as well as the rest of the 12pm lunch crew. Most especially, Chris and Jordan, without whom it would have been a lot less fun.

Most importantly, my thanks to Liv. You have been unfailingly patient throughout, and your support and encouragement have been an indispensable source of motivation. Finally, I would like to thank my family, who provided a country escape during COVID-19, where I could write in peace.

Abstract

Senescence is a state of proliferative arrest that is triggered through a range of harmful stimuli. Senescent cells are associated with the acquisition of an enhanced secretory profile known as the senescence-associated secretory phenotype (SASP), which has been demonstrated to confer a secondary senescence response upon neighbouring proliferating cells, in a process known as paracrine senescence. This work aims to characterise the contribution of a group of small lipid bilayer-bound particles, known as extracellular vesicles (EVs), to the induction of paracrine senescence, with a focus on emphasising the limitations of widely applied EV isolation methodologies in a senescence context.

First, models of oncogene-induced (OIS) and replicative (RS) senescence were established in IMR90 and adult human mammary fibroblasts respectively, with phenotypic characterisation performed via a high content analysis (HCA) approach. EVs were then isolated from these models via differential ultracentrifugation (dUC), with increased EV release identified following senescence induction in both settings. Proteomic profiling via mass spectrometry (MS) indicated that soluble components of the SASP co-isolate during dUC based procedures, hindering the utility of this widely used technique within senescence research. Size-exclusion chromatography (SEC) was established to overcome this limitation, facilitating a further, more comprehensive assessment of OIS derived EVs via MS. Furthermore, SEC allowed demonstration that EVs isolated from OIS fibroblasts mediate the induction of paracrine senescence in both proliferating fibroblasts and breast cancer cells. Finally, in order to probe the mechanisms underlying these responses, potential mechanistic leads (NOTCH1 and ADAM10/17) were identified from EV proteomic profiles and validated to be constituents of

OIS derived EVs. The functional importance of these targets in paracrine senescence was also investigated.

Overall, this work emphasises that EVs are distinct and functionally important mediators within the SASP, but that their investigation in a senescence setting requires careful attention to isolation rigor and stringency.

Contents

Figure List

Table List

List of Abbreviations

Abbreviation	Full Name
µg	Microgram
µL	Microlitre
µm	Micrometre
468s	MDA-MB-468
53BP1	p53-binding protein 1
8-oxo	8-Oxoguanine
a.u.	Arbitrary units
ADAM10	ADAM Metallopeptidase Domain 10
ADAM17	ADAM Metallopeptidase Domain 17
ALIX	Apoptosis-Linked Gene 2-Interacting Protein X
ANOVA	Analysis of variance
APH1	Anterior pharynx-defective 1
ASCs	Adipose tissue-derived mesenchymal stem cells
ATF6α	Activating Transcription Factor 6 alpha
ATM	Ataxia–telangiectasia mutated
ATR	Ataxia telangiectasia and Rad3-related protein
BMDCs	Bone marrow-derived dendritic cells
BMSCs	Bone marrow stem cells
BRAF	Serine/threonine-protein kinase B-Raf
BrdU	Bromodeoxyuridine
BSA	Bovine Serum Albumin
C	Celsius
C/EBPβ	CCAAT-enhancer-binding protein
$C0_2$	Carbon dioxide
CCFs	Cytoplasmic chromatin fragments
CCL2	Chemokine ligand 2 (monocyte chemoattractant protein 1)
CCL20	Chemokine ligand 20 (macrophage inflammatory protein-3)
CDC7	Cell division cycle 7-related protein kinase
CDK	Cyclin dependent kinase
CDKI	Cyclin dependent kinase inhibitor
cDNA	Complementary DNA
cGAS/STING	Cyclic GMP-AMP Synthase/ Stimulator of Interferon Genes
CM	Conditioned media
cm^2	Centimetre squared
COX2	Cyclooxygenase 2
CXCR2	Chemokine receptor 2
DAPI	4’,6-diamidino-2-phenylindole
DDR	DNA damage response
DGS	Density gradient separation
DLL4	Delta-Like Protein 4
DMEM	Dulbecco's Modified Eagle Medium
DMSO	Dimethyl sulfoxide
DNA	Deoxyribonucleic acid
DNMT1	DNA Methyltransferase 1

DS	Deep senescence
dsDNA	Double stranded DNA
DTT	Dithiothreitol
dUC	Differential ultracentrifugation
ECM	Extra-cellular matrix
ELISA	Enzyme-linked immunosorbent assay
EM	Electron microscopy
EndoG	Endonuclease G
EP	Early proliferative
EPHA2	Ephrin Type-A Receptor 2
ER	Endoplasmic reticulum
ESCRT	Endosomal sorting complexes required for transport
EVs	Extracellular vesicles
ExoFBS	Exosome depleted FBS (commercial product)
FA	Formic acid
FBS	Foetal bovine serum
FCM	Flow cytometry
G0	Quiescence
G1	Growth phase 1
G2	Growth phase 2
GAPDH	Glyceraldehyde 3-phosphate dehydrogenase
GATA4	Transcription Factor GATA-4
GL13	Biotinylated Sudan black B derivative
GO	Gene Ontology
GSH	Glutathione
GSTM2	Glutathione S-transferase Mu 2
H2O2	Hydrogen peroxide
HAECs	Human amniotic epithelial cells
HCA	High content analysis
HDFs	Human dermal fibroblasts
HES	hairy and enhancer of split-1
HEY	Hairy/enhancer-of-split related with YRPW motif protein 2
HGF	Hepatocyte growth factor
HMEC	Human mammary epithelial cell
HMF	Human mammary fibroblast
HRP	Horseradish peroxidase
HRS	Hepatocyte growth factor regulated tyrosine kinase substrate
HSCs	Hepatic stellate cells
HUVEC	Human umbilical vein endothelial cells
IF	Immunofluorescence
IFITM3	Interferon Induced Transmembrane Protein 3
IFN-γ	Interferon gamma
IHROM1	Rhomboid family member 1 (RHBDF1)
IHROM2	Rhomboid family member 2 (RHBDF2)
IKK	IkappaB kinase
IL-1α	Interleukin 1 alpha
IL6	Interleukin 6
IL8	Interleukin 8

ILV	Intraluminal vesicle
IPF	Idiopathic pulmometry fibrosis
IR	Ionising radiation
IRAK1	Interleukin-1 receptor-associated kinase 1
ISEV	International society for extracellular vesicles
JAG1	Jagged1
JAK	Janus kinase
Ki67	Antigen KI-67
LFQ	Label-free quantification
LMK	Lim Kinase
LP	Late passage
M	Mitotic phase
M	Molar
MAML1	Mastermind like transcriptional coactivator 1
MCH-II	Major histocompatibility complex class II
MDM2	Mouse double minute 2 homolog
MEFs	Mouse embryonic fibroblasts
MIP1β	Macrophage inflammatory protein-1 beta (CCL4)
miR	Micro RNA
MISEV	Minimum Information for the Study of Extracellular Vesicles
ml	Millilitre
mM	Millimolar
MMP	Matrix metalloproteinase
MPF	Mitotis-promoting factor (CDK1 and cyclin B complex)
mRNA	Messenger RNA
MS	Mass spectrometry
mTOR	Mammalian target of rapamycin
MV	Microvesicle
MVB	Multivesicular body
N1ICD	Notch-1 intracellular domain
NF-κB	Nuclear Factor kappa-light-chain-enhancer of activated B
ng	Nanogram
NIS	Notch Induced Senescence
NK cell	Natural Killer Cell
nSMase	Neutral sphingomyelinase-2
NTA	Nanoparticle tracking analysis
OA	Osteoarthritis
OHT	4-Hydroxytamoxifen
OIS	Oncogene induced senescence
p38MAPK	P38 mitogen-activated protein kinases
PAI-1	Plasminogen activator inhibitor-1
PBS	Phosphate buffered saline
PCR	Polymerase chain reaction
PDGF	Platelet-derived growth factor
PDGFAA	Platelet-derived growth factor
PDs	Population doublings
PEG	Polyethylene glycol
PEN2	Presenilin enhancer 2

PFA	Paraformaldehyde
pg	Picogram
PGE2	Prostaglandin E2
pH	Power of hydrogen
psen1	Presenilin-1
PTX	Paclitaxel
qRT-PCR	Quantitative Reverse Transcription PCR
RA	Rheumatoid arthritis
RB	Retinoblastoma
RIPA	Radio immunoprecipitation assay buffer
RNA	Ribonucleic acid
ROCK	RHO-associated protein kinase
ROS	Reactive oxygen species
RPM	Revolutions per minute
RS	Replicative senescence
RT	Room temperature
S	DNA synthesis
SAHF	Senescence-associated heterochromatin foci
SASP	Senescence-associated secretory phenotype
SA-β-gal	Senescence-associated beta-galactosidase
SBB	Sudan Black B
SCAPs	Senescent Cell Anti-Apoptotic Pathways
SEC	Size-Exclusion chromatography
SF	Synovial fluid
shRNA	Short hairpin RNA
siRNA	Small inhibitory RNA
SIRT1	Sirtuin-1
SP-IRIS	Single-Particle Interferometric Reflectance Imaging Sensor
TEAB	Triethylammonium bicarbonate buffer
TEM	Transmission electron microscopy
TEM	Transmission electron microscopy
TERRA	Telomeric Repeat-containing RNA
TGFβ	Transforming growth factor beta
TIS	Therapy-induced senescence
TRPS	Tunable resistive pulse sensing
TSAP6	Tumour suppressor-activated pathway 6
u	Unit
uPA	Urokinase-type plasminogen activator
UPR	Unfolded protein response
VEGF	Vascular endothelial growth factor
VPS32	Vacuolar protein sorting-associated protein 32
WCL	Whole cell lysate
X-gal	5-bromo-4-chloro-3-indolyl-β-D-galactopyranoside
Y-EVs	Young extracellular vesicles
αSMA	alpha smooth muscle actin
γH2AX	H2A histone family member X
γ-secretase	gamma secretase complex

1 Introduction

1.1 Senescence

1.1.1 The Cell Cycle

The division of eukaryotic cells is orchestrated in a highly regulated process known as the cell cycle (Figure 1.1). This is split into four distinct phases (G1, S, G2 and M) that are closely regulated at three key checkpoints (G1/S, G2/M and Spindle) (Schafer, 1998; Vermeulen, Van Bockstaele and Berneman, 2003). *In vivo* cells primarily exist in a reversible cell cycle arrest known as quiescence (G0) and only enter the cell cycle in G1 following sufficient mitogenic stimulation (Pardee, 1974). During G1, the cell is readied for DNA synthesis, which occurs during S phase. G2 then primes the cell for entry into the mitotic (M) phase (Malumbres and Barbacid, 2001; Massagué, 2004). During mitosis, chromosomes are sorted into daughter cells and cell division occurs through cytokinesis (Wieser and Pines, 2015). Progression through the cell cycle is driven by the interaction and complex formation between cyclin dependent kinases (CDKs) and cyclin sub-units (Satyanarayana and Kaldis, 2009; Lim and Kaldis, 2013). These allow advancement through regulatory checkpoints at which stage a cell is committed to the next phase of the cell cycle (Malumbres and Barbacid, 2001; Vermeulen, Van Bockstaele and Berneman, 2003).

The progression of the cell cycle is transcriptionally controlled by the E2F family of transcription factors, which are frequently termed “master regulators” (Dyson, 1998; Bertoli, Skotheim and De Bruin, 2013). In cells not under mitogenic stimulation, E2F mediated transcription is repressed though the binding of Retinoblastoma protein (RB) family members including RB, p130 and p107 (Dyson, 1998; Malumbres and Barbacid, 2001; Satyanarayana and Kaldis, 2009). Following sufficient mitogenic stimulation (including growth factor treatment), cells re-enter the cell cycle in G1, having advanced through the so-

called restriction point (Pardee, 1974). This transition is governed by the synthesis of cyclin D in response to growth factor stimulation, which is not constitutively expressed in G0 cells (Assoian and Zhu, 1997; Vermeulen, Van Bockstaele and Berneman, 2003). CDK4/6 facilitates phosphorylation of RB through the formation of complexes with cyclin D, leading to dissociation of RB from E2F (Massagué, 2004; Bertoli, Skotheim and De Bruin, 2013). Transcription of E2F target genes marks progression though the restriction point and cells are now committed to S phase (Vermeulen, Van Bockstaele and Berneman, 2003; Satyanarayana and Kaldis, 2009). The G1/S transition is itself mediated by the E2F transcriptional target cyclin E, though complex formation with CDK2. This leads to hyperphosphoryaltion of RB (a state that is retained through the rest of the cell cycle) and further expression of E2F transcriptional targets, including cyclin E and A (Malumbres and Barbacid, 2001; Vermeulen, Van Bockstaele and Berneman, 2003; Moser *et al.*, 2018). This feedback loop mediates the G1/S transition (Ohtsubo *et al.*, 1995; Massagué, 2004).

Following G1/S transition, cells are primed for DNA replication, with progress through S phase mediated by complexes of cyclin A and CDK2 (Girard *et al.*, 1991; Walker and Maller, 1991; Sherr, 2000). These complexes mediate both the activation of DNA synthesis and prevent further replication, ensuring DNA synthesis occurs only once per cell cycle (Coverley, Laman and Laskey, 2002; Woo and Poon, 2003). Progression through the G2/M phase checkpoint and entry into mitosis is governed by CDK1 and cyclin A complexes (Pagano *et al.*, 1992; Vermeulen, Van Bockstaele and Berneman, 2003). During mitosis, CDK1 and cyclin B complexes (also referred to as mitosis-promoting factor; MPF) regulate the initiation of both prophase and anaphase, with the latter leading to the degradation of cyclins and exit from mitosis into G1 of the following cell cycle (King, Jackson and Kirschner, 1994; Peters, 2006; Harashima, Dissmeyer and Schnittger, 2013).

Whilst cyclins and CDKs represent key facilitators of the cell cycle, additional mechanisms exist that maintain regulatory control of the process. Key to the G1/S checkpoint, are the cyclin-dependent kinase inhibitor (CDKI) families INK4 and Cip/Kip, which act to inhibit the formation of cyclin-CDK complexes and thus impede cell cycle progression (Malumbres and Barbacid, 2001; Vermeulen, Van Bockstaele and Berneman, 2003). The INK4A family of cyclin-dependent kinase inhibitor (CDKI) tumour suppressors include $p16^{INK4A}$ (p16), $p15^{INK4B}$ (p15), $p18^{INK4C}$ (p18) and $p14^{INK4D}$ (ARF), which bind to CDK4/6 thus inhibiting complex formation with cyclin D (Malumbres and Barbacid, 2001). Cip/Kip CDKIs including $p21^{WAF/CIP1}$ (p21), $p27^{KIP1}$ (p27) and $p57^{KIP2}$ (p57) produce a less specific inhibition, attenuating CDK interactions with cyclins A, B, D and E (Figure 1.1), thus inhibiting progression though all phases of the cell cycle (Sherr and Roberts, 1999; Lim and Kaldis, 2013). The inhibition of CDK4/6 and CDK2 during G1 prevents the phosphorylation of RB. Consequently, this hypophosphorylated RB retains its inhibitory effect on E2F thus preventing transition from G1 to S phase. This arrest of the cell cycle is key to the process of senescence induction, with both p16 and p21 recognised as markers of a senescence response (Munoz-Espin and Serrano, 2014).

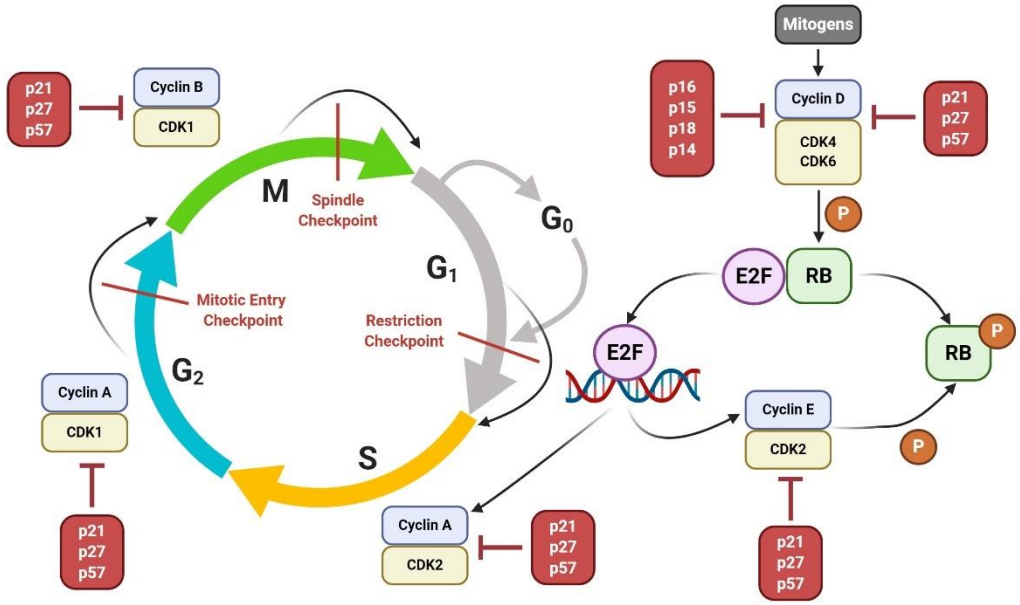

Figure 1.1: The Cell Cycle

The cell cycle is comprised of four phases and dictates the growth and division of cells. *In vivo*, cells predominantly exist in a state of quiescence (G0), only entering the cell cycle following sufficient mitogenic stimulation. Entry into the cell cycle occurs during growth phase 1 (G1) and progresses through the DNA synthesis (S), growth 2 (G2) and mitotic phases successively. Advancement through the cell cycle is controlled at regulatory checkpoints by the formation of complexes between cyclin dependent kinases (CDKs) and regulatory cyclin sub-units. During senescence, exit from the cell cycle occurs, mediated by the action of INK4A (p16, p15, p18 and p19) and Cip/Kip (p21, p27 and p57) cyclin dependent kinase inhibitors. This predominantly occurs during G1, where hypophosphorylation of retinoblastoma protein (RB) leads to inhibition of E2F family transcription factors and failure to advance through the G1/S restriction checkpoint. Based on (Vermeulen, Van Bockstaele and Berneman, 2003; Massagué, 2004)

1.1.2 Pathways of Senescence Induction

Senescence is a state of proliferative arrest typically characterised by exit from the cell cycle during G1 (Di Leonardo *et al.*, 1994; Serrano *et al.*, 1997; Campisi and D'Adda Di Fagagna, 2007). This process was first described by Leonard Hayflick, who observed that primary fibroblasts possessed finite proliferative potential *in vitro* (Hayflick and Moorhead, 1961). This limited proliferative capacity was demonstrated to result from the shorting of telomeres with successive rounds of the cell cycle, leading to a DNA damage response (DDR) and what is now referred to as replicative senescence (Harley, Futcher and Greider, 1990; Olovnikov, 1996; Bodnar *et al.*, 1998). It has subsequently emerged that senescence may be induced prematurely through a variety of potentially harmful stimuli (described in detail in section 1.1.7) (Sharpless and Sherr, 2015; Gorgoulis *et al.*, 2019). Whilst the pathways through which senescence induction occurs are highly cell type and inducing stimulus specific, two pivotal effectors have been widely described as key to the initiation and maintenance of senescence – the CDKIs p16 and p21.

Whilst not a universal requirement for the induction of senescence, many stimuli which trigger senescence initiate a DDR (Munoz-Espin and Serrano, 2014). This leads to the activation of kinases including ataxia-telangiectasia (ATM) and ataxia-telangiectasia and Rad3-related (ATR) that phosphorylate the checkpoint kinases CHK1 and CHK2 (Gire *et al.*, 2004; Campisi and D'Adda Di Fagagna, 2007). In turn, this leads to the phosphorylation of the transcription factor p53, attenuating the inhibitory binding of the ubiquitin ligase mouse double minute 2 homolog (MDM2; HDM2 human equivalent) which mediates the degradation of hypophosphorylated p53. Stabilisation of p53 leads to activation of the p21 promoter and transcription of p21 (Espinosa, Verdun and Emerson, 2003; Campisi and D'Adda Di Fagagna, 2007). The role of p21 as a CDKI then leads to the inhibition of cyclin E

and CDK2 complex formation, preventing phosphorylation of RB. Consequently, E2F transcriptional activity is repressed and cessation of the cell cycle occurs during G1 as described above (section 1.1.1).

Senescence induction may also occur through derepression of the CDKN2A locus. This has been observed in both ageing and following oncogene expression (Serrano *et al.*, 1997; Krishnamurthy *et al.*, 2004). This leads to expression of p16, which causes E2F inhibition though RB, via the blockade of cyclin D binding to CDK4/6 (Alcorta *et al.*, 1996; Sherr, 2001). Furthermore, the gene product $p14^{ARF}$ (ARF) is also encoded at the CDKN2A locus (Sherr, 2001). ARF contributes to the stabilisation of p53 and thus propagation of the p53/p21 pathway, through inhibition of MDM2 (Sherr and McCormick, 2002).

The relative contribution of the p21 and p16 pathways to the induction of senescence varies within specific cellular contexts. For example, epithelial cells have been demonstrated to undergo a p16 mediated senescence response before the critical shortening of telomeres (cellular senescence). Methylation of the p16 promoter then facilitates the reinstatement of cellular proliferation, which continues until telomere attrition triggers an exclusively p21 driven senescence response (Brenner, Stampfer and Aldaz, 1998; Garbe *et al.*, 2009). By contrast, both p21 and p16 have been demonstrated to contribute to the initiation and maintenance of senescence in fibroblasts. In fibroblast replicative senescence, p21 and p16 expression occurs sequentially, with p21 levels reaching a maximum several passages before the population has reached proliferative arrest. This then begins to decline, accompanied by a concurrent increase in p16 expression (Alcorta *et al.*, 1996). Furthermore, p16 has been demonstrated to maintain senescence-associated proliferative arrest following inhibition of the p53/p21 pathway, whilst inactivation of p53 reinstated proliferation in cells with low

levels of p16 (Beauséjour *et al.*, 2003). Additionally, a secondary senescence response may be initiated in proliferating fibroblasts treated with conditioned media from oncogene-induced senescence (OIS) cells. This occurs through activation of p21 and p15 pathways via transforming growth factor beta (TGFβ), a key component of the senescence-associated secretory phenotype (SASP) (section 1.1.4) (Coppe *et al.*, 2008; Acosta *et al.*, 2013). Models of replicative senescence and OIS are utilised within this work.

In summary, the proliferative arrest which occurs during senescence is initiated and maintained primarily though the actions of the p16 and/or p21 tumour suppressor pathways (Figure 1.2). However, the relative importance of each of these varies between both cell types and senescence inducing stimuli. Consequently, senescence represents a diverse set of phenomena, each of which differ within the context of their initiation. This heterogeneity is reflected in the diverse set of markers that have emerged as so-called “hallmarks” of senescence (Hernandez-Segura, Nehme and Demaria, 2018).

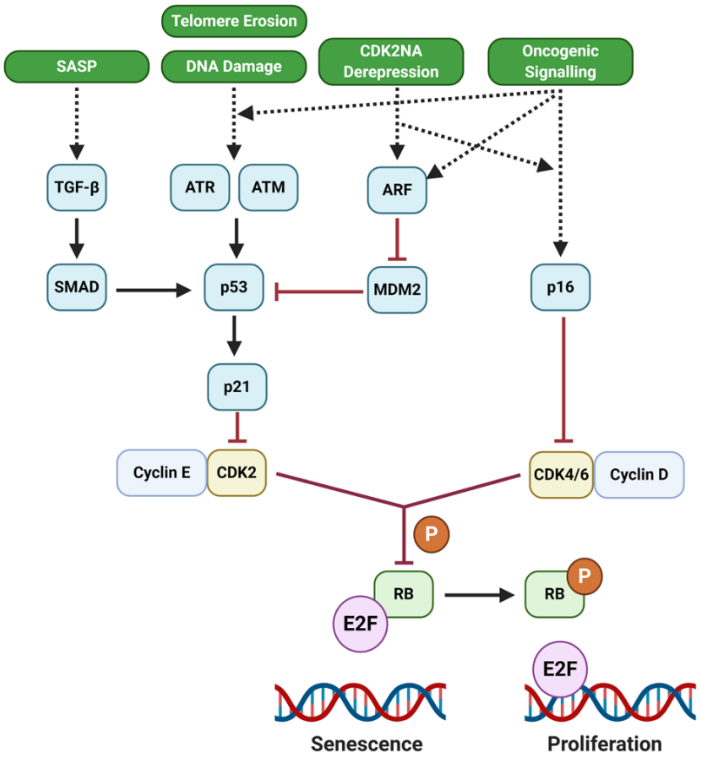

Figure 1.2: Pathways to Senescence Induction

Senescence induction may occur in response to a range of potentially harmful stimuli. Many of these lead to instigation of a DNA damage response (DDR) and activation of kinases including ataxia-telangiectasia (ATM) and ataxia-telangiectasia and Rad3-related (ATR). These lead to a signalling cascade which results in the activation of the transcription factor p53, which facilitates transcription of the cyclin dependent kinase inhibitor (CDKI) p21. The transcription of p16, another CDKI may also be elicited by senescence inducting stimuli, including oncogenic signalling and derepression of the CDK2NA locus. The later of these can also facilitate p21 expression through increased ARF expression, leading to inhibition of MDM2 and disinhibition of p53. Furthermore, secreted cytokines including TGF-β have been demonstrated to facilitate activation of p53. Following expression, the CDKIs act to inhibit complex formation between cyclin dependent kinases (CDKs) and regulatory cyclin sub-units. This leads to hypophosphorylation of retinoblastoma protein (RB) and inhibition of E2F family transcription factors, leading to cessation of the cell cycle and induction of senescence. Based on (Munoz-Espin and Serrano, 2014).

1.1.3 Phenotypic Markers of Senescence

As described in section 1.1.2, senescence represents a heterogeneous set of terminal cell fates that vary with cell type and senescence inducing stimuli. Whilst senescent cells share many common features, the diversity of potential cellular contexts has prevented the emergence of a universal "marker" of senescence. It is of particular importance to note that observation of a senescence phenotype must be carefully distinguished from other instances where cessation of cellular proliferation occurs, including quiescence and differentiation (Gorgoulis *et al.*, 2019). To achieve this, a panel of senescence "hallmarks" are often utilised, in order to compliment an observed loss of proliferation (Hernandez-Segura, Nehme and Demaria, 2018). In order to comprehensively classify senescence induction, it has been proposed that a three-step multi-marker workflow be employed. This includes: 1) a general screen for senescence induction; 2) verification with additional markers; and 3) sub-type classification (Gorgoulis *et al.*, 2019). The markers chosen within this framework will vary depending on the specific senescent context and are discussed in detail in this section (Figure 1.3). The development of a senescence-associated secretory phenotype (SASP) is examined in section 1.1.4.

1.1.3.1 Loss of Cellular Proliferation

As described in section 1.1.1, a G1 cell cycle arrest is fundamental to the process of senescence. Therefore, loss of cellular proliferation is an intrinsic hallmark of senescence. The loss of cellular proliferation markers are often used to demonstrate this phenomenon. Bromodeoxyuridine (BrdU) is a thymidine analogue that is incorporated into DNA during synthesis in the course of S phase (Nowakowski, Lewin and Miller, 1989). BrdU immunofluorescence (IF) staining can be used to demonstrate a lack of progression to S phase and thus indicate that a population of cells has undergone a G1 arrest. Similarly, Ki67

is a proliferation marker whose expression greatly increases during S phase (Lawless *et al.*, 2010). Therefore, negative Ki67 IF staining can also be used to indicate cell cycle arrest. Reduced cellular proliferation can also be identified through quantitation of cell numbers, such as via nuclei counts following 4,6-diamidino-2-phenylindole (DAPI) staining. Overall, whilst a key marker of senescence, loss of cellular proliferation alone is insufficient to distinguish senescence from cell fates such as quiescence and differentiation. It is also limited to *in vitro* assessment, as the vast majority of cells *in vivo* are in a state of G0 arrest (Vermeulen, Van Bockstaele and Berneman, 2003). Therefore, whilst an important marker, the loss of cellular proliferation alone cannot be considered an exclusive senescence marker.

1.1.3.2 Cyclin Dependent Kinase Inhibitor Expression

Closely linked to the loss of cellular proliferation described in section 1.1.2, senescence is associated with the engagement of the p16 and p21 tumour suppressor pathways. Therefore, identification of p16 and p21 upregulation are widely used to demonstrate the induction of a senescence response (Gorgoulis *et al.*, 2019). However, the relative importance of these pathways varies between different types of senescence and neither can be considered a universal marker. Furthermore, p21 activation is not restricted to senescence, mediating DDR responses such as apoptosis and DNA repair (Jung, Qian and Chen, 2010). Paradoxically, p21 has also been demonstrated to promote cell cycle progression by facilitating CDK4/cyclin D complex formation (Cheng, 1999). This is an illustrative example of the wider issues regarding senescence marker identification, as whilst extremely useful in many settings, p21 is neither exclusive to senescence nor present in all senescence models. This underpins the requirement for a panel of senescence markers to confidently detect senescence induction.

1.1.3.3 Cellular Morphology

Alterations in cell size and morphology were among the first phenotypic changes to be described as accompanying senescence (Cristofalo and Kritchevsky, 1969; Greenberg, Grove and Cristofalo, 1977; Wang and Gundersen, 1984). Phase contrast microscopy can readily visualise an increase in cell size following senescence induction, with heterogeneous size profiles emergent between different models of senescence (Hwang, Yoon and Kang, 2009). This increased size *in vitro* appears to be recapitulated *in vivo*, with senescence-associated beta-galactosidase (SA-β-gal) positive cells from a variety of mouse tissues demonstrating larger cell areas than negative counterparts following image-stream flow cytometry analysis (Biran *et al.*, 2017). Interestingly, it has recently been demonstrated that increased cell size during G1 arrest hinders cellular proliferation. Pharmacological blockade of CDK4/6 via the p16 mimetic palbociclib leads to an increase in cell size and a decreased DNA:cytoplasmic ratio. This is hypothesised to contribute to a process of "cytoplasmic dilution" whereby nucleic acid and protein production cannot support an increased demand following excessive cell growth. This leads to fundamental changes in the biochemical properties of the cytoplasm such as diffusion rates and viscosity. Palbociclib treatment in combination with mitogenic stimulation leads to excessive cell growth and inhibition of cellular proliferation upon cessation of treatment. Crucially, palbociclib treatment in the absence of growth factors did not lead to impairment of cellular proliferation with removal of the drug. Together, this data indicates that a process of cytoplasmic dilution, resulting from excessive cell growth, may contribute to the proliferative arrest associated with senescence (Neurohr *et al.*, 2019). This represents the first mechanistic implication of the widely reported increase in cell size that accompanies senescence, and indicates that excessive cell growth is a contributor to, as well as a consequence of, senescence induction.

As well as increasing in size, senescent cells have also been widely reported to acquire alterations in cellular shape (Hernandez-Segura, Nehme and Demaria, 2018). The specific nature of these morphological changes is heavily dictated by the cell type under investigation. However, common features include an irregular flattened morphology, which is distinct from that of the proliferating counterpart cells (Hwang, Yoon and Kang, 2009). Such striking alterations in cell shape might be predicted to arise from cytoskeletal modifications with senescence. Expression of vimentin, an intermediate filament protein, has been demonstrated to increase with replicative senescence (Nishio *et al.*, 2001; Nishio and Inoue, 2005). Moreover, reorganisation of vimentin from a disparate "fur" like network into discrete bundles that traverse the full length of the cell occurs (Nishio and Inoue, 2005). Senescence-associated changes in actin expression have also been investigated. However, contradictory studies have indicated that hydrogen peroxide (H_2O_2) and replicative senescence are not associated with changes in actin expression, but rather re-organisation (Chen *et al.*, 2000) and that replicative senescence is associated with a decrease in actin expression (Nishio and Inoue, 2005). Therefore, vimentin currently represents the most comprehensively described cytoskeletal component that alters following senescence induction. Interestingly, small inhibitory RNA (siRNA) inhibition of Activating Transcription Factor 6 (ATF6α), part of the unfolded protein response (UPR), recovers a proliferative morphology in replicatively senescent fibroblasts without altering DNA damage markers of senescence (Druelle *et al.*, 2016). Inhibition of cyclooxygenase-2 (COX-2) and prostaglandin E2 (PGE2), downstream effectors of the ATF6α, also leads to an uncoupling of senescence from morphological changes (Cormenier *et al.*, 2018). However, the specific mechanisms via which these pathways influence senescent cell morphology have not been fully described (Hernandez-Segura, Nehme and Demaria, 2018).

1.1.3.4 Nuclear Alterations

Changes in nuclear morphology have also been demonstrated to occur following senescence induction (Sadaie *et al.*, 2015). Both a reduction in intensity of DAPI staining and increased nuclear area have been reported following induction of therapy-induced senescence (TIS) (Zhao *et al.*, 2010; Studencka and Schaber, 2017). DAPI intensity has previously been used to stratify cell populations according to phase of the cell cycle and may provide a useful high throughput screening tool for demonstrating senescence induction (Zhao and Darzynkiewicz, 2013; Roukos *et al.*, 2015). These alterations in nuclear morphology have been attributed to changes in nuclear composition (Mehta *et al.*, 2007; Hernandez-Segura, Nehme and Demaria, 2018). Lamin B1, a structural nuclear envelope protein, has been demonstrated to decrease in senescent fibroblasts induced by x-ray irradiation, replicative arrest and oncogenic-Ras expression (Freund *et al.*, 2012). Impaired nuclear integrity following loss of Lamin B1 has been implicated in the emergence of cytoplasmic chromatin fragments (CCFs), which may underpin the reduced DNA content associated with senescence induction (Ivanov *et al.*, 2013). Furthermore, irradiation induced senescence is also associated with a loss of DNA, demonstrated by reduced DAPI intensity, attributed to release of mitochondrial endonuclease G (EndoG) and the degradation of damaged DNA (Studencka and Schaber, 2017). Therefore, alterations in nuclear morphology and reduced nuclear DNA content are widely reported in multiple models of senescence and these may arise from the loss of structural functionality of the nuclear envelope.

By contrast, the emergence of DAPI-dense nuclear foci known as senescence-associated heterochromatin foci (SAHF) has been primarily associated with induction of OIS (Narita *et al.*, 2003; Di Micco *et al.*, 2011; Sharpless and Sherr, 2015). Heterochromatin describes a configuration of genomic DNA and regulatory histones that is tightly bound, thus repressing

access to transcriptional machinery (Parry and Narita, 2016). In OIS, it has been proposed that promoters of genes critical to the propagation of cellular proliferation, such as E2F targets, are associated with heterochromatin proteins, facilitating cell cycle arrest (Narita *et al.*, 2003). However, if oncogenic RAS is expressed in cells that have been transduced with p53 short-hairpin RNA (shRNA), and consequently do not enter OIS, the appearance of SAHFs is retained (Di Micco *et al.*, 2011). Interestingly, whilst the total presence of heterochromatin was unchanged, the localisation to E2F target promoters was dramatically reduced, accounting for the re-establishment of cellular proliferation and reinforcing the previously described role of SAHFs in proliferative arrest (Di Micco *et al.*, 2011; Salama *et al.*, 2014). Overall, SAHFs represent the only notable example of a senescence marker principally described in the context of a single form of senescence (Gorgoulis *et al.*, 2019).

1.1.3.5 Increased Lysosomal Activity

One of the most widely reported markers of senescence is observation of increased lysosomal activity (Hernandez-Segura, Nehme and Demaria, 2018). In particular, the detection of increased SA-β-gal activity is often used to demonstrate acquisition of a senescence phenotype (Dimri et al., 1995). In senescence, due to high activity of SA-β-gal, a characteristic blue stain can be detected via use of the substrate 5-bromo-4-chloro-3-indolyl-β-D-galactopyranoside (X-gal) at a pH of 6.0, which is not seen in proliferating cells. However, it has been demonstrated that SA-β-gal activity may be detected in quiescent cells, in conditions of contact inhibition and serum starvation (Yang and Hu, 2005). Therefore, whilst a notable and well-described marker of senescent cells, SA-β-gal must be considered a more general marker of increased lysosomal activity, which is not itself, exclusive to a senescence phenotype (Hwang, Yoon and Kang, 2009; Gorgoulis *et al.*, 2019).

Despite the limitations that surround SA-β-gal, its popularity as a senescence marker has led to the emergence of other methods of lysosomal assessment. In particular, staining of lipofuscin aggregates (an indication of impaired lysosomal degradation) with Sudan Black B (SBB) stain has been reported as a method to demonstrate lysosomal accumulation (Georgakopoulou *et al.*, 2013; Evangelou *et al.*, 2017). A biotinylated SBB derivative (GL13) has recently become commercially available under the trade name SenTraGor™. These techniques provide some advantage over SA-β-gal as they are applicable to paraffin embedded tissue (Georgakopoulou *et al.*, 2013; Hernandez-Segura, Nehme and Demaria, 2018). However, the major limitation of SA-β-gal, that lysosomal accumulation is not exclusive to senescence, also applies to these techniques. Therefore, as discussed above, increased lysosomal activity must be applied in concert with other techniques in order to serve as a marker of senescence.

1.1.3.6 DNA Damage Markers

As described in section 1.1.2, the initiation of a DDR follows numerous senescence inducing stimuli (Munoz-Espin and Serrano, 2014). Senescent fibroblasts generated via both ionising radiation or replicative exhaustion demonstrate increased markers of DNA double strand breaks including p53 binding protein 1 (53BP1) and phosphorylated histone variant H2AX (γH2AX) (D'Adda Di Fagagna *et al.*, 2003). H2AX is phosphorylated by ATM and ATR kinases during the DDR cascade and contributes to recruitment of DNA repair complexes to sites of double strand breaks (Celeste *et al.*, 2002; Kuo and Yang, 2008). H2AX phosphorylation can also lead to the recruitment of 53BP1, which in turn promotes DNA repair of double strand breaks through non-homologous end-joining, (Panier and Boulton, 2014; Kocyłowski *et al.*, 2015). As with other markers of senescence, the use of DNA damage is limited by a lack of

specificity to senescence and the existence of senescence models that do not engage a DDR (Hernandez-Segura, Nehme and Demaria, 2018).

1.1.3.7 Mitochondrial Dysfunction

Mitochondrial dysfunction has been proposed as a "hallmark" of ageing and has also been associated with senescence (López-Otín *et al.*, 2013; Hernandez-Segura, Nehme and Demaria, 2018). Excessive reactive oxygen species (ROS) production by dysfunctional mitochondria has been described within replicative senescence (Passos *et al.*, 2007) and is believed to lead to an accumulation of damaged proteins and other cellular waste, which overwhelms lysosomal degradative capacity (Gorgoulis *et al.*, 2019; Vasileiou *et al.*, 2019). This is fundamental to the "garbage catastrophe" theory of ageing, in which export or degradation of damaged products is overcome by excessive demand (Terman *et al.*, 2010; Baixauli, López-Otín and Mittelbrunn, 2014; Picca *et al.*, 2019). Furthermore, mitochondrial dysfunction has been observed following H_2O_2 treatment in fibroblasts, also leading to an increase in intracellular ROS production and instigation of a senescence phenotype (Tai *et al.*, 2017). Therefore, mitochondrial dysfunction and the closely associated increase in ROS production can be considered potential markers of a senescence response.

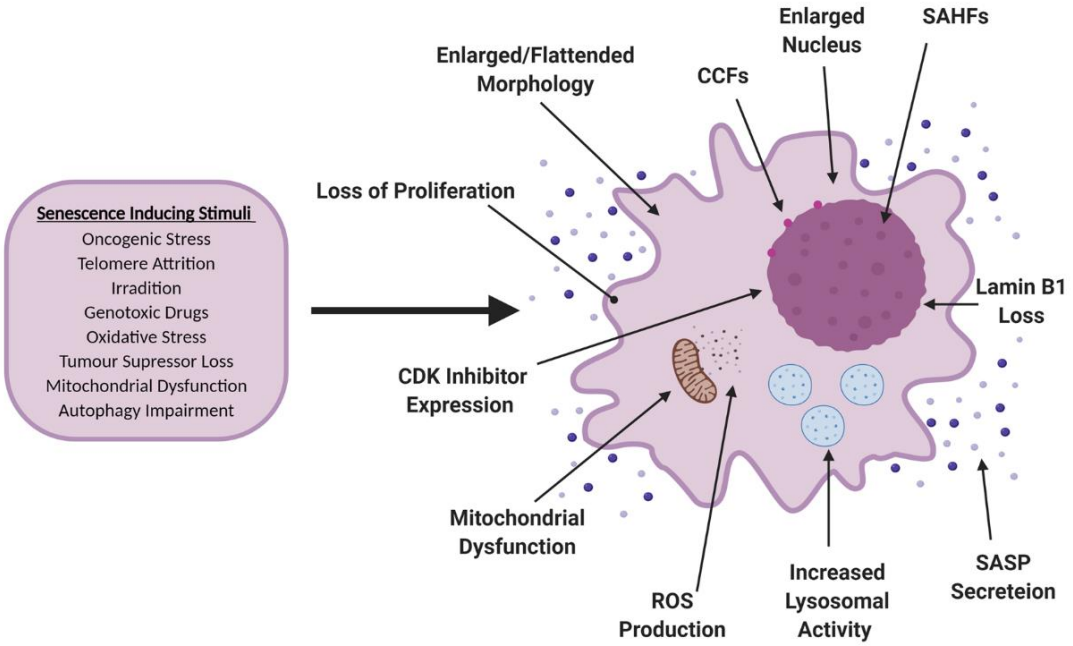

Figure 1.3: Common Markers of Senescence

Senescence induction may be triggered through a range of stimuli. This results the emergence of a heterogeneous array of markers that also depends on the cell type under insult. As no single universal marker of senescence has been described, confident classification is determined through investigation of a range of markers. Aside from the intrinsic loss of proliferation, these include acquisition of an enlarged cellular and nuclear morphology, loss of nuclear Lamin B1, appearance of senescence-associated heterochromatin foci (SAHFs), expression of cyclin dependent kinase inhibitors (CDKIs) increased cytoplasmic chromatin fragments (CCFs), increased lysosomal activity, mitochondrial dysfunction, increased production of reactive oxygen species (ROS) and acquisition of a senescence-associated secretory phenotype (SASP).

1.1.4 The Senescence-Associated Secretory Phenotype (SASP)

The senescence-associated secretory phenotype (SASP) is an enhanced secretory profile of inflammatory cytokines, chemokines, growth factors and proteases that accompanies the development of senescence. Whilst individual factors, such as plasminogen activator type-1 (PAI-1), had previously been considered markers of senescence induction, Coppé *et al*., (2008) were the first to comprehensively describe the secretome of senescent cells (Mu and Higgins, 1995; Coppe *et al.*, 2008). Through use of antibody arrays, investigators demonstrated that induction of senescence via both oncogenic-Ras expression and ionising radiation (IR) lead to secretion of a complex inflammatory secretome in both fibroblasts and epithelial cells (Coppe *et al.*, 2008). The composition of the secretome varied between both cell types and inducing stimuli, reflecting the heterogeneity in senescence phenotypes within different cellular contexts (Coppe *et al.*, 2008; Maciel-Barón *et al.*, 2016).

Whilst not present in all models of senescence, initiation of a DDR has been demonstrated to contribute to the development of the SASP (Rodier *et al.*, 2009; Coppé *et al.*, 2010). Interleukin 6 (IL-6) and IL-8 secretion, frequently used surrogate markers of the SASP, were demonstrated to increase following persistent DNA damage via both ionising radiation and proliferative arrest. This response was not recapitulated following transient DNA damage with low dose irradiation and was attenuated in cells depleted of ATM by shRNA. However, other identified factors (nine out of 14) were unaltered following ATM depletion demonstrating that a DDR is only partially involved in the development of the SASP (Rodier *et al.*, 2009). Furthermore, SASP production has been demonstrated to occur independently of a DDR (Freund, Patil and Campisi, 2011). Interestingly, neither the p16 nor the p53/p21 tumour suppressor pathways appear essential for SASP production. Senescent WI-38 fibroblasts have been demonstrated to continue SASP production following p53 ablation by

shRNA. Furthermore, p53 may repress development of an exaggerated SASP, as WI-38 fibroblasts induced by replicative exhaustion, irradiation and oncogenic-Ras develop a more potent SASP profile following p53 inactivation (Coppe *et al.*, 2008). Additionally, senescence induction by ectopic expression of p21 or p53 is not accompanied by development of a SASP (Coppé *et al.*, 2011). Moreover, SASP development occurs in WI-38s induced by both irradiation and oncogenic-Ras following p16 inhibition by shRNA. Therefore, whilst widely observed within a range of senescence models, SASP development appears to be uncoupled from tumour suppressor pathways (Coppé *et al.*, 2010).

Current understanding of the molecular pathways of the SASP are outlined in Figure 1.4. The mitogen-activated protein kinase p38 (p38MAPK) signalling cascade has been demonstrated to be essential to the induction of oncogenic-Ras induced senescence (Wang *et al.*, 2002; Deng *et al.*, 2004). The development of a potent SASP in these cells has also been linked to p38MAPK activity, as pharmacological inhibition was demonstrated to lead to a reduction in 65 out 83 SASP factors in oncogenic-Ras induced HCA2 fibroblasts. This result was recapitulated in irradiation induced HCA2s, with 25 out of 37 factors reducing following p38MAPK inhibition. These emphasise that the SASP is variable between senescence models and, whilst 19 out of 23 common factors between both models reduced following p38MAPK inhibition, that SASP composition is likely be driven by more than one pathway (Freund, Patil and Campisi, 2011). Importantly, p38MAPK was also demonstrated to drive the activation of the transcription factor NF-κB, with NF-κB knockdown via shRNA sufficient to prevent p38MAPK induced SASP production (Freund, Patil and Campisi, 2011).

NF-κB is a pro-inflammatory transcription factor that is upregulated during OIS and has been implicated as a major contributor to the direct transcription of many SASP factors (Chien *et*

al., 2011). As well as via p38MAPK, NF-κB activation occurs through interleukin-1α (IL-1α), an initiating factor within the SASP, which acts to regulate the development of a mature SASP composition, including both IL-6 and IL-8 (Orjalo *et al.*, 2009). This occurs through a positive feedback loop, as IL-1α is a transcriptional target of NF-κB. Furthermore, this system is modulated by the microRNAs (miRs) miR-146a and miR-146b, which reduce expression of the IL-1α signalling cascade component interleukin 1 receptor-associated kinase (IRAK1), and are themselves upregulated via NF-κB (Bhaumik *et al.*, 2009). IL-1α is also regulated by the molecular target of rapamycin (mTOR), a kinase whose pharmacological inhibition has been demonstrated to extend the life span of mice (Harrison *et al.*, 2009). mTOR inhibition with rapamycin leads to reduced mRNA expression of NF-κB targets, including IL-6 and IL-8, as well as potent suppression of IL-1α signalling, whilst ectopic expression of IL-1α recovers rapamycin induced SASP suppression (Laberge *et al.*, 2015; Faget, Ren and Stewart, 2019). Activation of NF-κB also occurs following cyclic GMP–AMP synthase (cGAS) / stimulator of interferon genes (STING) signalling in response to CCFs, which accumulate during senescence due to downregulation of cytoplasmic DNases (Dou *et al.*, 2017; Glück *et al.*, 2017; Takahashi *et al.*, 2018). The initiation of a DDR (a key facet of many senescence models) has also been demonstrated to contribute to NF-κB activation. This occurs through stabilisation of GATA4, a transcription factor which upregulates IL-1α and thus contributes to the complex feedback loop that mediates the maturation of SASP composition (Kang *et al.*, 2015; Faget, Ren and Stewart, 2019).

Another key transcription factor activated though IL-1α signalling is CCAAT/enhancer-binding protein beta (C/EBPβ) (Orjalo *et al.*, 2009). Similar to IL-1α mediated activation of NF-κB, C/EBPβ is essential to the development of the full SASP composition including IL-6 and IL-8 (Acosta *et al.*, 2008; Kuilman *et al.*, 2008). Factors within this developed SASP have

been demonstrated to reinforce senescence in an autocrine manner via the CXCR2 chemokine receptor (Acosta *et al.*, 2008). The contribution of C/EBPβ to SASP composition has also been demonstrated to depend on NOTCH1 signalling during OIS. Early during OIS, the composition of the SASP is geared towards TGFβ secretion, whilst activation of C/EBPβ is repressed. NOTCH1 mediates a switch to a C/EBPβ driven pro-inflammatory secretome, which is characterised by an increased IL-6 and IL-8 secretion.

The vast majority of studies investigating the SASP have focused upon the soluble constituents. However, extracellular matrix components and shed ectodomains were also identified during early characterisation of the SASP (Coppé *et al.*, 2010). It has since emerged that approximately 10% of the OIS SASP composition is comprised of shed ectodomains with a third of those released through cleavage by the sheddase A Disintegrin and metalloproteinase domain-containing protein 17 (ADAM17) (Morancho *et al.*, 2015). Interestingly, reports into the activity of ADAM17 within senescence are not harmonious, with ADAM17 (and the closely related ADAM10) activity demonstrated to increase in oncogenic-Ras induced PC-3 prostate cancer cells (Effenberger *et al.*, 2014), but not in MCF7 breast cancer cells induced via oncogenic p95HER2 (Morancho *et al.*, 2015). Whilst both reports demonstrated that ADAM17 contributed to SASP composition, the changes in both expression and activity of sheddases within senescence remain poorly described.

In summary, the molecular controls of the SASP are complex and not fully appreciated. The SASP develops kinetically across the course of senescence induction and varies in both potency and composition between models of senescence and cell types. However, it is clear that the SASP comprises a plethora of soluble inflammatory factors as well as shed ectodomains and extracellular matrix components.

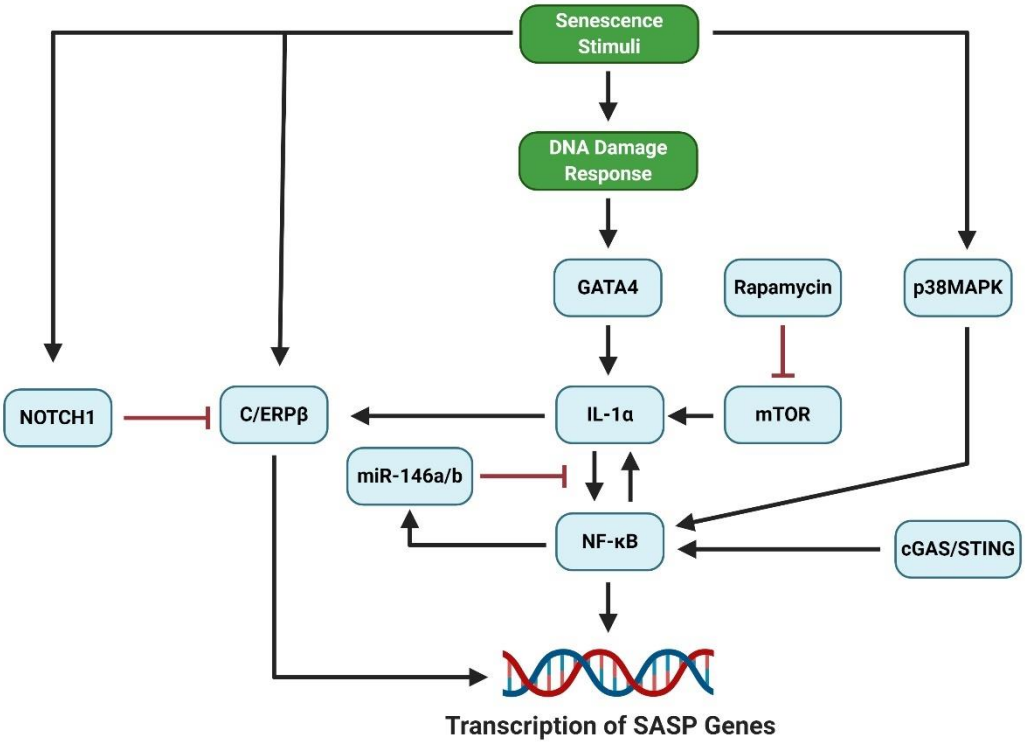

Figure 1.4: Molecular Pathways of the Senescence-Associated Secretory Phenotype (SASP)

Acquisition of a senescence-associated secretory phenotype (SASP) occurs following senescence induction through a range of damaging stimuli. The composition of the SASP is not static and kinetically develops following senescence induction. SASP constituents also vary between cell types and following different senescence inducing stimuli. NF-κB and C/ERPβ are key transcription factors mediating SASP composition. Based on (Faget, Ren and Stewart, 2019).

1.1.5 Replicative Senescence

As stated above, the phenomenon of senescence was first described by Hayflick and Moorhead in 1961, though observation of replicative exhaustion following ~50 "sub-cultivations" of human fibroblasts in culture (Hayflick and Moorhead, 1961). This finite proliferative potential has since been termed the "Hayflick-limit" and is used to describe the number of population doublings required for cells to enter a state of replicative senescence (Figure 1.5). This process has been demonstrated to arise through initiation of a DDR in response to telomere shortening with consecutive rounds of the cell cycle (Herbig *et al.*, 2004).

Telomeres are repetitive DNA sequences (5' – TTAGGG – 3') which serve as protective caps at the end of chromosomes (Blackburn and Gall, 1978; Blackburn, 2001). Telomeres are eroded with successive rounds of the cell cycle, due to the so called "end-replication problem". This was first described in 1971 by Olovnikov in a Russian language publication (Olovnikov, 1971) where the author speculated that incomplete replication of DNA ends ("marginotomy") could underpin the senescence responses observed by Hayflick (Olovnikov, 1973, 1996). The distinction of being the first manuscript to describe this phenomenon is often attributed to (Watson, 1972), who independently described a similar phenomenon, albeit without linking to Hayflick's work (Olovnikov, 1996; Greider, 1998). Regardless, the concept centres on fact that DNA synthesis occurs in a 5' to 3' direction. In order to synthesise the 3' to 5' lagging strand, short RNA primers are used to generate Okazaki fragments, which are in turn extended, and primers both removed and replaced by DNA polymerase. However, the primer of the final Okazaki fragment cannot be replaced with DNA, leading to incomplete replication following removal and overall shortening of the chromosome (Vega, Mateyak and Zakian, 2003; Chow *et al.*, 2012). Telomeres serve a

protective function due to their position on the end of chromosomes, which allows them to be eroded rather than critical coding regions (Blackburn and Gall, 1978). This process occurs with each round of the cell cycle, with telomeres becoming progressively shorter (Harley, Futcher and Greider, 1990). Eventually, telomeres reach a critical length, where their role as a "buffer" against the end-replication problem can no longer be served, leading to instigation of a DDR and entry into a state of replicative senescence (Bodnar *et al.*, 1998; Fagagna *et al.*, 2003).

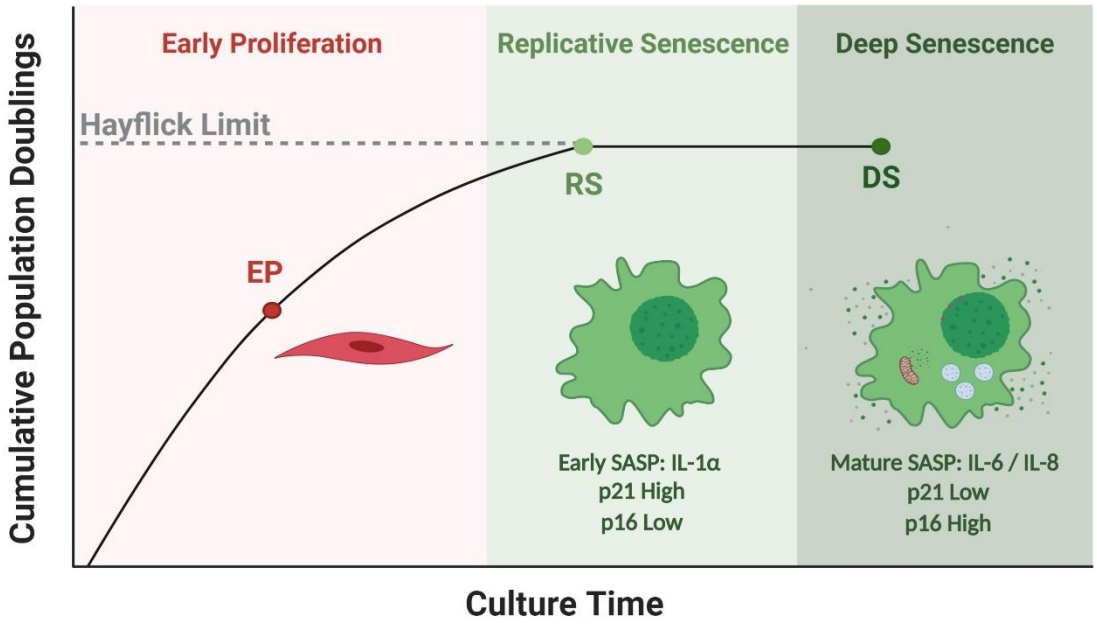

Figure 1.5: Replicative senescence of fibroblasts and the Hayflick Limit

The finite proliferative capacity of cells *in vitro* was first demonstrated by Hayflick and Moorhead in 1961. Early proliferative (EP) cells are serially passaged reach until they reach a maximum cumulative number of population doublings. At this point they are considered to have entered replicative senescence (RS), having reached their Hayflick limit. The senescence response then develops into a stable phenotype known as deep senescence (DS). The initiation and maintenance of these responses is mediated by expression of the tumour suppressors p21 and p16, which have an inverse relative abundance during RS and DS. Furthermore, during the transition of RS to DS, the senescence-associated secretory phenotype (SASP) of the cells develops, from an early IL-1α composition to a developed, mature IL-6/IL-8 dominated makeup.

1.1.6 Oncogene-Induced Senescence

Distinct from telomere dependent proliferative potential, senescence may be induced prematurely through expression of oncogenes including Ras (Serrano *et al.*, 1997), MEK (Lin *et al.*, 1998) and BRAF (Zhu *et al.*, 1998) in a process termed oncogene-induced senescence (OIS). OIS was first described in normal human fibroblasts (IMR90 and WI-38), mouse embryonic fibroblasts (MEFs) and immortalised rat fibroblasts (REF52), through transduction with activated ras allele ($HRas^{V12}$). This lead to supra-physiological expression of HRas protein, between 5 and 10 times greater than endogenous levels. Consequently, cellular proliferation was restricted through a G1 arrest characterised by reductions in hyperphosphorylated RB, cyclin A and CDK2 activity. This was accompanied by established senescence markers, including expression of both p16 and p21, along with increased SA-β-gal activity and acquisition of an enlarged flattened morphology. Crucially, these phenotypes emerged within 10 days of transduction, demonstrating OIS to be a rapid, premature response (Serrano *et al.*, 1997). Subsequently, initiation of OIS has been demonstrated to occur in response to the expression of other oncogenes including MEK and BRAF (Lin *et al.*, 1998; Zhu *et al.*, 1998). These *in vitro* studies are supported by *in vivo* evidence that highlight a potential physiological role of OIS as an important tumour suppressor response (Campisi and D'Adda Di Fagagna, 2007). Mice expressing oncogenic $KRas^{V12}$ acquire fewer malignant tumours (adenocarcinoma) and more pre-malignant tumours (adenoma) than control mice. The adenomas displayed characteristics of *in vitro* senescence markers including increased expression of p16, reduced expression of Ki67 and increased SA-β-gal activity, whereas adenocarcinomas did not. The authors speculated that initiation of OIS *in vivo* acts to inhibit tumour development, thus serving as a tumour suppressor mechanism (Collado *et al.*, 2005; Campisi and D'Adda Di Fagagna, 2007). The physiological roles of senescence induction, including tumour suppression, are discussed further in section 1.1.9.

1.1.7 Other Types of Senescence

Replicative exhaustion and oncogene expression represent two potential stressors that may elicit a senescence response. However, a wide range of other stimuli have also been demonstrated to induce senescence. Premature senescence may occur following challenge with a variety of deleterious agents including cytotoxic drugs (Petrova *et al.*, 2016), irradiation (Studencka and Schaber, 2017), H_2O_2 (Chen and Ames, 1994), tumour suppressor loss (Chen *et al.*, 2005), autophagy impairment (Tai *et al.*, 2017) and mitochondrial dysfunction (Wiley *et al.*, 2016). Senescence can also propagate between cells through processes of secondary senescence. This involves the transmission of senescence to neighbouring proliferating cells through a variety of mechanisms.

The first indications that senescence could propagate through a population of cells was demonstrated by a so called "bystander effect". Replicatively senescent MRC5 fibroblasts were demonstrated to induce a DDR in neighbouring proliferating cells, although this could not be recapitulated through use of conditioned media or trans-well co-culture experiments (Nelson *et al.*, 2012). The breakthrough publication to investigate this bystander effect senescence was Acosta *et al.* (2013), who implicated paracrine signalling of the SASP as a major effector of secondary senescence (Acosta *et al.*, 2013). Conditioned media collected from OIS (RAS, RAF and MEK) IMR90s was demonstrated to inhibit both cell proliferation and BrdU incorporation, as well as increase SA-β-gal activity. This inhibition of cellular proliferation was demonstrated up to 10 days following the cessation of treatment. Inhibition of p16, p21 and p53 by siRNA in treated cells attenuated this paracrine induction, indicating that both tumour suppressor pathways are involved in mediating paracrine senescence. Numerous factors were demonstrated to be critical to mediating this function of the SASP including TGFβ, VEGF, CCL2 and CCL20. Of these, the role TGFβ was identified as

the most uniquely paracrine, with a less significant role in the autocrine reinforcement of OIS than the other factors. Pharmacological TGFβ pathway inhibition was confirmed to attenuate paracrine senescence in a mechanism that relied upon both p15 and p21 (Acosta *et al.*, 2013).

Understanding of secondary senescence has recently been extended to include a juxtacrine-induced response through the expression of NOTCH1 ligands (Jagged 1, JAG1) on the surface of senescent cells (Hoare *et al.*, 2016; Parry *et al.*, 2018; Teo *et al.*, 2019). This NOTCH-induced senescence (NIS) was demonstrated to occur through lateral induction from both OIS IMR90s and senescent cells induced via ectopic expression of the intracellular domain of NOTCH1 (N1ICD; Figure 1.6) (Hoare *et al.*, 2016; Hoare and Narita, 2018). Interestingly, expression of NOTCH1 and cleavage of its functional intracellular domain has been demonstrated to increase early during the induction of OIS, followed by a reduction in N1ICD cleavage from day 4. This is kinetically associated with a shift in secretome composition from a predominantly TGF-β high SASP, to an IL-6/IL-8 profile dependent on C/EBPβ (Hoare *et al.*, 2016). Ectopic expression of N1ICD also suppresses appearance of SAHFs in OIS cells, in an effect recapitulated though juxtacrine NOTCH1 signalling via JAG1 ligands on neighbouring cells (Parry *et al.*, 2018). Therefore, the role of NOTCH1 signalling within senescence is complex. NOTCH1 expression increases in OIS and mediates the composition of the SASP. NOTCH1 ligands on senescent cells may drive neighbouring proliferating cells into a senescent phenotype in a juxtacrine mechanism of secondary senescence. Finally, the cleavage of N1ICD and activation of NOTCH1 signalling pathways supress development of a full OIS phenotype. Overall, senescent cells have been demonstrated to propagate senescence to neighbours through both paracrine and juxtacrine signalling. The physiological consequences of this are discussed in section 1.1.9.

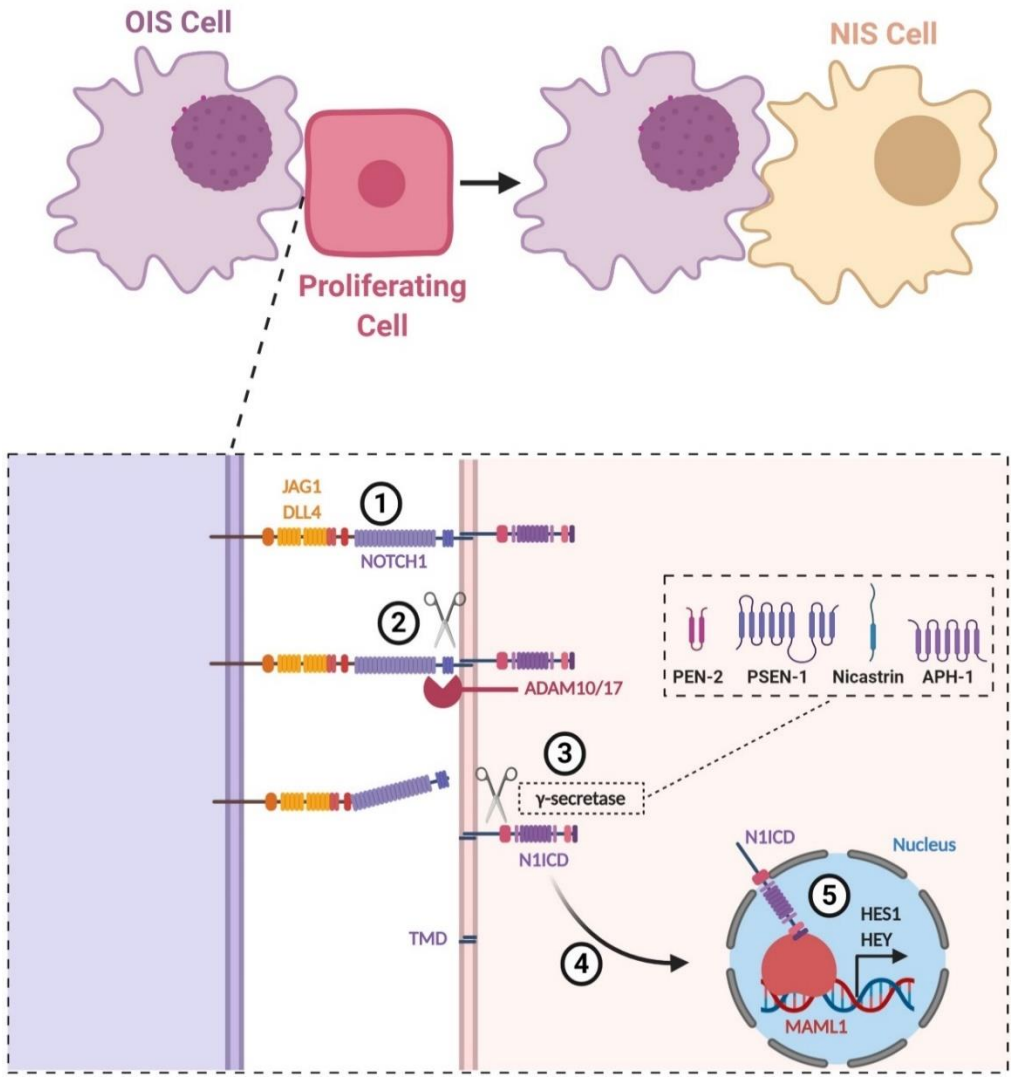

Figure 1.6: NOTCH induced senescence via canonical NOTCH1 signalling

Expression of NOTCH1 ligands such as JAG1 and DLL4 on the surface of oncogene-induced senescent cells mediates induction of a form of secondary senescence referred to as NOTCH-induced senescence (NIS). This occurs through canonical NOTCH1 juxtacrine signalling. 1) Binding of NOTCH1 ligands to the extracellular domain of the NOTCH1 receptor facilitates 2) Cleavage by ADAM10 and ADAM17 sheddases, which causes disengagement of the extracellular domain and leads to 3) cleavage of the NOTCH1 intracellular domain (N1ICD) by the γ-secretase complex (comprising PEN-2, PSEN-1, Nicastrin and APH-1). 4) N1ICD translocates to the nucleus leading to activation of MAML1 transcription factor and transcription of NOTCH1 responsive genes HES1 and HEY. This may be recapitulated experimentally though ectopic expression of N1ICD. Based on (Bray, 2016).

1.1.8 Senescence Reversal

Senescence has widely been considered a terminal cell fate characterised by an irreversible cell cycle arrest. Whilst bypass of senescence has been demonstrated as a pro-tumorigenic effect that occurs following hypermethylation of the p16 promotor in epithelial cells (section 1.1.2), these "bypassed" cells fundamentally differ from those early in their proliferative potential (Garbe *et al.*, 2014; Lowe *et al.*, 2015). Therefore, whilst these cells re-establish proliferation following cellular senescence, they are not considered "reversed" to an early proliferative state. However, this was recently achieved through the ablation of p16 via siRNA inhibition in adult human mammary epithelial cells (HMECs) (Lowe *et al.*, 2015). This resulted in increased BrdU incorporation, reduced SA-β-gal activity and a reversion of DNA methylation profile to that of early proliferating cells. This work is supported by previous studies, which have demonstrated senescence reversal in MEFs (Dirac and Bernards, 2003; Sage *et al.*, 2003) and human foetal fibroblasts (Gire and Wynford-Thomas, 1998; Beauséjour *et al.*, 2003). A protocol for the reversal of senescence in adult fibroblasts has also recently been developed within the Bishop lab. by Elly Tyler, details of which are described within her PhD thesis (Thesis:(Tyler, 2016)) and section 2.6.

1.1.9 Senescence *in vivo*

Since Hayflick and Moorhead first described the proliferative arrest associated with replicative senescence, there has been widespread interest in determining the physiological purpose of senescence induction (van Deursen, 2014). An early concept proposed that senescence could serve as a protective function against the malignant transformation of cells by restricting proliferation (Campisi and D'Adda Di Fagagna, 2007). This was supported by both the observation that replicative senescence occurs as a consequence of telomere attrition, and by the discovery of OIS (Serrano *et al.*, 1997; Bodnar *et al.*, 1998). This would

position senescence as an evolutionarily beneficial process, which promotes organismal survival by providing a barrier to cancer development (Campisi, 2001). However, as first predicted by Hayflick and Moorhead, the loss of proliferation and long term persistence of senescent cells has also been proposed as a key mechanism to the tissue dysfunction and loss of regeneration that accompanies ageing (Campisi and D'Adda Di Fagagna, 2007). Furthermore, the secretion of SASP factors has been identified to contribute to an increased proliferation of premalignant cells (Krtolica *et al.*, 2001). This paints a paradoxical picture of senescence *in vivo*, having both a bright, beneficial role in tumour suppression and a dark, detrimental role in ageing. These contradictory functions are harmonised in the evolutionary theory of "antagonistic pleiotropy", which stipulates that, due to human lifespan being historically much shorter, mechanisms that are beneficial in early life may develop despite detrimental consequences with age. Individuals would be afforded protection by such mechanisms and thus reach reproductive age, before experiencing the harmful long-term effects in later life, where selection pressure is less (Rauser, Mueller and Rose, 2006; Campisi and D'Adda Di Fagagna, 2007). The physiological relevance of senescence has more recently been extended to include other key processes such as wound-healing (Demaria *et al.*, 2014) and embryonic development (Muñoz-Espín *et al.*, 2013). This is section will discuss the proposed physiological roles of senescence in turn.

1.1.9.1 Senescence and Ageing

As described in section 1.1.3, the classification of senescence is often hindered by a paucity of universally applicable markers. This is exacerbated *in vivo*, where the majority of cells are arrested, thus preventing characterisation of proliferative potential. Despite this, some *in vitro* markers may be observed in an *in vivo* setting, and have led to a clear association between senescence and ageing (Sharpless and Sherr, 2015). One widely applied method is

the identification of p16 positive cells, which has led to the detection of senescent cell accumulation in a variety of tissues from both mice and humans (Nielsen *et al.*, 1999; Krishnamurthy *et al.*, 2004; Ressler *et al.*, 2006). This observation lead researchers to investigate if there was a causal link between the accumulation of senescent cells with aging and the development of age-related pathologies (van Deursen, 2014). This connection was first investigated in a progeroid mouse model of premature ageing (BubR1), where investigators utilised a transgene, INK-ATTAC, which contained a fragment of the p16 promoter and was thus only transcribed in p16 positive (equated to senescent) cells. INK-ATTAC encodes a caspase-8 containing fusion protein that dimerises (and becomes active) upon treatment with a small molecule AP20187. Therefore, this model triggers apoptosis in p16 positive cells, thus facilitating their clearance. Through the INK-ATTAC model, investigators demonstrated attenuation of age-related pathologies including loss of adipose tissue and skeletal muscle as well as reduced cataracts of the eye (Baker *et al.*, 2011). Building on this work, the INK-ATTAC model was applied in naturally aged mice. In a seminal publication, Baker et al., (2016) demonstrated that clearance of p16 positive cells alleviated a range of age-related-pathologies and, strikingly, extended the median lifespan of experimental mice (Baker *et al.*, 2016). This provided compelling evidence that the accumulation of senescent cells with age contributes to the development of age-related pathologies. There is now a growing interest in the therapeutic clearance of senescent cells through pharmacological methods, “senolytics”, which is discussed in section 1.1.10.1.

1.1.9.2 Immune-Clearance of Senescent Cells

The accumulation of senescent cells has been demonstrated to contribute to age-related pathologies as described above (Baker *et al.*, 2016). However, the mechanisms through which this accumulation occurs are not entirely clear. It is conceivable that exposure to

stressful stimuli across an organism's lifespan could lead to a general increase in senescent cell numbers (van Deursen, 2014). Alternatively, impairment of mechanisms responsible for the clearance of senescent cells could also contribute to the observed accumulation with age. Age has been previously been associated with a decline of immune function, referred to as immunosenescence, which renders the elderly more susceptible to infectious diseases and less responsive to vaccination (Nikolich-Žugich, 2008; Dewan *et al.*, 2012; Boraschi and Italiani, 2014). This is believed to arise through compositional and functional alterations in immune cell sub-types, leading to a low level, chronic state of sterile inflammation known as "inflammageing" (Franceschi, 2007; Boraschi and Italiani, 2014). Interestingly, inflammageing has also been proposed to occur as a consequence of senescent cell accumulation, possibly through the SASP (Franceschi and Campisi, 2014).

The clearance of senescent cells through immune function was first demonstrated by Xue *et al.,* (2007), whereby p53 activation in hepatoblasts (liver progenitor cells), transplanted into mouse livers, led to the development of a senescence phenotype. These senescent cells were demonstrated to be cleared by innate immune cells (Xue *et al.*, 2007). Krizhanovsky et al., (2008) developed this concept further, through use of macrophage inflammatory protein-1β (MIP-1β, also known as CCL4) induced fibrosis of mouse livers. This lead to accumulation of senescent hepatic stellate cells (HSCs), which were demonstrated to contribute to the restriction of fibrotic progression. The gene expression profile of the senescent HSCs was shown to be upregulated for factors that enhance natural killer (NK) cell function, including the chemokine IL-8 and the adhesion molecule CD58. NK cells were also demonstrated to selectively clear senescent IMR90s induced by replicative, therapy-induced and oncogene-induced senescence *in vitro*. This was recapitulated *in vivo*, where use of an NK cell neutralising antibody led to an increase in senescent cell accumulation and stimulation of NK

activity reduced the number of senescent HSCs (Krizhanovsky *et al.*, 2008). Further exploring the interaction between senescent cells and the immune system, oncogenic NRas induced senescence was investigated in hepatocytes (Kang *et al.*, 2011). Immune cells were demonstrated to cluster around the senescent hepatocytes and the number of these senescent cells notably decreased from 12 days after NRas transduction. In transgenic mice with defective NK cell and macrophage responses, this reduction was not observed suggesting these cells are key mediators of the clearance of OIS cells *in vivo* (Kang *et al.*, 2011). Overall, these studies provide compelling evidence that senescent cells facilitate their own clearance through SASP signalling to immune cells. This integrated system of removal may represent a mechanism to prevent the deleterious effects of senescent cell accumulation observed in ageing, aligning closely to the antagonistic pleiotropy theory of ageing described above (Campisi and D'Adda Di Fagagna, 2007; van Deursen, 2014).

1.1.9.3 Wound Healing

Whilst Baker *et al.,* (2016) demonstrated that senescent cells contribute to the development of age-related pathologies, they also observed a beneficial effect of senescent cells to wound healing, as this was impaired following senescent cell clearance (Baker *et al.*, 2016). This corroborated a previous a report, which utilised another p16 dependent model of senescent cell clearance (p16-3MR), which is inducible upon treatment with ganciclovir. Demaria *et al.,* (2014) demonstrated transient accumulation of senescent cells in wounds, peaking 6 days after injury and returning to baseline by day 9. The clearance of senescent cells 24 hours after injury extended the time required for complete wound closure, and the final healed wound possessed increased levels of fibrosis characterised by increased collagen deposition. This was accompanied by alterations in MMP production (increased MMP-10 and -13; decreased MMP-2) and senescent cells induced via ionising radiation were demonstrated to

produce increased levels of collagen. Intriguingly, the SASP profile of senescent cells found in the wounds had an unusual composition, secreting very high levels of PDGF-A and VEGF, whilst not producing IL-6 or TGFβ. Interestingly, senescent cell clearance also depleted the number of myofibroblasts, an effect that could be rescued though PDGF-A treatment, along with normal wound closure kinetics. Overall, this study emphasised the nuances of SASP composition, implicating the development of a bespoke SASP to promote wound healing though stimulation of myofibroblast differentiation (Demaria *et al.*, 2014). This critical role in a homeostatic process emphasises that senescence contributes to more than pathological ageing and suggests that therapeutic strategies of senescence clearance might be associated with adverse effects.

1.1.9.4 Embryonic Development

The majority of research into senescence has focused on a response to some form of insult, be that replicative exhaustion, DNA damage or oncogenic stimulation. A less widely described process involves the contribution of senescence to embryonic development, which occurs through a programmed system of senescent cell accumulation and clearance (Munoz-Espin and Serrano, 2014). Senescence markers have been identified in embryos from mice, humans, chickens and quail, implicating senescence as a conserved feature across vertebrates during development (Nacher *et al.*, 2006; Muñoz-Espín *et al.*, 2013; Storer *et al.*, 2013). Of particular note is p21, without which morphological abnormalities occur during embryonic development. Importantly, developmental senescence does not appear to be associated with appearance of a DDR, emphasising the heterogeneous nature of senescence responses (Muñoz-Espín *et al.*, 2013).

1.1.10 Therapeutic Modulation of Senescence

1.1.10.1 Senolytics

The compelling evidence for a causal role of senescent cells within the development of age-related pathologies described above, has led to a rapidly increasing interest in the therapeutic modulation of senescence. Similar to the work of Baker et al., (2016), the selective clearance of senescent cells has become the focus of most therapeutic strategies, with the emergence of an array of "senolytic" agents (Kirkland *et al.*, 2017). The first description of senolytics was made by Zhu *et al.,* (2015), who identified the existence of pro-survival anti-apoptotic pathways in senescent cells, termed senescent-cell anti-apoptotic pathways (SCAPs), through use of DNA microarrays and siRNA inhibition (Zhu *et al.*, 2015; Kirkland *et al.*, 2017). A targeted drug screen of 46 candidate molecules identified the compounds Dasatinib (a tyrosine kinase inhibitor) and Quercetin (a PI3 kinase inhibitor) as the most promising senolytic candidates *in vitro*. Dasatinib appeared to be more effective in the selective clearance of senescent preadipocytes, whereas Quercetin displayed preferential action in HUVECs. A combination treatment with both compounds overcame this cell type specificity, leading to a potent clearance of both cell types. Importantly, this effect appeared to translate *in vivo* where the combination treatment reduced the number of senescent adipose cells in aged mice along with improved cardiovascular function and extended the lifespan of progeroid mice (Zhu *et al.*, 2015). More recently, Dasatinib and Quercetin were used to recover age-related physical decline of naturally aged mice and, strikingly, also caused an extension of lifespan (Xu *et al.*, 2018). These seminal publications sparked an enormous research effort to discover more compounds that could selectively clear senescent cells.

The third senolytic agent described was ABT263, more commonly referred to as Navitoclax, which was demonstrated to reduce the survival of senescent WI-38 fibroblasts induced by irradiation, replicative exhaustion and oncogenic-Ras expression (Chang *et al.*, 2016). This was further validated in additional human and mouse cells in order to demonstrate a less cell type specific response than that of Dasatinib and Quercetin. The authors also demonstrated that oral delivery of Navitoclax cleared senescent cells in irradiated and naturally aged mice, with associated rejuvenation (Chang *et al.*, 2016). This reported effect of Navitoclax was swiftly supported by a second publication, which was under review at the time of the first (Zhu *et al.*, 2016). Navitoclax promotes apoptosis by inhibiting BCL-2 and BCL-xL anti-apoptotic proteins, continuing the SCAP focused development of senolytics. A similar SCAP mediated senolytic action was demonstrated through use of a FOXO4-peptide, which facilitates a p53 dependent apoptosis response (Baar *et al.*, 2017). Subsequently, a range of other publications have found novel senolytics targeting SCAPs including the Quercetin analogue Fisetin (Zhu *et al.*, 2017) and the Navitoclax predecessor ABT-737 (Yosef *et al.*, 2016). More recently, a new class of senolytic agent have been described, the cardiac glycosides (Guerrero *et al.*, 2019; Triana-Martínez *et al.*, 2019). These agents disrupt the electrochemical stability of senescent cells though binding of sodium/potassium pumps, leading to depolarisation and apoptosis. The membrane potential of senescence cells is higher than that of proliferating cells, making them more susceptible senolysis through this mechanism (Guerrero *et al.*, 2019; Triana-Martínez *et al.*, 2019).

The rapid development of senolytics has already led to their clinical assessment. Senolytics are unlikely to represent a panacea against all possible age-related pathologies and are currently under clinical assessment for treatment of osteoarthritis (OA), idiopathic pulmonary fibrosis (IPF) and diabetic kidney fibrosis. Navitoclax, under the trade name

UBX0101, is currently in Phase II clinical trial (ClinicalTrials.gov Identifier: NCT04129944) to assess efficacy in the treatment of OA of the knee, having successfully navigated a Phase I tolerability trial (ClinicalTrials.gov Identifier: NCT03513016). This followed pre-clinical work in mice, which demonstrated that Navitoclax restricted the development of naturally occurring and traumatic OA (Jeon *et al.*, 2017). Senescent cells have also been identified as mediators of IPF in mice (Schafer *et al.*, 2017). Recently, a phase I clinical trial (ClinicalTrials.gov Identifier: NCT02874989) demonstrated Dasatinib and Quercetin were well tolerated in IPF patients and some physical function benefits were demonstrated (Justice *et al.*, 2019). Finally, Dasatinib and Quercetin have recently been demonstrated in a phase I clinical trial (ClinicalTrials.gov Identifier: NCT02848131) to reduce senescent cell numbers in humans. Intriguingly, the treatment also reduced circulating SASP factors, the suspected instigators of senescent cell driven age-related pathologies (Hickson *et al.*, 2019). Overall, whilst promising, clinical research into senolytics is in its infancy and there are significant hurdles that must be overcome before senolytics emerge as therapeutically available agents.

1.1.10.2 Therapy-induced senescence (TIS)

Therapy-induced senescence (TIS) describes the induction of a senescence response in cancer cells through use of pharmacological agents. The bypass of senescence is an essential step in the malignant transformation of cells, with most cancer cells possessing mutations in key senescence effectors such as p21 and p16 (Hanahan and Weinberg, 2011). However, cancer cells have been identified which retain p16 expression and are, incidentally, often associated with a poor clinical outcome (Hui *et al.*, 2000). Nevertheless, whilst cancer cells may bypass CDKI mediated cessation of proliferation, many retain the capacity to undergo senescence in response to chemotherapeutic agents, such as doxorubicin, suggesting that

the pathways which facilitate senescence induction may be repressed, as opposed to absent, within these cells (Ewald *et al.*, 2010). Therefore, there is clinical interest in the induction of senescence as a therapeutic approach within cancer. This has led to the development of palbociclib, a p16 mimetic which inhibits CDK4/6 and which has shown clinical utility in the treatment of a subset of advanced breast cancer (Finn *et al.*, 2009, 2016; Pernas *et al.*, 2018). However, there are some concerns with such therapeutic approaches. These principally stem from the demonstration that senescent cells are deleterious in ageing (section 1.1.9.1) and that the SASP has the capacity to be pro-tumorigenic (section 1.1.9). Recently, an interesting novel use of senolytics in combination with senescence inducing agents in the treatment of cancer has been proposed. This "one-two punch" based approach utilises induction of senescence in order to render cancer cells vulnerable to senolytic clearance. This has recently been utilised in the clearance of liver cancer cells (Wang *et al.*, 2019). Pharmacological inhibition of CDC7, a kinase involved in DNA replication, was demonstrated to induce senescence in liver cancer but not proliferating cells. This was then combined with an mTOR inhibitor, AZD8055, which led to apoptosis of the induced senescent cells *in vitro*. This was recapitulated *in vivo* where CDC7 inhibition in combination with AZD8055 restricted tumour growth to a greater extent than sorafenib, a current clinically used therapeutic (Wang *et al.*, 2019). Overall, this novel approach utilises the potent anti-tumorigenic action of senescence induction, without any potentially deleterious effects of senescent cell accumulation.

1.1.10.3 Other Therapeutic Strategies

Senolysis refers to the selective clearance of senescent cells. However, as described in section 1.1.9, senescence has been demonstrated to have beneficial effects, most notably in wound healing (Demaria *et al.*, 2014). There is some concern that depletion of senescent cells may also cause dysfunction of tissue architecture, as the regenerative tissue capacity in geriatrics may be insufficient to restore these lost cells (Janzen *et al.*, 2006). An alternative

to senolytic development is the search for “senomorphic” or “senostatic” agents, which modulate the senescence phenotype, in particular the SASP, whilst retaining the cell itself. As NF-κB is a significant driver of the SASP, its inhibition might be predicted to diminish the deleterious effects of the senescent cells. This was recently demonstrated through inhibition of the upstream kinase IκB kinase (IKK), which lead to restriction of age-related pathologies in progeroid mice (Tilstra *et al.*, 2012). Similarly, inhibition of Janus kinases (JAK), a key component of canonical cytokine signalling pathways, attenuates the SASP of both preadipocytes and HUVECs. JAK inhibition also improved physical function in aged mice, not unlike that achieved with senolytic agents (Xu *et al.*, 2015, 2018). However, in general, the field has committed more significant research effort to the development of senolytics. Nevertheless, it is prudent that an alternative strategy is also being actively pursued, in order to develop a more diverse set of therapeutic strategies.

1.2 Extracellular Vesicles (EVs)

1.2.1 Classifications of Extracellular Vesicles

Extracellular vesicles (EVs) is an umbrella term used to encompass the heterogeneous range of lipid bound particles secreted by cells (Witwer and Théry, 2019). EVs represent a diverse set of mediators, which are defined by both their size and route of biogenesis (Colombo, Raposo and Thery, 2014) (Figure 1.7). The term EV is often qualified to reflect a more context specific usage, such as inclusion of an indicator to the relative size (e.g. small EV) (Kowal *et al.*, 2016). Historically, the nomenclature surrounding EVs has lacked standardisation and inconsistent usage across the literature has emerged (Gould and Raposo, 2013). Whilst EVs had been observed through electron microscopy previously (Aaronson *et al.*, 1971), Trams *et al*., (1981) were the first to use the popular term "exosomes" to described vesicles "derived from specific domains of the plasma membrane" (Trams *et al.*, 1981). Inconsistent usage of the term exosomes was then applied to vesicles derived from multivesicular bodies (MVBs) (Johnstone *et al.*, 1987). These vesicles had been discovered earlier by two groups investigating the transferrin receptor in reticulocytes (Harding, Heuser and Stahl, 1983; Pan and Johnstone, 1983). Through immuno-gold labelling, trafficking of the receptor to multivesicular endosomes (equivalent to MVBs) was identified, and more specifically, tracked to the intraluminal vesicles (ILVs) which give MVBs their name. These vesicles were observed to be released by exocytosis through MVB fusion with the plasma membrane, hence their subsequent designation as exosomes (Johnstone *et al.*, 1987). However, use of the term exosome did not remain exclusive to the description of endosome-derived vesicles and was often used to describe the second major subclass of EVs – microvesicles (MVs). These vesicles are shed directly from the plasma membrane and have been referred to previously as ectosomes (Witwer and Théry, 2019). A confounding factor that had added to this confusion is the paucity of accepted biomarkers of these vesicular subtypes. This has resulted in vesicles often being defined predominantly by size, with the vast majority of

experimental methods for their isolation also relying on size-separation (Gardiner *et al.*, 2016). Whilst exosomes have typically been regarded as smaller, ranging from 30-150nm in diameter, the broad size range of MVs, 50-1,000nm, makes this an imperfect solution, with experimental procedures considered to produce a varied set of vesicles. In order to achieve some level of standardisation, as well as to reflect the current uncertainties surrounding both biomarkers and experimental procedures, the International Society of Extracellular Vesicles (ISEV) has attempted to define a consensus position within the field with regard to nomenclature (Lotvall *et al.*, 2014; Théry *et al.*, 2018). As such, the broad term extracellular vesicle (EV) is generally preferred, unless specific determination of biogenesis can be demonstrated (Witwer and Théry, 2019). Therefore, EV is used throughout this thesis, with indications of potential subclasses noted where appropriate

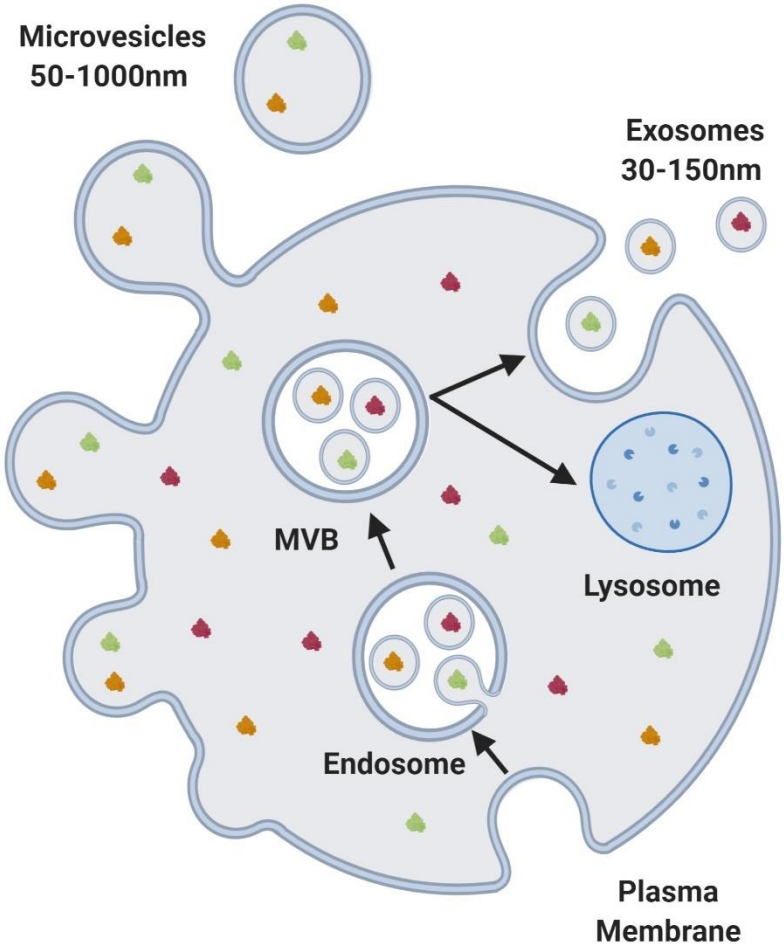

Figure 1.7: Classification of Microvesicles and Exosomes

Extracellular vesicles (EVs) is a term to describe small lipid bilayer bound particles secreted by cells. There has been inconsistent usage of nomenclature within the field, but EVs are widely considered to predominantly comprise two main subclasses. These may be distinguished by both their size and biogenesis. Microvesicles (MVs) are shed directly from the plasma membrane and have a broad size range of 50-1,000nm. In contrast, exosomes are small vesicles (30-150nm) and have an endosomal origin. They form as intraluminal vesicles (ILVs) within multivesicular bodies (MVBs). These may be trafficked to lysosomes for degradation or to the plasma membrane where they are released as exosomes. Adapted from (Colombo, Raposo and Thery, 2014).

1.2.2 Extracellular Vesicle Biogenesis

As described above, one of the defining characteristics of EV subtypes is variation between the routes to biogenesis. Two main varieties of EV have been described within the literature, exosomes and microvesicles, although considerable heterogeneity is likely to exist within these subsets in terms of both composition and function (Kowal *et al.*, 2016; van Niel, D'Angelo and Raposo, 2018). In the broadest sense, these two categories are divided by the endosomal origin of exosomes, whilst MVs are directly shed from the plasma membrane (Colombo, Raposo and Thery, 2014).

1.2.2.1 MVB and ILV Biogenesis

The generation of MVBs is fundamental to the process of exosomal biogenesis (Figure 1.8). This first requires endosome formation, which occurs via inward budding of the plasma membrane (Klumperman and Raposo, 2014). Subsequent budding of the endosomal membrane leads to formation of ILVs contained within larger a MVB, with the ILV membrane orientation matching that of the plasma membrane (Stoorvogel *et al.*, 1991; Colombo, Raposo and Thery, 2014). The formation of MVBs is mediated by the endosomal sorting complex required for transport (ESCRT), which is a group of ~30 proteins that act in sequence to recruit other ESCRT members or accessory proteins (Hurley, 2008; Colombo, Raposo and Thery, 2014). ESCRT-0 has been demonstrated to facilitate the recruitment of ubiquitinated membrane cargos, which allows clustering in the regions of the endosomal membrane fated for ILV formation (Wollert and Hurley, 2010). A component of ESCRT-0, hepatocyte growth factor regulated tyrosine kinase substrate (HRS), then recruits the ESCRT-I component TSG101, which is subsequently responsible for the recruitment of the ESCRT-II protein Apoptosis-Linked Gene 2-Interacting Protein X (ALIX; Gene Name: PDCD6IP), which in turn leads to recruitment of ESCRT-III (Colombo, Raposo and Thery, 2014). ESCRT-I and ESCRT-II

also possess ubiquitin binding domains, which maintains the recruited cargos within regions of the endosomal membrane, facilitating sorting into ILVs (Baietti *et al.*, 2012). Both ESCRT-I and ESCRT-II have been demonstrated to lead to curvature and budding of the endosomal membrane, which encloses cytoplasmic cargo within what will subsequently become the ILV lumen (Wollert and Hurley, 2010). ESCRT-III components are responsible for the final scission event that disengages the bud from the endosomal membrane, by acting to draw the membrane across the "neck" of the bud, thus leading to ILV formation (Wollert *et al.*, 2009; Wollert and Hurley, 2010). Additionally, it has been demonstrated that the presence of the proteoglycan syndecan within the endosomal membrane may lead to ILV formation through complexing with ALIX via the adaptor protein syntenin. ALIX then promotes recruitment of vacuolar protein sorting-associated protein 32 (VPS32) a component of ESCRT-III, which leads to ILV generation (Baietti *et al.*, 2012). However, whilst the ESCRT-dependent pathway is the most clearly described process of ILV formation, evidence suggests that it may also occur in an ESCRT-independent manner (van Niel, D'Angelo and Raposo, 2018).

The first indication of a ESCRT-independent route for ILV generation came through demonstration that knockdown of the ESCRT components HRS (ESCRT-0), TSG101 (ESCRT-I), VPS22 (ESCRT-II) and VPS24 (ECRT-III) via siRNA, was insufficient to prevent ILV formation within MVBs (Stuffers *et al.*, 2009). This supported a previous finding by Trajkovic *et al*., (2008), who demonstrated that knockdown of ESCRT components including ALIX and TSG101 did not lead to a complete impairment of exosome release. Instead, the investigators identified that exosomes were enriched for several types of lipid, including cholesterol, sphingolipids and, crucially, ceramide. Ceramide is generated from sphingomyelin via the enzymatic activity of sphingomyelinases. Use of the neutral sphingomyelinase (nSMase) inhibitor GW4869 led to a reduction in exosome release, corroborated via use of two

additional nSMase inhibitors. The authors speculated that the cone-like shape of ceramide may contribute to curvature of endosomal membranes thus facilitating the formation of ILVs (Trajkovic *et al.*, 2008). The work of Trajkovic *et al.*, (2008) was carried out in oligodendroglial cells but has subsequently been contradicted in a MNT-1 melanoma cell line, where use of GW4869 did not inhibit ILV generation. These investigators identified the tetraspanin CD63 as a crucial mediator of ILV formation, as siRNA inhibition led to a dramatic reduction in the number of ILVs observed by electron microscopy (van Niel *et al.*, 2011). Other tetraspanins, including CD9, have also been implicated in exosome biogenesis, with particular regard to sorting of specific cargos (Chairoungdua *et al.*, 2010). It has been proposed that the structure of the tetraspanins may facilitate invagination of the endosomal membrane following their clustering within micro-domains (van Niel, D'Angelo and Raposo, 2018). Therefore, whilst the pathways that underpin the formation of exosomes have not been fully elucidated, there appears to be both an ESCRT-dependent and independent routes to ILV generation.

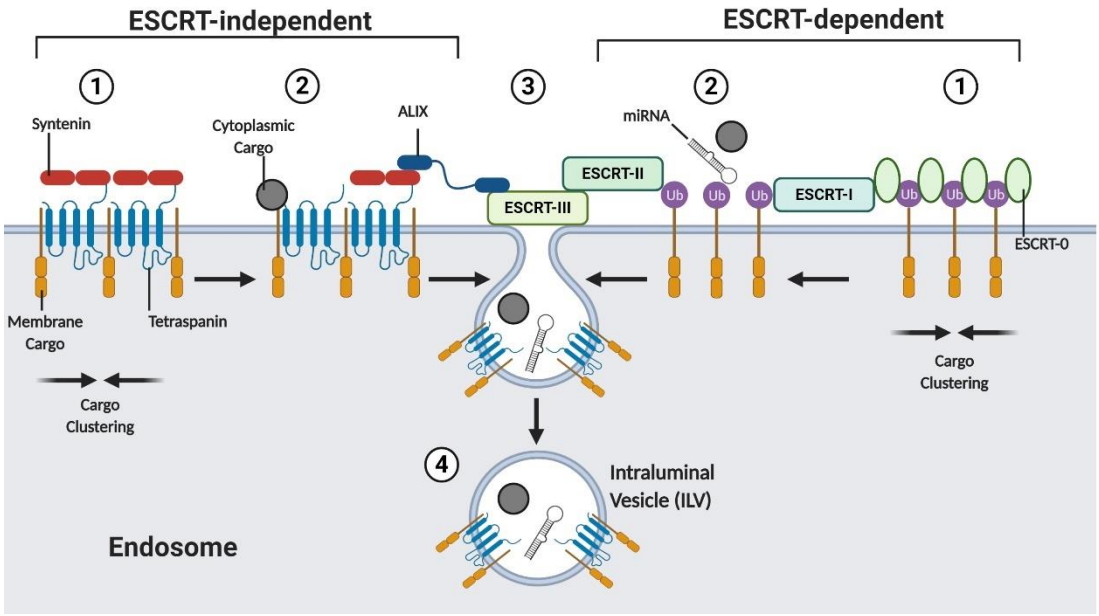

Figure 1.8: Mechanisms of ILV Biogenesis

The formation of intraluminal vesicles (ILVs) is critical to the biogenesis of exosomes. This process occurs through inward budding of endosomal membranes leading to subsequent designation as multivesicular bodies (MVBs). The process of ILV formation has been demonstrated to occur via two main pathways. The first, the ESCRT dependent pathway, sees clustering of ubiquitinated membrane proteins on the endosomal surface via the subunit ESCRT-0. A series of subsequent ESCRT subunits then facilitate membrane curvature and scission, leading to formation of an ILV. This process has also been demonstrated to occur via an ESCRT independent route, with tetraspanins clustering within microdomains on the endosomal membrane facilitating ILV generation. The ESCRT-II component ALIX may has also been demonstrated to facilitate the generation of ILVs through binding to syntenin adaptor proteins that are in turn bound to syndecan membrane domains. The accumulation of luminal cargos such as miRNA and cytoplasmic proteins is less well described and may occur due to proximity to the endosome or through active trafficking. Adapted from (van Niel, D'Angelo and Raposo, 2018).

1.2.2.2 ILV Trafficking and Release

Following their generation within MVBs, ILVs face one of two main fates. The first is trafficking to the plasma membrane, where they may be released by exocytosis as exosomes. The second is to undergo degradation following fusion of the MVB with lysosomes. Indeed, exosome secretion increases in cells treated with the lysosome inhibitor Bafilomycin A1 (Eitan *et al.*, 2016; Villarroya-Beltri *et al.*, 2016). The processes that determine the fate of MVBs have not been well described, however, the lipid composition of the MVB membrane may contribute, as enrichment of cholesterol leads to a bias towards exosome secretion (Möbius *et al.*, 2003). Furthermore, those MVBs that form through the syndecan–syntenin–ALIX axis appear to exclusively release ILVs as exosomes (Baietti *et al.*, 2012; van Niel, D'Angelo and Raposo, 2018). This is mediated by RAB7, as inhibition via siRNA led to a reduction in exosome secretion (Baietti *et al.*, 2012). RAB7 has previously been demonstrated to play a role in the development of endosomal compartments and is a member of the wider RAB superfamily of small GTPases, which are crucial effectors of ILV trafficking and release (Rink *et al.*, 2005; Colombo, Raposo and Thery, 2014). For instance, the RAB27 isoforms A and B were identified as mediators of exosome production through an shRNA screen in HeLa cells, where they were demonstrated to facilitate MVB fusion with the plasma membrane (Ostrowski *et al.*, 2010). Similarly, RAB35 was shown to act in a similar manner to RAB27 in mouse oligodendroglial cells, promoting the secretion of exosomes by facilitating plasma membrane fusion (Hsu *et al.*, 2010). Furthermore, RAB11 has also been demonstrated to contribute to exosome production from K562 erythroleukemia cells (Savina, Vidal and Colombo, 2002; Colombo, Raposo and Thery, 2014). Overall, the intracellular trafficking of ILVs, as well as their subsequent release as exosomes, appears to have a significant RAB GTPase mediated component (van Niel, D'Angelo and Raposo, 2018).

1.2.2.3 Microvesicle Biogenesis

The processes that lead to MV generation have been less clearly described than those of exosomes. The most obvious distinction is that MVs are shed directly from the plasma membrane, contrasting the endosomal origin of exosomes. Changes in lipid organisation within the plasma membrane have been demonstrated to promote curvature thus facilitating MV formation (Piccin, Murphy and Smith, 2007; van Niel, D'Angelo and Raposo, 2018). Furthermore, RHO small GTPases and RHO-associated protein kinase (ROCK) have been implicated as crucial effectors of MV generation via regulation of actin in cancer cells. MV production requires extension of actin filaments and formation of a ring-like structure, in order to be released from the plasma membrane. This is impaired by the regulatory protein cofilin, which usually facilitates the disassembly of actin filaments. Lim kinase (LIMK) activation by ROCK, facilitates phosphorylation and inactivation of cofilin, thus leading to actin filament elongation and MV production (Li *et al.*, 2012). Interestingly, despite being widely considered markers of exosomal biogenesis, ESCRT complex members have also been demonstrated to contribute to MV formation. TSG101 and the ESCRT recycling ATPase VPS4 were demonstrated to facilitate MV generation in HEK-293T cells (Nabhan *et al.*, 2012). Furthermore, ESCRT-0 and ESCRT-I depletion in *C. elegans* embryos was demonstrated to inhibit MV release from the plasma membrane (Wehman *et al.*, 2011). This common contribution of ESCRT proteins to the biogenesis of both MVs and exosomes prevents their confident usage as unique markers of exosome biogenesis, contributing to the widespread difficulty in identifying subclasses of extracellular vesicles (Hurley, 2015; van Niel, D'Angelo and Raposo, 2018).

1.2.3 Extracellular Vesicle Cargo and Composition

By virtue of their origin, EVs are compositionally dependent upon their producing cell. Therefore, all cargos and constituents are derived directly from the parental cell. As such, EVs have been described as “miniature versions of the cell”, representing the cellular composition at the precise point of biogenesis (Saleem and Abdel-Mageed, 2015). However, this is not entirely accurate, as EVs are preferentially enriched in a range of cargos, and also possess a heterogeneous composition between subtypes (Willms *et al.*, 2016). Of particular note, is an identified enrichment in a range of factors involved in EV biogenesis, notably the ESCRT components ALIX and TSG101, as well as the tetraspanins CD9, CD63 and CD81 (Théry *et al.*, 2001). These have been observed widely and are considered general EV markers (Lotvall *et al.*, 2014). However, due to heterogeneity across EV subtypes, no single marker is considered truly universal, as no marker has been described as common within all EVs (Kowal *et al.*, 2016). This underpins the use of more general terminology to describe bulk populations of vesicles, as specific subtypes cannot currently be confidently identified (Witwer and Théry, 2019).

Because EVs derive both membrane and luminal cargos directly from producing cells, their potential compositional components are as varied as that of the cells themselves, as well as all the specific contexts those cells may be in. In general, EVs have been demonstrated to contain a range of protein and nucleic acid cargoes, as well as a variety of compositional lipid components (Colombo, Raposo and Thery, 2014). Lipids are a fundamental constituent of EVs, given that they are considered lipid bilayer bound particles (Witwer and Théry, 2019). Work by Llorente *et al.,* (2013), demonstrated that PC-3 prostate cancer cell derived EVs, comprised a distinct lipid profile compared to their producing cells. Specifically, EVs were associated with enrichment of cholesterol, glycosphingolipids, phosphatidylserine and

sphingomyelin (Llorente *et al.*, 2013). It is not clear whether these changes are specific to PC-3 cell derived EVs or represent a more widely associated EV profile. Lipids have, in general, garnered significantly less research attention than the other predominant EV cargos – proteins and nucleic acids (Colombo, Raposo and Thery, 2014).

Many EV protein constituents are involved in surface interactions with recipient cells. These are considered in more detail in section 1.2.4. In fact, the proteomic composition of EVs has been characterised in such a variety of circumstances, that several online compendiums (such as www.ExoCarta.org) exist to catalogue the data. To date, approximately 25% of proteins have been identified in human EVs in some context (Mathivanan *et al.*, 2012; Keerthikumar *et al.*, 2016). Therefore, it is prudent to assess the protein content of EVs within specific circumstances, such as within senescence and ageing (described in detail – section 1.3). Generally, profiling of the proteomic content of EVs is performed through mass spectrometry (MS), due to the high level of sensitivity, low required sample volume and extensive data sets produced (Bandu, Oh and Kim, 2019). MS has proved a critical tool within EV research and was utilised in the detection of the majority of proteins now considered canonical EV "markers" (Théry *et al.*, 2001). However, its utility within EV research is hindered by the inherent limitations of EV isolation techniques, many of which are subject to non-vesicular protein contamination (section 1.2.5). Furthermore, the huge variety in producing cells, as well as subtypes of EV, has led to enormous diversity in the proteomic characterisation of EVs (Willms *et al.*, 2016).

Nucleic acids have received widespread research attention since they were first identified as EV cargos. This was demonstrated by Valadi et al., (2008), who showed that messenger RNA (mRNA) and miRNA could be transferred between murine mast cells. Importantly, these

nucleic acids were demonstrated to have functional potential, as the delivered mRNA possessed the capacity to facilitate translation in recipient cells (Valadi *et al.*, 2007). This was built upon by Pegtel *et al.*, (2010), who further demonstrated that miRNAs from B-cell derived EVs could regulate protein expression in treated dendritic cells (Pegtel *et al.*, 2010). These studies have prompted significant research interest, as EV mediated transfer of nucleic acids represents a form of cellular communication that is distinct from the wider soluble secretome. However, in order to fully appreciate these differences, it is important to understand the mechanisms through which EVs may engage recipient cells.

1.2.4 Extracellular Vesicle Uptake and Signalling

Following their release, EVs may interact with recipient cells through a number of mechanisms (Figure 1.9). These include endocytosis, macropinocytosis, phagocytosis, clathrin/caveolin mediated endocytosis, direct membrane fusion and receptor/ligand binding (Figure 1.9) (Mulcahy, Pink and Carter, 2014; van Niel, D'Angelo and Raposo, 2018). There is some distinction to be made between the binding of EVs with a recipient cell through a combination of receptors and ligands, compared to the internalisation of the entire vesicle itself. However, the two concepts intersect, as EV uptake is facilitated by binding to specific surface receptors (van Niel, D'Angelo and Raposo, 2018). This has been demonstrated via the loss of EV uptake following proteinase K treatment of ovarian cancer cells (Escrevente *et al.*, 2011). Such mechanisms may allow a more specific route to signalling, than could be achieved through general uptake systems. This is likely facilitated by heterogeneity in EV and cell membrane compositions (Mulcahy, Pink and Carter, 2014). Indeed, integrins on the surface of EVs have been demonstrated to facilitate uptake through interaction with adhesion molecules on the surface of dendritic cells (Morelli *et al.*, 2004; van Niel, D'Angelo and Raposo, 2018). Furthermore, different cells uptake EVs with different levels of efficiency,

such as a demonstrated reduction in T-cell uptake compared to peritoneal exudate cells (Zech *et al.*, 2012; Mulcahy, Pink and Carter, 2014). The actual mechanisms through which cells internalise EVs are broadly covered by the term "endocytosis", although greater specificity has been widely demonstrated (Figure 1.9) (Doherty and McMahon, 2009; Mulcahy, Pink and Carter, 2014). Vesicles may also directly fuse with the plasma membrane, leading to cytoplasmic delivery of luminal cargos (Parolini *et al.*, 2009). This represents a potential route through which vesicular payloads may be delivered to a target cell. Alternatively, following endocytosis, "back-fusion" of the EV with the endosomal membrane could facilitate a similar cytoplasmic delivery (van Niel, D'Angelo and Raposo, 2018). The engagement of such mechanisms currently underpin our understanding as to the routes through which functional delivery of luminal EV cargos, such as nucleic acids, occurs (Valadi *et al.*, 2007; Mulcahy, Pink and Carter, 2014).

Contrasting vesicular uptake, engagement of EVs with receptors on the surface of recipient cells has been demonstrated to activate intracellular signalling cascades in a variety of contexts (van Niel, D'Angelo and Raposo, 2018). This was first demonstrated through the observation of augmented T-cell IL-2 secretion following antigen presentation by MHC-II molecules on the surface of B-lymphocyte derived EVs (Raposo *et al.*, 1996). Furthermore, Cossetti *et al*., (2014) demonstrated that interferon gamma (IFN-γ) bound to its receptor, interferon gamma receptor 1 (Ifngr1), on the surface of EVs, could engage STAT1 signalling in recipient NIH 3T3 fibroblasts. Investigators noted that a greater response was elicited in cells treated with EVs compared to soluble IFN-γ at a 100 times greater concentration than that measured in the EVs by ELISA. This suggests that EVs may augment the activity of soluble mediators, possibly by conferring additional stability than the soluble form (Cossetti *et al.*, 2014).This was supported by Webber *et al.,* (2015), who demonstrated that EV-associated

TGFβ1 promoted the differentiation of lung fibroblasts into myofibroblasts, characterised by expression of alpha smooth muscle actin (αSMA). Whilst this also occurred in response to soluble TGFβ1, the EV-associated form of the cytokine produced an altered secretory profile, with increased expression of several growth factors (uPA and HGF) and downregulation of others (PDGF-AA and IGFBP-3). Furthermore, increased proliferation of HUVECs was demonstrated through treatment with conditioned media (CM) from the EV treated fibroblasts, compared to media derived from cells treated with a concentration-matched level of soluble TGFβ1. Importantly, the fibroblast differentiation (and derived CM effect) could be attenuated by TGFβ1 receptor inhibition, through use of the small molecule SB431542 (Webber *et al.*, 2015). Together, these studies demonstrate that activation of intracellular signalling pathways can occur in response to EV engagement with cell surface receptors. Clearly, these responses will be highly context specific, relying on the composition of both producing and recipient cell, as well as any heterogeneity within EV subtypes. However, through both uptake mechanisms and receptor signalling, EVs have been demonstrated to be functionally relevant contributors to cellular communication (Mulcahy, Pink and Carter, 2014; van Niel, D'Angelo and Raposo, 2018).

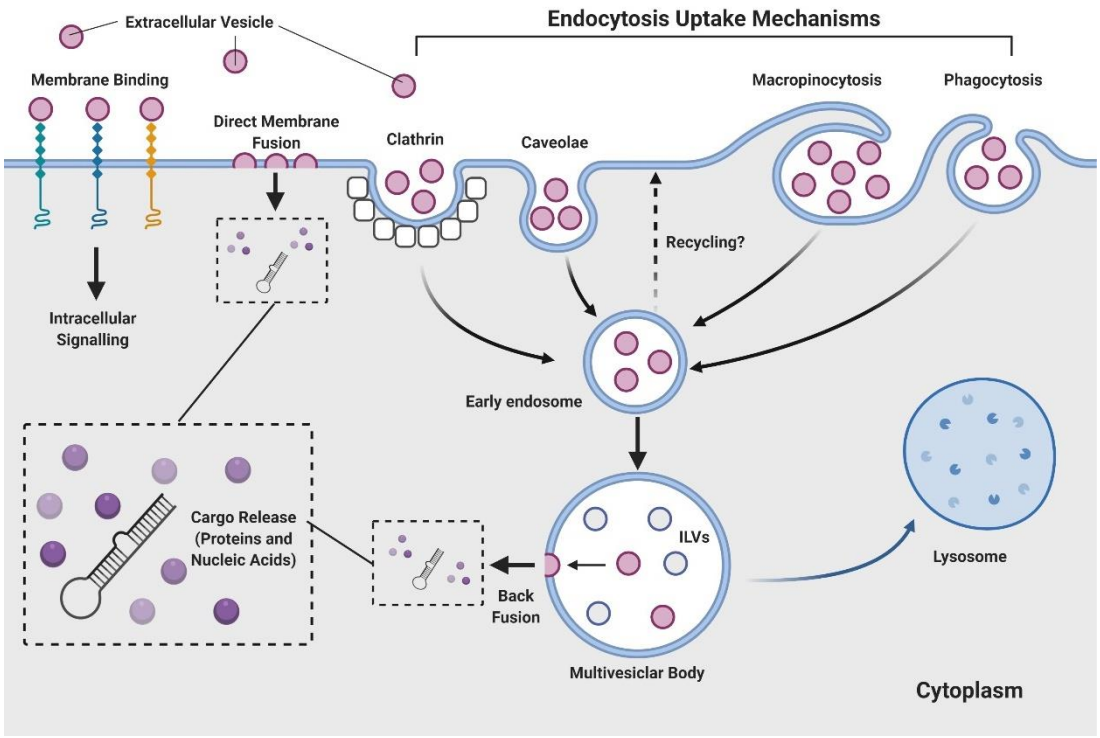

Figure 1.9: Mechanisms of Extracellular Vesicle Signalling

Extracellular vesicles (EVs) may engage with recipient cells through interactions with the cell surface or internalisation of the vesicle itself. Receptors and ligands on the surface of EVs can interact with corresponding counterparts of the cell surface and trigger intracellular signalling cascades. Furthermore, EVs may fuse with the plasma membrane, leading to direct cytoplasmic delivery of luminal cargo. Alternatively, EVs may be taken up through a range of mechanisms broadly falling under the term endocytosis. These may be mediated though formation of clathrin pits or caveolae on the cell surface, or through more general uptake mechanisms such as macropinocytosis and phagocytosis. Once internalised within endosomes, EVs may "back-fuse" with the endosomal membrane leading to cytoplasmic delivery of luminal cargo. Conversely, the endosome may be fated for lysosomal degradation, leading to breakdown of the internalised EVs. Adapted from (van Niel, D'Angelo and Raposo, 2018).

1.2.5 Influence of the 3D Environment on EV Production and Function

The vast majority of research investigating EVs has been performed in two-dimensional (2D) cell culture models. This is perhaps unsurprising, as these systems are the fundamental backbone of biomedical research and are generally considered the "standard" for *in vitro* investigations (Tibbitt and Anseth, 2009; Thippabhotla, Zhong and He, 2019). However, it is now widely appreciated that these 2D systems fail to fully represent the three dimensional (3D) conditions in which cells are found *in vivo*, leading to inconsistencies between physiological conditions and the experimental systems that aim to model them (Tibbitt and Anseth, 2009). In particular, cells in 2D lack the complex interactions with the surrounding extracellular matrix (ECM) that are found *in vivo*, which have been demonstrated to alter fundamental cellular processes including morphology, proliferation and differentiation (Baker and Chen, 2012). Recently, this has been extended to include the rate of EV production, with several investigations identifying an increase in EV production from cells cultured using 3D cell culture models (Rocha et al., 2019; Thippabhotla, Zhong and He, 2019). Furthermore, both the protein and RNA cargo of EVs has been demonstrated to alter with 3D cell culture, suggesting that 2D systems may provide inaccurate representation of EV composition *in vivo* (Rocha et al., 2019). This provides an important caveat to the work presented in this thesis, as only 2D cell culture was utilised and thus may be restricted by the inherent limitations associated with this form of cell culture. In the context of senescence, it would represent interesting future work to investigate the changes in EV production and function in 3D, particularly given the potential for ECM remodelling afforded by components of the SASP, such as matrix metalloproteinases (MMPs) (Ghosh et al., 2020). However, this work aims to explore the biological fundamentals of EVs within senescence by utilising a more conventional 2D cell culture system.

1.2.6 Methods of Extracellular Vesicle Isolation

As discussed above, significant heterogeneity exists between subtypes of EVs. Furthermore, no marker can be considered exclusively vesicular, as all cargos are derived from parental cells (van Niel, D'Angelo and Raposo, 2018). This makes both confident classification of EV subtypes and distinction from cellular material difficult, hence the use of generic, all-encompassing terminology (Witwer and Théry, 2019). Current understanding of EVs broadly separates subclasses into plasma membrane shed MVs and endosome derived exosomes (Colombo, Raposo and Thery, 2014). One commonly reported distinction between these groups is a disparity in size profile, with exosomes generally considered smaller. However, the extensive range of possible MV sizes, many of which overlap those of exosomes, makes this a flawed means of distinction (Lotvall *et al.*, 2014). Indeed, it has been proposed that EVs should be classified according to their size (e.g. small, medium and large), without any attempt to describe their route of biogenesis, as this cannot confidently be attributed to bulk isolates (Kowal *et al.*, 2016). This proposal stems from the fact that the majority of methods for the isolation of EVs are based upon the separation of particles according to size (Gardiner *et al.*, 2016). However, within these size-based classifications, enrichment will occur for particular groups of EVs. For example, a population of small EVs may be described as enriched for exosomes, whilst a population of large EVs may be enriched for MVs. This concept of enrichment as opposed to isolation is helpful, particularly when combined with appropriately cautious nomenclature, as it allows the nuances of EV heterogeneity to be accurately represented. It is important to note that any employed isolation technique should be tailored to the experimental questions and downstream applications. Equally, all techniques will have some level of bias towards a particular population of EVs and results observed are unlikely to be universally applicable to all other settings. With these caveats in mind, this section will describe the methods that have been applied for the isolation of EVs.

1.2.6.1 Differential Ultracentrifugation (dUC)

Application of a series of increasingly fast centrifugation steps, the final of these being an ultracentrifugation step, is comfortably the most widely applied method for the isolation of EVs (Gardiner *et al.*, 2016). The general principle behind this technique is that larger particles will sediment at slower speeds, allowing them to be removed in the early stages, whilst smaller particles will be pelleted in the final steps (Figure 1.10) (Livshits *et al.*, 2015). Within the field, the number, speed and duration of centrifugation steps employed to isolate EVs have ranged widely. Furthermore, variation exists between different centrifugation rotors, particularly in the clearance factor (K-factor), which is a measure of the efficiency with which the rotor pellets particles at its maximum speed (this may be adjusted for any given revolutions per minute (RPM). Additionally, each individual particle within a sample has a specific sedimentation coefficient, which dictates its movement within a liquid based upon the physical characteristics of both particle and medium. Through a combination of both K-factor and sedimentation co-efficient, a particular particle will pellet from a given medium within a specific time using a specific rotor (Cvjetkovic *et al.*, 2014). This is overviewed in Figure 1.11. These variables present a problem, as direct comparison between protocols requires detailed information about rotor specifications, which have not been consistently reported within the literature. Therefore, comprehensive methodological reporting is now a minimal experimental requirement, as determined by ISEV (Lotvall *et al.*, 2014). As a general principle, at least three steps are usually employed to pellet vesicles according to size, largely based on a protocol described by Théry *et al.,* (2006). A step of approximately 2000 *x g* is used to remove large MVs (such as apoptotic bodies) as well as any other cellular debris. A second 10,000 *x g* step is employed to pellet MVs and a final 100,000 *x g* step used to pellet exosomes (Théry *et al.*, 2006). As described above, overlap between the sizes of these vesicles makes each of these steps an enrichment for the intended subtype rather than a true isolation, with use of the terms large, medium and small EVs more appropriately

describing the composition of the final pellets (Kowal *et al.*, 2016). Through dUC, EVs have been successfully obtained from a wide range of biological fluids and cell culture supernatants (Gardiner *et al.*, 2016).

Despite its widespread popularity, dUC has several drawbacks as a method of EV isolation. The first of these is the physical disruption of the vesicles due to the high forces involved with ultracentrifugation, which hinders yield and can lead to a broad range of particle sizes (Lobb *et al.*, 2015; Taylor and Shah, 2015). It is also a technique not suitable for clinical application, due to a high level of user variability and complications resulting from variable viscosity of patient samples (e.g. plasma) (Lamparski *et al.*, 2002; Lobb *et al.*, 2015). However, perhaps the most significant drawback to dUC is its relative lack of purity. One proposed method of purity assessment is to observe the ratio of particles and protein within an EV sample. By this measure, dUC performs poorly compared to methods such as sucrose gradient separation (Webber and Clayton, 2013). This effect may be driven by the co-isolation of proteins alongside EVs during dUC and may be a more significant problem depending on both the starting material (e.g. cell culture supernatant vs patient plasma) or intended downstream applications (Van Deun *et al.*, 2014). Recently it has been comprehensively demonstrated by Foers *et al.,* (2018) that dUC EV preparations are associated with considerable soluble protein contamination. Electron microscopy of EVs isolated from the synovial fluid (SF) or rheumatoid arthritis (RA) patients, demonstrated significant isolation of non-vesicular material by dUC. Immunoblotting demonstrated that, whilst EV markers were enriched, presence of contaminating serum albumin, apolipoprotein A-I and the extracellular matrix (ECM) component fibronectin were also identified. Furthermore, application of size-exclusion chromatography (SEC) largely avoided these centrifugation-related issues (Foers *et al.*, 2018). Therefore, whilst a popular technique that

has been demonstrated to successfully isolate EVs from starting material, dUC is associated with significant limitations with regard to the purity of the final EV product, in particular due to co-isolation of non-vesicular proteins.

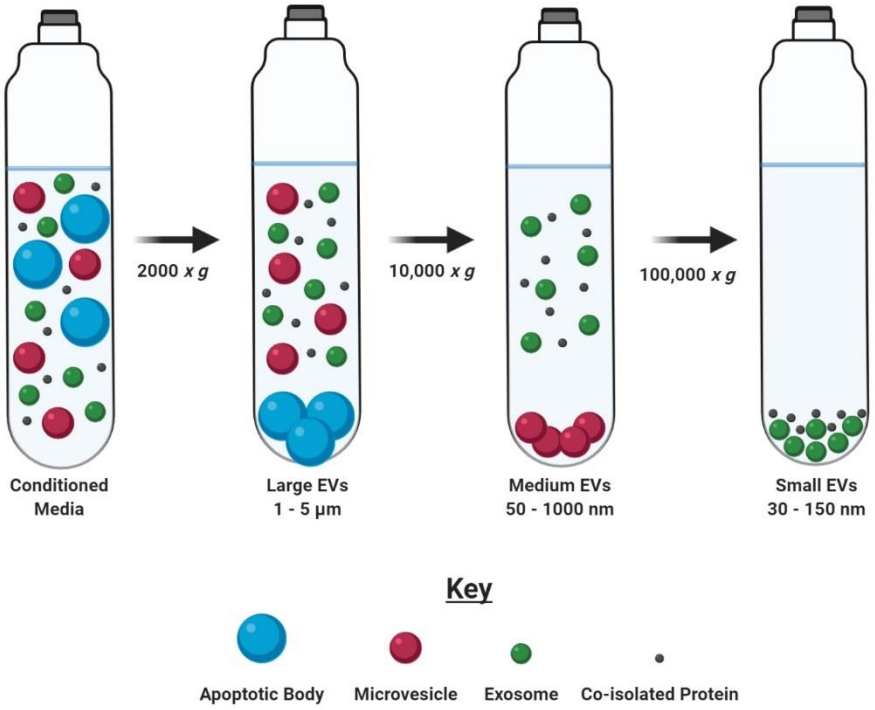

Figure 1.10: Principles of Differential Centrifugation

Extracellular vesicles (EVs) may be isolated from a starting medium by subjecting it centrifugation spins of increasingly faster speeds (differential ultracentrifugation, dUC). This separates vesicles into pellets based upon their size, allowing broad separation between large, medium and small EVs including apoptotic bodies, microvesicles and exosomes. However, this process has also been demonstrated to co-isolate additional protein and other contaminants.

(1) $$K = \frac{2.53 \times 10^5 * \ln(r_{max}/r_{min})}{(RPM/1000)^2}$$

(2) $$S = \frac{m}{6\pi\eta r}$$

(3) $$T = \frac{K}{S}$$

Figure 1.11: Principles of Particle Sedimentation

The particles that are isolated by a particular rotor is determined by: 1) The K-factor (K) of that rotor, which corresponds to the revolution per minute (RPM) and minimum/maximum radii from the centre of rotation (rmax and rmin), and 2) the sedimentation coefficient (S) of the particles, which is dependent of the mass (m) and radii (r) of the particles, and the viscosity (η) of the medium. 3) The time of centrifugation (T) required for any individual particle by a specific rotor can then be determined via the K-factor and sedimentation co-efficient. Adapted from (Cvjetkovic *et al.*, 2014).

1.2.6.2 Size-Exclusion Chromatography (SEC)

As described above, size-exclusion chromatography (SEC) presents some advantages over dUC as an isolation technique, mainly in the form of a greater separation of vesicles from soluble proteins (Foers *et al.*, 2018). SEC generally involves use of a column comprising sepharose beads, which in turn contain a pore of 30-70nm. This pore increases the path length through the column for any loaded particles smaller than the pore size. This means large particles pass straight through the column and are often eluted in the void volume. By contrast, smaller particles pass through the column more slowly, distributing in fractions according to size (Böing *et al.*, 2014). In general, EVs are eluted in earlier fractions than soluble proteins, and SEC has been demonstrated to provide excellent separation between vesicles and protein (Benedikter *et al.*, 2017; Koh *et al.*, 2018). However, as with dUC, because SEC utilises size to separate vesicles, it does not provide any sort of indication to the class of EVs obtained. Furthermore, SEC columns are not readily scalable, which may present problems depending on the volume of starting material. One solution to this issue is to incorporate SEC as a purification step following concentration through techniques such as dUC or filtration (Nordin *et al.*, 2015; Gardiner *et al.*, 2016). Overall, SEC represents a useful alternative or complimentary technique to the widely employed dUC, due to greater overall purity in the final EV product.

1.2.6.3 Density Gradient Separation (DGS)

As discussed above, a key aim of EV isolation methodologies is the separation of a pure vesicular population from an initial medium, without the co-isolation of non-vesicular factors. Density gradient separation (DGS) employs ultracentrifugation to separate EVs within a gradient comprised of either sucrose or iodixanol (OptiPrep^{TM}) (Tauro *et al.*, 2012). This often employs a multi-step process where EVs are initially isolated via dUC and then purified by DGS. During this process, EVs of different densities (a physical property largely dependent on size) separate within the gradient, which can then be collected in fractions (Iwai *et al.*, 2016). This also leads to separation of vesicles and protein, with little overlap between fractions (Foers *et al.*, 2018). However, as with all isolation techniques, DGS possesses limitations. For example, the high osmotic pressure associated with sucrose gradients may cause structural damage to the isolated vesicles, although this problem may be circumvented through use of iodixanol (Iwai *et al.*, 2016). Furthermore, the density of EVs has been demonstrated to overlap significantly with that of high-density lipoprotein (HDL), which is a significant contaminant of DGS preparations, particularly those derived from biological fluids (Foers *et al.*, 2018; Onódi *et al.*, 2018). Additionally, due to the use of multiple centrifugation steps, isolation recovery yield is often low with DGS, limiting potential downstream processes (Tauro *et al.*, 2012; Onódi *et al.*, 2018). Whilst DGS has been used with some success in combination with SEC, this also suffered from issues of yield (Karimi *et al.*, 2018). Overall, DGS should be considered a complimentary technique to be paired with other methods of EV isolation where downstream applications require a high level of purity.

1.2.6.4 Precipitation Based Assays

Numerous kits are commercially available that are intended to provide a quick and easy method of EV isolation (Rider, Hurwitz and Meckes Jr., 2016). These often comprise volume-excluding polymers such as polyethylene glycol (PEG), which precipitate biological material by sterically excluding them from regions of solvent occupied by the polymer (Atha and Inghamg, 1981; Rider, Hurwitz and Meckes Jr., 2016; Brennan *et al.*, 2020). Acetate based assays have also been employed, in which negatively charged components of the EV membrane, such as phosphatidylserine, are neutralised, leading to hydrophobic interaction, aggregation and subsequent precipitation of the vesicles (Brownlee *et al.*, 2014). However, these precipitation-based assays are associated with significant limitations, which principally stem from the fact that the underlying principles employed are not exclusive to EVs. For instance, high concentrations of albumin were co-precipitated with EVs isolated from human plasma samples (Lobb *et al.*, 2015). Furthermore, precipitation-based techniques were demonstrated to produce less enrichment for EV markers, despite having a higher overall protein concentration (Van Deun *et al.*, 2014). This supports the concept that precipitation of non-vesicular proteins occurs alongside EVs, potentially compromising downstream applications.

1.2.7 Methods of Extracellular Vesicle Characterisation

As described throughout section 1.2.5, current understanding of EV biology is hampered by technical limitations in both isolation and characterisation. The latter of these is particularly hindered by the small size of EVs, which limits application of standard microscopy and flow cytometry techniques. Nevertheless, a range of approaches have been employed to visualise and characterise EVs.

1.2.7.1 Electron Microscopy (EM)

The first studies to identify the existence of EVs did so through application of electron microscopy techniques (Trams *et al.*, 1981; Harding, Heuser and Stahl, 1983; Pan and Johnstone, 1983). The majority of investigations utilise transmission electron microscopy (TEM), which has a resolution of around 1-3nm, thus allowing clear visualisation of even the smallest EVs (Coumans *et al.*, 2017). TEM requires the fixation and dehydration of samples before imaging, which has been demonstrated to alter EV morphology, resulting in a "cup shape" that has been erroneously reported as an EV specific characteristic (Raposo *et al.*, 1996; van Niel, D'Angelo and Raposo, 2018). This issue is avoided through use of cyro-EM, where samples may be maintained in a hydrated state, thus retaining their conventional spherical morphology (Coumans *et al.*, 2017). EM may also be combined with immuno-gold labelling, whereby gold particles are conjugated to an antibody, thus allowing identification of specific surface proteins. This technique was used in early EV investigations to follow the trafficking of the transferrin receptor to ILVs (Harding, Heuser and Stahl, 1983; Pan and Johnstone, 1983; Coumans *et al.*, 2017). Whilst EM may be considered the gold standard for characterisation of individual EVs, it is not high-throughput, requires significant operator training and does not provide a measurement of sample concentration (Rikkert *et al.*, 2019).

Therefore, it is often used to validate the successful isolation of EVs and combined with additional methods of characterisation.

1.2.7.2 Nanoparticle Tracking Analysis (NTA)

Nanoparticle tracking analysis (NTA) is a technique that aims to determine the size of particles based upon their Brownian motion, a characteristic whereby particles in suspension randomly move (Dragovic *et al.*, 2011). NTA utilises a laser beam, the light of which is scattered by the suspended particles and detected by a microscope. This scattering of light is recorded by a video camera, whilst tracking software is employed to follow the displacement of particles between frames. This is combined with the physical characteristics of the suspension fluid (temperature and viscosity) and allows determination of the size of each tracked particle via the Stokes-Einstein equation (Figure 1.12) (Filipe, Hawe and Jiskoot, 2010; Dragovic *et al.*, 2011; Gardiner *et al.*, 2013). In simple terms, smaller particles have greater Brownian motion than larger particles in the same fluid, thus tracking movement allows an estimation of size to be made (Gardiner *et al.*, 2014). Because the microscope visualises a suspension chamber of a known volume, a concentration of tracked particles can also be determined (Dragovic *et al.*, 2011). Therefore, NTA has become a widely employed technique to characterise the size and concentration of EV preparations (Gardiner *et al.*, 2016).

However, NTA is not without limitations. The most glaring of these, is that NTA is simply a measurement of light scattered by particles of a specific size and cannot confidently separate EVs from any contaminating materials (Coumans *et al.*, 2017). In this sense, it is a measurement of a physical property of EVs, as opposed to any biological characteristic. However, NTA can be combined with fluorescent probes, such as lipid binding dyes, that

allow some level of confidence that measured particles are EVs (Gardiner *et al.*, 2013). However, NTA is not able to determine the subcellular origin of the detected EVs and thus cannot be used to define EV subtypes. It has also been suggested that NTA may be less reproducible than other techniques (Filipe, Hawe and Jiskoot, 2010; Hole *et al.*, 2013; Bachurski *et al.*, 2019). However, with these caveats in mind, NTA does provide a relatively simple technique to determine the concentration and size of EVs, without the need for labelling or sample processing. Many of the limitations posed may be offset through combination with other techniques such as immunoblotting and EM. This approach is recommended by ISEV in order to minimise the relative limitations of each individual technique (Lotvall *et al.*, 2014). Therefore, NTA is a widely accepted method for EV characterisation. However, other techniques have also been described.

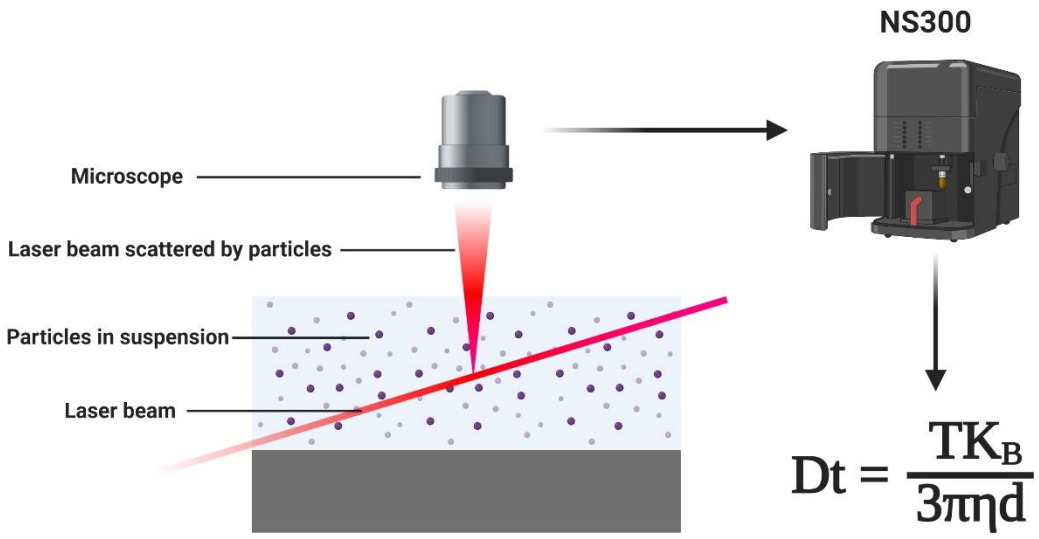

Figure 1.12: Principles of Nanoparticle Tracking Analysis (NTA)

Nanoparticle tracking analysis (NTA) is based on the principle of Brownian motion, the movement of particles based upon size. A laser beam is applied to particles in suspension, the movement of which causes light to be scattered. This is then detected by a microscope and the light scatter is tracked by software such as that in the NS300 system. The scattered light is dependent on the relative speed that at which the particles are moving, which is in turn dependent on the size of the particles. Therefore, by tracking the scattered light the Stokes-Einstein equation may be applied to calculate the diameter of the particles (d) using the temperature (T) of the sample and the viscosity (η) of the suspension fluid using Boltzmann's constant (K_B). Based on (Hole *et al.*, 2013).

1.2.7.3 Tunable Resistive Pulse Sensing

Tunable resistive pulse sensing (TRPS) involves continuous measurement of a current across a pore, which can be used to calculate the electrical resistance of the pore itself. As vesicles are forced through the pore by both voltage and pressure, the resistance in the pore increases, recorded as a decrease in current. This is proportional to the volume of vesicles traversing the pore, which can then be calculated (Coumans *et al.*, 2014). Furthermore, the count of current-decrease events may also be used to determine the particle concentration of a sample. However, as with NTA, this system does not distinguish between EVs and non-vesicular material (Coumans *et al.*, 2017). Furthermore, the system also relies heavily on the pore size, as inclusion of particles or contaminants larger than the pore may clog and damage the system, leading to unreliable results (Coumans *et al.*, 2014). Finally, the system has no facility to determine any compositional characteristics of the measured EVs.

1.2.7.4 Flow Cytometry (FCM)

In conventional flow cytometry (FCM), cells are passed sequentially through a laser beam leading to the scattering of light, which allows determination of cell size (forward angle scatter) and granularity (side scatter) (Adan *et al.*, 2017). Early attempts to evaluate EVs by FCM utilised polystyrene beads to construct calibration curves against which EV samples could be compared (Coumans *et al.*, 2017). However, this is a flawed approach, as EVs have a different refractive index to the calibration beads, resulting in inaccurate comparisons (van der Pol *et al.*, 2014). Furthermore, the small size of EVs produces an issue of sensitivity, as the EV scattered light is often indistinguishable from background noise. This means that often only the largest EVs are detected, leading to inaccurate size measurements (Harrison and Gardiner, 2012). Additionally, due to their small size, multiple vesicles are often included as one “event”, leading to coincidence artefacts and inaccurate data output (Van Der Pol *et*

al., 2012; Coumans *et al.*, 2017). Finally, the use of fluorescent FCM in an EV setting is limited, as antigen availability is much lower on the surface of EVs than on cells. This once again limits the intensity of signal generated, thus hindering detection (Coumans *et al.*, 2017). Overall, it is a consequence of repurposing a technique designed for cells that limits the utility of FCM as a method of EV characterisation.

However, recently, a purpose built form of EV FCM has become commercially available – nanoFCM. This system overcomes many of the limitations of the standard technique as it has a lower resolution limit of 40nm for EVs, as opposed to 1000nm reported for FCM (Van Der Pol *et al.*, 2012; Tian *et al.*, 2020). Furthermore, EV subpopulations may be assessed through fluorescent staining for the EV markers CD9, CD63 and CD81 (Tian *et al.*, 2018). Recently, this technique was used to assess EVs isolated by dUC, SEC, ultrafiltration and several precipitation based kits successfully (Tian *et al.*, 2020). Overall, this system would appear to have several advantages over techniques such as NTA as it is capable of determining particle size, concentration and, more importantly, potential heterogeneity with EVs based upon fluorescently detected markers. Whilst an exciting new technology, its relative infancy has prevented widespread adoption to date.

1.2.7.5 Single particle interferometric reflectance imaging sensing (SP-IRIS)

The development of new technologies to characterise EVs has begun to address some of the major limitations within the field. This can be seen with nanoFCM and greater elucidation of EV subtype compositions. Similarly, single particle interferometric reflectance imaging sensing (SP-IRIS) has recently been deployed in the form of the ExoView system (Daaboul *et al.*, 2016; Bachurski *et al.*, 2019). This technique utilises a micro-array of capture spots, which is able to immune-capture EVs positive for the tetraspanins CD9, CD63 and CD81. Furthermore, additional fluorescent antibodies may be incorporated to identify other surface markers of interest. The resolution limit is 50nm but, crucially, those EVs detected will have an associated profile of all three tetraspanins (Bachurski *et al.*, 2019). This is important as it has previously been indicated that sub-populations of EVs may be identified by the combination of tetraspanins expressed (Kowal *et al.*, 2016). An obvious limitation of this technique is that it is not suitable for EVs that do not express any of the tetraspanins. However, this is also a strength, as it overcomes the misidentification of non-vesicular particles that confounds other systems (Bachurski *et al.*, 2019). Another important advantage is that, depending on the sample, no EV isolation method need be pre-applied (Daaboul *et al.*, 2016). This overcomes a major hurdle in terms of practicality and yield that has hindered EV research to date. Overall, it is encouraging to see the emergence of new technologies that attempt to overcome many of the issues that have hampered EV research. Whilst widespread adoption is likely to take time, the application of more rigorous characterisation methodologies may expand our understating of EV heterogeneity.

1.3 Extracellular Vesicles in Senescence and Ageing

1.3.1 Changes in Extracellular Vesicle Production in Senescence

As described in section 1.1.4, the secretory phenotype of the SASP has become a hallmark of senescent cells (Coppe *et al.*, 2008; Hernandez-Segura, Nehme and Demaria, 2018). This enhanced secretome has typically been regarded as comprising predominantly soluble factors, complemented by shed ectodomains (Coppe *et al.*, 2008; Morancho *et al.*, 2015). However, recent reports have described a vesicular component to the secretory profile of senescent cells, which is exaggerated from that associated with proliferating or quiescent counterparts (Takasugi, 2018; Wallis, Mizen and Bishop, 2020). This was first reported by Lehmann *et al.,* (2008), who observed that EV secretion increased in human prostate cancer cells that had undergone premature senescence in response to ionising radiation. The authors also described an increase in EV release from replicatively senescent human dermal fibroblasts (HDFs), which suggested that this may be a feature of multiple types of senescence (Lehmann *et al.*, 2008). A previous report had established that tumour suppressor-activated pathway 6 (TSAP6) and vacuolar protein sorting-associated protein 32 (VPS32), both p53 targets, were responsible for an increase in EV secretion following p53 activation in response to ionising radiation in non-small cell lung cancer cell lines (Yu, Harris and Levine, 2006). Expanding on this, EV secretion was demonstrated to increase following DNA damage, triggered by ionising radiation or actinomycin D treatment, in MEFs and bone marrow-derived dendritic cells (BMDCs), respectively. This was demonstrated to occur in a p53 dependent manner, as the increased production of EVs was lost in cells from TSPAN6 knockout mice, indicating a possible link between this key effector of senescence and EV production (Lespagnol *et al.*, 2008). Whilst a less explicit association, p53 has also been reported to mediate an increase in Rab27b expression in senescent SVts8 fibroblasts, once again linking p53 to EV biogenesis. More recently, Takasugi *et al.,* (2017) demonstrated that EV production increased in TIG-3 human fibroblasts in response to replicative, oncogene

induced and therapy-induced senescence (Takasugi *et al.*, 2017). This work has been followed by a flurry of publications reporting increased EV secretion in models of replicative (Mensà *et al.*, 2020; Riquelme *et al.*, 2020), oncogene-induced (Borghesan *et al.*, 2019), therapy-induced (Kavanagh *et al.*, 2017), H_2O_2-induced (Terlecki-Zaniewicz *et al.*, 2018) and irradiation-induced (Basisty *et al.*, 2020) senescence. Overall, in a phenotype reminiscent of the SASP, senescence has been widely associated with an increase in EV production (Wallis, Mizen and Bishop, 2020).

It is currently unclear how the establishment of a senescence phenotype may lead to an increase in EV secretion. Choi *et al.,* (2020) have sought to provide some clarity using HDFs, which have undergone senescence in response to replicative exhaustion. The authors demonstrated that RS HDFs are associated with increased nSMase activity. As described in section 1.2.2.1, this enzyme has been shown to be a crucial mediator of EV production and its inhibition with GW4869 was demonstrated to reduce EV release by HDFs (Choi, Kil and Cho, 2020). Furthermore, increased nSMase activity has been linked to excessive ROS production, another senescence-associated phenomenon, with antioxidant treatment demonstrated to attenuate EV production from senescent HDFs (Hernandez-Segura, Nehme and Demaria, 2018; Choi, Kil and Cho, 2020). Additionally, the authors postulated that dysfunctional lysosomal activity in senescent cells is directly linked with increased EV secretion. Pharmacological restoration of lysosomal function in senescent HDFs, through lowering of lysosomal pH, reduced EV production. Furthermore, increasing lysosomal pH in proliferating HDFs conferred a vesicular secretory level equitable to that of senescent cells (Choi, Kil and Cho, 2020). Together, this suggests a link between the altered lysosomal activity of senescent cells and an increased rate of EV production.

1.3.2 Changes in Extracellular Vesicle Cargoes in Senescence

The biogenesis of EVs necessitates that they derive all compositional components directly from their producing cell (van Niel, D'Angelo and Raposo, 2018). Therefore, alterations in cellular composition can lead to subsequent changes in EV cargoes. Senescent cells are compositionally distinct from their proliferating counterparts and a growing body of evidence suggests the same is true of the EVs produced by these cells (Takasugi, 2018; Wallis, Mizen and Bishop, 2020). This section will discuss the alterations in senescent cell derived EV cargos in the context of proteins, nucleic acids and lipids, as well as the associated functional consequences of these constituents.

1.3.2.1 Proteins

EVs have recently emerged as an additional layer of complexity to the predominantly soluble secretome of senescent cells (Takasugi, 2018; Basisty *et al.*, 2020). Whilst identification of EVs themselves has become more routine as a result of techniques such as NTA (Bachurski *et al.*, 2019) and EM (Rikkert *et al.*, 2019), as well as the identification of widely accepted biomarkers (Théry *et al.*, 2018), distinction between EV constituent proteins and other secreted factors remains technically challenging (Foers *et al.*, 2018). Nevertheless, efforts to characterise the change in EV protein content following senescence induction have recently escalated. Having described an increase in EV production in four distinct models of senescence, Takasugi *et al.*, (2017) assessed the proteomic composition of therapy-induced senescent RPE-1 epithelial cells following doxorubicin treatment. The ephrin receptor A2 (EphA2) was identified as the second most abundantly enriched protein, the first being histone H4, which the authors attributed to the presence of CCFs in senescent cells. EphA2 was further demonstrated to increase in both RS and OIS TIG-3 fibroblasts. The investigators also established that the proliferation of MCF7 breast cancer cells could be potentiated by

treatment with TIS RPE-1 derived EVs, as well as CM from TIS RPE-1s and RS TIG-3s, an effect which was lost if the CM was depleted of EVs. EphA2 was demonstrated to be crucial to these EV mediated effects, with shRNA ablation of EphA2 attenuating the increase in cancer cell proliferation elicited by both TIS RPE-1 EVs as well as TIS RPE-1 and TIG-3 CM. EphA2 was demonstrated to act via ephrin A1 on the surface of the cancer cells in a reverse signalling mechanism that was not recapitulated in non-cancerous RPE-1s, as ephrin A1 expression was lower in those cells. Recombinant EphA2 could not recapitulate the effect of the EV-associated form, suggesting that incorporation within EVs potentiated its function. This is reminiscent of studies that describe a more potent effect of EV-associated factors than a soluble form of the same protein, specifically interferon gamma (IFN-γ) (Cossetti *et al.*, 2014) and TGFβ (Webber *et al.*, 2015). This opens the possibility that EVs may augment the signalling properties of soluble proteins, including SASP components (Takasugi, 2018).

The role of EVs within TIS has recently been explored further in Cal51 triple negative breast cancer cells. Kavanagh et al., (2017) demonstrated that following senescence induction with paclitaxel (PTX), EV secretion increased. Furthermore, proteomic analysis of these EVs demonstrated increased expression of 142 proteins. Of these, authors validated the increased expression of annexin V, sodium/potassium ATPase and α-tubulin, involved in apoptosis/chemoresistance, ATP regulation and PTX mediated senescence induction respectively. Pathway analysis also indicated that 69/142 of the proteins with increased abundance in EVs were predicted to enhance cellular proliferation. The investigators suggested that cells might preferentially sort proteins into EVs for removal, in order to maintain survival following stressful stimuli. Furthermore, as the fluorescent PTX analogue Flutax-2 was observed in EVs, and as EV biogenesis inhibition with GW4869 decreased

cellular proliferation, it was proposed that EVs might also represent a route through which cancer cells enforce chemoresistance and maintain proliferation (Kavanagh *et al.*, 2017).

The process of paracrine senescence, described in section 1.1.7, is one of the key functions of the SASP, as well as a suspected contributor to the age-related pathologies associated with senescence (Acosta *et al.*, 2013; Baker *et al.*, 2016). Whilst previous studies had demonstrated that senescent cell derived EVs were functionally active, given they could increase the proliferation of cancer cells, Borghesan *et al.,* (2019) were the first to directly describe a contribution to paracrine senescence. The investigators demonstrated that HFFF2 human foreskin primary fibroblasts treated with OIS cell derived EVs had reduced cellular proliferation, as well as increased expression of p16, p53 and DNA damage foci. Supporting this finding, conditioned media and trans-well investigations demonstrated that OIS mediated paracrine senescence could be attenuated by treating conditioning cells with nSMase inhibitors. The implication of this finding is that EVs are a major contributor to the paracrine senescent effects of the SASP. In order to characterise the composition of EVs derived from senescent cells, HFFF2s induced by both OIS and DNA damage following etoposide treatment were investigated by mass spectrometry. Among common factors differentially expressed in both models, as well as unique to the EVs, interferon-induced transmembrane protein 3 (IFITM3) was identified as a possible functional EV cargo through a CM siRNA screen. This was validated through both IFITM3 siRNA and shRNA inhibition of EV producing HFFF2s, which attenuated the upregulation of p16 and IL-8 in cells treated with the EVs (Borghesan *et al.*, 2019). Overall, this data indicates that EVs are contributors to paracrine senescence, in an effect partially mediated by IFITM3.

A key issue when establishing the composition of senescent cell derived EVs, is the context dependent nature of their constituents. This mirrors the SASP, where components vary with both cell type and inducing stimuli (Coppe *et al.*, 2008). Recently, a solution to this heterogeneity has been produced through development of a SASP "Atlas". Investigators collated mass spectrometry data from CM derived from fibroblasts stimulated by therapy, oncogene and irradiation-induced senescence, as well as epithelial cells stimulated by irradiation. This was supported by proteomic profiling of EVs derived from the OIS and IR fibroblast models (Basisty *et al.*, 2020). This work confirmed that EV composition varied with senescence model, emphasising this fundamental challenge with both senescence and EV research. Whilst a commendable endeavour, the utility of the SASP Atlas would be greatly enhanced if it were to have a facility for submission. This could allow the development of a collaborative repository of datasets similar to that of ExoCarta (Simpson, Kalra and Mathivanan, 2012), which would facilitate a more comprehensive record of the heterogeneity in SASP composition. As it stands, the SASP Atlas allows comparison of an inputted gene list and the stored data sets. It is interesting to note that neither EphA2 nor IFITM3 were identified in any of the SASP Atlas components, highlighting the challenge facing the field when attempting to compose a complete SASP profile across models and cell types. It is also important to note that without standardisation of variables such as EV isolation, CM incubation time and cell numbers, the number of potentially confounding factors is extensive. However, the SASP Atlas clearly corroborates previous studies, which indicate that EVs are compositionally distinct from the from the soluble proteins that have canonically comprised the bulk of the SASP (Takasugi, 2018; Wallis, Mizen and Bishop, 2020).

1.3.2.2 Nucleic Acids

Having been established as abundant components within the secretome of senescent cells, understanding whether EVs carry out functions distinct from those of the soluble SASP has become a key research question. The EV mediated transfer of nucleic acids represents a potential route through which such discrete functional roles may occur. This principle was first described by Valadi et al., (2007), with demonstration of EV mediated transfer of functional mRNA between mast cells (Valadi *et al.*, 2007). Subsequently, the role of EV facilitated transfer of nucleic acids has become widely investigated in the senescence field. This section will address these studies according to the subtype of nucleic acid investigated: miRNA, DNA and Telomeric repeat containing RNA (TERRA).

1.3.2.3 miRNA

Within senescence, miRNAs have been described as contributors to the maintenance of p16 dependent cellular senescence in epithelial cells (Overhoff *et al.*, 2014). More recently, miRNAs have also been observed to stimulate the development of RS in MEFs (Xu *et al.*, 2019). Therefore, EV resident miRNAs have become the focus of significant research attention in order to explore potential roles in the modulation of senescence responses. This was first investigated by Weiner-Gorzel *et al.,* (2015) who identified that miR-433 expression in ovarian cancer cells instigated a senescence response through ablation of CDK6. Investigators identified that EVs isolated from three ovarian cancer cell lines expressing miR-433 were associated with increased levels of the miRNA. Furthermore, confocal microscopy demonstrated that EVs were delivered to treated cells, raising the possibility that EVs may facilitate a route to secondary senescence induction (Weiner-Gorzel *et al.*, 2015). This initial study was recently expanded upon by Fulzele *et al.,* (2019), through demonstration that oxidative stress induced senescence in both mouse myoblasts and human myotubes

contained increased levels of miR-34a, which the authors also demonstrated to be elevated with age in mice. Importantly, the myoblast EVs were shown to elicit a paracrine senescence response in treated bone-marrow stem cells (BMSCs), determined through increased SA-β-gal activity. The investigators also observed that the p53 suppressor Sirtuin 1 (SIRT1) could be downregulated in BMSCs following treatment with EVs from miR-34a overexpressing cells, suggesting a possible mechanism for the proposed senescent cell derived EV mediated paracrine senescence (Yamakuchi and Lowenstein, 2009; Fulzele *et al.*, 2019). This has since been elaborated by Mensa *et al.,* (2020), through investigation of the "MiRome" in senescent HUVECs and derived EVs. Investigators first established that EVs were released in greater quantities from RS HUVECs than from the proliferating counterparts. Comprehensive analysis of all miRNAs in proliferating and senescent HUVECs, as well as the derived EVs, identified five that were differentially expressed in both senescent HUVECs and their EVs, a number that was reduced to two following qRT-PCR validation. These were miR-21-5p and miR-217. This was further validated through a demonstrated increase in expression of both miRNAs in human aortic endothelial cells (HAECs) induced by replicative exhaustion, as well as HAECs and HUVECs following TIS. These miRNAs had previously been established as inhibitors of both SIRT1 and DNA Methyltransferase 1 (DNMT1). The investigators demonstrated that treatment of proliferating HUVECs with senescent HUVEC derived EVs led to a reduction of both SIRT1 and DNMT1, accompanied by reduced Ki67 expression and increased expression of p16, IL-6 and IL-8 (Mensà *et al.*, 2020). Together, this data indicates that functional transfer of miRNAs via replicatively senescent cell derived EVs is a contributor to paracrine senescence, in a process dependent on the inhibition of SIRT1 and DNMT1. This suggests EVs may have a role as mediators within the "dark" detrimental effects of the SASP (Wallis, Mizen and Bishop, 2020).

By contrast, miRNAs transported by EVs have also been suggested to contribute to the beneficial side of the SASP, in particular in wound healing (Fafián-Labora and O'Loghlen, 2020; Wallis, Mizen and Bishop, 2020). Terlecki-Zaniewicz *et al.,* (2019) demonstrated that miR-23a-3p encapsulated within EVs was responsible for an enhanced wound healing effect upon treatment of keratinocytes in scratch assays. These EVs had been isolated from HDFs induced by oxidative stress through H_2O_2 treatment (Terlecki-Zaniewicz *et al.*, 2019). The same investigators had previously established that under these conditions, HDFs secrete more EVs than quiescent cells maintained under contact inhibition (Terlecki-Zaniewicz *et al.*, 2018). In this earlier report, it was demonstrated that senescent cell derived EVs possessed a distinct miRNA profile, which kinetically developed with the long-term maintenance of senescence. Target prediction of the top 20 most abundant EV miRNAs implicated a potential role as negative regulators of apoptosis. Indeed, the senescent cell derived EVs were demonstrated to confer an anti-apoptotic effect upon treated fibroblasts that were exposed to acute stress through H_2O_2 treatment, although this was not explicitly attributed to the miRNA cargo (Terlecki-Zaniewicz *et al.*, 2018). Together, these studies indicate that senescent cell derived EVs are functionally relevant contributors to the SASP and, importantly, have a diverse set of both beneficial and detrimental roles, with many of these effects mediated by the transfer of functional miRNAs (Wallis, Mizen and Bishop, 2020).

1.3.2.4 Telomeric Repeat-Containing RNA (TERRA) and Telomeric DNA

As described in section 1.1.5, replicative senescence occurs as a direct consequence of the erosion of telomeres due to the end-replication problem. Telomere attrition has been demonstrated to lead to an increase in the presence of TERRA within cells, although a direct link to senescence has not currently been demonstrated (Cusanelli, Romero and Chartrand, 2013; Takasugi, 2018). EVs isolated from human lymphoblastoid cells have been

demonstrated to contain TERRA, whilst cells treated with these EVs display an upregulation in inflammatory cytokines, including the canonical SASP factor IL-6 (Wang *et al.*, 2015; Wang and Lieberman, 2016). However, a limited number of research publications have investigated this phenomenon and a clear link directly to senescence is still lacking. Indeed, contradictory evidence has proposed that cytoplasmic telomere repeats may exert anti-inflammatory response through inhibition of cGAS/STING (Bonafè, Sabbatinelli and Olivieri, 2020). Therefore, the presence and consequences of telomeric components within senescent cell derived EVs remains unclear.

1.3.2.5 DNA

As described in section 1.1.4, the increased presence of CCFs has become an established hallmark of senescence, with an intrinsic link to SASP modulation through cGAS/STING mediated activation of NF-κB (Ivanov *et al.*, 2013; Dou *et al.*, 2017; Glück *et al.*, 2017). The potential secretion of these DNA fragments within EVs has recently been investigated by Takahashi *et al.,* (2017). Investigators demonstrated that inhibition of EV secretion via siRNA ablation of ALIX and Rab27a, as well use of nSMase inhibitors, lead to increased apoptosis of RS and OIS TIG-3 fibroblasts. The use of the same treatments also caused an increase in DNA damage in proliferating fibroblasts, whilst knockdown of DDR response kinases ATM and ATR via siRNA was sufficient to attenuate this effect. The authors concluded that EVs were thus functioning as a homeostatic mechanism to prevent DDR activation. In order to demonstrate that this occurred through the removal of damaged cytoplasmic DNA fragments, immuno-gold labelling was used to identify double stranded DNA (dsDNA) in EVs via EM, as well as the histone proteins H3 and H4. This was supported by rescue of DNA damage through use of a dsDNA endonuclease, following inhibition of EV secretion. The authors went on to demonstrate that the cGAS/STING/IFN-γ axis was key to mediating the onset of the aberrant

DDR following blockade of EV secretion (Takahashi *et al.*, 2017). This elegantly returns to some of the earliest concepts surrounding the biological function of EVs, namely their role as a mechanism of "waste disposal" (Johnstone, 1992; Wallis, Mizen and Bishop, 2020). Finally, the investigators demonstrated that the CCF containing EVs could evoke a DDR in treated fibroblasts, suggesting a more malign influence in the form of paracrine senescence than the predominantly beneficial contribution to cellular homeostasis demonstrated within the producing cells.

1.3.2.6 Lipids

There is a paucity of research investigating the lipid composition of senescent cell derived EVs, particularly when compared to the abundance of publications investigating constituent proteins and nucleic acids (Wallis, Mizen and Bishop, 2020). Recently, lipidomic assessment of OIS fibroblast derived EVs has been performed by several groups. Buratta *et al.,* (2017) demonstrated that EVs possessed a distinct lipid profile from the cells from which they were derived. Investigators highlighted EV enrichment of lyso-phospholipid and reduced abundance of phosphatidylserine (Buratta *et al.*, 2017). A subsequent study supported this proposed differential lipid content, with EVs from OIS fibroblasts possessing greater levels of saturated and polyunsaturated fatty acids compared to the producing cells (Sagini *et al.*, 2018). Complimenting previous reports, the lipid profile of EVs has also been described to contribute to EV mediated paracrine senescence. Khayrullin *et al.,* (2019) demonstrated that C24:1 ceramide was abundantly present in EVs isolated from elderly volunteers. Mouse serum derived EVs were then loaded with this very long chain ceramide, which were then used to treat BMSCs. These EV treatments lead to a paracrine senescence effect, demonstrated by increased SA-β-gal staining. The authors indicated that this may suggest that EVs contribute to secondary senescence induction (Khayrullin *et al.*, 2019). Overall, it

remains unclear as to how the lipid profile of EVs changes following senescence induction and to what extent the lipid composition of EVs determine their functional effects.

1.3.3 Changes in Extracellular Vesicle Production with Age

The emerging consensus across multiple models of senescence, investigated in a variety of cell types, suggests that EV production increases following senescence induction (Takasugi, 2018; Fafián-Labora and O'Loghlen, 2020). However, a less clear picture has developed in terms of the change in EV production during ageing. Alberro *et al.,* (2016) noted that in subjects aged 79-92, the level of serum IL-6 was greater than that seen in individuals aged 21-50. However, this was not the case with EVs isolated from the same volunteers, with no change across any age-groups observed (Alberro *et al.*, 2016). A subsequent investigation noted a decrease in the plasma EV concentration with age, assessed in 74 participants ranging from 30 – 65 (Eitan *et al.*, 2017). The investigators also demonstrated that both smoking and increased body mass index (BMI) had some correlation to an increased level of plasma EVs. Interestingly, both these factors are also associated with enhanced levels of senescence induction (Nyunoya *et al.*, 2006; Ogrodnik *et al.*, 2019). The range in ages assessed between these conflicting studies makes assessment difficult and may be a contributing factor to the differences observed. More recent investigations also contradict these early findings, with Im *et al.,* (2018) demonstrating an increase in EV secretion in elderly volunteers aged 63-90, compared to young volunteers aged 23-45 (Im *et al.*, 2018). This observation was supported by recent work in a mouse model of normal ageing, which demonstrated a correlation between increased age and the level of plasma EV like particles positive for TSG101, CD63 and CD81, acquired from either young (3 months) or old (18-21 month) mice. The investigators made an important observation in that depending on their selected method of EV characterisation, an entirely contrary result was observed. In this

case, use of NTA demonstrated a decrease in EV concentration, contradicting western blot and flow cytometry data (Alibhai *et al.*, 2020). This emphasises the importance of utilising multiple methodologies when investigating EVs, as contaminants (in this case lipoproteins) can often obfuscate the true nature of the EVs present. Determination of the level of EV production may also be confounded by age-related pathologies. The investigation by Im *et al.,* (2018) describe above, also noted that young patients with gastric cancer secreted more EVs than healthy volunteers of a comparable age (Im *et al.*, 2018). Increased EV levels have also been observed in the plasma of patients with COPD, as well as from isolated chondrocytes derived from the cartilage of osteoarthritis patients (Tan *et al.*, 2017; Jeon *et al.*, 2019). Overall, due to the array of potentially confounding factors that undermine comparison between these studies, it is difficult to draw as firm a conclusion as to the change in EV production with age, as that which can be drawn for senescent cells.

1.3.4 Changes in Extracellular Vesicle Cargoes with Age

To understand the consequences of altered levels of EV secretion within both age and age-related pathology, it is also important to appreciate any compositional changes that may also occur in these circumstances. EVs isolated from healthy elderly subjects have been demonstrated to possess a reduced capacity to facilitate osteogenic differentiation of adipose tissue-derived mesenchymal stem cells (ASCs) compared to EVs of young donors. This was attributed to an increase in miR-31 content, demonstrated by a rescue of differentiation through use of an anti-miR-31 nucleic acid inhibitor (Weilner, Schraml, *et al.*, 2016). The same group also demonstrated that the carbohydrate binding protein Galectin-3 is present at reduced levels in EVs isolated from the plasma of elderly volunteers (older than 55) compared to young participants (younger than 25). The EVs from the old subjects were also less efficient at stimulating the osteogenic differentiation of ASCs than those from the

young volunteers (Weilner, Keider, *et al.*, 2016). Further supporting these findings, is evidence that osteogenic differentiation of mouse BMSCs may be attenuated through treatment with EVs isolated from the bone marrow of aged mice. These EVs were shown to be associated with increased levels of miR-183-5p, which could independently cause comparable inhibition of osteogenic differentiation. Whilst not direct evidence that this miRNA is the effector of the EV mediated response, investigators did demonstrate EV uptake, thus providing a rationale that delivery miR-183-5p may be a feasible underlying mechanism (Davis *et al.*, 2017). Further evidence to indicate that EV cargo change with age comes through the demonstration that macrophage derived EVs are associated with increased mRNA levels of IL-6 and IL-12, when isolated from old subjects aged 65-90 compared to young volunteers aged 21-45 (Mitsuhashi *et al.*, 2013). Changes in the nucleic acid content of EVs derived from the plasma of frail aged (71–89 years) individuals has also been demonstrated when compared to that of healthy aged and young (23–35 years) subjects, with 8 miRNAs (miR-10a-3p, miR-92a-3p, miR-185–3p, miR-194–5p, miR-326, miR-532–5p, miR-576–5p, and miR-760) identified to be differentially expressed (Ipson *et al.*, 2018). Further supporting these observations is evidence from Alibhai *et al.,* (2020) who demonstrated that six miRNA increased (miR-146a, miR-21, miR-22, miR-223, miR-145, and let-7a) and two decreased (miR-212 and miR-455) in EVs isolated from elderly mice compared to young counterparts. Several of the increased miRNA were able to recapitulate an immunomodulatory effect on macrophages that had been observed following treatment with the old EVs, specifically an increased production of TGFβ and IL-10, suggesting that they may be functionally delivered cargos in ageing (Alibhai *et al.*, 2020).

Mirroring the observation above from Ipson *et al.,* (2018), that fragility associated with pathological ageing is accompanied by changes in EV cargo, diseases associated with

advanced age have also been observed to lead to alterations in EV composition and function. EVs isolated from acute coronary syndrome patients (43-93 years) have been demonstrated to contribute to a process of secondary senescence, characterised by endothelial dysfunction and oxidative stress (Abbas *et al.*, 2017). EVs isolated from the plasma of elderly volunteers aged 75-83, were demonstrated to contribute to increased calcification of human aortic smooth muscle cells compared to EVs isolated from young subjects aged 20-28. The EVs from aged individuals were demonstrated to be enriched for proteins considered pro-calcific including annexin A2, annexin A6 and BMP2 (Alique *et al.*, 2018). Furthermore, OA is a pathology closely associated with ageing. Work by Jeon *et al.,* (2019) demonstrated that EVs derived from chondrocytes isolated from OA patients contributed to a paracrine senescence response in treated non-senescent chondrocytes, demonstrated by an increase in SA-β-gal staining. Investigators attributed these effects to reduced levels of EV associated miR-140-3p and increased miR-34a-5p, which are associated within increased chondrocyte dysfunction and the onset of senescence respectively. Furthermore, EVs isolated from elderly healthy and OA subjects aged (70-80) were demonstrated to contain 22 differentially expressed miRNAs, which the authors postulated as potential biomarkers of OA. Additionally, the investigators demonstrated that young mice treated with EVs from aged mice displayed increased pain and less leg function than controls, indicating that EVs may act to propagate the development of OA.

Finally, two recent studies have focused on the inverse situation to the majority of investigations described here, namely the contribution of EVs from young individuals or proliferating cells upon old subjects or senescent cells. The first publication by Yoshida *et al.,* (2019), demonstrated that an extracellular form of nicotinamide phosphoribosyltransferase (eNAMPT) was exclusively contained in EVs and that the levels of this decreased with age in

both humans (37-80 years) and mice (young, 4-6 months; old, 18-26 months). Furthermore, old mice treated with EVs isolated from the plasma of young mice were demonstrated to display increased levels of physical activity and, remarkably, had an extended median lifespan of 10% (Yoshida *et al.*, 2019). Supporting this finding is recent work by Fafián-Labora *et al.,* (2020), who investigated the functions of EVs isolated from primary fibroblasts derived from young individuals (Y-EVs; 1-4 years). Treatment of fibroblasts from old individuals (67-81 years) with Y-EVs reduced the appearance of senescence markers including p16, p21, SA-β-gal and IL-8, along with increasing expression of BrdU and increased cellular proliferation. Furthermore, OIS HFFF2s treated with EVs derived from proliferating control cells displayed reduced mRNA expression of several SASP components as well as both p16 and p21. Through the proteomic assessment described in Borghesan *et al.,* (2019), glutathione-related protein (GSTM2) was identified as a potential functional candidate, validated by western blot to be increased in both EVs from control HFFF2s and Y-EVs. Treatment of old fibroblasts with Y-EVs was also demonstrated to prevent accumulation of 8-Oxo-2'-deoxyguanosine (8-oxo) and γH2AX, indicating inhibition of oxidative stress. The EV-associated GSTM2 was demonstrated to be functional, increasing the formation of glutathione (GSH) in treated old fibroblasts, which was positioned as key component of the rejuvenating properties of Y-EVs. Finally, *in vivo* investigation demonstrated that aged mice (22-25 months) treated with Y-EVs displayed reduced levels of SA-β-Gal in kidney, lung and adipose tissues. Furthermore, these tissues were also associated with reduced ROS levels and increased GST activity. Overall, this work elegantly demonstrated the potential of EVs isolated from young cells to ameliorate senescence *in vitro* and *in vivo*, at least partially through the action of EV-associated GSTM2 (Fafián-Labora, Rodríguez-Navarro and O'Loghlen, 2020). The work presented in these two studies presents EVs from proliferating cells as an intriguing avenue for the development of therapeutic approaches aimed at attenuating pathological ageing.

1.4 Thesis Hypothesis

This work aims to explore the change in composition and function of extracellular vesicles (EVs) following the induction of senescence. It was hypothesised that EVs derived from senescent cells contain a distinct profile of protein constituents from those isolated from proliferating cells. Furthermore, it was hypothesised that these cargos facilitate the propagation of a secondary senescence response, so called paracrine senescence, to proliferating cells, in a distinct manner from that of the canonical soluble SASP. Additionally, it was hypothesised that application of rigorous EV isolation methodologies are essential to the accurate functional and compositional profiling of senescent cell derived EVs, due to the previously reported obstacle of co-isolating soluble proteins.

1.5 Project Aims

- **Establish and validate experimental models of senescence**
    - Induction of oncogene-induced senescence (OIS) in IMR90 fibroblasts
    - Induction of replicative senescence (RS) in adult human mammary fibroblasts (HMFs)
    - Investigation of the senescent secretome using an established model of senescence reversal in HMFs

- **Establish methodology for the isolation and compositional assessment of EVs from senescent cells**
    - Validate isolation of EVs through differential ultracentrifugation (dUC)
    - Validate isolation of EVs through size-exclusion chromatography (SEC)
    - Characterise the proteomic composition of senescent cell derived EVs

- **Characterise contribution of EVs to the process of paracrine senescence**
    - Investigate paracrine senescence through conditioned media and EV treatment investigations
    - Probe potential mechanisms identified during compositional characterisation investigations

2 Material and Methods

2.1 Cell Culture and Reagents

Unless otherwise indicated, all reagents were sourced from Sigma UK. All cells were maintained under conditions of 37°C with 5% CO_2 and demonstrated to have a negative mycoplasma status regularly. Cells were cultured in T25/75/150 flasks (Corning, UK). Unless otherwise stated, cells were medium changed every two to three days. Cells were frozen at densities not exceeding 1e6 cells/ml in 2ml cryovials using 1ml freezing medium comprising 90% foetal bovine serum (FBS, Labtech.com, UK) and 10% dimethyl sulfoxide (DMSO). Antibiotics were not used in culture media aside from experiments utilising EV treatments. In these cases, 50units/ml penicillin and 50µg/ml streptomycin (Life Technologies, UK) were included in the media.

IMR90 *ER:STOP* (vector) *or ER:RAS* (OIS) foetal lung fibroblasts were kindly donated by Juan Carlos Acosta (MRC Institute of Genetics & Molecular Medicine, Edinburgh), having been generated according to this group's published protocol (Hari *et al.*, 2019). Cells were cultured using Dulbecco's Modified Eagle Medium (DMEM; Life Technologies, UK) containing 10% FBS and 2mM L-Glutamine (Life Technologies, UK). Cells were thawed from stocks as required, seeded at a density of 2,000-10,000 cells/cm^2, passaged on a weekly basis. These cells were used in experiments investigating OIS, which are described further in section 2.2. OIS was selected as a model due to the expedient nature of senescence induction and the previously reported potency of the OIS SASP, thus providing potential advantage over other models of premature senescence e.g. IR induced senescence (Coppe *et al.*, 2008). As these cells are not immortalised, all investigations were carried out within three passages of thawing to prevent the confounding influence of replicative senescence. Normal adult human mammary

fibroblasts (HMFs) were donated by Elly Tyler (Bishop Lab, Blizard Institute) having previously been acquired from Martha Stampfer (Lawrence Berkeley National Laboratory, Berkeley). Cells were derived from tissue collected from a 16-year-old donor following a reduction mammoplasty procedure (Stampfer *et al.*, 1981). Cells were cultured in the same medium as IMR90s with the addition of 10µg/ml bovine pancreas insulin using a seeding density of 10,000 cells/cm^2. These cells were serial passaged every seven days until observation of replicative senescence, as described in section 2.3. This model was selected due to its previous comprehensive characterisation within the group (Thesis:(Tyler, 2016)). It is important to note that these cells were derived from a single patient and the associated Hayflick proliferation profiles of cells from other individuals may vary significantly. This is discussed further in section 3.7.

MDA-MB-468 triple negative basal-like breast cancer cells (468s) were purchased from ATCC (HTB-132). These were cultured using high glucose DMEM supplemented with 10% FBS, 2mM L-Glutamine and 1mM Sodium Pyruvate. Cells were seeded at a density of 10,000 cells/cm^2, passaged weekly for a maximum of 10 passages and used in the experiments described in sections 5.3, 5.5 and 5.6. These cells were selected due to previous characterisation of senescence induction via High Content Analysis (HCA) within the group (Preprint(Moore *et al.*, 2018)). The cells were used to serve as a means of assessing the potential pro-/anti-tumorigenic effects of the SASP that has been previously reported (Campisi and D'Adda Di Fagagna, 2007).

2.1.1 Antibodies

For the immunoblotting and immunofluorescence procedures described in sections 2.5 and 2.12, the antibodies utilised are described in Table 1.

Target	Antibody	Supplier	Dilution
p21	12D1	Cell Signalling, UK	IF: 1:2,000 WB: 1:1,000
p16	10883-1-AP	Protein-Tech, UK	IF: 1:2,000 WB: 1:1,000
Ki67	NCL-Ki67p	Novocastra, UK	IF: 1:1,000
IL-6	AB-206-NA	R and D Systems, UK	IF: 1:500 WB: 1:250
IL-8	AF-208-NA	R and D Systems, UK	IF: 1:500 WB: 1:500
GAPDH	ab9485	Abcam, UK	WB: 1:5,000
β-Tubulin	E1C601-1	EnoGene, UK	WB: 1:20,000
Lamin B1	ab16048	Abcam, UK	WB: 1:1,000
CD9	CD9-A1	System Biosciences, UK	WB: 1:1,000
TSG101	ab30871	Abcam, UK	WB: 1:1,000
Calnexin	ab22595	Abcam, UK	WB: 1:1,000
NOTCH1	4147	Cell Signalling, UK	WB: 1:1,000
N1ICD	4380	Cell Signalling, UK	WB: 1:1,000
ADAM10	14194	Cell Signalling, UK	WB: 1:1,000
ADAM17	ab2051	Abcam, UK	WB: 1:1,000
HRP goat anti-rabbit	65-6120	Invitrogen, UK	WB: 1:5,000
HRP rabbit anti-goat	P0160	Dako, UK	WB: 1:5,000
Goat anti-rabbit-Alexa 546	A11035	Thermo-Fisher, UK	IF: 1:500
Rabbit anti-goat-Alexa 546	A21446	Thermo-Fisher, UK	IF: 1:500

Table 1: Antibody List

2.2 Oncogene-Induced Senescence Induction

OIS induction was carried out through use of *ER:RAS* IMR90 fibroblasts. These cells express a fusion protein comprising oncogenic HRas coupled to an oestrogen receptor (ER) hormone binding domain. This construct is activated through treatment with 4-Hydroxytamoxifen (OHT) (Reuter and Khavari, 2006). Control *ER:STOP* cells were utilised as a proliferating control, which express a constuct comprising the ER hormone binding domain alone (Boumendil *et al.*, 2019). In the interest of clarity, *ER:RAS* cells are refered to as **OIS** and ER:STOP as **vector** throughout this report.

In the course of this project several induction schedules were optimised, with the final protocol used for the majority of experiments presented here. This is summarised in Figure 2.1, along with an explanation of the initial protocols and corresponding experiments. In the final schedule (schedule three), vector and OIS IMR90s were seeded at 10,000 cells/cm^2. One day post seeding, these were treated with 200nM OHT prepared in DMEM with 10% FBS. Cells were cultured for 72 hours to day four at which point media was changed to one comprising DMEM, 200nM OHT and 1% “exosome-depleted FBS” (Gibco, UK). Media was collected on day eight for downstream experiments and EV isolation. Concurrently, cells were passaged and seeded into 96-well plates. These were cultured for a further five days at which point senescence characterisation was performed by high content analysis (HCA).

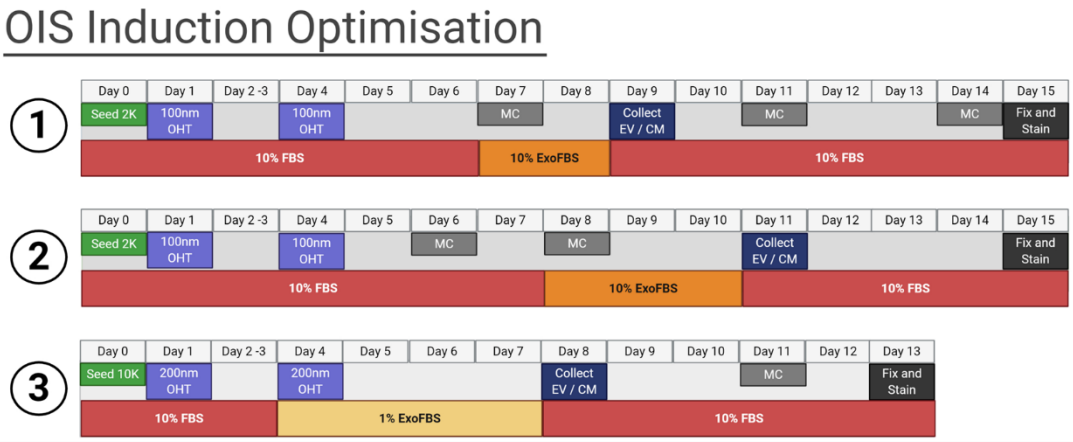

	Mass Spectrometry	Section	Other Experiments (Figure)
Schedule 1	MS1	4.5	None
Schedule 2	MS2	4.7	Time-Course Optimisation (3.12) Fraction Particle/Protein Assessment (4.13 / 4.14) Fraction IL-8 Assessment (4.15)
Schedule 3	MS3	4.8	All remaining OIS experiments

Figure 2.1: Optimisation of OIS Induction Schedule

Throughout the course of this work, the schedule used for the induction of oncogene-induced senescence has undergone several optimisations (schedule 1, 2 and 3). The bulk of the work has been performed using the optimised schedule 3. However, several key experiments (including the first and second rounds of mass spectrometry – MS1 and MS2) were performed using earlier iterations. This figure illustrates the three schedules in detail along with which experiments (and figures) correspond to which schedule.

2.3 Replicative Senescence Induction

Validation of RS induction in HMFs using a panel of senescence markers has previously been established within the Bishop Lab (section 3.5) and is employed here as a complimentary system to OIS. HMFs were serially passaged from a variety of initial cell stocks (provided by Elly Tyler) at passages ranging from nine to 22. Cells were considered to have reached replicative senescence (RS) at passage 29, as this was the point at which an increase in population doublings was no longer observed. To allow development of a deep senescence (DS) phenotype, with an elaborated and mature SASP, experiments were conducted at passage 29 + three weeks (Passos *et al.*, 2010; Tyler, 2016). By contrast, cells were considered early proliferative (EP) between passages 10 and 16, where cells were readily proliferating, with population doublings (PDs) remaining consistent between weekly passages. For phenotypic assessment, cells were seeded at 10,000 cell/cm^2 and cultured for six days. At this point fixation and immunofluorescence, staining was performed according to section 2.4. For other experiment specific culture conditions, see sections 2.8 and 2.10.

2.4 Immunofluorescence Staining

Immunofluorescence staining was performed in either 6-well or 96-well plates depending on experimental requirements. Cells in culture were fixed through use of 3.7% paraformaldehyde (PFA) comprising 5% sucrose. Fixation occurred at room temperature (RT) for 15 minutes and was both preceded and followed by a Phosphate Buffered Saline (PBS) wash. Permeabilisation of cell membranes was then performed for 15 minutes at RT via a solution of 0.1% Triton X-100, followed by a further PBS wash. In experiments where cellular proliferation and morphology measurements were investigated alone, this was followed by a two hour incubation with both 4',6 -diamidino-2 phenylindole (DAPI) (Sigma UK, D8417, 1µg/µl) and HCS Cell Mask Deep Red (Cell Mask 0.1µg/ml) (Thermo-Fisher UK, C10046,

1:50,000). Where antibody staining was required, an initial 30 minute blocking step using 0.25% (w/v) bovine serum albumin in PBS (PBS/BSA) was employed following permeabilisation. Primary antibody incubations were then carried out overnight at 4°C in working dilutions of PBS/BSA. The following morning, cells were washed at RT with PBS/BSA for 30 minutes followed by RT incubation for two hours with DAPI, Cell Mask and the relevant Alexa Fluor-546 conjugated secondary antibody (1:500, Invitrogen). Final wash steps were then applied, including a 30 minute PBS/BSA incubation followed by three washes in PBS. Plates were then imaged using an IN Cell 2200 automated microscope (GE). A full list of antibodies is included in section 2.17 as a table.

2.5 High Content Analysis (HCA)

Images were acquired through the IN Cell 2200 using magnifications of 10-20X and four fields of view. The images were assessed via the IN Cell Developer software version v1.9.2. (GE) high content analysis (HCA) system. DAPI and Cell Mask staining were used to develop nuclear and cellular image masks respectively. The individual targets comprising these masks were then linked to create a "nucleated cell" target set, upon which subsequent analyses were applied (Figure 2.2). The morphology of nucleated cells was then assessed, according to the measures described in Table 2. Values from each individual measure were used to generate Z-scores relative to the proliferating control. This was performed according to the equation: ***Score =*** *(mean value of three independent experiments for senescent experimental condition – mean value of three independent experiments for proliferating control condition) / Standard Deviation (SD) of proliferating control condition*. The Z-scores were combined in heat maps, in order to illustrate the morphological profile of the imaged cells. In heat maps, forced maximum (+/- five Z-scores) and minimum (+/- one Z-scores) thresholds were applied to facilitate comparison between measures. It is important to emphasise that Z-scores were

not used to determine statistically significant change but rather as an indication of positive or negative modulation of each measure by providing a means of scaling. An overview of the HCA morphology workflow is outlined in Figure 2.3.

Immunostaining for changes in the senescence markers p16, p21, Ki67, IL-6 and IL-8. A comparison between proliferating and senescence conditions was determined by calculating percentage positivity of each marker. This was based upon the raw grey-scale values detected and thresholded based on signal detected in the secondary only control. The presence of senescence-associated heterochromatin foci (SAHFs) was determined through quantitation of nuclei positive for DAPI foci as a percentage of the total nuclear count.

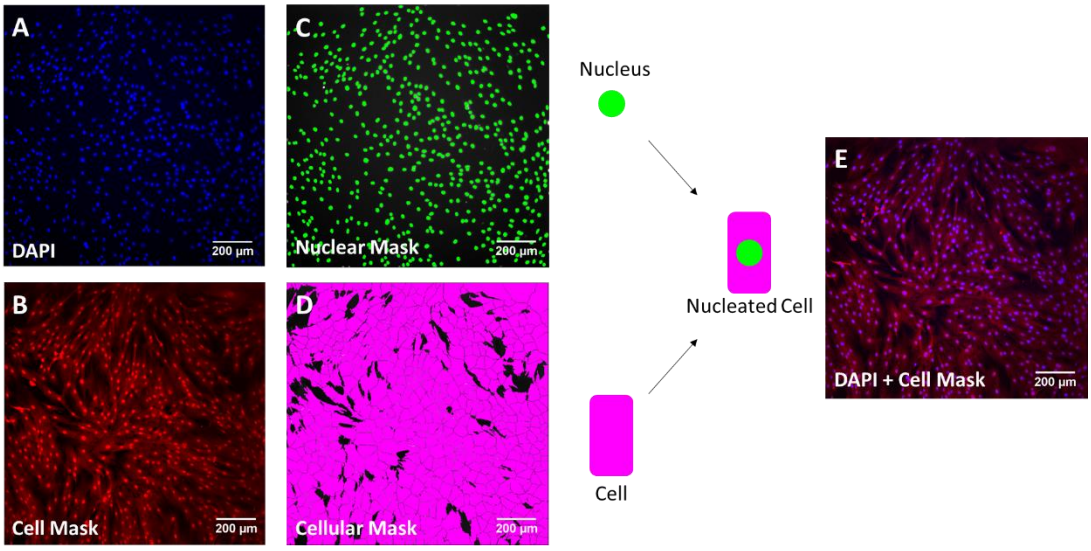

Figure 2.2: Principle of High Content Analysis (HCA)

Following immunofluorescence staining with A) DAPI (blue) and B) Cell Mask (red) (section 2.4) cells were assessed by high content analysis (HCA). Staining was used to generate C) nuclear mask (green) and D) cellular mask (pink) to quantitate nuclei and cells, respectively. These targets were linked into E) "nucleated cell" target set upon which all analysis, including morphological measures (Table 2), was performed. Scale bars = 200µm.

Measure Name	Measure Explanation
Cell Number	Mean Count of Nucleated Cells
Cell Area	Mean Area of Nucleated Cells
Nuclear Area	Mean Area of Nuclei in Nucleated Cells
Cytoplasmic/Nuclear Ratio	Mean Cell Area / Nuclear Area
DAPI Density	Mean DAPI Grey Levels in Nuclear Mask
Nuclear Form Factor	Mean Nuclear Circularity (Ranging 0 -1 where 1 is a circle)
Cellular Protrusions	Mean Count of End Nodes within Nucleated Cells
Cellular Form Factor	Mean Cellular Circularity (Ranging 0 -1 where 1 is a circle)
Major Axis Length	Longest Axis within Nucleated Cell
Minor Axis Length	Shortest Axis within Nucleated Cell
Cellular Elongation	Minor Axis/ Major Axis

Table 2: HCA Morphology Measures

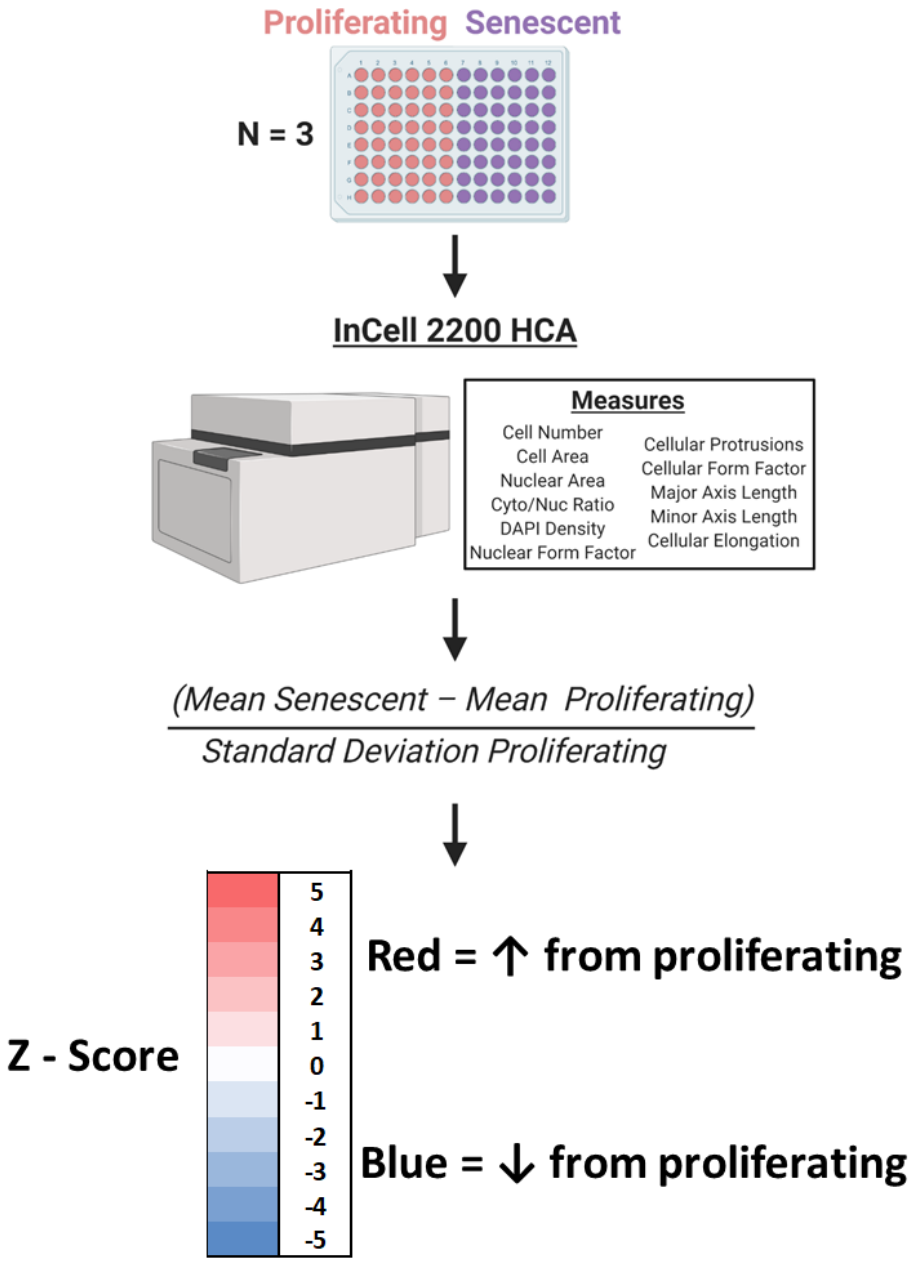

Figure 2.3: Schematic of HCA Morphology Analysis Workflow

Morphological analysis by HCA was used to assess senescence induction. Proliferating and senescent cells from three independent experiments were imaged via the InCell 2200 microscope and images subject to HCA using the InCell Developer software. Morphology measures were quantitated and mean values used to determine Z-Scores (change in standard deviation from the proliferating condition). These were displayed as heat maps with red indicating positive modulation and blue negative modulation from the proliferating condition. White indicates no change.

2.6 Senescence Reversal

The reversal of senescence in RS cells has been demonstrated within the Lab (Lowe *et al.*, 2015) and all siRNAs employed have been previously validated (Table 3) (Thesis:(Tyler, 2016)). Here, both reversal and downstream analysis was carried out in DS HMFs by Kishan Vara, a supervised MSc student. Senescent HMFs seeded at 15,000 cells/cm^2 in 6 well format and were treated with 30nM siRNA using 6.5µl of the transfection reagent Dharmafect 2 (GE Healthcare, UK). Two siRNAs, targeting p16 and p21 respectively, were used in combination for senescence reversal, whilst a fluorescently tagged negative control siRNA targeting cyclophilin B (siGLO) was also employed, having been demonstrated not to alter either the EP or DS phenotype. Cells were reverse transfected on the day of seeding and media changed 24 and 48 hours later. After a further 72 hours had elapsed, cells and associated conditioned media were collected for immunoblotting, qRT-PCR and ELISA assessment.

siRNA (Target)	Accession number	Supplier	siRNA Target sequence
siGLO (PPIB)	NM_000942	Dharmacon, UK	GAGCCCAGAUCAACCUUUA
p16 (CDKN2A)	NM_000077	QIAGEN, UK	TACCGTAAATGTCCATTTATA
p21(CDKN1A)	(Pool of four siRNAs) NM_078467 NM_000389 NM_001220778 NM_001220777 NM_001291549	GE, UK	(Pool of four siRNAs) CTACCTTGAAGCTGAAACA CGCTACCTTGAAGCTGAAA GCTACCTTGAAGCTGAAAC GCTGACACTACGCGATTAC

Table 3: siRNAs Used in Senescence Reversal Protocol

2.7 Quantitative Reverse Transcription Polymerase Chain Reaction (qRT-PCR)

As with the senescence reversal investigations, all qRT-PCR experiments were carried out through supervision of Kishan Vara. Following either application of the reversal protocol or using EP and DS cells, cell lysis was performed using 400µl of QIAzol lysis reagent (Qiagen, UK). RNA extraction was performed using miRNeasy Mini Kit according to manufacturer's instructions (Qiagen, UK). RNA Reverse transcription reactions were carried out using a starting RNA concentration of 100ng/µl prepared in RNase-free water. 3µl of RNA was added to a reaction mixture comprising 1ul each of oligo(dT)18 (50µM; Millipore, UK) and deoxynucleotides triphosphate (10mM; Thermo Scientific, USA) and made up to 13µl with RNase-free water. This reaction was performed at 65°C for 5 minutes, followed by a 5 minute incubation on ice. This reaction mixture was then made up to 20µl through addition of 4µl 5x first strand buffer (Invitrogen, UK), 1µl dithiothreitol (0.1M; Invitrogen, UK), 1µl RNase inhibitor (40u/µl; Invitrogen, UK) and 4 µl superscript III reverse transcriptase (200u/µl; Invitrogen, UK). This mixture was incubated at 50°C for 45 minutes and then at 70°C for 15 minutes to produce cDNA. Standard curve serial dilutions were then prepared for target genes described in Table 3, alongside a previously validated housekeeper control, Glyceraldehyde 3-phosphate dehydrogenase (GAPDH). 2µl cDNA was added to reaction mixtures comprising 12.5µl 2x SYBR Green PCR Master-mix (Applied Biosystems, UK), 0.2µl forward and reverse primers (20µM; Eurofins Genomics, UK) and made up to 25µL using ultrapure water. qRT-PCR was carried out via using 7500 Real-time PCR system (Applied Biosystems, UK) according to the schedule in Table 4. CT values for each target gene was normalised to the GAPDH, which was validated to remain constant between samples.

Target	Sequence (5’ to 3’)	Direction
GAPDH	GGCTGCTTTTAACTCTGG	FWD
	GGAGGGATCTCGCTCC	REV
p21	TGTCCGTCAGAACCCATGC	FWD
	AAAGTCGAAGTTCCATCGCTC	REV
p16	CCAACGCACCGAATAGTTACG	FWD
	GCGCTGCCCATCATCATG	REV
IL-6	AATTCGGTACATCCTCGACGG	FWD
	TTGGAAGGTTCAGGTTGTTTTCT	REV
IL-8	AAGGAAAACTGGGTGCAGAG	FWD
	ATTGCATCTGGCAACCCTAC	REV
IL-1α	AGTGCTGCTGAAGGAGATGCCTGA	FWD
	CCCCTGCCAAGCACACCCAGTA	REV
IL-1β	TGCACGCTCCGGGACTCACA	FWD
	CATGGAGAACACCACTTGTTGCTCC	REV

Table 4: qRT-PCR Primer Sequences

Step	Temperature (°C)	Time	Cycles
Denature	95	10 minutes	1
Denature	95	15 seconds	40
Anneal and Extend	60	1 minutes	
Hold	72		1
Melt Curve	95	15 seconds	1
	60	1 minute	1
	95	15 seconds	1
	60	15 seconds	1

Table 5: qRT-PCR Reaction Protocol

2.8 Extracellular Vesicle Isolation

2.8.1 Differential Ultracentrifugation (dUC)

EVs were isolated from conditioned media generated through a range of conditions. However, in all cases, culture medium was prepared with "exosome-depleted FBS", which was established to contain negligible levels of EVs (Section 4.3). In the OIS model, three induction schedules were utilised as described above, with a range of media volumes collected from varied final cell numbers (**Schedule 1,** 20ml collected from one T150 flask (30ml total), Vector: 8.9e6 cells, OIS: 1.7e6 cells ; **Schedule 2,** 160ml collected from six T150 flasks (180ml total), Vector 5.1e7 cells, OIS: 1.6e7 cells; **Schedule 3**, 80ml collected from three T150 flasks (90ml total), Vector: 6.1e6 cells, OIS: 4.3e6 cells; mean cell numbers).

In the HMF model, a single protocol was used, in which cells were seeded at day zero and cultured to day four. At this point cells were changed to medium containing ExoFBS and cultured for a further 72 hours. At day seven, medium was collected for EV isolation (20ml collected from two T75 flasks or one T150 flask (30ml total), EP: 4.9e6 cells; LP: 1.6e6 cells; mean cell numbers). EP HMFs seeded at 7,500 cell/cm^2 were used alongside cells that were between passage 26 and 28 seeded at 15,000 cells/cm^2. RS was imminent in these cells, having reached close to the maximum number of population doublings observed in HMFs (i.e. passage 29). However, as some level of cellular proliferation persisted, these passages cannot be considered senescent. Therefore, they have been designated as late passage (LP), likely comprising a significant proportion of cells that have entered RS.

The collected media was centrifuged (2,000 *x g*; 4°C; 10 minutes) in order to pellet large EVs such as apoptotic bodies. The resultant supernatant was decanted into 50ml polypropylene tubes (Nalgene UK, 3118-0050) and subject to a high speed centrifugation (10,000 *x g*; 4°C;

30 minutes) in order to remove medium sized EVs including MVs (Sorvall RC6+ High Speed Rotor: SS-34; RPM: 9130; k-factor: 3,598.4). The cleared supernatant was then decanted into 30ml Oak Ridge polycarbonate tubes (Thermo Scientific, UK) and ultracentrifuged (100,000 *x g*; 4°C; one-hour 30 minutes) in order to achieve a population of small EVs enriched for exosomes (Sorvall Discovery 100 SE Rotor: T-865; RPM: 31,300; k-factor: 223.1). The final pellet was resuspended in 250µl sterile PBS.

2.8.2 Size-Exclusion Chromatography (SEC)

In order to concentrate EVs from a large starting volume, dUC was performed according to the protocol described, apart from a modified final resuspension volume of 500µl PBS. This dUC product was then loaded onto qEV original size-exclusion chromatography columns, which were first equilibrated with 10ml sterile PBS (Izon Science, UK). Twenty fractions of 500µl were then collected consecutively as per the manufacturer's instructions, with the first six comprising void volume. Columns were washed with 10ml sterile PBS in-between experiments, and reused a maximum of five times. However, for preparations used in EV treatment experiments, samples were prepared from fresh columns.

2.9 Nanoparticle Tracking Analysis (NTA)

NTA was carried out using the Nanosight NS300 system (Malvern-Panalytical, UK). EV dilutions were prepared in sterile PBS to produce a final volume of 1ml. The magnitude of this dilution was determined by the final particles per frame of captured videos, which were required to be between 15 and 80 particles/frame in order to both generate sufficient particle tracks and avoid particle masking. However, in order to preserve sample volume and enable other methods of analysis, a maximum dilution of 1:50 was used. A minimum of three

60-second videos were acquired at camera level 15, whilst analysis was performed at detection threshold 3 in software version NTA 3.2.

2.10 "Exosome-Depleted FBS" Growth Rate Experiment

EP HMFs were seeded in 6-well plates at 10,000 cell/cm^2. These cells were maintained in standard culture medium until day 4, at which point cells were changed into medium containing 10% "exosome-depleted FBS" or standard FBS as a control. Cells were cultured for a further two days at which point fixation and immunofluorescence staining was performed (section 2.4). Cellular proliferation and morphology characterisation was then carried out according to the processes in section 2.5.

2.11 Freezing Stability Experiment

In order to assess the optimum storage conditions of isolated EV preparations, DMEM 10% FBS was subjected to the dUC EV isolation procedure. Samples were analysed by NTA on the day of isolation in order to determine the concentration of newly prepared samples. Remaining sample volume was then aliquoted and stored at either 4°C or -80°C. After one week, an aliquot from each condition was thawed and assessed by NTA. Following a further 4 weeks, remaining aliquots from each temperature were also assessed by NTA. Samples were disposed of following thawing to avoid the confounding issue of multiple freeze/thaw cycles.

2.12 Western Blotting

2.12.1 Sample Preparation

Whole cell lysates (WCL) were collected through the resuspension of cell pellets using a lysis solution comprising RIPA buffer and 4% protease cocktail inhibitor (Roche, UK). These pellets contained a known cell number via use of a haemocytometer. The lysate was vortexed for 30 seconds and incubated on ice for five minutes, followed by an additional 30 second vortex. Lysate protein concentration was then measured through use of a DC protein assay kit and BSA standard curve (Bio-Rad, UK). Protein concentrations between 2-5µg were then combined with 6X Laemmli sample buffer (Alfa Aesar, UK) and boiled at 95°C for 5 minutes. WCL samples were then ready for loading. Importantly, whilst the majority of WCL samples were prepared with standardised protein concentrations as described, in a number of experiments protein from an equal number of cells was prepared. This was to account for the size differential between proliferating and senescent cells, which results in an equal protein level from a lower number of senescent cells. In such instances, Lamin B1 is used as a loading control in order to demonstrate that observed changes are not due to excessive loading in the senescent condition (Freund *et al.*, 2012). This is not the preferred method of analysis and is clearly indicated where used.

In order to determine the protein concentration of EV samples, microBCA protein assays were performed (Thermo-Fisher, UK). However, as there was no intention to draw direct comparison to WCL samples, EV preparations isolated via dUC were used to produce samples containing an equal number of particles (3e9 particles) prior to loading. In situations where EV particle numbers were limited, such as in preparations isolated by SEC, an equal volume (25µl) of sample was prepared, determined by the maximum loading volume of the gel. EV

samples were then combined with sample buffer and boiled at 95°C for 5 minutes. No direct lysis step was used.

2.12.2 SDS-PAGE and Immunoblotting

Following sample preparation, gels were constructed, and used to separate protein according to size, via the Mini-PROTEAN III system (Bio-Rad, UK). The same system was used to transfer protein to a nitrocellulose membrane (GE, UK). This was then blocked at RT in 0.05% (v/v) Tween-20, 5% (w/v) Marvel semi-skimmed milk in PBS (PBS-T-milk) for one hour. Membranes were then incubated overnight at 4°C with primary antibody prepared in PBS-T-M on a roller. The following morning, HRP-conjugated secondary antibodies appropriate for the primary were then used to incubate the membranes, both preceded and followed by a wash step comprising three PBS-T washes for five minutes on a roller. Membranes were then incubated with Enhanced Chemiluminescence reagent (GE Healthcare, UK) and used to expose photographic film (GE Healthcare, UK). Densitometry was performed using ImageJ software, with intensity in condition of interest normalised to loading control.

2.13 Mass Spectrometry (MS) Analysis

2.13.1 Sample Preparation

All steps described here were performed in collaboration with Natasa Josipovic and Argyris Papantonis (Institute of Pathology, Göttingen) through the CECAD proteomic facility (University of Cologne). EV or CM samples were prepared according to the protocols described in sections 2.8. Samples were combined in an equal ratio with a solution comprising 8M Urea, 50mM Tetraethylammonium bromide (TEAB) and protease cocktail inhibitor. This then underwent a series of 30 second sonication steps, with 30 second rest intervals for 10 minutes. Samples were then centrifuged at 20,000 *x g* for 15 minutes. 5mM Dithiothreitol (DTT) was then added to the collected supernatant, followed by a one-hour incubation at 25°C. Subsequently, 40mM chloroacetamide (Merck, Germany) was added for 30 minutes at 25°C in the absence of light. A 4-hour incubation with 0.1µg/µl of Lysyl Endopeptidase (Wako, Germany) at RT was then performed, followed by 0.1µg/µl Trypsin (Serva, Germany) overnight. The following morning, addition of 1% of formic acid (FA; Honeywell, Germany) was carried out. Sequential washes with methanol (VWR, Germany), 0.1% FA in 80% acetonitrile (Merck, Germany) and 0.1% FA in water were then used to activate stage tips, followed by sample loading. The tips then underwent additional wash steps with 0.1% FA in water and 0.1% FA in 80% Acetonitrile, were left to dry and subsequently stored at 4°C. Label-free mass spectrometry was performed using a nanoHPLC coupled to a Thermo Q-exactive MS/MS. Protein quantification and annotation was performed via MaxQuant, using default settings for label-free detection (Cox and Mann, 2008). For each detected protein, iBAQ intensity values were then converted to LFQ intensities using the Perseus software platform (Tyanova *et al.*, 2016).

2.13.2 Data Analysis

MS data was generated from vector and OIS samples according to the senescence induction schedules described in section 2.2. MS1 utilised triplicate EV samples prepared by dUC from both OIS and vector cells. Generated gene lists were ranked in each condition according to mean label-free quantification (LFQ) values in order to indicate the abundance of each protein. These were also used to determine fold change values from the vector condition. FunRich version 3.1.3 was then used to explore Gene Ontology (GO) terms associated with each sample, with cellular compartment terms ranked based upon the percentage of genes identified. In MS2, CM, SEC fraction 8 and SEC fraction 20 samples isolated from OIS cells were investigated in triplicate. Mean LFQ intensities were calculated for all identified genes in each sample and GO terms were then examined using FunRich as in MS1. In order to further examine the compositional makeup of each sample, localisation classifications were attributed to each gene according to those described in Protein Atlas (www.proteinatlas.org). Each gene was designated as intracellular, membrane or secreted, with genes able to receive multiple designations. Genes identified in each sample were then collated in lists according to Protein Atlas categorisation. Fraction 8 genes were then assessed using the PANTHER DB pathway analysis tool (http://www.pantherdb.org/) in order probe potential functional targets. MS3 utilised the same sample types as MS2 but were collected from both OIS and vector cells. Mean LFQ intensity values were compared through principal component and hierarchical clustering analysis using R version 3.6.3. Each sample type (CM, Fraction 8, Fraction 20) were also compared between vector and OIS conditions in order to calculate mean LFQ intensity fold changes. Finally, GO terms were explored in fraction 8 samples according to predicted cellular compartment within the gene ontology database. MS1, MS2 and M3 data are found in appendices 1, 2 and 3 respectively and a summary schematic may be found in Figure 2.4.

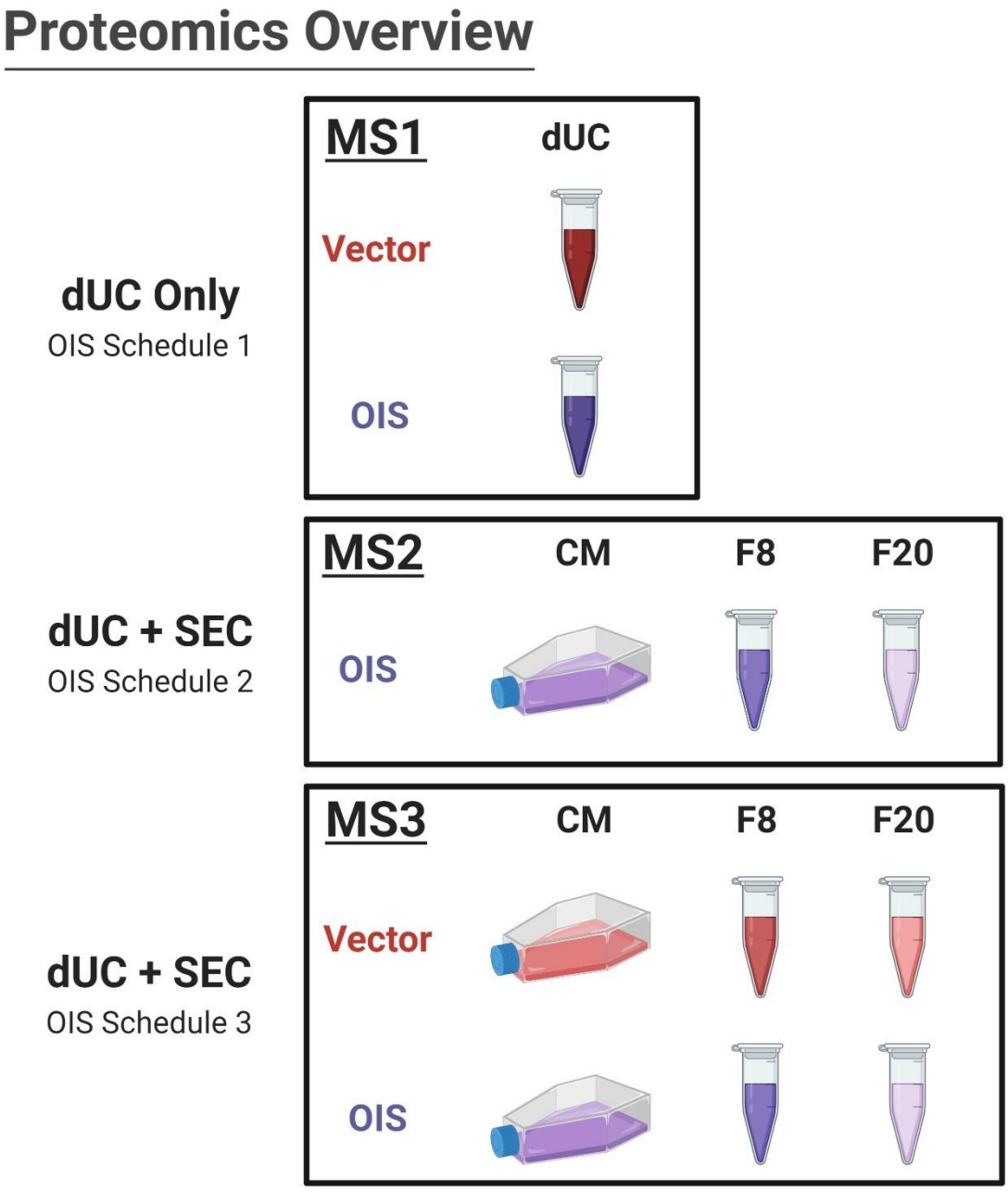

Figure 2.4: Overview of Mass Spectrometry Proteomic Investigations

Three rounds of mass spectrometry were performed (MS1, MS2 and MS3). MS1 investigated EV samples isolated by differential ultracentrifugation (dUC) from vector and OIS IMR90s. MS2 investigated conditioned media (CM) and size-exclusion chromatography (SEC) fractions 8 and 20 (F8 and F20) isolated from OIS IMR90s only. MS3 investigated CM, F8 and F20 from both vector and OIS IMR90s. OIS induction schedules 1-3 are described in Figure 2.1.

2.14 Enzyme-Linked Immunosorbent Assay (ELISA)

Conditioned media samples were generated according to the senescence induction and EV isolation schedules described in sections 2.2, 2.3 and 2.8. Following a clearance centrifugation step of 2000 *x g,* media was analysed through use of commercial ELISA sets (R&D Systems, Human IL-6 DuoSet ELISA DY206; R&D Systems, Human IL-8 DuoSet ELISA DY208). EV samples were prepared according to the protocols in section 2.8 and analysed with the same ELISA kits without pre-application of lysis. Analytes were assessed at an absorbance of 450/570nm via a CLARIOstar Plus multi-mode plate reader (BMG Labtech).

2.15 Conditioned Media and EV Treatment Investigations

Treatment experiments were performed with conditioned media and EV samples in several contexts. Figure 2.5 summarises the treatment regimens, including dosing schedule and treatment volumes.

2.15.1 Conditioned Media Investigations

Conditioned media (CM) samples were prepared from OIS cells according to the conditioning and clearance protocols described in section 2.8. For HMFs, EP cells were seeded at 6,785 cell/cm^2 and DS at 25,477 cell/cm^2 in order to achieve a final cells per microlitre of condition media comparable to that described in (Acosta *et al.*, 2013). In investigations using IMR90s and HMFs, the CM was combined in a 3:1 ratio with a 4X cocktail of medium components comprising 40% FBS DMEM and 8mM L-glutamine, in accordance with the protocol described in (Acosta *et al.*, 2013). Control medium was composed of serum free DMEM supplemented with the 4X cocktail. Vector IMR90 or EP HMFs were seeding in 96 well plates at 10,000 cells/cm^2. These were treated with 120µl of CM + 4x cocktail. Treatment was performed one

day after cell seeding and repeated following an additional 72 hours. After cells were cultured for a further 48 hours, fixation and staining was carried out according to the protocol described in section 2.4. Due to differences in standard culture medium, the MDA-MB-468 treatment experiments were performed with some modification. The vector and OIS media was collected and cleared as described in section 2.8. However, a dose of 10µl CM was added to each well of 468s seeded at 10,000 cells/cm^2 with an identical dose regime to the IMR90/HMF investigations.

2.15.2 Extracellular Vesicle Treatment Investigations

Following isolation through SEC, EV samples were used to treat IMR90 or 468 cells cultured in 96-well plates. In all cases cells were seeded at 10,000 cells/cm^2 and doses of 10µl per well were applied in addition to 120µl of appropriate standard culture media. Dosing regimens were identical to those of conditioned media investigations, with doses at 24 and 96 hours post-seeding. Assessment by HCA was then performed following the standard fixation procedure. EV samples used in these experiments included fraction 8 and 20 from OIS and fraction 8 from vector IMR90s, whilst a PBS vehicle control was included in each experiment.

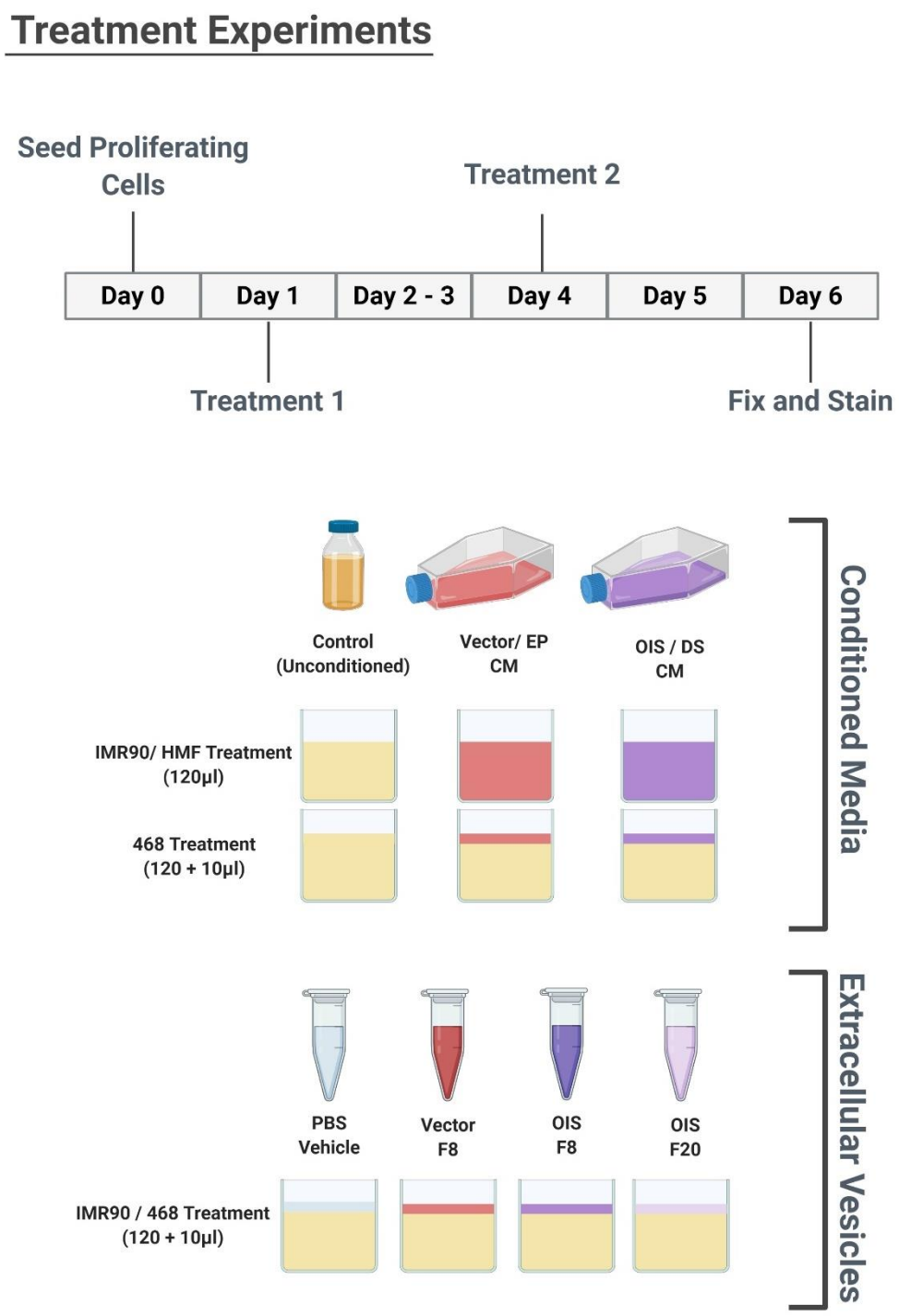

Figure 2.5: Treatment Experiment Summary

2.16 NOTCH1/ADAM Inhibitor Conditioned Media Experiments

IMR90 vector and OIS cells were cultured in 6-well plates and subject to the final OIS induction schedule described in section 2.2 with some modification. At day four, cells were treated with either 500nM of the ADAM17 inhibitor TMI005, 10µM of the γ-secretase inhibitor DAPT or DMSO vehicle control. DAPT was selected as a potent inhibitor of NOTCH1 signalling that has previously been utilised in a senescence setting (Hoare *et al.*, 2016). TMI005 has been reported as a potent inhibitor of ADAM17 but it important to acknowledge that the compound also inhibits MMPs (Shu *et al.*, 2011; Richards *et al.*, 2012). Cells were cultured for a further four days at which point conditioned media was collected and prepared in accordance with the protocol described in section 2.15.1. MDA-MB-468 cells were then treated with conditioned media according to the schedule also described in section 2.15.1. It is important to note that this experiment was only performed with N=1, with one technical replicate on conditioning plate and four on treatment plate.

2.17 Statistical Analysis

GraphPad Prism version 7 was used to conduct all statistical tests, details of which may be found in figure legends. As standard, unpaired Student's t-test and Ordinary One-way ANOVA analyses were used, in order to compare means between two and multiple conditions, respectively. Tukey's post-hoc tests were performed following ANOVA, in order to make multiple comparisons between conditions. Statistical significance was defined according to the following p value representations: ∗ $p < 0.05$; ∗∗ $p < 0.01$; ∗∗∗ $p < 0.001$; ∗∗∗∗ $p < 0.0001$. Unless otherwise stated, error bars represent standard deviation (SD) of ≥3 independent experiments with at least three technical replicates throughout.

2.18 Diagrams and Schematics

All diagrams and schematics have been prepared using BioRender – www.biorender.com

3 Results 1: Establishing Models of Senescence and Characterising Phenotype

3.1 Introduction

As described in section 1.1, senescence is a terminal cell fate characterised by a loss of cellular proliferation in response to a variety of potential harmful stimuli. These stimuli have been demonstrated to drive a context dependent response, with the emergent phenotype dependent not only on the particular senescence trigger, but also on the cell type under insult. Consequently, this leads to varied secretory profiles emerging between different models of senescence, with the SASP driven by both cell type and senescence inducer. Whilst this is true of *in vitro* models of senescence, it becomes of greater significance when considering the consequences of senescence *in vivo,* where specific types of senescence in specific cells/tissues contribute to a diverse range of biological responses (section 1.1.9). Therefore, senescence cannot be considered a single uniform phenomenon and, as such, it is useful to employ a variety of experimental models when investigating it.

Oncogene-induced senescence (OIS) is one of the most widely applied models of senescence and has a well-characterised and potent SASP (section 1.1.6). A popular system for studying OIS involves expression of oncogenic HRas in IMR90 foetal lung fibroblasts, often coupled to the oestrogen receptor (ER) in an inducible fusion protein system (section 2.2). This allows investigation of OIS in an expedient manner, whilst also generating a robust and well-described phenotype. By contrast, the induction of replicative senescence (RS) in primary adult cells is a more laborious endeavour and less widely used. These cells must be serially passaged over many months until observable population doublings stop as cells reach their Hayflick limit (section 1.1.5). The rationale for investigating senescence in this protracted

experimental system is to recapitulate a phenotype reflective of ageing in adult cells. Therefore, both models have advantages and limitations but provide useful complimentary systems in which to study the broad phenomena of “premature” and “replicative” senescence. The *ER:RAS* model of OIS and a primary adult human mammary fibroblast (HMF) model of RS are used here.

Finally, as a potentially useful experimental tool, the process of senescence reversal was also investigated (section 1.1.8). In conjunction with the model of RS, siRNA inhibition of key tumour suppressors p16 and p21 were used to rejuvenate deeply senescent cells. This work was performed through supervision of a Regenerative Medicine MSc student, Kishan Vara and based upon work established previously within the lab by Elly Tyler (Thesis:(Tyler, 2016)).

Overall, by setting up these experimental systems and characterising the senescence phenotypes, the next set of experiments investigating the extracellular vesicle (EV) component of the SASP were facilitated.

3.2 Chapter Hypothesis and Aims

The aim of this chapter was to establish models of senescence in order to facilitate the subsequent isolation of EVs. Expression of an inducible HRas construct in IMR90 fibroblasts and serial cultivation of adult human mammary fibroblasts (HMFs) were hypothesised to generate models of oncogene-induced (OIS) and replicative (RS) senescence, respectively. Validation of senescence induction was performed through characterisation of canonical senescence markers along with a high content analysis (HCA) based screening assessment of senescence-associated morphological changes. The acquisition of a senescence-associated secretory phenotype (SASP) was also investigated in both models. Finally, use of a previously validated siRNA reversal protocol in RS HMFs was hypothesised to attenuate expression of the SASP and investigated though supervision of an MSc student.

The aims of this chapter are as follows:

- To characterise oncogene-induced senescence (OIS) in IMR90 HRas:ER fibroblasts.
    - To validate loss of cellular proliferation and changes in canonical senescence markers by high-content analysis (HCA) microscopy
    - To establish a high-throughput, unbiased set of morphological measures to characterise senescence induction
    - To validate the OIS SASP

- To characterise replicative senescence (RS) in primary adult human mammary fibroblasts (HMFs)
    - To validate RS induction by HCA

- To establish the SASP of RS HMFs

- To characterise senescence reversal in RS HMFs through use of siRNA
  - To validate the re-establishment of cellular proliferation and ablation of canonical senescence markers
  - To characterise the secretome of rejuvenated HMFs

3.3 Characterising the Oncogene- Induced Senescence (OIS) Phenotype of IMR90 HRas:ER Fibroblasts

Oncogene-induced senescence (OIS) has been widely modelled through use of an inducible HRas:ER fusion protein construct in IMR90 foetal lung fibroblasts. The validation of senescence induction generally requires the observation of changes in a panel of senescence markers, as no single marker is considered universal. Here, the expression of tumour suppressor proteins (p21 and p16) were combined with assessment of cellular proliferation (reduction in cell number and Ki67 expression) as well as the acquisition of senescence-associated heterochromatin foci (SAHFs). These canonical markers of senescence induction were complimented with an unbiased high-content analysis assessment of changes in cellular and nuclear morphology. Cell area has been widely reported to increase with senescence induction, with senescent cells previously described as having an enlarged, flattened morphology (section 1.1.3.3). Furthermore, acquisition of enlarged irregular nuclei with low DAPI staining have been previously used to identify senescent cells (section 1.1.3.4). Here, these features were assessed using a range of morphological measures, in order to establish a senescence-associated morphological profile. Overall, these markers were considered as a collective in order to assess the induction of OIS.

Firstly, whole cell lysate (WCL) was collected from vector control and OIS cells at day eight of the OIS induction schedule. Day eight was selected following extensive optimisation of the OIS induction schedule (section 2.2), which sought to balance the seeding density and proliferation of the vector control cells (and thus prevention of contact inhibition) with development of an OIS phenotype. In particular, the elaboration of a SASP (section 3.4). Immunoblotting was then performed in order to assess the expression of the tumour suppressors p21 and p16. The OIS WCL was associated with an increased expression of both

these canonical senescence markers compared to the vector control (vector p21, 0.07 ± 0.01 a.u.; OIS p21, 0.72 ± 0.10 a.u.; vector p16, 0.02 ± 0.01 a.u.; OIS p16, 0.43 ± 0.10; Figure 3.1 A-D). This provided evidence that the senescence induction protocol led to an increase in tumour suppressor expression, as previously reported (Serrano et al., 1997). The next step was to assess the localisation of these proteins and combine with additional senescence markers.

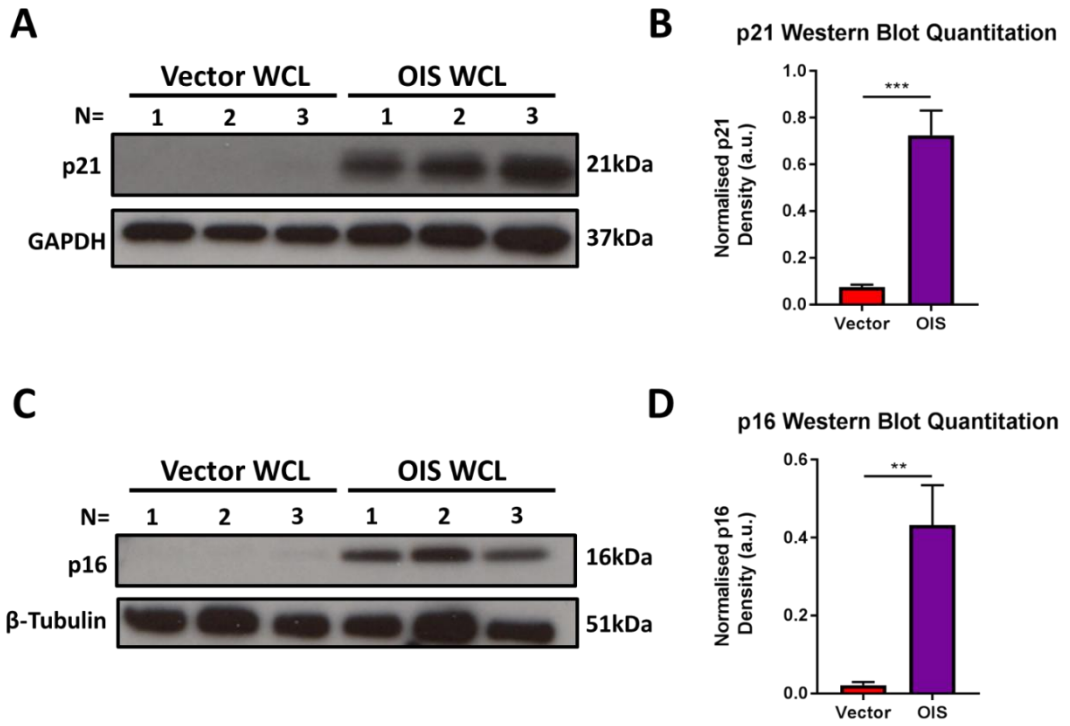

Figure 3.1: Western blot analysis of canonical senescence markers p21 and p16

Immunoblot analysis of whole cell lysate (WCL) from vector and OIS IMR90s for senescence markers p21 and p16. A-B) Immunoblot and densitometry quantitation for p21 and GAPDH loading control. C-D) Immunoblot and densitometry quantitation for p16 and β-tubulin loading control. Each lane contains a sample prepared during an independent experiment. N=3 independent experimental replicates (1 technical replicate per experiment). Quantitation performed via Image J with normalisation to loading control in each lane. Statistical analysis performed via unpaired Student's t-test (section 2.17).

Next, vector and OIS cells were passaged into 96 well plates on day eight of the induction schedule. These were then cultured to day 13 at which point the plates were fixed. Immunofluorescence staining was then used to assess the induction of senescence. HCA assessment demonstrated a reduction in cell number in the OIS cells compared to the vector control (vector, 4631 ± 535.7; OIS, 909.8 ± 184.4; Figure 3.2A). Cellular morphology was visualised using the nucleic acid dyes DAPI and Cell Mask. HCA analysis was used to unbiasedly assess a panel of 10 morphological measures (Figure 3.2B): cell area (vector, 922.2 ± 63.64μm^2; OIS, 3951±695.6 μm^2), nuclear area (vector, 206.6 ± 0.7219 μm^2; OIS, 303.2 ± 10.53 μm^2), cytoplasmic/nuclear ratio (vector, 3.514 ± 0.2925; OIS, 12.76 ± 2.449) , DAPI density (vector, 4760 ± 216.9 a.u.; OIS, 3173 ± 170.6 a.u.), Nuclear form factor (vector, 0.7936 ± 0.01385; OIS, 0.7514 ± 0.01378), cellular protrusions (vector, 4.403 ± 0.3185; OIS, 16.82 ± 0.695), cellular form factor (vector, 0.6371 ± 0.278; OIS, 0.3085 ± 0.01248), Major axis length (vector, 42.11 ± 1.4 μm; OIS, 86.29 ± 6.877 μm), minor axis length (vector, 24.41 ± 0.5097 μm; OIS 42.43, ±3.525 μm) and cellular elongation (vector, 0.58 ± 0.008918 ; OIS, 0.49 ± 0.002648), all of which were found to significantly change in the OIS cells compared to the vector control. This demonstrates that the use of HCA allows assessment of a large number of morphological parameters, of which OIS cells produced a district profile. To increase the applicability of this to other models of senescence induction, as well as compare between different measures, Z-scores were calculated based on the standard deviation from the control cells for each parameter (section 2.5). This method of analysis allows a broad assessment of senescence induction to be made based upon “senescence-associated” changes in morphological characteristics (Figure 3.3). In order to validate this approach, it was important to assess additional canonically described senescence markers.

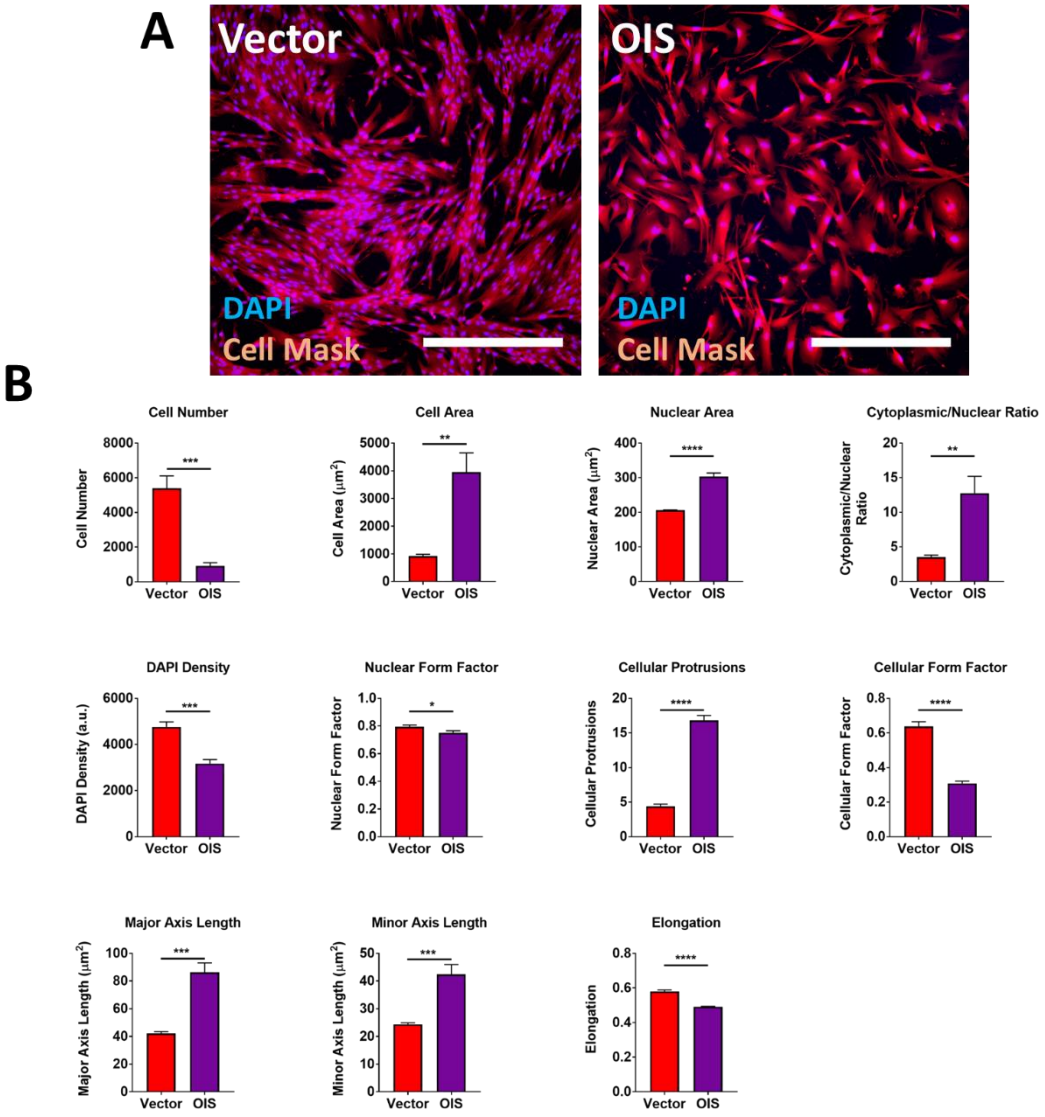

Figure 3.2: High Content Analysis (HCA) of oncogene-induced senescence proliferation and morphology

HCA analysis was performed on vector and OIS IMR90s to assess a panel of morphological measures. A) Representative immunofluorescence images for DAPI (blue) and Cell Mask (red) staining in OIS and vector control IMR90s following senescence induction. B) Quantitation of HCA cell number and morphology measures. N=3 independent experimental replicates (3 technical replicates per experiment). Statistical analysis performed via unpaired Student's t-test per measure (section 2.17). Scale bars = 250µm. Four fields of view.

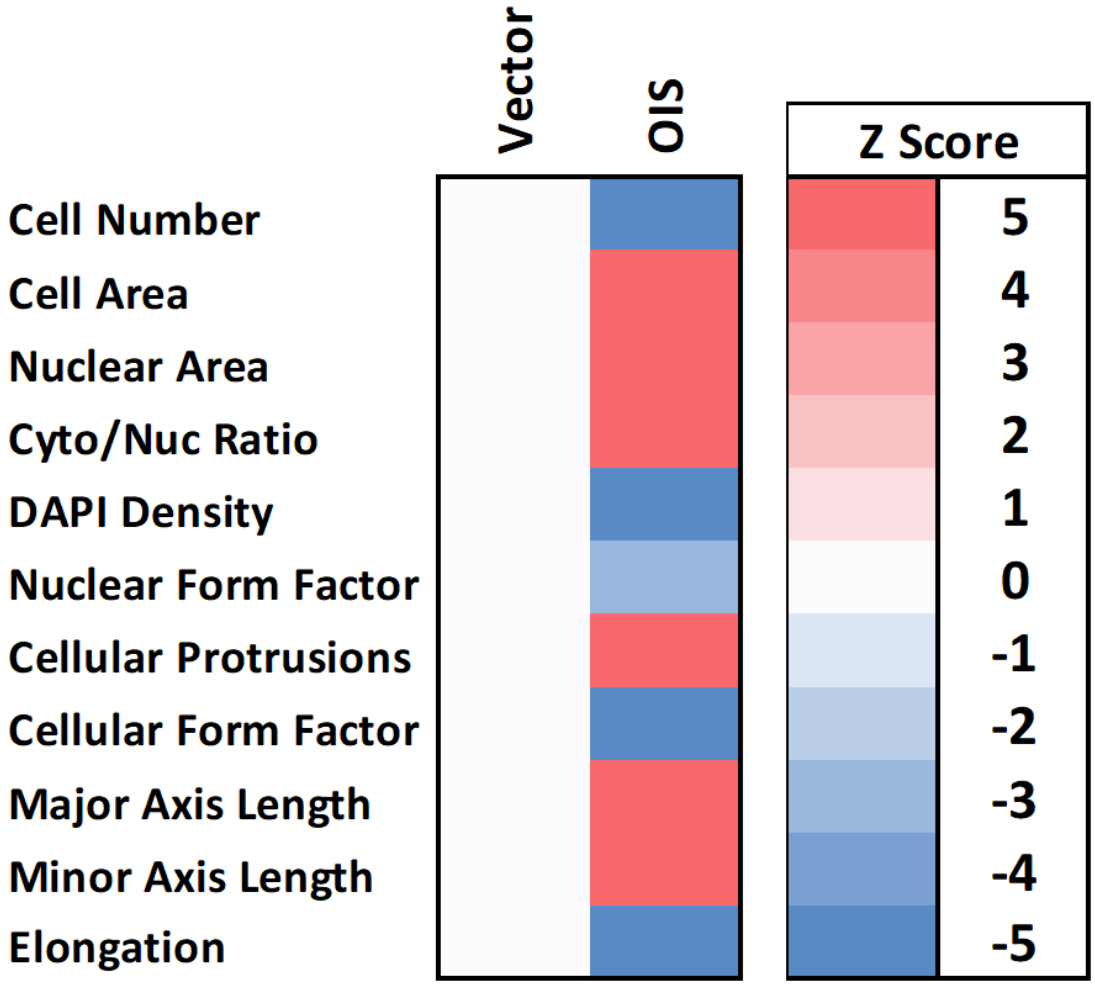

Figure 3.3: Heat map showing from morphological measure Z-scores following oncogene-induced senescence induction in IMR90 fibroblasts

HCA morphological measures were converted to Z-scores according to the change from the vector control condition (section 2.5). Positive and negative modulation of each measure is demonstrated by a change of at least +/- one Z-score (standard deviation) from the vector condition and indicated as red (increase) or blue (decrease), respectively. White indicates no change from the control. N=3 independent experimental replicates (3 technical replicates per experiment)

Having established through immunoblotting that the tumour suppressors p21 and p16 were upregulated in the OIS cells following induction, immunofluorescence staining was performed in order to visualise the localisation of these proteins. Both nuclear p21 and p16 were demonstrated to increase within the OIS cells (p21, 72.83 ± 9.835 percentage positive; p16, 99.05 ± 0.686 percentage positive; Figure 3.4 and 3.5) when compared to the proliferative control (p21, 29.11 ± 3.291 percentage positive; p16, 28.27 ± 10.35 percentage positive; Figure 3.4 and 3.5). Impaired cellular proliferation had been established in the OIS cells, as demonstrated by a reduction in cell number, and was further supported by a reduction in Ki67 staining compared to the vector control (vector, 45.35 ± 4.853 percentage positive; OIS, 4.755 ± 3.68 percentage positive; Figure 3.6). Finally, the presence of SAHFs was investigated, as these are often seen as a more specific marker of OIS. The number of foci was assessed per nuclei in brackets of 1-3 (vector, 1.29 ± 0.89%; OIS, 26.41 ± 1.57%), 4-6 (vector, 0.25 ± 0.23%; OIS, 23.54 ± 1.62%), 7-9 (vector, 0.06 ± 0.06%; OIS, 17.67 ± 0.80%) and 10+ (vector, 0.02 ± 0.02%; OIS, 9.15 ± 1.23%) (Figure 3.7). Each group saw significantly more foci in the OIS cells than the vector control. Therefore, assessment of canonical senescence markers demonstrated the successful induction of OIS. Importantly, these were supported by a HCA based morphological panel, which was employed to establish the induction of a senescence-associated morphology in subsequent experiments. Overall, it was concluded that the OIS induction schedule was successful in producing a canonical senescence response. The secretory phenotype of the OIS cells was then investigated.

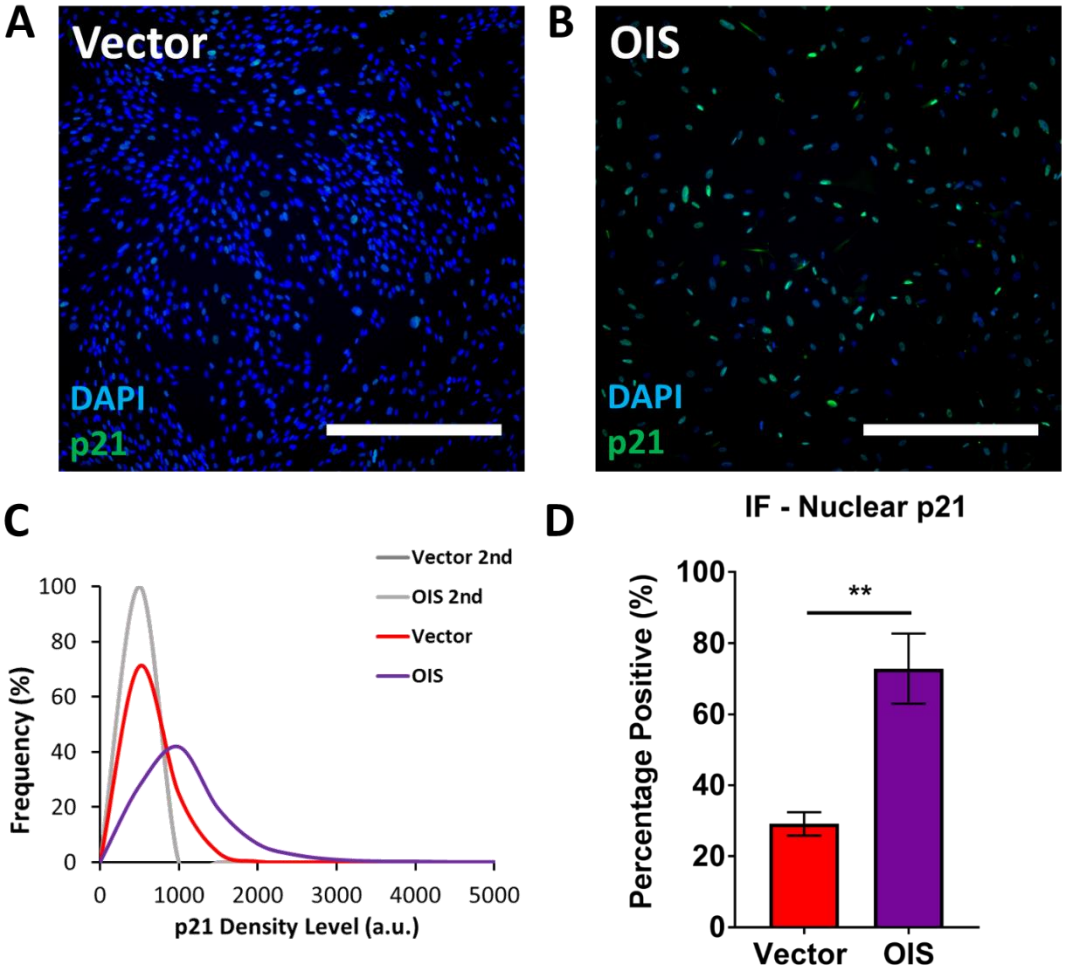

Figure 3.4: Immunofluorescence staining by high-content microscopy of senescence marker p21

Immunofluorescence staining for p21 was assessed in vector and OIS IMR90s. **A-B)** Representative images for DAPI (blue) and p21 (green) staining in OIS and vector control IMR90s following senescence induction. **C)** Frequency distribution of p21 density levels in all targets, including secondary only control conditions (2nd). **D)** Quantitation of p21 nuclear staining percentage positivity compared to secondary only control. N=3 independent experimental replicates (3 technical replicates per experiment). Statistical analysis performed via unpaired Student's t-test (section 2.17). Scale bars = 500µm. Four fields of view.

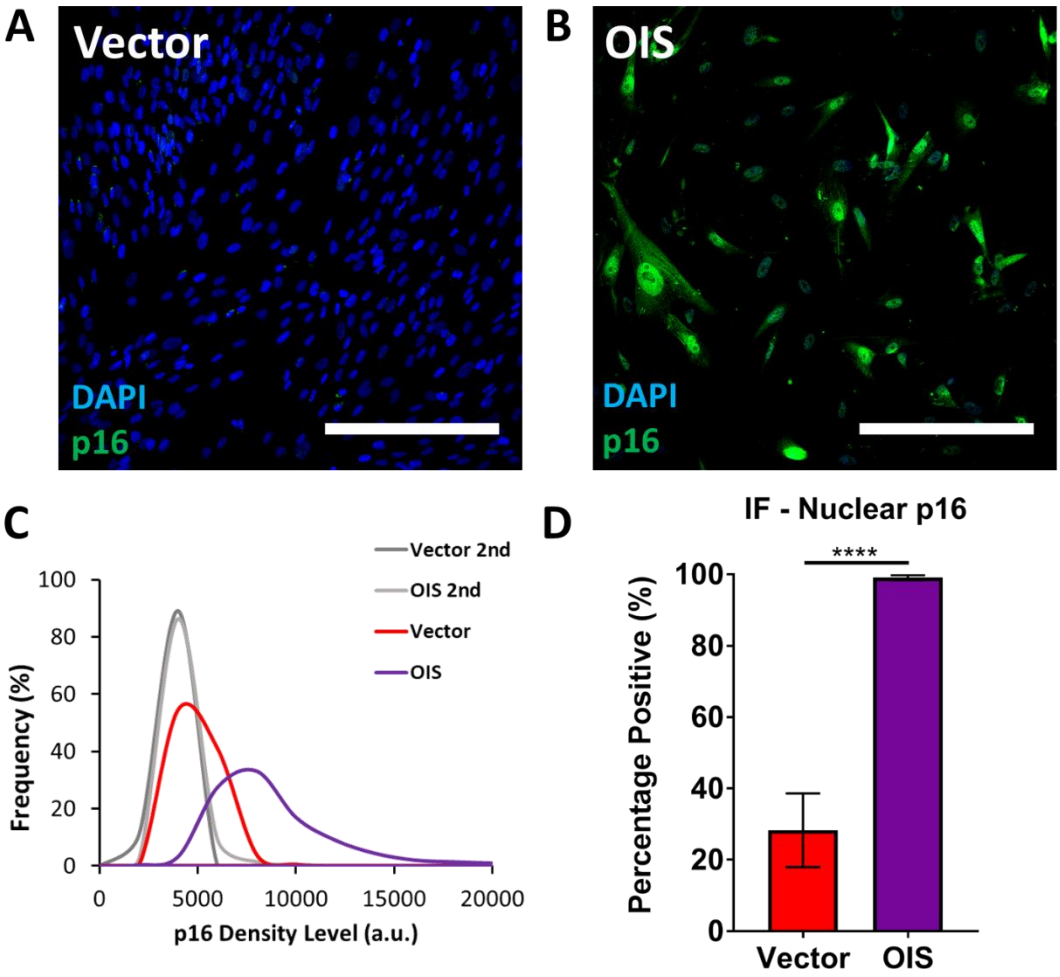

Figure 3.5: Immunofluorescence staining by high-content microscopy of senescence marker p16

Immunofluorescence staining for p16 was assessed in vector and OIS IMR90s. **A-B)** Representative images for DAPI (blue) and p16 (green) staining in OIS and vector control IMR90s following senescence induction. **C)** Frequency distribution of p16 density levels in all targets, including secondary only control conditions (2nd). **D)** Quantitation of p16 nuclear staining percentage positivity compared to secondary only control. N=3 independent experimental replicates (3 technical replicates per experiment). Statistical analysis performed via unpaired Student's t-test (section 2.17). Scale bars = 250µm. Four fields of view.

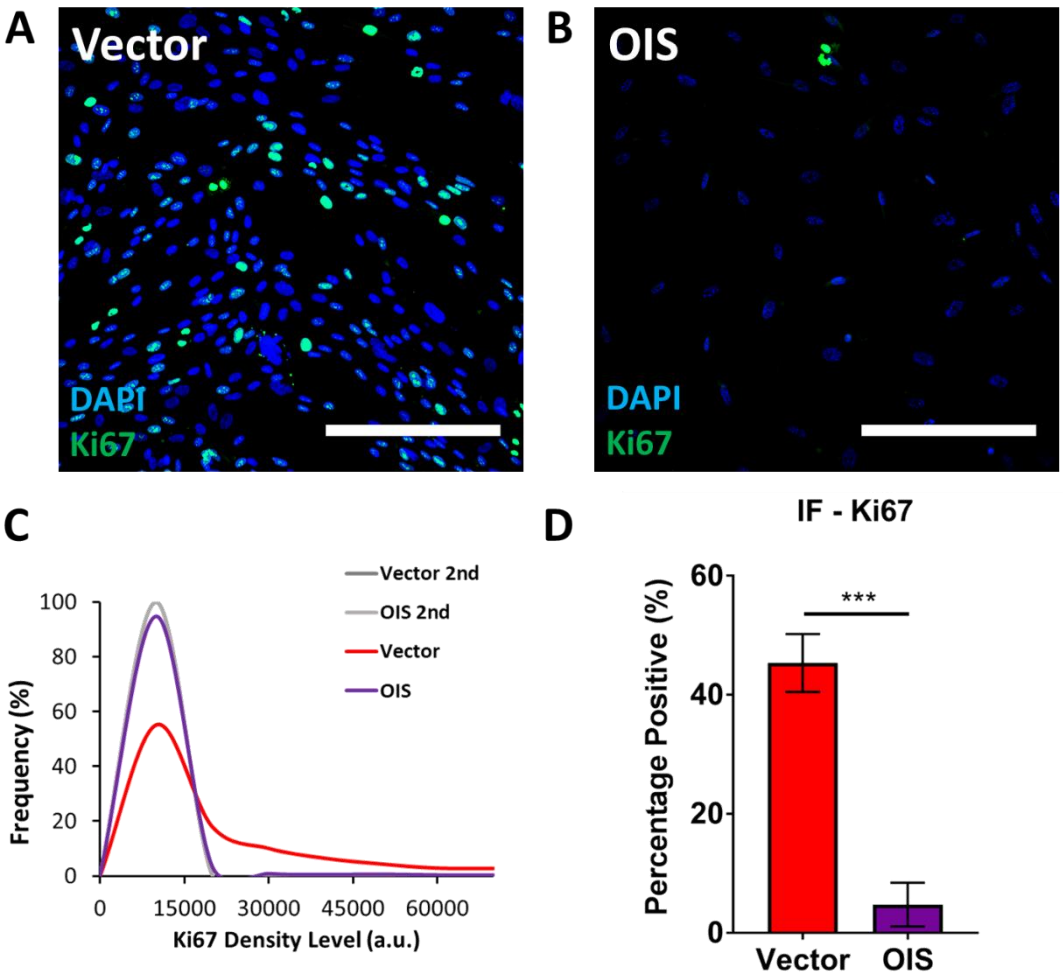

Figure 3.6: Immunofluorescence staining by high-content microscopy of proliferation marker Ki67

Immunofluorescence staining for Ki67 was assessed in vector and OIS IMR90s. **A-B)** Representative images for DAPI (blue) and Ki67 (green) staining in OIS and vector control IMR90s following senescence induction. **C)** Frequency distribution of Ki67 density levels in all targets, including secondary only control conditions (2nd). **D)** Quantitation of Ki67 staining percentage positivity compared to secondary only control. N=3 independent experimental replicates (3 technical replicates per experiment). Statistical analysis performed via unpaired Student's t-test (section 2.17). Scale bars = 250µm. Four fields of view.

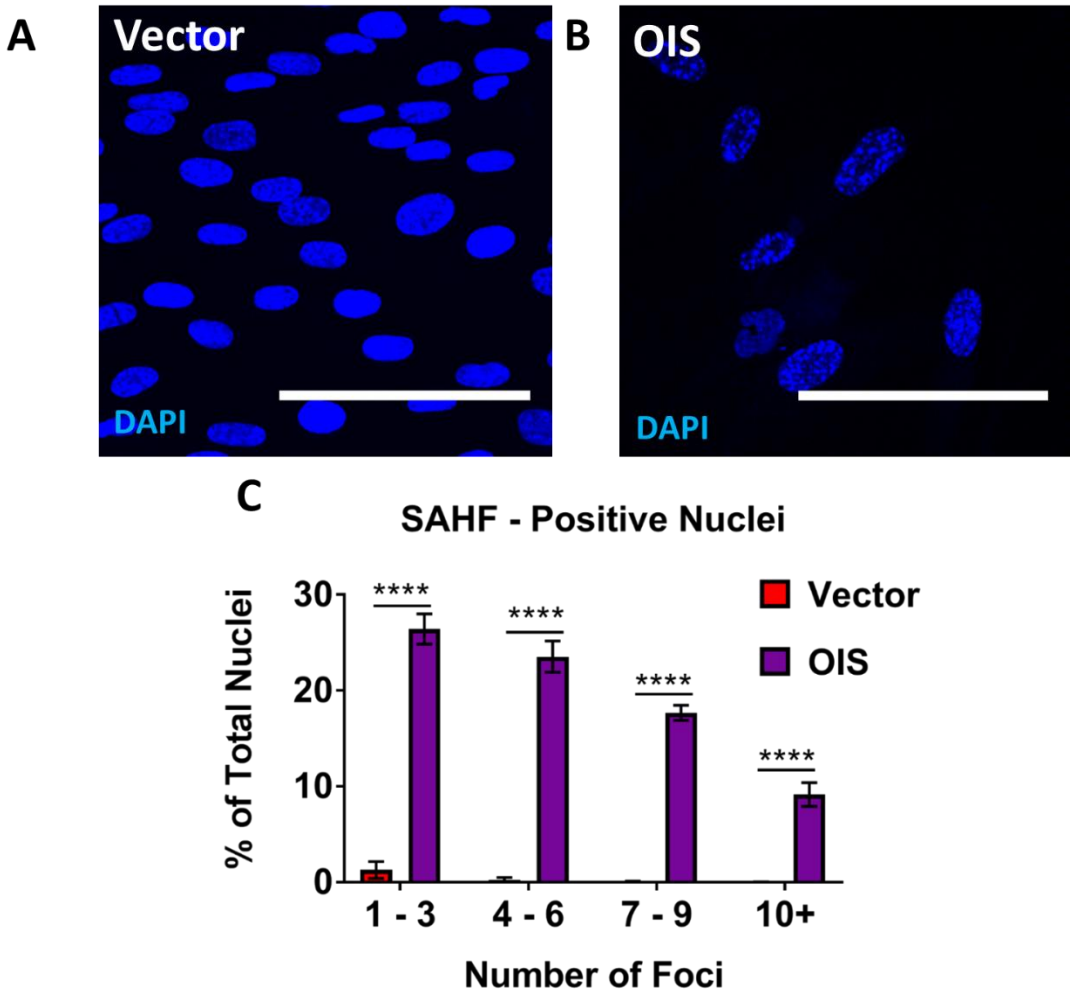

Figure 3.7: Immunofluorescence staining by high-content microscopy of senescence-associated heterochromatin foci (SAHF)

Immunofluorescence staining for SAHF was assessed in vector and OIS IMR90s. **A-B)** Representative images for DAPI (blue) staining in OIS and vector control IMR90s following senescence induction. **C)** Quantitation of nuclei positive for at least one foci as a percentage of the total nuclei in that condition. N=3 independent experimental replicates (3 technical replicates per experiment). Statistical analysis performed via unpaired Two Way ANOVA with Bonferroni's post-hoc test (Section 2.17). Scale bars = 125µm. Four fields of view.

3.4 Characterising OIS Senescence Associated Secretory Phenotype (SASP)

One of the key hallmarks of senescence induction is the acquisition of an enhanced secretory phenotype, the SASP. The SASP of OIS cells has been extensively investigated, with IL-6 and IL-8 frequently described as canonical markers (section 1.1.4). WCL from vector and OIS cells was assessed for these SASP components by immunoblotting. Both IL-6 and IL-8 were exclusively seen in the WCL from OIS cells. Whilst the IL-8 can confidently be described as increasing with senescence induction (vector, 0.02 ± 0.01 a.u.; OIS, 2.36 ± 1.08 a.u.; Figure 3.8), the IL-6 blot must be treated with some caution. This is because Lamin B1 was also assessed as the IL-6 blot loaded according to cell number. As Lamin B1 is downregulated in senescence, the rationale for its use as a loading control is to demonstrate that wells have not been overloaded (section 2.12). As this downregulation was not demonstrated, a conclusion cannot be drawn concerning the change in IL-6 based on this blot.

Next, immunofluorescence staining was performed, in order to determine the localisation of SASP proteins within the OIS cells. Whilst IL-8 was demonstrated to increase in OIS (vector, 2.256 ± 2.701 percentage positive; OIS, 31.95 ± 7.107 percentage positive; Figure 3.10), there was no observable difference between the OIS and vector cells in terms of IL-6 expression (vector, 23.72± 13.68 percentage positive; OIS, 33.49 ± 21.56 percentage positive; Figure 3.9). However, analysis was confounded by intra-experimental variability, so conclusions regarding IL-6 expression in OIS were not drawn. Whilst IL-8 data had thus far supported the literature, increased in IL-6 with OIS induction has not yet been demonstrated. Therefore, attention turned to assessing the secreted form of the proteins.

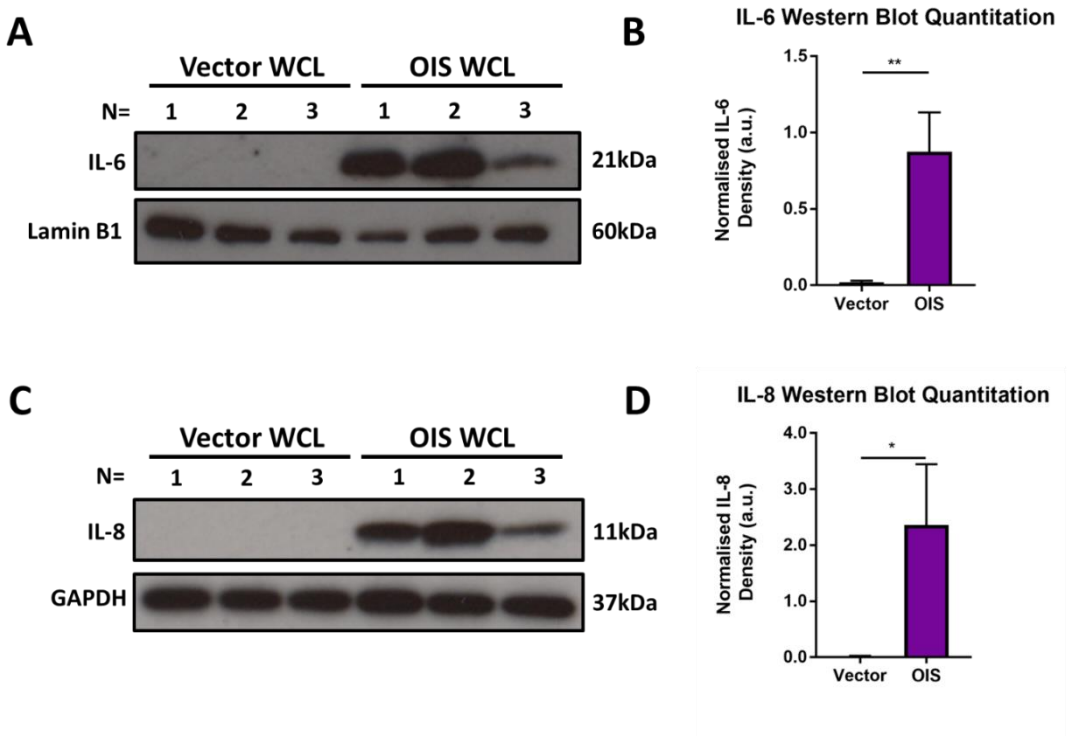

Figure 3.8: Western blot analysis of the canonical SASP markers IL-6 and IL-8

Immunoblot analysis of whole cell lysate (WCL) from vector and OIS IMR90s for senescence-associated secretory phenotype (SASP) markers IL-6 and IL-8. **A-B)** Immunoblot and densitometry quantitation for IL-6 and Lamin B1 loading control. **C-D)** Immunoblot and densitometry quantitation for IL-8 and GAPDH loading control. Each lane contains sample prepared during an individual experiment. N=3 independent experimental replicates (1 technical replicate per experiment). Quantitation performed via Image J with normalisation to loading control in each lane. Statistical analysis performed via unpaired Student's t-test (section 2.17).

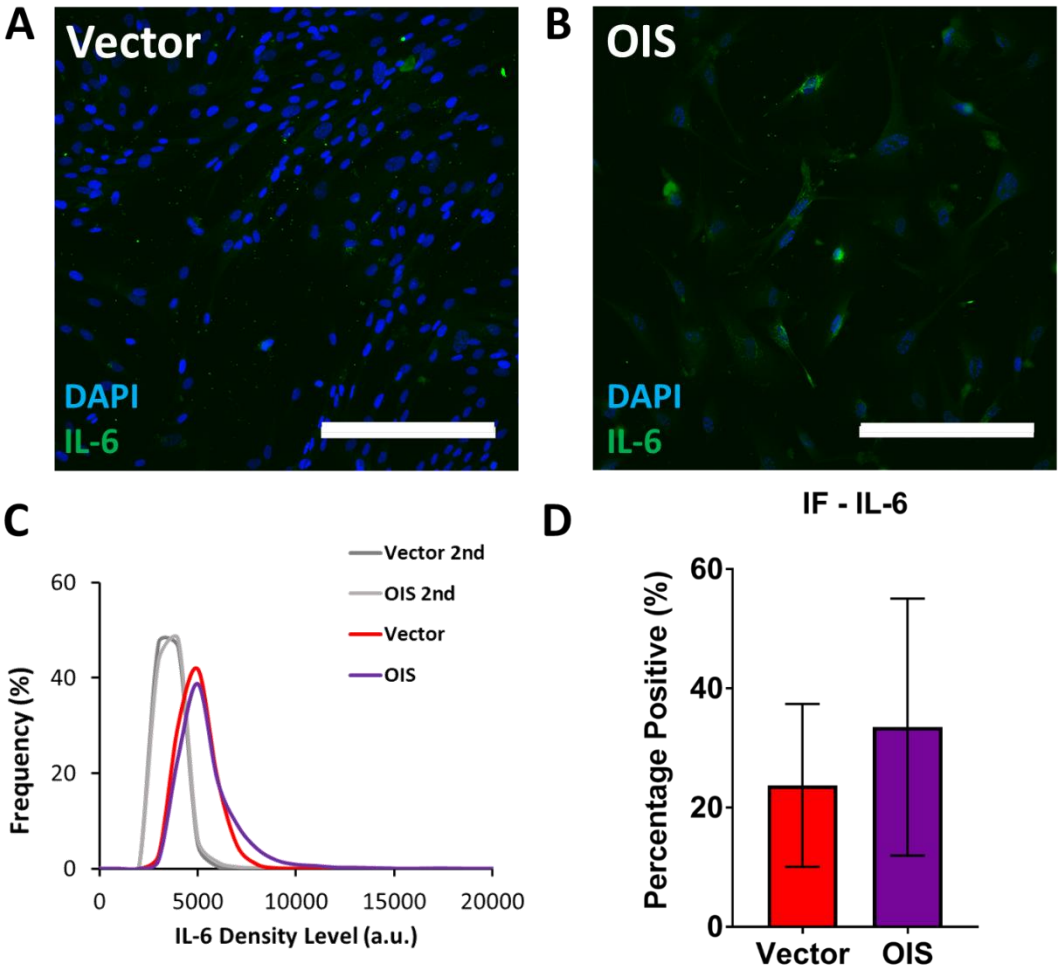

Figure 3.9: Immunofluorescence staining by high-content microscopy of SASP marker IL-6

Immunofluorescence staining for IL-6 was assessed in vector and OIS IMR90s. **A-B)** Representative images for DAPI (blue) and IL-6 (green) staining in OIS and vector control IMR90s following senescence induction. **C)** Frequency distribution of IL-6 density levels in all targets, including secondary only control conditions (2nd). **D)** Quantitation of IL-6 staining percentage positivity compared to secondary only control. N=3 independent experimental replicates (3 technical replicates per experiment). Statistical analysis performed via unpaired Student's t-test (section 2.17). Scale bars = 250µm. Four fields of view.

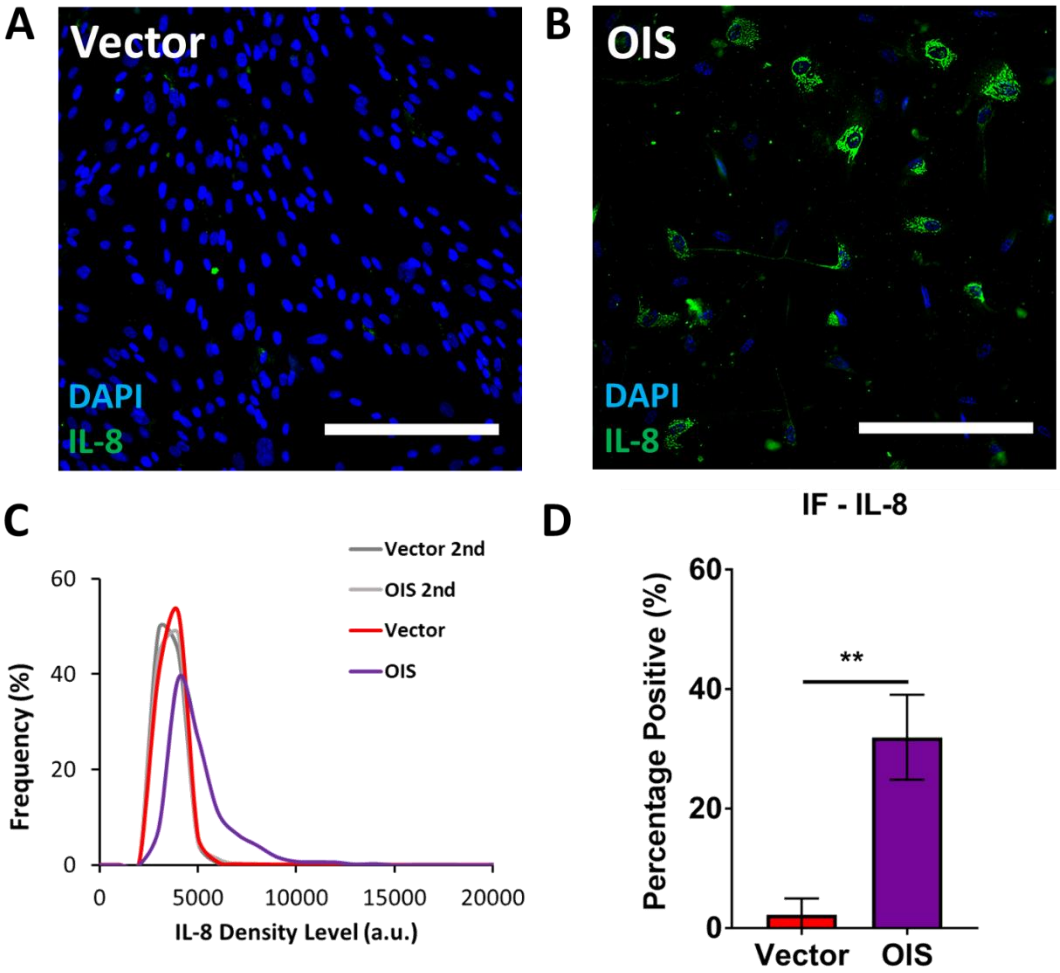

Figure 3.10: Immunofluorescence staining by high-content microscopy of SASP marker IL-8

Immunofluorescence staining for IL-8 was assessed in vector and OIS IMR90s. **A-B)** Representative images for DAPI (blue) and IL-8 (green) staining in OIS and vector control IMR90s following senescence induction. **C)** Frequency distribution of IL-8 density levels in all targets, including secondary only control conditions. **D)** Quantitation of IL-8 staining percentage positivity compared to secondary only control. N=3 independent experimental replicates (3 technical replicates per experiment). Statistical analysis performed via unpaired Student's t-test (section 2.17). Scale bars = 250µm. Four fields of view.

The secretion of IL-6 and IL-8 by the OIS cells was assessed by ELISA. Here, both IL-6 and IL-8 were demonstrated to increase compared to the proliferating control (vector IL-6, 57 ± 29.44 pg/ml; OIS IL-6, 8192 ± 981.1pg/ml; vector IL-8, 189.3 ± 259.6 pg/ml; OIS IL-8, 30978 ± 4248 pg/ml; Figure 3.11 A-B). It was notable, that the IL-8 concentration was substantially greater than that observed for IL-6. When combined with the immunoblotting and immunofluorescence data, IL-8 was selected as reliable marker of the OIS SASP that could be confidently assessed in subsequent experiments.

It was proposed that the difficulties in IL-6 characterisation might be due to variability within the composition of the SASP. Therefore, the levels of IL-6 and IL-8 were assessed across the course of OIS induction (schedule two), with samples collected at two day intervals between day four and day 16. This demonstrated that both IL-6 and IL-8 increased between day four and day 12. However, this was followed by a subsequent reduction from day 14, dramatically in the case of IL-8 (Figure 3.12). The kinetics of SASP development are incompletely understood and represent an intriguing area for future work (section 6.2). Despite not being the point of maximum SASP production during schedule two, a conditioning period between day four and day eight was selected for EV isolation experiments. This balanced the level of SASP production with the proliferation of vector cells, as well as a higher seeding density used in protocol three. In order to prevent contact inhibition and quiescence, this earlier time-point was selected. However, this data indicates that characterisation of later time-points may be of interest when exploring the development of the SASP (section 6.2).

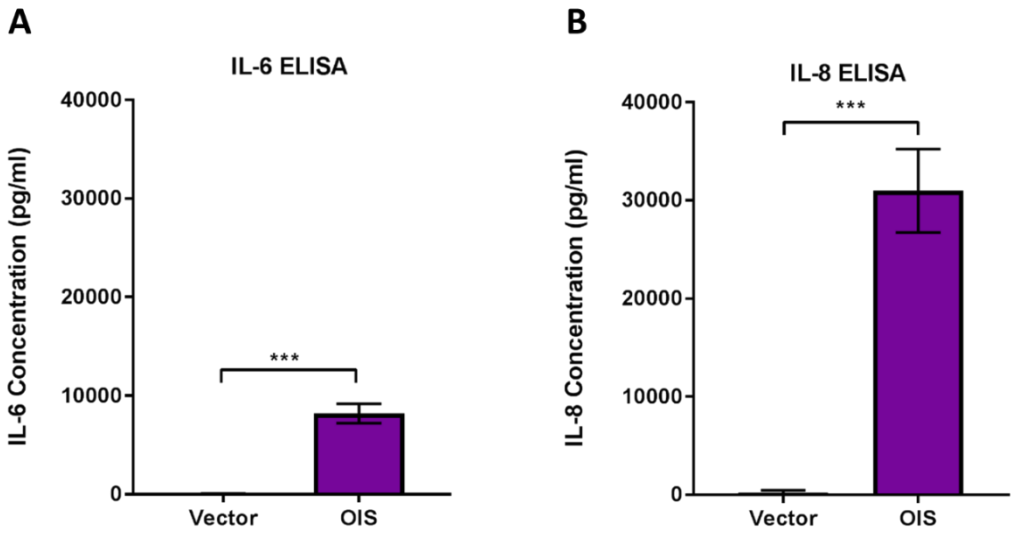

Figure 3.11: ELISA analysis of conditioned media from OIS and vector cells for canonical SASP markers IL-6 and IL-8

Conditioned media was collected from vector and OIS IMR90s between day four and day eight of the OIS induction schedule three. This media was assessed by ELISA for **A)** IL-6 and **B)** IL-8. N=3 independent experimental replicates (3 technical replicates per experiment). Statistical analysis performed via unpaired Student's t-test (section 2.17).

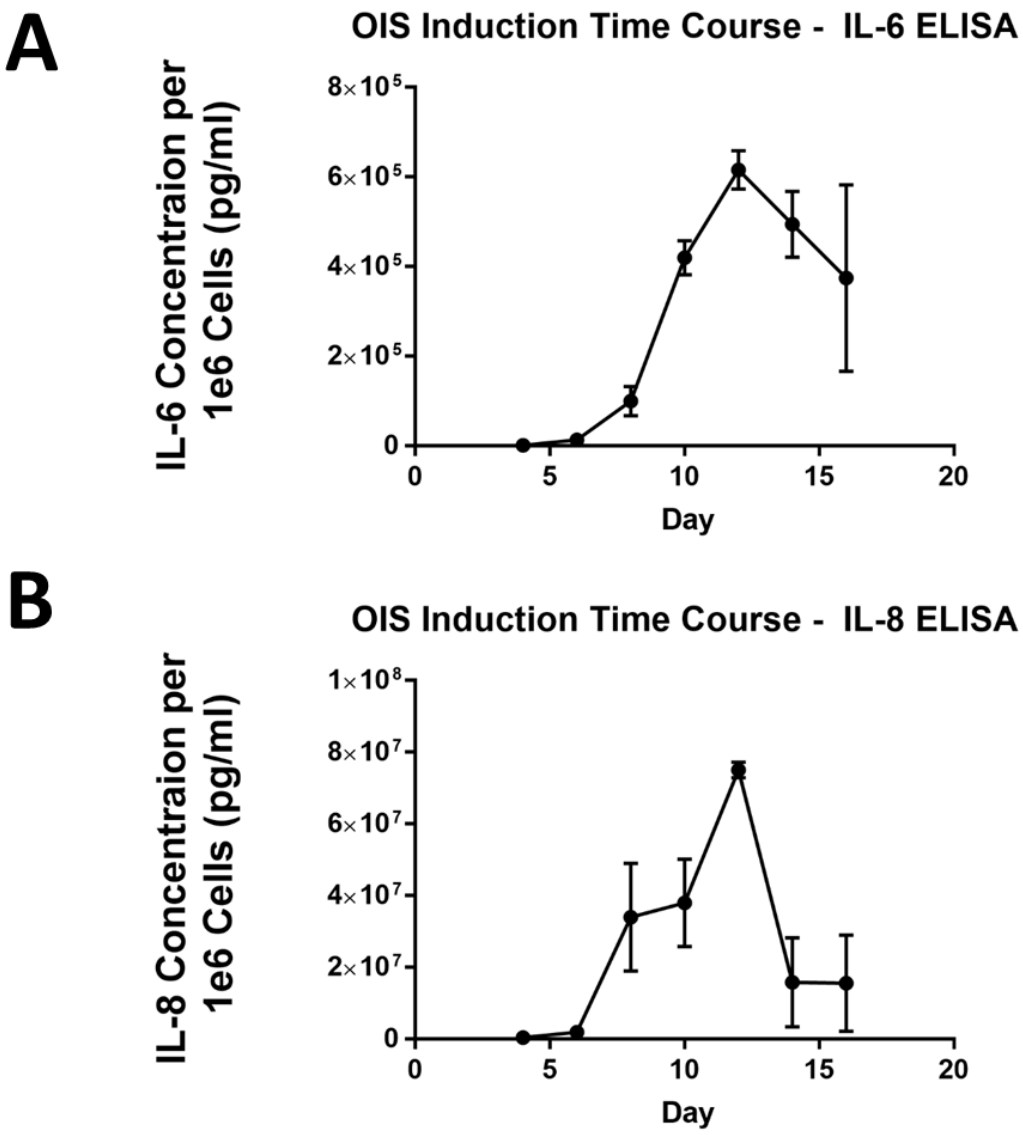

Figure 3.12: ELISA analysis of conditioned media from OIS cells collected between days 4-16

Conditioned media was collected from OIS IMR90s every two days between day four and day 16 following OIS induction (schedule two). This media was assessed by ELISA for **A)** IL-6 and **B)** IL-8. N=3 independent experimental replicates (3 technical replicates per experiment).

3.5 Characterising the Replicative Senescent (RS) Phenotype of Human Mammary Fibroblasts (HMFs)

Having successfully validated the induction of OIS in IMR90s, a model of replicative senescence (RS) was then pursued. Primary adult human mammary fibroblasts were selected, as these had already been extensively characterised within the lab (Thesis:(Tyler, 2016)). Importantly, the SASP of the RS HMFs has not been previously established. HMFs were serially passaged on a weekly basis until the point of replicative senescence (RS). This was established to occur at passage 29, at which point the cells had undergone ~35 population doublings (PDs), in line with previous investigations (Romanov *et al.*, 2001). Cells were then maintained for a further 3 weeks to allow for the establishment of a long-term stable state of deep senescence (DS). The HMF Hayflick curve (Figure 3.13A) demonstrated relatively consistent population doublings until around passage 16. Therefore, passages up to this point were considered to be "early proliferative" (EP). With these parameters established, the phenotype of the DS cells could characterised.

Given that the model of RS had been previously well established within the lab and that the cells were considered precious given they take ~200 days to generate, limited characterisation was performed. Immunofluorescence demonstrated a loss of proliferation in the DS cells compared to the EP, characterised by a reduced cell number (EP, 15572; DS, 2948). The panel of senescence-associated morphological changes also suggested induction of senescence, with alterations in cell area (EP, 1571; DS, 5600.137 μm^2), nuclear area (EP, 206; DS, 297μm^2), cytoplasmic/nuclear ratio (EP, 6.64; DS, 18.78), DAPI density (EP, 9579; DS, 3370 a.u.), nuclear form factor (vector, 0.901; DS, 0.853), cellular protrusions (EP, 3.88; DS, 9.10), cellular form factor (EP, 0.710; DS, 0.549), major axis length (EP, 53.58; DS, 99.31 µm),

minor axis length (EP, 33.91; DS, 60.41 μm) and cellular elongation (EP, 0.633; DS, 0.608) all observed (Figure 3.14). Importantly, this data must be viewed with caution as it represents only N=1 with technical replicates. However, it indicates that the cells which underwent serial passaging to passage 29 +3 weeks are morphologically distinct from the EP HMFs and that they have impaired proliferative capacity. Furthermore, this data is supported by previous evidence that HMFs at passage 29+3 weeks are positive for canonical senescence markers, reinforcing the assertion that a DS phenotype has been established (Stampfer *et al.*, 1981; Tyler, 2016). Therefore, whilst not definitively demonstrated to the highest possible standard here, it is reasonable to consider the likely establishment of RS. Throughout this work, this model has been predominantly used in a supportive capacity, to compliment evidence from OIS. If future work were to focus on the cells generated here, it would essential to comprehensively validate the induction of RS beforehand. With these caveats in mind, investigation into the composition of the RS SASP was then performed.

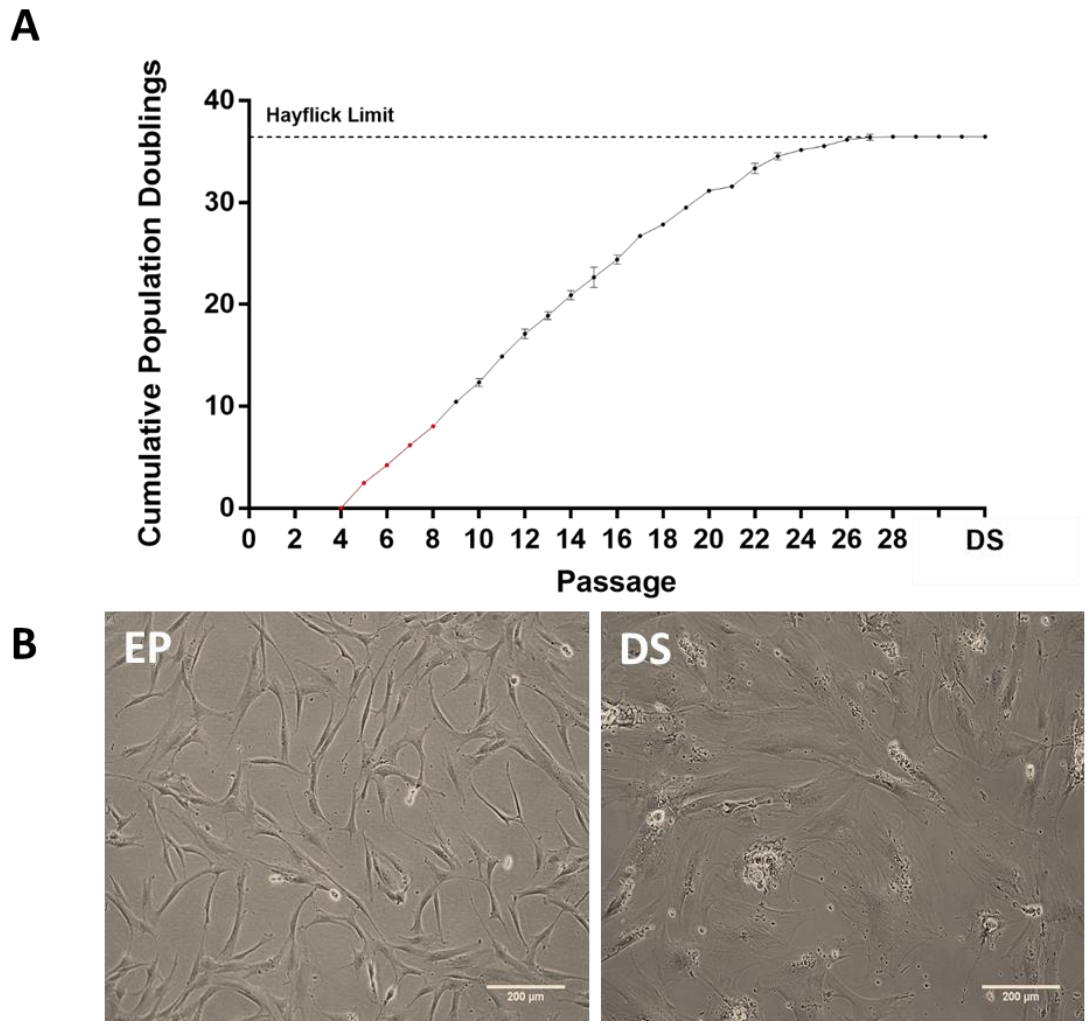

Figure 3.13: Hayflick curve and phase images of primary human mammary fibroblasts (HMFs) during culture from early proliferation (EP) to deep senescence (DS)

Human mammary fibroblasts (HMFs) were serially passaged to replicative senescence, having been previously passaged by Elly Tyler (Bishop Lab; Red line) and were acquired at passage nine. **A)** Hayflick curve demonstrating cumulative population doubling with passage number. Cells were defined as replicatively senescent (RS) at passage 29 and deeply senescent (DS) at 29 +3 weeks. N≥2 all passage apart from N=1 passage 18-21. Red line indicates cells cultured by Elly Tyler. **B)** Brightfield phase images of EP (passage 10) and DS (passage 29 + 11 weeks). Scale bar = 200µm.

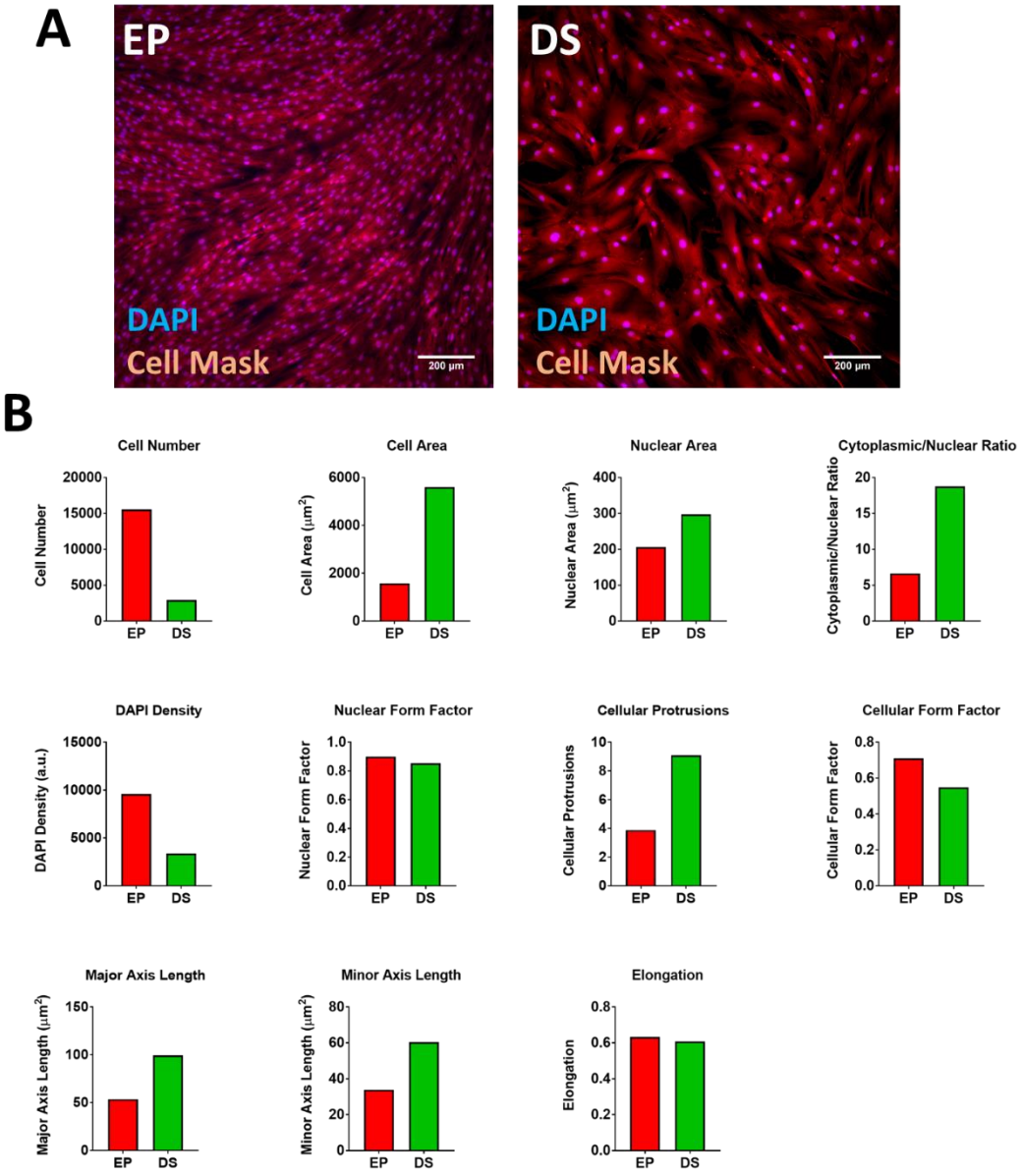

Figure 3.14: High Contentment Analysis (HCA) of Replicative Senescence in Human Mammary Fibroblasts (HMFs) – Proliferation and Morphology

HCA analysis was performed on early proliferative (EP) and deeply senescent (DS) human mammary fibroblasts (HMFs) to assess a panel of morphological measures. **A)** Representative immunofluorescence images for DAPI (blue) and Cell Mask (red) staining in EP and DS HMFs. **B)** Quantitation of HCA cell number and morphology measures. N=1 independent experimental replicate (3 technical replicates per experiment). Scale bars = 200µm.

Whilst well described as a model, the secretome of RS HMFs has not been established previously. In order to parallel the work in the OIS model, IL-6 and IL-8 were once again investigated as canonical markers of the SASP. Through immunoblotting (carried out through supervision of MSc student Kishan Vara), it was observed that IL-6 expression increased in the DS cells compared to the EP control (EP IL-6, 1 ± 0 fold change; DS IL-6, 30.39 ± 3.77; Figure 3.15). Intriguingly, this was not the case for IL-8, despite it being the more prominent marker of the OIS SASP (EP IL-8, 1 ±-0; DS IL-8, 0.57 ± 0.11; Figure 3.15). It should be noted that cells were loaded based upon cell numbers with Lamin B1 serving as a loading control with OIS samples included for reference. Interestingly, IL-6 in the OIS samples was observed to increase compared to the vector, which had not been fully demonstrated in section 3.4 (vector, 1.069 ± 0.06 fold change; OIS, 18.82 ± 3.83 fold change; Figure 3.15). The OIS lysates were collected at day 11 post-seeding (schedule two), which may account for this observed difference. Therefore, it appears that IL-6 forms a part of the RS HMF SASP whereas IL-8 does not. This highlights the context dependent nature of the SASP, with the RS and OIS models appearing quite different in composition. This also emphasises the benefit of utilising multiple senescence models, as senescence cannot be considered a homogenous phenomenon.

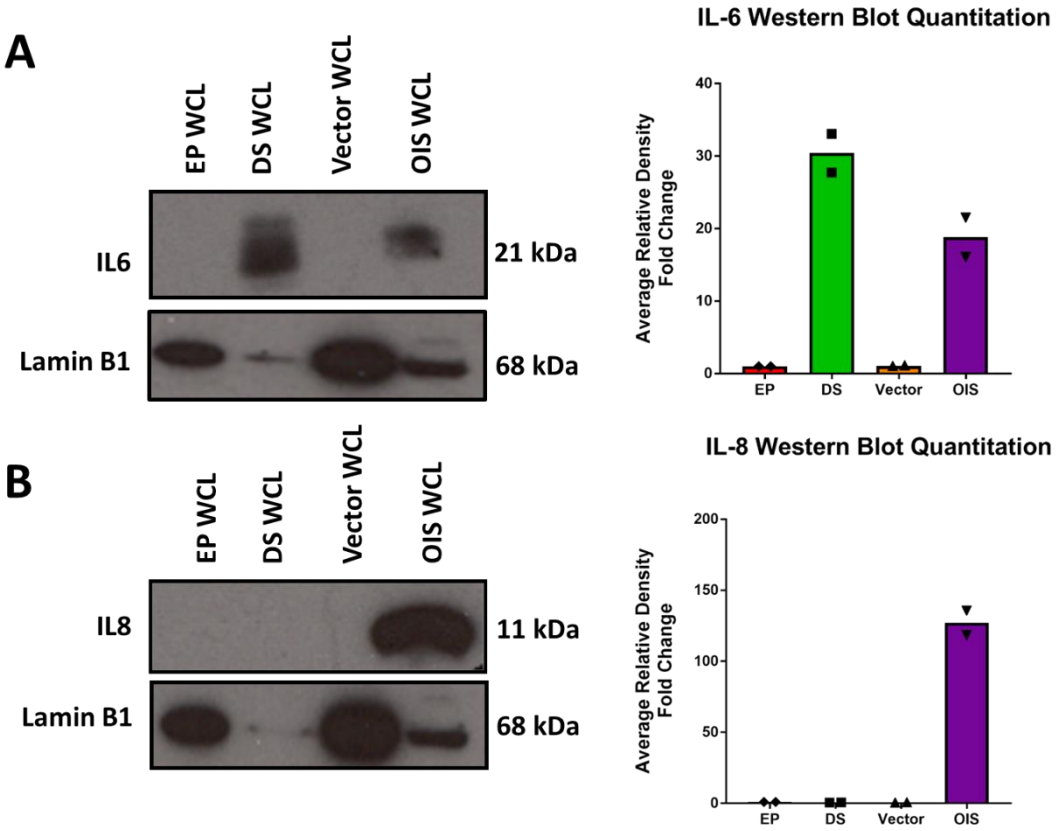

Figure 3.15: Assessment of the senescence-associated secretory phenotype (SASP) of replicatively senescent human mammary fibroblasts (HMFs)

Immunoblot analysis of whole cell lysate (WCL) from early proliferative (EP) and deeply senescent (DS) human mammary fibroblasts (HMFs) and vector and OIS IMR90s for the senescence-associated secretory phenotype (SASP) markers IL-6 and IL-8. **A-B)** Representative immunoblot and densitometry quantitation for IL-6 and Lamin B1 loading control. **C-D)** Immunoblot and densitometry quantitation for IL-8 and Lamin B1 loading control. N=2 independent experimental replicates (1 technical replicate per experiment). Quantitation performed via Image J with normalisation to loading control in each lane.

3.6 Senescence Reversal in HMFs

Senescence has previously been described as an irreversible arrest of the cell cycle. However, this concept has recently been challenged, with the demonstration that RS reversal can be initiated through use of siRNA knockdown of p16 and p21 (Thesis:(Tyler, 2016)). This system presents opportunities to investigate pathways that are intrinsic to the senescence process, as well as potential to uncouple senescence hallmarks, such as loss of proliferation and SASP production. The secretome of reversed HMFs has not been previously explored, although that of reversed HMECs indicates that senescence reversal sees ablation of SASP production (Lowe *et al.*, 2015). The work presented within this section was carried out through supervision of a Regenerative Medicine MSc student – Kishan Vara. The objectives were to establish the p16+p21 siRNA reversal protocol in RS HMFs and characterise the SASP of the reversed cells. It is important to acknowledge that all work in this section used only two independent experimental replicates and has not, therefore, been statistically assessed.

Firstly, it was important to assess the successful reversal of RS in the HMFs. Senescence reversal was demonstrated through re-establishment of cellular proliferation. This was observed through an increase in cell number in p16+p21 siRNA cells compared to the untreated DS cells and the siGLO control (DS, 1 ± 0 fold change; siGLO, 1.00 ± 0.03 fold change; 1.89 ± 0.27 fold change; Figure 3.16). Next, p21 and p16 were assessed by qRT-PCR. In the p16+21 siRNA treated cells, the level of both p16 (DS, 1 ± 0 fold change; siGLO, 1.176 ± 0.09 fold change; p16+p21, 0.2684 ± 0.03 fold change; Figure 3.17A) and p21 (DS, 1 ± 0 fold change; siGLO, 1.159 ± 0.08 fold change; p16+p21, 0.161 ± 0.14 fold change; Figure 3.17B) mRNA were lower than that of DS and siGLO conditions. When taken with previously generated data, RS reversal in the HMFs was concluded to have been successful. Therefore, attention turned towards assessing the secretome of these reversed cells.

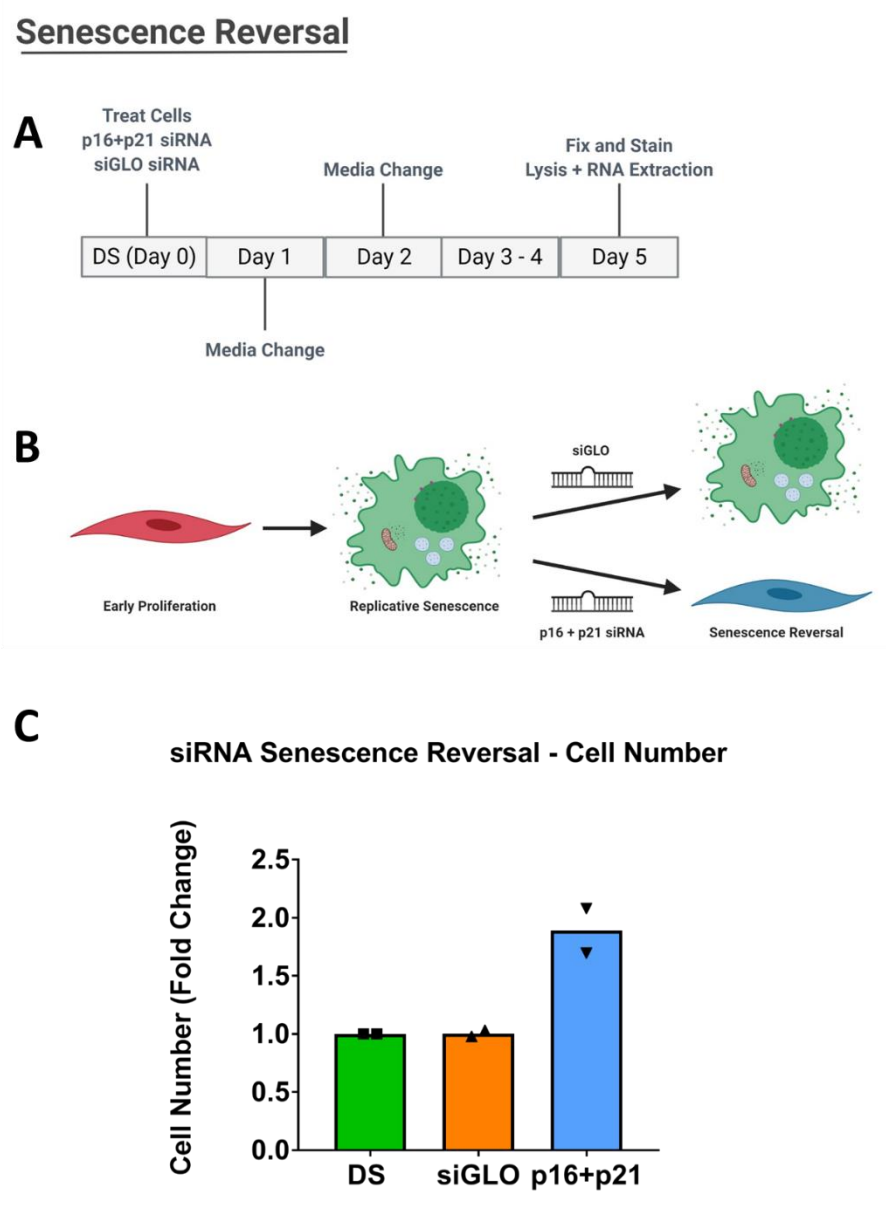

Figure 3.16: Assessment of siRNA senescence reversal via immunofluorescence through re-establishing cellular proliferation

Deeply senescent (DS) human mammary fibroblasts (HMFs) were treated with siGLO or p16+p21 siRNA or left as an untreated control. A) Timeline for siRNA reversal protocol B) Schematic indicating previously established reversal of HMF RS senescence via use of p16+p21 siRNA 3) HCA assessment of cell numbers. Normalisation to untreated DS control was performed. N=2 independent experimental replicates (2 technical replicate per experiment).

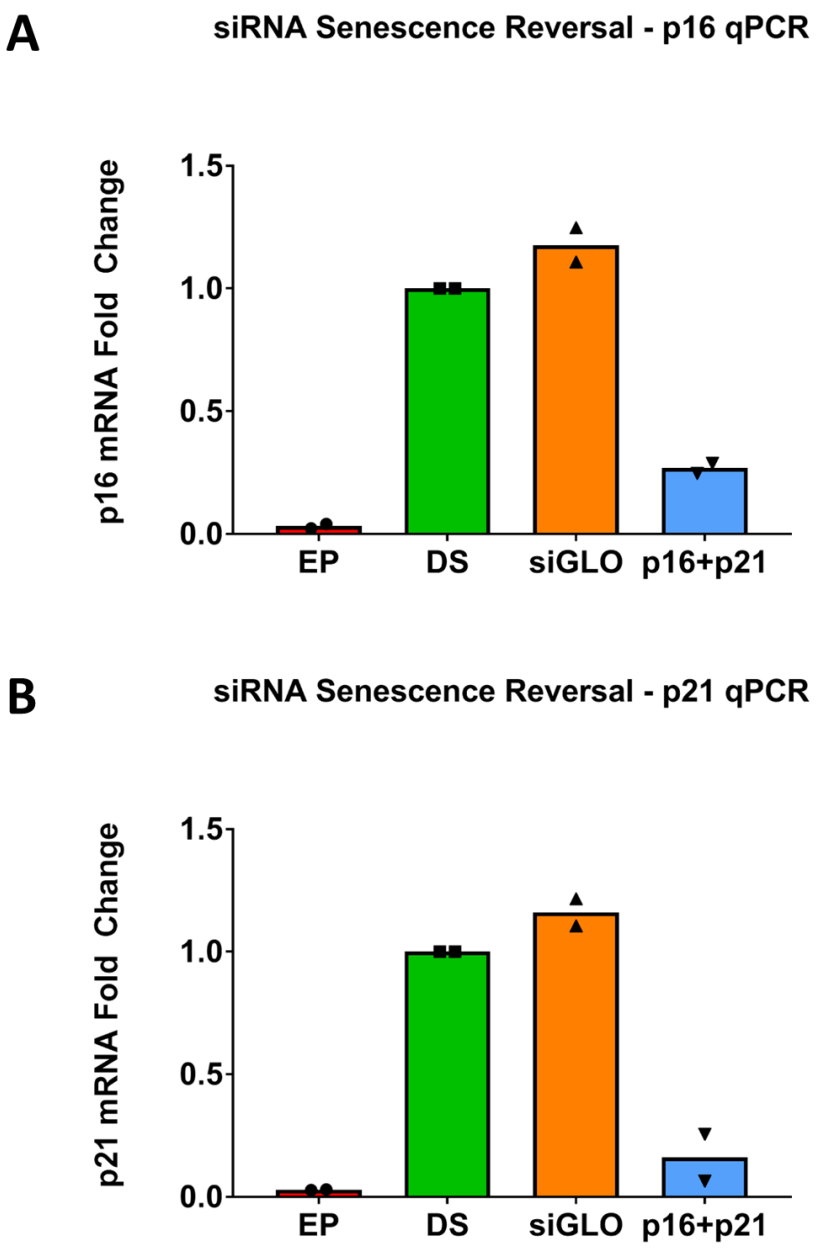

Figure 3.17: qRT-PCR analysis of p21 and p16 expression in human mammary fibroblasts (HMFs) following siRNA senescence reversal

Deeply senescent (DS) human mammary fibroblasts (HMFs) were treated with siGLO or p16+p21 siRNA and compared to early proliferating (EP) and DS controls. Assessment of **A)** p16 and **B)** p21 mRNA expression was then made by qRT-PCR. Relative expression was calculated through normalisation to a GAPDH housekeeper and fold change relative to the DS condition was determined. N=2 independent experimental replicates (2 technical replicate per experiment).

As described previously, the SASP varies between cells types and senescence triggers, as emphasised by the lack of IL-8 production in the RS HMFs observed through immunoblotting. This was once again demonstrated, as negligible IL-8 mRNA was observed in either EP or DS samples by qRT-PCR and did not change following siRNA treatments (EP, 1 ± 0 fold change; DS, 1.742 ± 0.71 fold change; siGLO, 1.131 ± 0.45 fold change; p16+p21, 5.646 ± 3.00 fold change; Figure 3.18A). By contrast, IL-6 mRNA was observed in both the DS and siGLO conditions, and was found to decrease with use of p16+p21 siRNA (EP, 1 ± 0 fold change; DS, 258.4 ± 39.5 fold change; siGLO, 232.5 ± 30.41 fold change; p16+p21, 52.92 ± 34.68 fold change; Figure 3.18A). In order to explore the effect of reversal on the SASP further, IL-1α and IL-1β were also assessed by qRT-PCR. IL-1α was demonstrated to remain unchanged from the levels observed in the DS and siGLO conditions, significantly above that of the EP cells (EP, 1 ± 0 fold change; DS, 50.93 ± 5.87 fold change; siGLO, 43.01 ± 2.70 fold change; p16+p21, 48.53 ± 3.769 fold change; Figure 3.18B). Intriguingly, IL-1β was seen to increase dramatically in the reversed cells (EP, 1 ± 0 fold change; DS, 64.1 ± 0.08 fold change; siGLO, 54.3 ± 1.71 fold change; p16+p21, 234.9 ± 5.82 fold change; Figure 3.18B). This suggests that the reversed secretory phenotype may be more complex than simply reverting to that of the EP condition.

As IL-6 has thus far been considered the most well described marker of the RS HMF SASP, the abundance of protein secretion was then investigated in the rejuvenated cells. The level of IL-6 secretion appeared to decrease in the p16+p21 conditioned verses the siGLO control, although this was not a statistically significant response (siGLO, 138.8 ± 91.71pg/ml; 10.82, ± 3.08pg/ml; Figure 3.19). The high variability between experiments highlights the importance of sufficiently powered experiments and producing at least one further replicate for N=3 would be a significant improvement to this experiment.

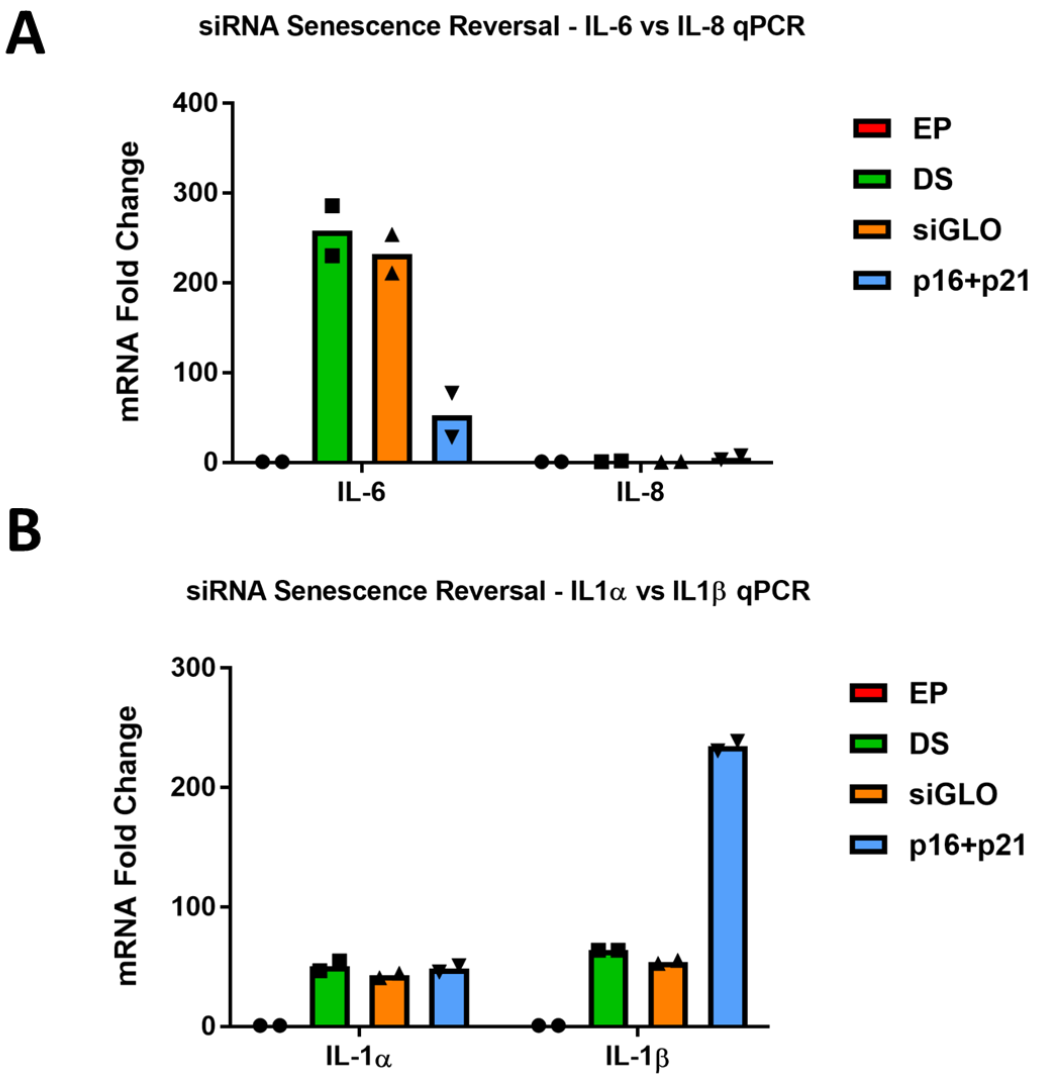

Figure 3.18: qRT-PCR analysis of IL-6, IL-8, IL-1α and IL-1β expression in human mammary fibroblasts (HMFs) following siRNA senescence reversal

Deeply senescent (DS) human mammary fibroblasts (HMFs) were treated with siGLO or p16+p21 siRNA. Assessment of **A)** IL-6 and IL-8 and **B)** IL-1α and IL-1β mRNA expression was then made by qRT-PCR. Relative expression was calculated through normalisation to a GAPDH housekeeper and fold change relative to the DS condition was determined. N=2 independent experimental replicates (2 technical replicate per experiment)..

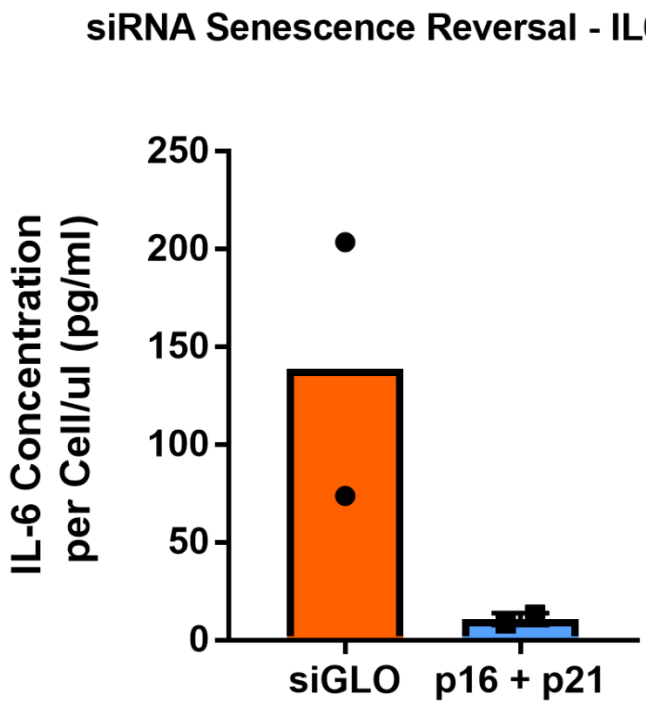

Figure 3.19: ELISA analysis of conditioned media from human mammary fibroblasts (HMFs) following siRNA senescence reversal

Deeply senescent (DS) human mammary fibroblasts (HMFs) were treated with siGLO or p16+p21 siRNA. Conditioned media was collected and assessed by ELISA for IL-6. N=2 independent experimental replicates (3 technical replicate per experiment).

3.7 Summary

In this chapter, two models of senescence have been investigated. The first, OIS in IMR90s, is one of the most extensively characterised models within the literature. Here, senescence induction was confirmed through the characterisation of multiple orthogonal markers including tumour suppressor expression (p16 and p21), loss of cellular proliferation (cell number and Ki67) and the appearance of SAHFs. This data was complimented by an HCA morphological assessment, which allowed unbiased characterisation of a panel of measures assessing cellular and nuclear shape. This panel demonstrated that OIS was associated with an overall increased cellular area, whilst this enlarged shape was also more irregular than that of the proliferating vector control. These cellular changes were also reflected in the nuclear morphology, where OIS was associated with large irregularly shaped nuclei, which possessed weak DAPI staining. The morphological alterations that accompany senescence induction were some of the first phenotypes identified in senescent cells (Hwang, Yoon and Kang, 2009). More recently, this increased size has been mechanistically linked to senescence induction through a process of "cytoplasmic dilution" (Neurohr *et al.*, 2019). This is corroborated here, by the observed increase in cytoplasmic to nuclear ratio. Together, this data demonstrates that HCA is a powerful tool when assessing the induction of a senescence phenotype. Whilst not representing a comprehensive characterisation, it allows a reliable "first pass" with which to classify senescence induction (section 6.4). Therefore, this was used in combination with proliferation data in section 5, in order to determine paracrine senescence induction.

Whilst the OIS model represents an expedient method of investigating senescence, RS (occurring as a result of telomere attrition) has been positioned as an important contributor to ageing (Lee *et al.*, 1998). RS was investigated by culturing adult HMFs to their Hayflick

limit, the point at which population doublings are no longer observed. This has previously been determined to occur at ~35 PDs, an observation reproduced here. This model takes >200 days to produce and is both labour and resource intense. Therefore, these cells were considered extremely precious and not used to reproduce characterisation experiments that had been conducted previously, apart from a preliminary validation via HCA comparison of proliferation and morphology (Thesis:(Tyler, 2016)). Overall, throughout this project, the OIS model was used as the primary experimental setting. This is in part due to the relative availability of senescent cells within each model, but also due to the exaggerated phenotype in OIS. The intended workflow was to develop experimental protocols and validate reagents in OIS, then moving into the complimentary RS system. However, OIS was eventually taken forward as the sole model of investigation as the project developed (sections 5 and 6). The use of a comprehensively characterised RS model would support many of the overall project conclusions, as a model that more faithfully recapitulates an ageing phenotype. However, this was reprioritised as future, complimentary work (section 6.2). It is important to acknowledge that the proliferation profile of comparable HMF samples from different biological donors may differ significantly from that investigated here. As such, future work would benefit from the investigation of cells from different donors to account for the potential heterogeneity in senescence responses. The broader implications of such sources of heterogeneity are discussed further in section 6.2.

The SASP is a defining hallmark of senescence induction and has been well characterised in OIS. Here, the canonical SASP factor IL-8 was validated by immunoblotting, immunofluorescence and ELISA. IL-6 was also investigated in each of these settings but was only fully validated by ELISA. Therefore, IL-8 was considered a more reliable marker of the OIS SASP and utilised as such in subsequent investigations. Preliminary exploration of the

kinetics of OIS induction were also carried out. It has previous been demonstrated that SASP composition varies during OIS induction (Hoare *et al.*, 2016). When selecting a protocol for EV isolation in section 5, this data was intended to establish a point at which the cells were producing the most potent secretome, as this was hypothesised to be a point in which EVs may also be produced. However, as the OIS induction schedule was optimised, with particular regard to initial seeding densities, the issue of contact inhibition and quiescence in the control condition became a more significant priority. Therefore, a conditioning time between day four and eight was selected, in line with previous studies (Acosta *et al.*, 2013). However, the time-course data here indicates that future work investigating the development of the OIS SASP, particularly at later time-points, would be valuable. Furthermore, the differences in RS and OIS SASP composition, particularly in terms of IL-8, further support the context dependent nature of the SASP, justifying further investigation in additional models (section 6.2).

The reversal of replicative senescence via siRNA has previously been established within the group (Thesis:(Tyler, 2016)). However, the secretome of reversed HMFs has not previously been established. Through supervision of an MSc student, this was explored using a previously validated combination of p16+p21 siRNA, with cellular proliferation successfully reinstated. Successful knockdown of p16 and p21 mRNA was confirmed by qRT-PCR, validating the experimental approach. Finally, SASP production was assessed by both qRT-PCR and ELISA. qRT-PCR corroborated immunoblotting data, which demonstrated that the RS SASP comprised IL-6 but not IL-8. IL-6 expression was also demonstrated to decrease upon senescence reversal. Interestingly, IL-1α and IL-1β expression did not decrease with reversal. This is intriguing, as it suggests the cells retain a “senescent” secretory profile, although one that comprises only certain factors. As IL-1α has been described as an early SASP factor, it

may be that cells have been reverted to an early part of the senescence induction process, or are re-entering senescence. However, it may also indicate that certain factors are more important within the SASP and warrants further investigation.

Overall, this chapter has established two models of senescence in which to study extracellular vesicles (EVs). OIS was comprehensively characterised and will form the basis of the majority of subsequent experiments. Importantly the OIS SASP was also characterised and demonstrated to contain a significant IL-8 component. Whilst a model RS was also established, this will serve as a complimentary system to the main OIS focus. Future work from this chapter includes further exploration of the kinetics of SASP production (section 6.2) and use of siRNA senescence reversal in order to explore the mechanisms behind SASP composition and production (section 6.5).

4 Results 2: Isolating Extracellular Vesicles (EV) from Senescent Cells

4.1 Introduction

As discussed in section 1.2, extracellular vesicles (EVs) represent a heterogeneous set of lipid bound nanoparticles that can be defined based on their size and route of biogenesis. These are most commonly broken down into two main groups: microvesicles and exosomes. However, the process of practically separating EVs into these distinct populations is hindered by the lack of unique, subset specific markers. Consequently, isolation methodologies broadly focus on separating EVs based upon physical characteristics, with the most common methods using size. However, due to overlapping size profiles, this is imperfect, and cannot confidently be considered to produce homogenous vesicle preparations. Therefore, the generic term “extracellular vesicle” is employed to reflect this ambiguity. However, each particular isolation methodology is usually aimed towards the enrichment of a specific EV subtype. Here, the isolation methods employed are done so with the intention of enriching for exosomes, but it important to acknowledge that a mixed EV population will in fact be produced.

This chapter focusses on the isolation and characterisation of EVs from senescent cells. Differential ultracentrifugation (dUC) was initially used to isolate EVs from both the OIS and RS senescence models. Nanoparticle-tracking analysis (NTA) was then employed to characterise both the size and concentration of the EVs produced. Next, proteomic assessment was performed, with the aim of characterising the cargo and composition of senescent cell derived EVs.

In order to explore the limitations of dUC, size-exclusion chromatography (SEC) was then employed as a complimentary isolation technique. This highlighted advantages and limitations of both methodologies, whilst a second round of proteomics was performed in order to emphasise the advantages of SEC in a senescence setting. This primarily stemmed from a greater separation between the soluble and vesicular portions of the senescent secretome, allowing more robust characterisation of EV composition to be made. Finally, a third round of proteomics was performed in order to confidently profile the changes in EV protein content following OIS induction.

4.2 Chapter Hypothesis and Aims

The aim of this chapter was to establish a rigorous protocol for the isolation of extracellular vesicles from senescent cells in order to facilitate compositional profiling via mass spectrometry (MS). It was hypothesised that differential ultracentrifugation (dUC) represents an effective method of EV isolation, albeit one potentially hindered by a lack of separation between EVs and co-isolated soluble proteins. Size-exclusion chromatography (SEC) was hypothesised to represent a purification method to serve as a useful adjunct to dUC. MS was employed as a method of global proteomic profiling in order characterise the change in EV composition following senescence induction, as well asses the relative suitability of each EV isolation technique.

The aims of this chapter are as follows:

- To validate that differential ultracentrifugation (dUC) can be used to isolate extracellular vesicles (EVs)
- To isolate extracellular vesicles (EVs) from senescent cells by dUC
    - To validate the presence of canonical EV markers by immunoblotting
    - To assess the change in EV production in senescence by nanoparticle tracking analysis (NTA)
- To isolate EVs from senescent cells by size-exclusion chromatography (SEC)
    - To establish the optimal isolation methodology for the assessment of EVs from senescent cells
- To characterise the cargo and composition of senescent cell derived EVs by mass spectrometry (MS)

4.3 Establishing a Protocol of EV Isolation via Differential Centrifugation

4.3.1 Use of Exosome Depleted FBS (ExoFBS)

Differential ultracentrifugation (dUC) is the most widely applied method for the isolation of EVs and was selected as a starting point to generate preparations from senescent cells (Figure 4.1) (Gardiner *et al.*, 2016). However, before culture media is conditioned in advance of EV isolation, it is important to ensure that there are no vesicles from any other source that may contaminate the final preparation. It has previously been demonstrated that foetal bovine serum (FBS) represents a potential source of these contaminating vesicles (Tosar *et al.*, 2017). This is a complication, as it requires cells to be cultured in either serum free or EV depleted media. Following application of the dUC protocol, a high number of EVs were confirmed to be present within DMEM supplemented with 10% FBS (DMEM 10%; 4.3E+10 ± 4.9E+09 Particles/ml; Figure 4.2) in comparison to the serum free control (DMEM 0%; 1.2E+08 ± 7.2E+07 Particles/ml; Figure 4.2). Extensive attempts to deplete this through longer ultracentrifugation procedures (up to 6 hours) were unsuccessful and so strategy turned towards use of commercially available products. DMEM supplemented with 10% "exosome-depleted FBS" (ExoFBS) was demonstrated to contain a negligible number of vesicles (1.8E+08 ± 3.1E+07 Particles/ml; Figure 4.2) compared to standard FBS (4.3E+10 ± 2.0E+09 Particles/ml; Figure 4.2) and was comparable to the serum free media (DMEM 0%; 1.2E+08 ± 7.2E+07 Particles/ml; Figure 4.2). Therefore, DMEM supplemented with ExoFBS was considered a viable alternative to standard FBS and taken forward for further validation.

A possible alternative to commercially depleted FBS is the use of a chemically defined cell culture medium. This was not pursued for three reasons: 1) A lack of established defined media for the cells used in both senescence models; 2) The need to move between multiple cell types and senescence models; and 3) The extensive characterisation of the RS model

with media containing FBS previously. The later of these points was also an important consideration when optimising the use of ExoFBS. In particular, there was a concern that during the manufacturing process, factors other than EVs may also be depleted. As comparisons between proliferating and senescent cells would constitute many subsequent experimental objectives, it was important to establish that use of ExoFBS did not stimulate a senescence response, particularly in the EP HMFs. To assess this, EP cells were cultured with DMEM supplemented with 10% FBS or 10% ExoFBS (Figure 4.3) and incubated for 48 hours. No differences were observed in either cell number (10% FBS, 14,963 ± 615; 10% ExoFBS, 13,482 ± 920; Figure 4.3) or any morphological measure between conditions. Importantly, the OIS phenotype was also demonstrated to be robust following culture with ExoFBS between days four and eight as described in section 3.3. Whilst not a comprehensive assessment of the possible changes in proliferation with ExoFBS in all following experimental conditions, the advantage of ExoFBS demonstrated by NTA, combined with an absence of growth impairment in the EP HMFs, was considered sufficient to justify the use of ExoFBS as a culture supplement during EV conditioning.

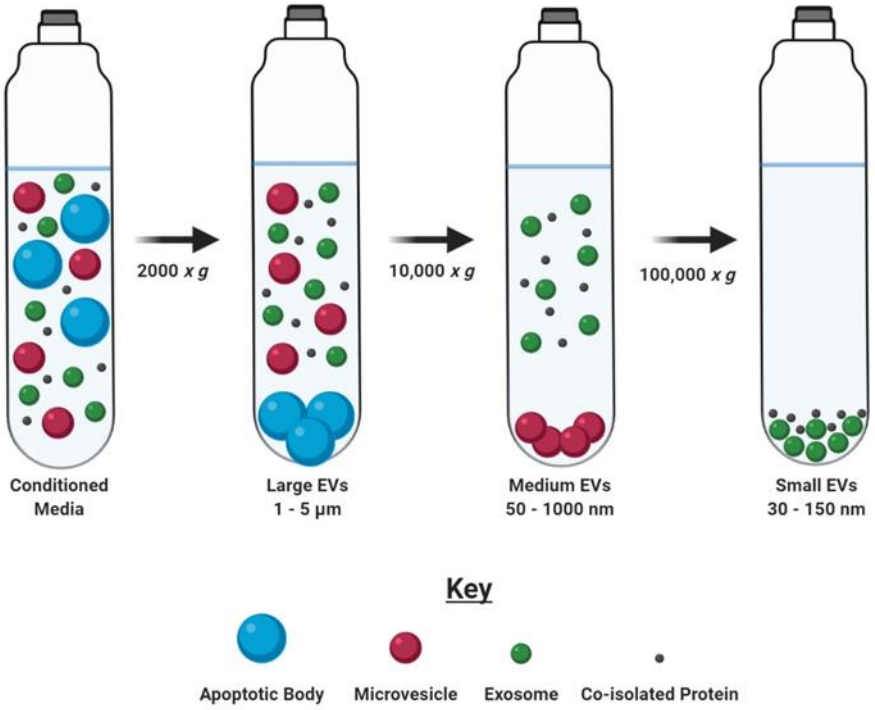

Figure 4.1: Schematic of EV Isolation Procedure by Differential Centrifugation (dUC)

As described in section 1.2.5.2, EVs may be isolated from cell culture medium by differential ultracentrifugation (dUC). This facilitates the clearance of large and medium sized EVs (such as apoptotic bodies and microvesicles) from the supernatant in earlier steps. A final 100,000 *x g* product is then produce, which is enriched for small EVs (such as exosomes) but may contain some co-isolation of protein.

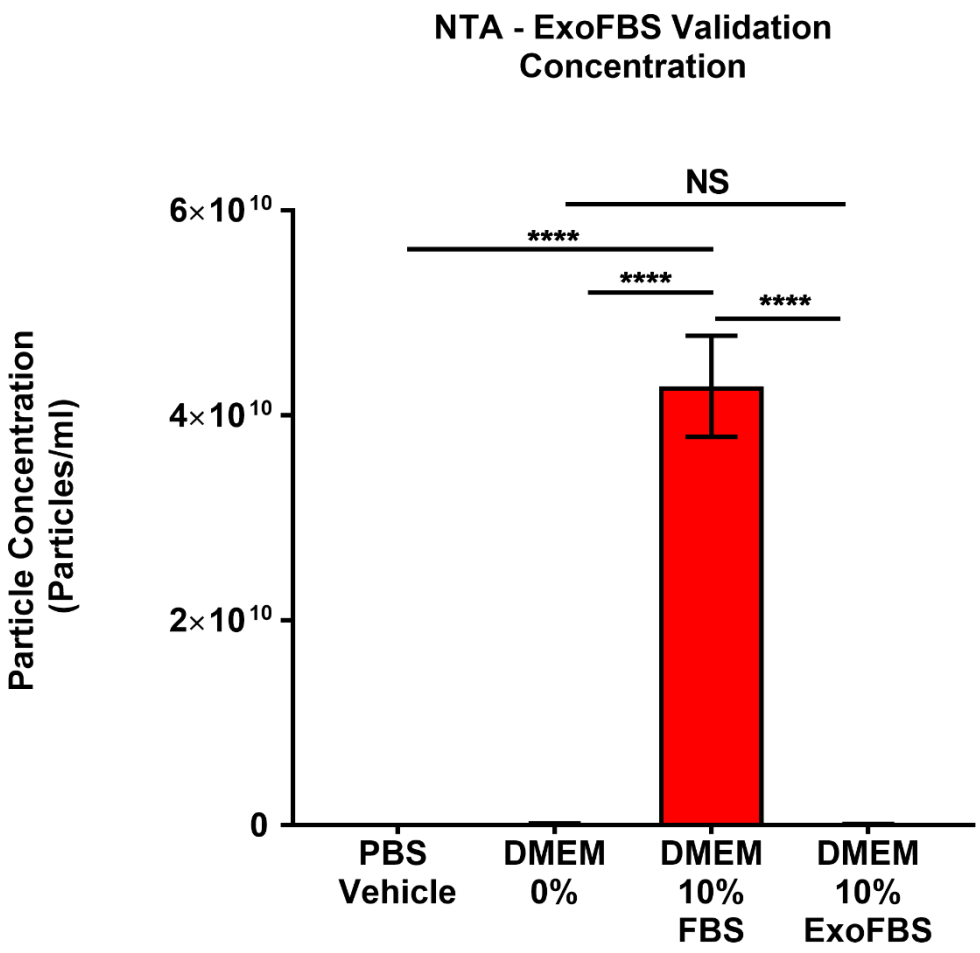

Figure 4.2: Nanoparticle Tracking Analysis (NTA) of DMEM culture medium containing foetal bovine serum (FBS) or exosome-depleted FBS (ExoFBS)

Extracellular vesicles (EVs) were isolated by differential ultracentrifugation (dUC) from serum free media (DMEM 0%), media containing 10% foetal bovine serum (DMEM 10% FBS) and media containing a commercial EV depleted FBS (DMEM 10% ExoFBS). These preparations were assessed by nanoparticle tracking analysis (NTA) alongside a PBS vehicle control. N=3 independent experimental replicates (1 technical replicate per experiment). Statistical analysis performed via One-way ANOVA with Tukey's post-hoc test (section 2.17).

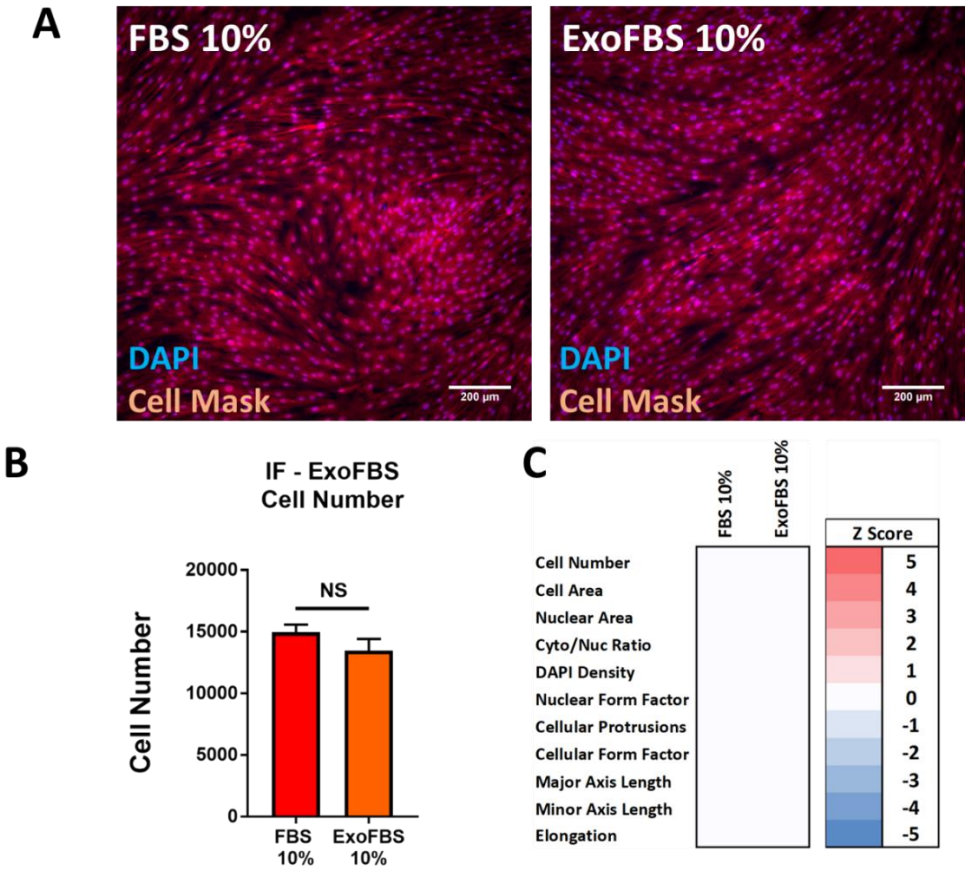

Figure 4.3: Immunofluorescence high content analysis (HCA) of human mammary fibroblasts (HMFs) cultured with medium containing foetal bovine serum (FBS) or EV-depleted FBS (ExoFBS)

Early proliferating human mammary fibroblasts (HMFs) were cultured for 48 hours in media containing 10% foetal bovine serum (10% FBS) or media containing a commercial EV depleted FBS (10% ExoFBS) and assessed by HCA. **A)** Representative immunofluorescence images for DAPI (blue) and Cell Mask (red) staining in HMFs. **B)** HCA morphology measures were converted to Z-scores according to the change from the FBS 10% control condition (see methods). Positive and negative modulation of each measure is demonstrated by a change of at least +/- one Z-score from the FBS 10% condition and indicated as red or blue respectively. White indicates no change from the control. N=3 independent experimental replicates (2 technical replicates per experiment). Statistical analysis performed via One-way ANOVA with Tukey's post-hoc test (section 2.17). Scale bars = 200µm. Four fields of view.

4.3.2 Assessing the Long Term Stability of EVs

In order to assess the optimum method for long-term storage of EV preparations, EVs were isolated from DMEM supplemented with 10% FBS. These were then aliquoted and stored at either 4°C or -80°C. Consistency of both particle concentration and size were then assessed by NTA. Measurements were taken at zero days, one week and five weeks post-isolation. No concentration changes were observed at zero days (4.3E+10 ± 4.9E+09 Particles/ml; Figure 4.4A), one week (4°C, 3.92E+10 ± 3.45E+09; -80°C, 4.54E+10 ± 5.08E+09 Particles/ml; Figure 4.4A) or five weeks (4°C, 4.34E+10 ± 2.09E+09; -80°C, 4.41E+10 ± 6.25E+09 Particles/ml; Figure 4.4A). Size differences were also not seen at zero days (88 ± 2.5 nm; Figure 4.4B), one week (4°C, 82 ± 4.0; -80°C, 84 ± 5.1 nm; Figure 4.4B) or five weeks (4°C, 87 ± 7.2; -80°C, 81 ± 1.7 nm; Figure 4.4B). Consequently, it was decided that long-term storage would be performed at -80°C as this has been described previously in the literature (Witwer *et al.*, 2013). It is important to emphasise that this work utilises FBS derived EVs and there is an assumption that those from cells will behave in a similar manner. Equally, no analysis of freeze-thaw cycles has been made. However, from a logistical perspective the use of freshly isolated preparations was not feasible for all experiments. Despite this, the NTA data suggests that preparations are reasonably robust and steps were taken to minimise freeze-thaw cycles and maintain integrity by storing EVs on ice when thawed.

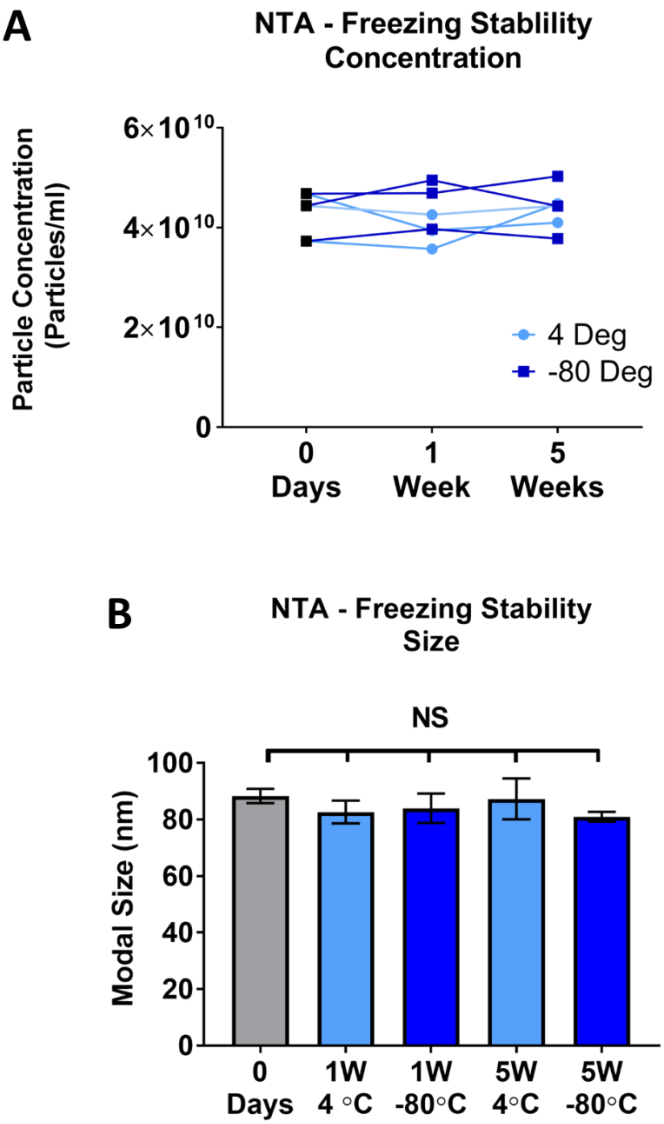

Figure 4.4: Nanoparticle Tracking Analysis (NTA) of EVs isolated from foetal bovine serum (FBS) and stored at either 4°C or -80°C

Extracellular vesicles (EVs) were isolated by differential ultracentrifugation (dUC) from unconditioned media containing 10% foetal bovine serum and assessed by nanoparticle tracking analysis (NTA). Aliquots were stored at either 4°C or -80°C for one and five weeks with NTA assessment at these time points. **A)** NTA particle concentration measurements. **B)** NTA particle size measurements. N=3 independent experimental replicates (1 technical replicate per experiment). Statistical analysis performed via One-way ANOVA with Tukey's post-hoc test (section 2.17).

4.4 Isolating EVs from Models of Oncogene-Induced and Replicative Senescence

Having established that particles of ~100nm could be isolated from FBS, the dUC protocol was then applied to conditioned media from vector control and OIS cells in order to isolate EVs. Here, an increase in particle concentration was observed in OIS samples (4.48E+11 ± 9.57E+09 Particles/ml; Figure 4.5A) compared to those from vector cells (2.13E+11 ± 2.06E+10 Particles/ml; Figure 4.5A), with the modal sizes also observed at ~100nm (vector, 85.3 ± 5.3 nm; OIS, 102.5 ± 14.3 nm; Figure 4.5B). This size profile reflects that which would be anticipated for a population of EVs enriched for exosomes, supporting previous data that suggests senescent cells have an increased rate of EV production (Section 1.3.1). Next, the same dUC protocol was applied to conditioned media from early proliferating (EP; P12-13) and late passage (LP; P26-29) HMFs. The LP cells have a very slow PD rate but are not considered to have reached the point of replicative senescence. However, an observable increase in particle concentration (per cell) was identified in the LP derived samples (4630 ± 969.7 Particles/ml; Figure 4.6A) compared to those from EP cells (603 ± 636.9 Particles/ml; Figure 4.6A). Once more, these displayed a modal size broadly consistent with EVs enriched for exosomes (EP, 86.27 ± 11.98; DS, 86.33 ± 5.508; Figure 4.6B). This suggests that RS is also associated with an increased production of EVs. However, due to the relative expediency of the OIS model, coupled with greater availability of senescent cells, it was decided at this point to focus on further validation of EV isolation in OIS and return to the RS model at a later point (section 6.2).

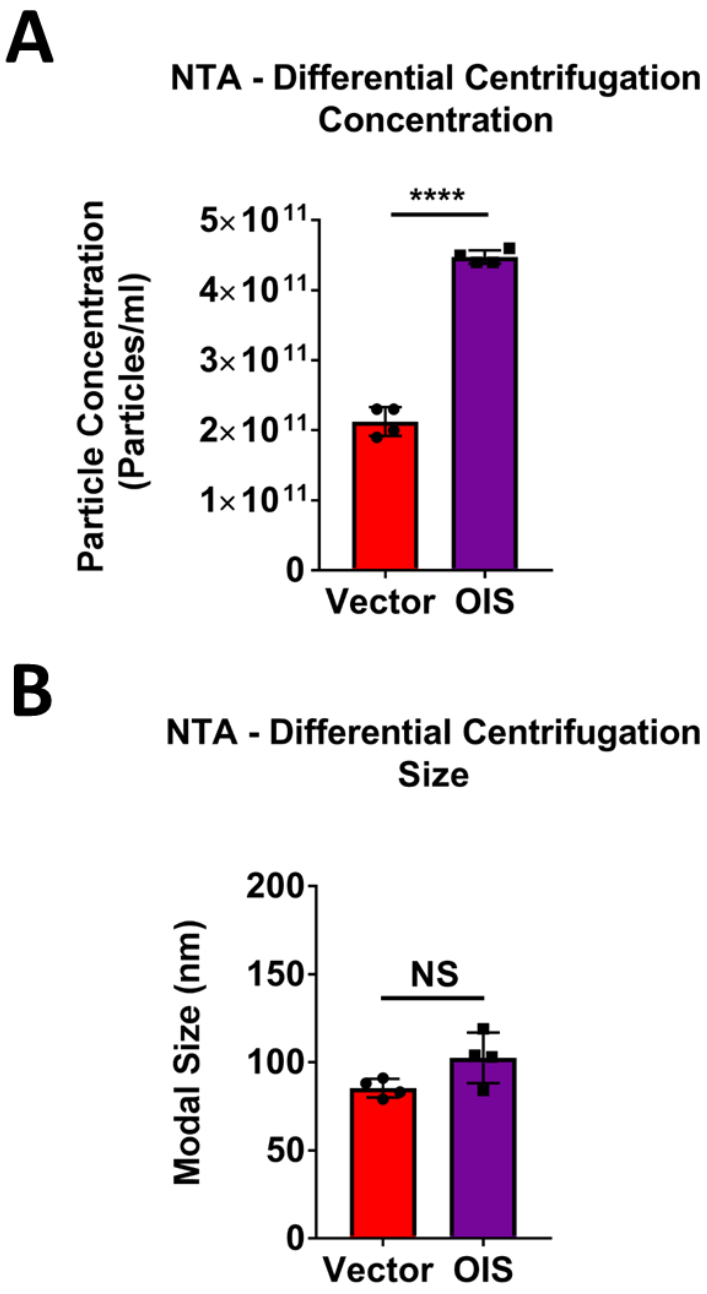

Figure 4.5: Nanoparticle Tracking Analysis (NTA) of EVs isolated from vector or oncogene-induced senescent (OIS) IMR90 fibroblasts by differential centrifugation

Extracellular vesicles (EVs) were isolated by differential ultracentrifugation (dUC) from vector control and OIS IMR90s. Nanoparticle tracking analysis (NTA) was then performed to determine **A)** particle concentration and **B)** particle size measurements. N=4 independent experimental replicates (1 technical replicates per experiment). Statistical analysis performed via unpaired Student's t-test (section 2.17).

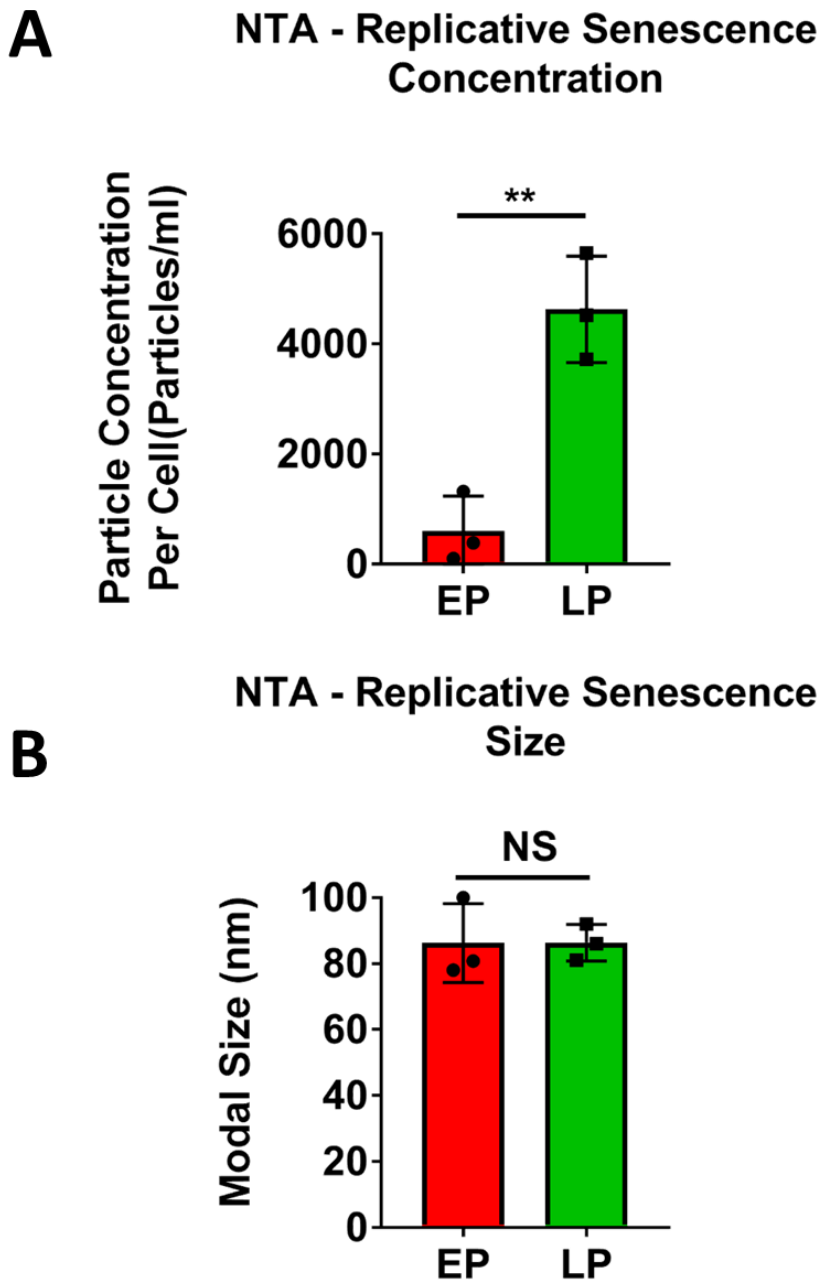

Figure 4.6: Nanoparticle Tracking Analysis (NTA) of EVs isolated from early or late passage human mammary fibroblasts (HMFs) by differential centrifugation

Extracellular vesicles (EVs) were isolated by differential ultracentrifugation (dUC) from early proliferative (EP) and late passage (LP) human mammary fibroblasts (HMFs). Nanoparticle tracking analysis (NTA) was then performed to determine **A)** particle concentration and **B)** particle size measurements. N=3 independent experimental replicates (1 technical replicate per experiment). Statistical analysis performed via unpaired Student's t-test (section 2.17).

Much like senescence, there is no universal marker of EVs. This makes it difficult to classify preparations as containing exclusively one subclass of vesicle confidently. However, as stated above (section 4.1), the dUC protocol is aimed at producing an EV population that is enriched for exosomes. Therefore, markers of the exosomal biogenesis pathway may be used to identify the presence (if not exclusivity) of exosomes within the final EV pellet. Immunoblotting was carried out to determine the presence of the ESCRT I protein TSG101, as well as the tetraspanin CD9. Both of these were identified in dUC EV preparations from both the vector and OIS cells (Figure 4.7). The blots were loaded with matched particle numbers based upon NTA data. However, only TSG101 gave consistent band intensity between the proliferating and OIS samples. This may reflect heterogeneity within the isolated vesicles, as EVs have previously been described which lack CD9 (Kowal *et al.*, 2016). Next, in order to establish that the majority of isolated EVs were derived from an endosomal origin, the endoplasmic reticulum (ER) protein calnexin was investigated (Figure 4.7). Proteins from non-endosomal organelles are often employed as "negative" exosome markers, in order to demonstrate the absence of additional EV subclasses, which are proposed to be more susceptible to incorporation of such "contaminating" protein (Théry *et al.*, 2018). Interestingly, calnexin was detectable in EV samples from both vector and OIS cells, indicating the presence of EVs other than exosomes. However, the most pertinent comparison that should be made is that between the relative abundance of calnexin and TSG101 within the EV and WCL samples. In the WCL, there is strong expression of calnexin with no observable detection of Tsg101 at this exposure. Conversely, in the EV samples, there is greater expression of Tsg101 than that seen for calnexin. This suggests that the EV samples are enriched for exosomal markers and have lower abundance of non-exosomal protein than observed in the WCL. Together with the NTA data, which suggests that the isolated particles are ~100nm in diameter, this indicates that the dUC protocol has successfully isolated a population of EVs that is enriched for exosomes.

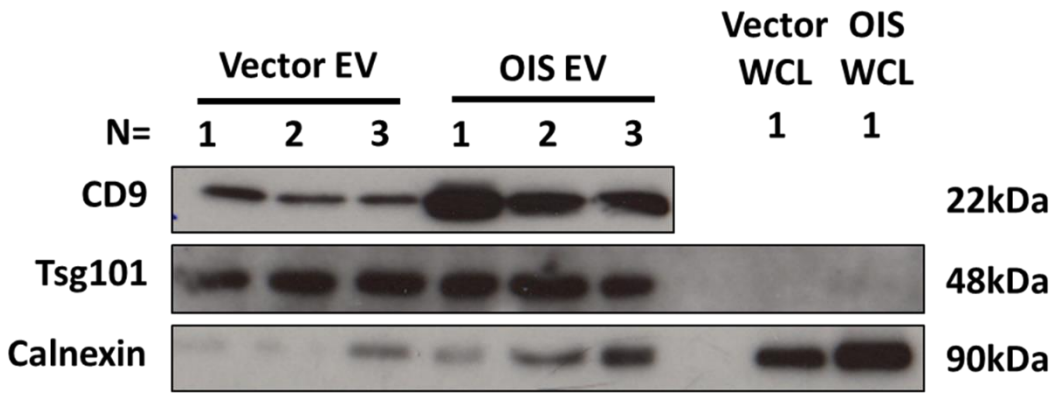

Figure 4.7: Western blot analysis of EVs and whole cell lysate (WCL) from vector or oncogene-induced senescent (OIS) IMR90 fibroblasts by differential centrifugation

Immunoblot analysis of extracellular vesicles (EV) isolated by differential ultracentrifugation (dUC) and whole cell lysate (WCL) from vector and OIS IMR90s for TSG101 and calnexin. CD9 was investigated in the EV samples only. Each lane contains sample prepared during an individual experiment. EV: N=3 independent experimental replicates (1 technical replicate per experiment) WCL: N=1 independent experimental replicate (1 technical replicate per experiment).

4.5 Proteomic Analysis 1: Differential Centrifugation OIS and Vector (EVs)

Following validation that the dUC protocol isolated EVs, attention turned to characterising the overall composition of the vesicles, as well as exploring any changes that occurred with the induction of OIS. Proteomic analysis was performed by MS, with an initial proof-of-principle experiment aimed at understanding the feasibility of characterising the EVs in this manner. As such, whilst the starting cell number was consistent, following senescence induction, EVs were generated from fewer OIS cells than those from the vector control. Equally, given the reported lack of precision associated with NTA as a technique, no attempt was made to match for particle numbers as with immunoblotting. Therefore, for clarity, more EVs from fewer OIS cells were analysed than from the vector control and, unsurprisingly, differential expression was observed between the two conditions (Figure 4.8A). Overall, 571 proteins were detected in both samples, with increased abundance of 131 and decreased abundance of 80 in OIS. Importantly, proteins with increased abundance included key markers of senescence (HRAS), endosomal biogenesis (PDCD6IP/ALIX) as well as the validated tetraspanin CD9. Interestingly, several proteins previously identified in the OIS SASP were also identified at increased levels (CXCL8; PLAU; MMP1; MMP14). This highlighted the potential that EVs may have the capacity to act as "carriers" or "facilitators" of the SASP. However, it also demonstrated the possibility that components of the secretome other than EVs may be isolated during the dUC process. Indeed, gene-ontology assessment of cellular compartments indicated that of the top 50 most abundantly expressed proteins in each condition, a significant portion were associated with either the "extracellular region" or "extracellular space" (Figure 4.8B). These terms suggested that there was the potential for soluble protein contamination of the final EV pellet, a limitation of dUC that has been reported previously (Foers *et al.*, 2018). In a senescence setting, this may represent a significant limitation, as the SASP represents a major source of potential soluble contamination. Therefore, in order to validate the presence of SASP factors within the EV

samples, IL-8 was assessed by ELISA. This clearly demonstrated an increased IL-8 content in the OIS EV samples (885.9 ± 128.2pg/ml; Figure 4.9) compared to the vector control (13.63 ± 14.91pg/ml; Figure 4.9). Therefore, it was concluded that this preliminary round of proteomic assessment had to be treated with caution, as the identified factors could not confidently be designated as either cargo or contaminant. Consequently, attention turned to whether an alternative or complimentary isolation method would be more appropriate in a senescence setting.

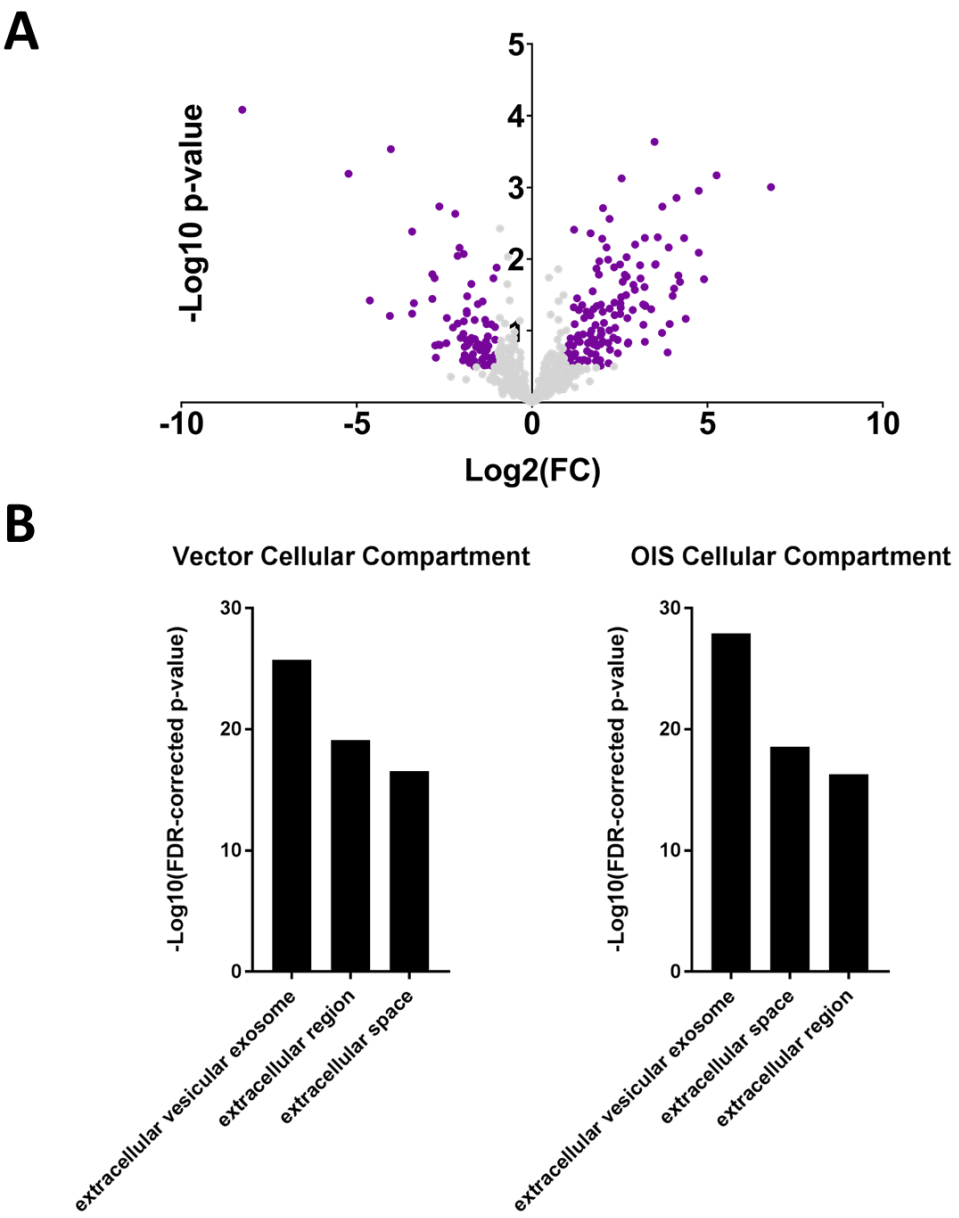

Figure 4.8: Volcano Plot and Gene Ontology Cellular Compartment Terms for EV Samples Isolated from vector or oncogene-induced senescent (OIS) IMR90 fibroblasts by differential centrifugation (dUC)

Extracellular vesicles (EV) isolated by differential ultracentrifugation (dUC) from vector and OIS IMR90s were analysed by mass spectrometry. **A)** Volcano plot demonstrating Log2 fold change (Log2FC) in protein expression between OIS and vector samples. **B)** Gene ontology cellular compartment terms in vector and OIS samples. N=3 independent experimental replicates (1 technical replicate per experiment).

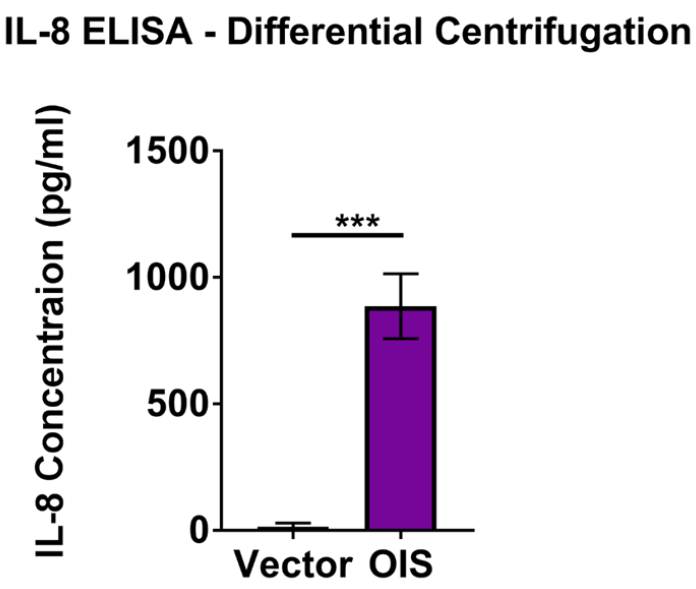

Figure 4.9: IL-8 ELISA analysis for extracellular vesicle (EV) samples isolated from vector or oncogene-induced senescent (OIS) IMR90 fibroblasts by differential centrifugation

Extracellular vesicles (EV) isolated by differential ultracentrifugation (dUC) from vector and OIS IMR90s were assessed by ELISA for the senescence-associated secretory phenotype (SASP) marker IL-8. N=3 independent experimental replicates (3 technical replicates per experiment). Statistical analysis performed via unpaired Student's t-test (section 2.17).

4.6 Purification of EV Isolation procedure via Size Exclusion Chromatography (SEC)

4.6.1 Assessing EVs Isolated by SEC by NTA and Immunoblotting

One key advantage of dUC is the ability to concentrate EVs from a large starting volume into a small final preparation. Given that dUC had also been established as successfully isolating EVs from senescent cells, it was not abandoned as a technique outright. However, as described in the previous section, the final dUC preparations required further assessment, and possibly further purification. Size-exclusion chromatography (SEC) was selected as a complimentary, adjunct technique, as one of the main purported advantages is the separation of soluble and vesicular material. Commercially available Izon qEV columns were selected, as there is significant literature support for their use (Lobb *et al.*, 2015). The final dUC pellet was loaded into these columns and twenty sequential fractions were collected, as per the manufacturer's instructions (Figure 4.10). Previous reports suggest that Fractions 7-10 (particularly Fraction 8), should contain the vesicles, whilst the later fractions (particularly Fraction 20), should contain soluble contaminants. As a starting point, Fraction 8 was collected from vector control and OIS samples. Particle concentration and size measurements were assessed by NTA in the same manner as those from the dUC protocol. Whilst modal sizes in both samples remained ~100nm (vector, 92.28 ± 7.667 nm; OIS, 107.2 ± 11.06 nm; Figure 4.11B) the particle yield was impaired, with the OIS sample approximately five times lower following SEC (dUC, 4.48E+11 ± 9.57E+09 Particles/ml; SEC, 8.79E+10 ± 2.11E+10 Particles/ml). Despite this, there was still a significantly higher production of particles in the OIS sample (8.79E+10 ± 2.11E+10 Particles/ml; Figure 4.11A) compared to the vector control (1.65E+10 ± 8.35E+09 Particles/ml; Figure 4.11A). In order to validate that the isolated particles were EVs, immunoblotting was once again performed for TSG101, CD9 and calnexin (Figure 4.12). However, due to the lower particle numbers observed by NTA, loading

was performed based on the maximum volume of sample that could be added per well, in order to increase the probability of observable bands. This decision appears to have been prudent, as the particle, concentration in the vector samples was too low for marker detection. However, in the OIS samples, clear CD9 expression could be observed, along with weaker (but detectable) TSG101 expression. Interestingly calnexin bands could still be observed (albeit faintly) and the relative difference to TSG101 expression between EV and WCL was maintained. When coupled with the NTA data, it was concluded that the addition of SEC to the dUC protocol still allowed the isolation of a population of small EVs enriched for exosomes, albeit with a much lower recovery yield.

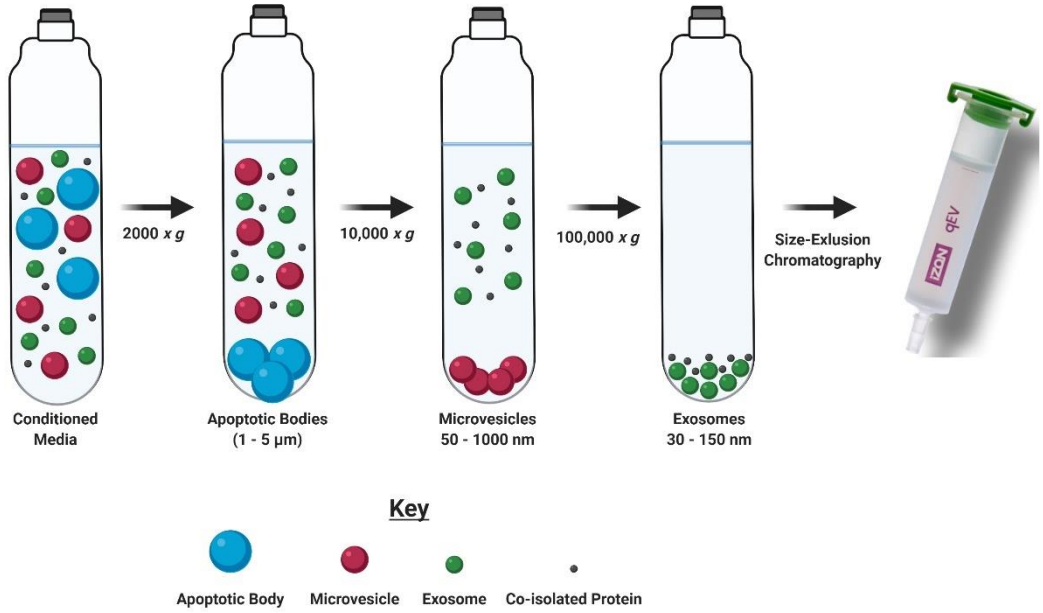

Figure 4.10: Schematic of EV Isolation Procedure by Size-Exclusion Chromatography

The differential ultracentrifugation (dUC) protocol employed in section 2.3 was adjusted to include a final size-exclusion chromatography step. This involved the loading of the dUC product (EVs + co-isolated protein) into a SEC column, from which 20 sequential fractions were then collected. Manufacturer's suggested EVs should be anticipated within Factions 7-10, whilst protein should be separated into later fractions.

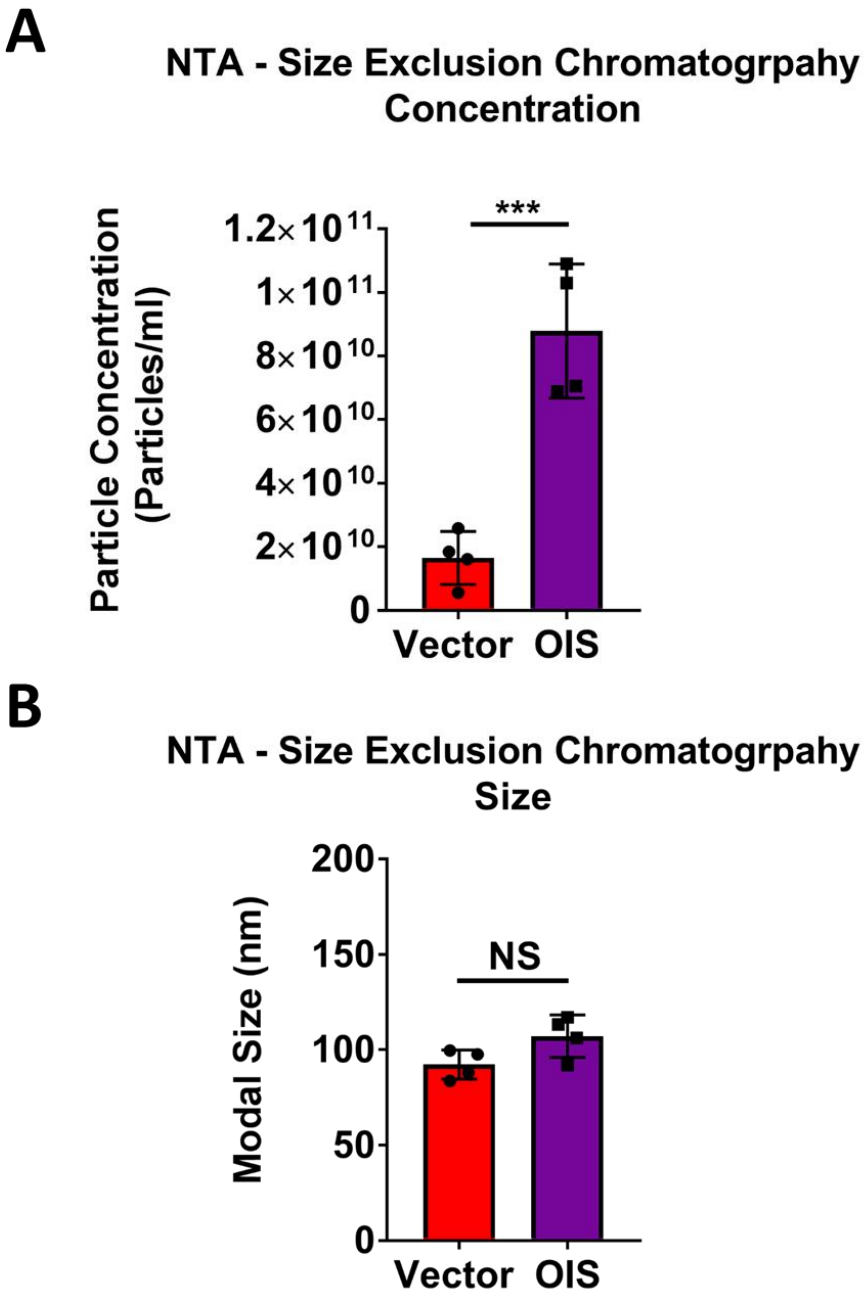

Figure 4.11: Nanoparticle Tracking Analysis (NTA) of EVs isolated from vector or oncogene-induced senescent (OIS) IMR90 fibroblasts by size-exclusion chromatography

Extracellular vesicles (EVs) were isolated by size-exclusion chromatography (SEC) from vector control and OIS IMR90s. Nanoparticle tracking analysis (NTA) was then performed on Fraction 8 samples to determine **A)** particle concentration and **B)** particle size measurements. N=4 independent experimental replicates (1 technical replicate per experiment). Statistical analysis performed via unpaired Student's t-test (section 2.17).

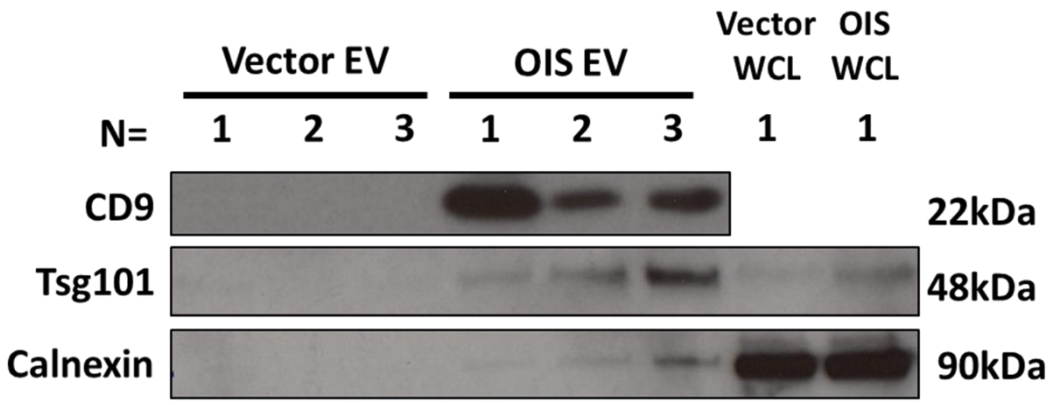

Figure 4.12: Western blot analysis of EVs and whole cell lysate (WCL) from vector or oncogene-induced senescent (OIS) IMR90 fibroblasts by size-exclusion chromatography

Immunoblot analysis of extracellular vesicle Fraction 8 (EV) isolated by size-exclusion chromatography (SEC) and whole cell lysate (WCL) from vector and OIS IMR90s for CD9, TSG101 and calnexin. Each lane contains sample prepared during an individual experiment. EV: N=3 independent experimental replicates (1 technical replicate per experiment) WCL: N=1 independent experimental replicates (1 technical replicate per experiment).

4.6.2 Further Analysis of All SEC Fractions in Vector and OIS Samples

In order to further assess SEC as an isolation technique, all fractions from vector and OIS samples were assessed for particle concentration by NTA, as well as protein concentration by microBCA. In the vector samples (Figure 4.13), there was a small increase in protein concentration in Fractions 7-10, which was associated with a modest increase in particle concentration, peaking in Fraction 8. In later fractions, there was a steady increase in protein concentration between Fractions 15-20. Importantly, this was not associated with an increase in particle concentration, with the Fraction 8 particle concentration (7.73E+09 ± 2.10E+09 Particles/ml; Figure 4.13B) significantly higher than that of Fraction 20 (7.33E+08 ± 5.92E+08 Particles/ml; Figure 4.13B). In the OIS samples, a similar trend was observed, with an overall increased protein and particle concentration in the EV Fractions 7-10 than those observed in the vector samples. Once again, whilst protein concentration increased steadily between Fractions 15-20, this was not associated with an increase in particle number. As such, the particle concentration in OIS Fraction 20 (3.73E+09 ± 1.66E+09 Particles/ml; Figure 4.14B) was significantly lower than that seen in the in Fraction 8 (4.63E+10 ± 1.76E+10 Particles/ml; Figure 4.14B). The Fraction 8 concentration is not comparable to that seen in Figure 4.11, as a different OIS isolation schedule had been (schedule 2). Overall, analysis of all fractions in both the vector and OIS samples indicates that SEC is efficient at separating EVs into Fractions 7-10 (with the highest concentration in Fraction 8), whilst soluble, non-EV protein, which is co-isolated during the dUC process, is confined to Fractions 15-20. Therefore, it become important to explore whether the SASP proteins identified in dUC EV samples by MS and ELISA, were associated with the SEC "EV" or "soluble" fractions. Consequently, all fractions from the OIS samples were assessed for IL-8 concentration by ELISA. A modest peak in IL-8 concentration was observed in Fractions 7-10 (most prominently in Fraction 8). However, a far greater IL-8 content was observed in the later fractions, with a steady increase between Fractions 15-20. This resulted in a significantly greater IL-8 content

in Fraction 20 (190.1 ± 45.43 Particles/ml; Figure 4.15) than Fraction 8 (36.77 ± 24.47 Particles/ml; Figure 4.15B). The implication of this finding was that whilst some IL-8 may be associated with the EVs, the vast majority could be considered a soluble, contaminating by-product of the dUC isolation procedure. Therefore, this would represent a major advantage of SEC by providing a means of dissecting the vesicular and soluble portions of the senescent secretome. However, as the relative loss of yield represented a substantial limitation of SEC, it was decided to explore the composition of Fraction 8 and Fraction 20 in more detail, in order to present a more comprehensive rationale for the use of SEC in subsequent experiments.

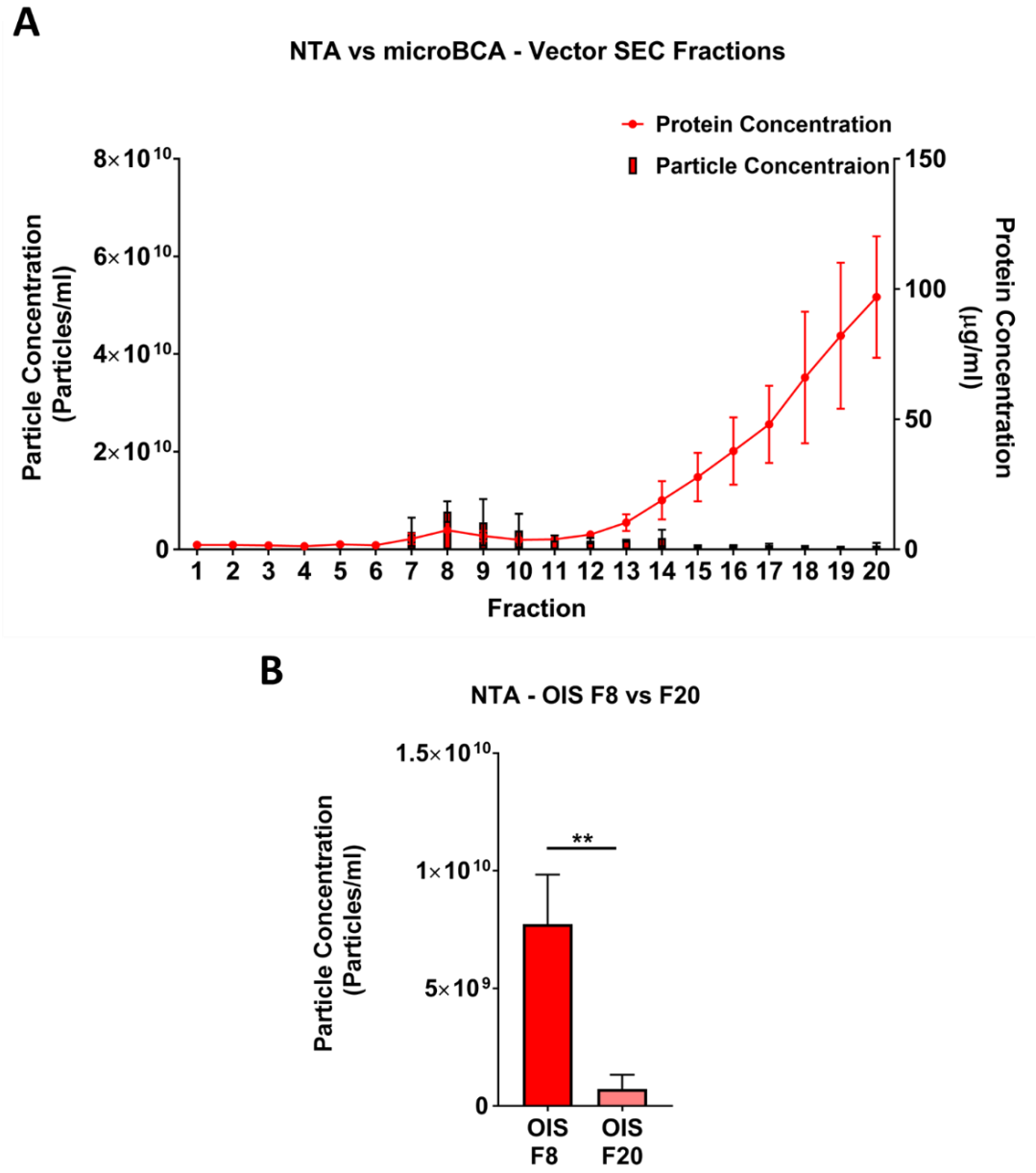

Figure 4.13: microBCA and nanoparticle tracking analysis (NTA) of EV fractions from vector IMR90 fibroblasts isolated by size-exclusion chromatography (section 2.8.2)

Extracellular vesicles (EVs) were isolated by size-exclusion chromatography (SEC) from vector control IMR90s. **A)** Nanoparticle tracking analysis (NTA) was performed on Fractions 6-20 and microBCA protein concentration measured in Fraction 1-20. **B)** Comparison of NTA concentration data for Fractions 8 and 20. N=3 independent experimental replicates (NTA, 1 technical replicate per experiment; microBCA, 3 technical replicates per experiment). Statistical analysis performed via unpaired Student's t-test (section 2.17).

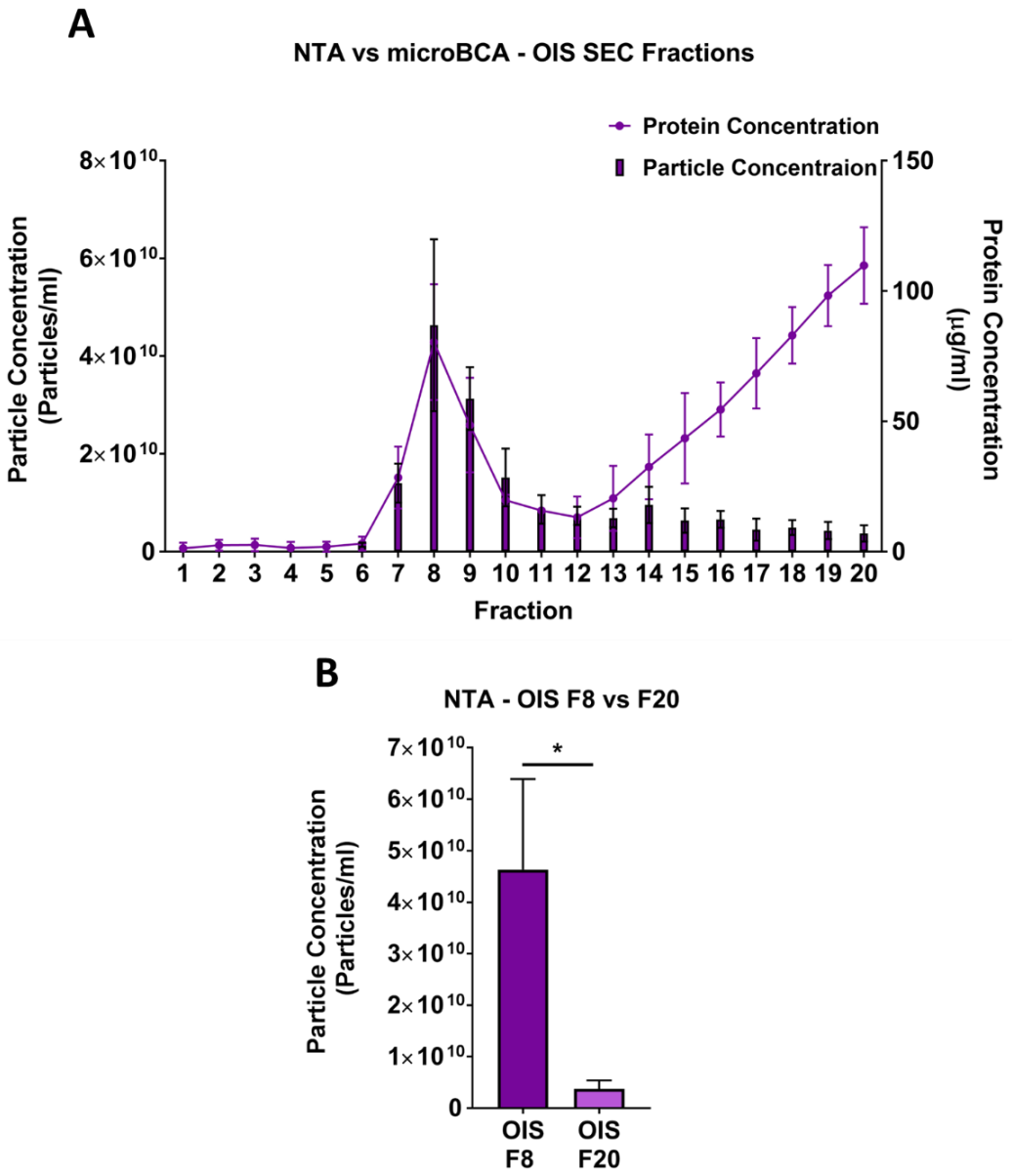

Figure 4.14: microBCA and nanoparticle tracking analysis (NTA) of EV fractions from oncogene-induced senescent (OIS) IMR90 fibroblasts isolated by size-exclusion chromatography (section 2.8.2)

Extracellular vesicles (EVs) were isolated by size-exclusion chromatography (SEC) from OIS IMR90s. **A)** Nanoparticle tracking analysis (NTA) was performed on Fractions 6-20 and microBCA protein concentration measured in Fraction 1-20. **B)** Comparison of NTA concentration data for Fractions 8 and 20. N=3 independent experimental replicates (NTA, 1 technical replicate per experiment; microBCA, 3 technical replicates per experiment). Statistical analysis performed via unpaired Student's t-test (section 2.17).

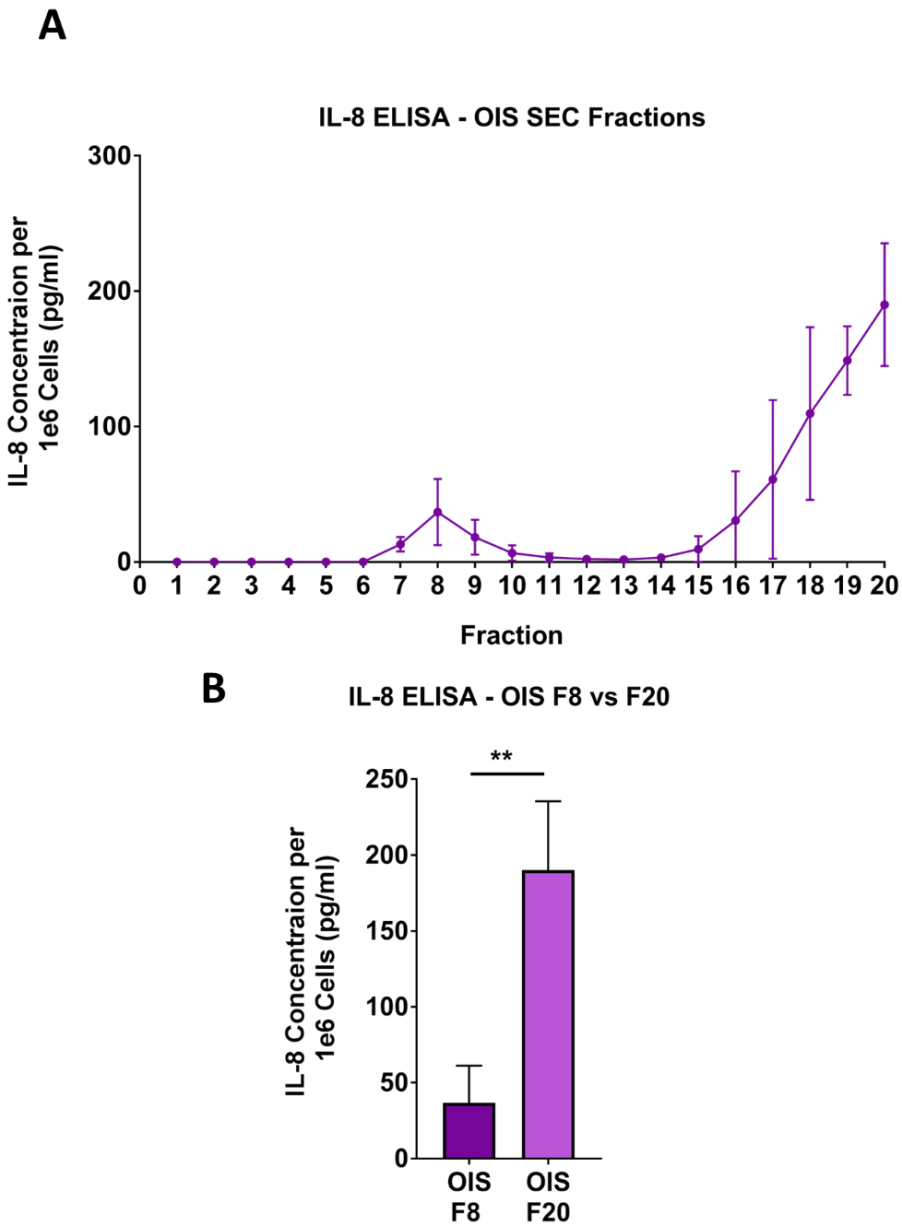

Figure 4.15: IL-8 ELISA analyses of EV fractions from oncogene-induced senescent (OIS) IMR90 fibroblasts isolated by size-exclusion chromatography (section 2.8.2)

Extracellular vesicles (EVs) were isolated by size-exclusion chromatography (SEC) from OIS IMR90s. **A)** All Fractions 6-20 were assessed by ELISA for the senescence-associated secretory phenotype (SASP) component IL-8 **B)** Comparison of IL-8 concentration data for Fractions 8 and 20. N=3 independent experimental replicates (3 technical replicates per experiment). Statistical analysis performed via unpaired Student's t-test (section 2.17).

4.7 Proteomic Analysis 2: Size-Exclusion OIS (Conditioned Media, Fraction 8 and Fraction 20)

Analysis of SEC fractions indicated that, whilst producing a lower overall EV recovery yield than dUC, greater separation between the vesicular and soluble secretomes was also achieved. Fraction 8 was designated as the primary EV fraction, whilst Fraction 20 was designated as representing the co-isolated, soluble contaminating protein. Along with total conditioned media samples, these fractions were analysed by MS, in order to further explore the relative compositions between sample types, as well as provide justification for use of SEC over dUC. Because these samples were fundamentally different, no attempt was made to normalise based on protein or particle concentrations. The first, and perhaps most striking finding, were the differences in total unique proteins identified within the different samples. (Fraction 8, 698; Fraction 20 14; Conditioned Media, 78; Figure 4.16). In order to explore this further, GO pathway analysis was performed (Figure 4.17). Cellular compartment terms indicated that whilst the CM and Fraction 20 samples had enrichment for EV proteins, they also possessed significant representation from the extracellular region and extracellular space, i.e. secreted protein. In contrast, Fraction 8 was associated with strong enrichment for EVs but also for proteins of the plasma membrane and cytosol. This reinforces the concept that Fraction 8 contains small membrane bound vesicles, which include cytoplasmic contents derived from the parental cell, validating SEC as an isolation procedure. This was supported by protein localisation data from Protein Atlas (Figure 4.18), which demonstrated that proteins considered membrane bound or intracellular were primarily enriched into Fraction 8, accounting for the disparity in total unique proteins seen in that fraction. Conversely, secreted proteins displayed little enrichment between samples, which was also the case for a list of canonical SASP factors identified from (Coppé *et al.*, 2010) (Figure 4.19). This highlights the benefits of SEC as an isolation technique, as without it, these secreted proteins would be a confounding influence in all subsequent proteomic and functional

experiments. Therefore, it was accepted that SEC provided sufficient benefits over dUC to accept the loss of yield. Consequently, efforts turned to producing a comprehensive and rigorous assessment of the changes in EV composition following OIS induction, by using SEC as a more robust and stringent technique.

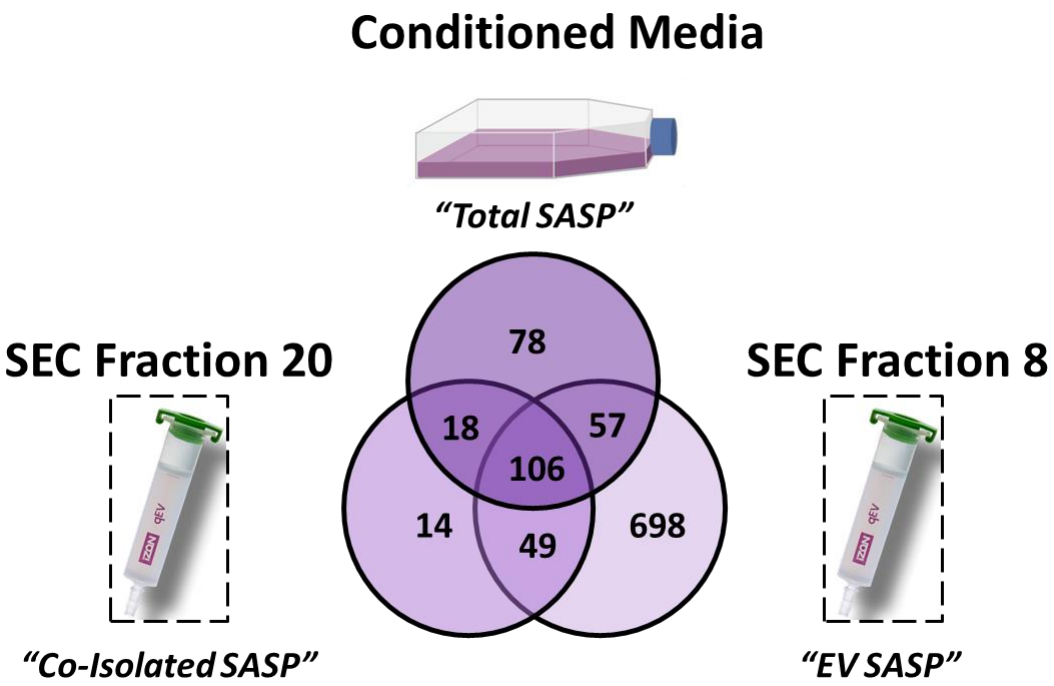

Figure 4.16: Schematic of conditioned media (CM), SEC Fraction 20 and SEC Fraction 8 from oncogene-induced senescent (OIS) IMR90 fibroblasts

Conditioned media (CM), SEC Fraction 20 and SEC Fraction 8 samples from oncogene-induced senescent (OIS) IMR90 fibroblasts were assessed by mass spectrometry (MS). Proteins are identified within each sample type are indicated in the Venn diagram. N=3 independent experimental replicates (1 technical replicate per experiment).

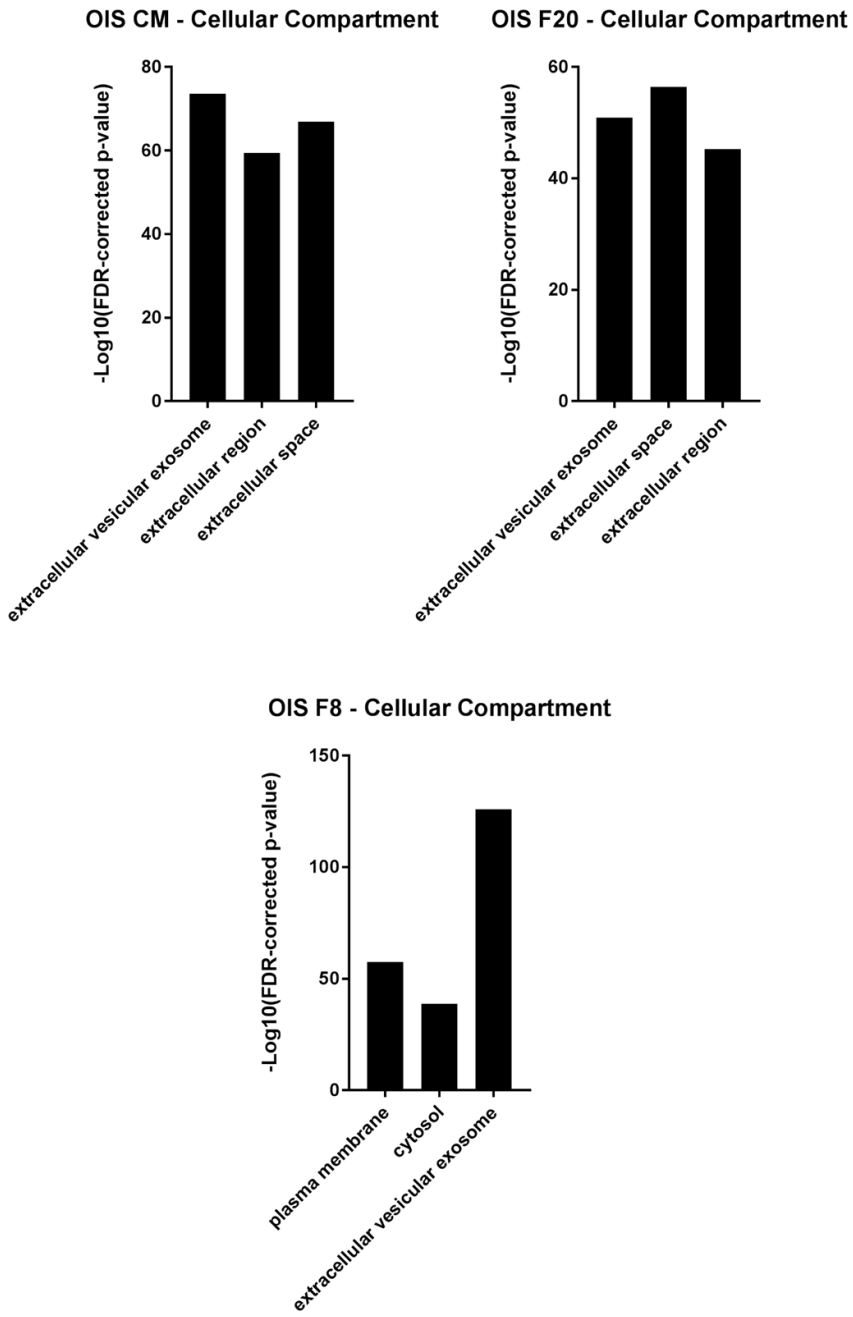

Figure 4.17: Gene ontology cellular compartment terms for conditioned media (CM), SEC Fraction 20 and SEC Fraction 8 from oncogene-induced senescent (OIS) IMR90 fibroblasts

Conditioned media and size-exclusion chromatography (SEC) Fractions 8 and 20 from OIS IMR90s were analysed by mass spectrometry. Gene Ontology cellular compartment terms were then assessed for all proteins identified in each sample type. N=3 independent experimental replicates (1 technical replicate per experiment).

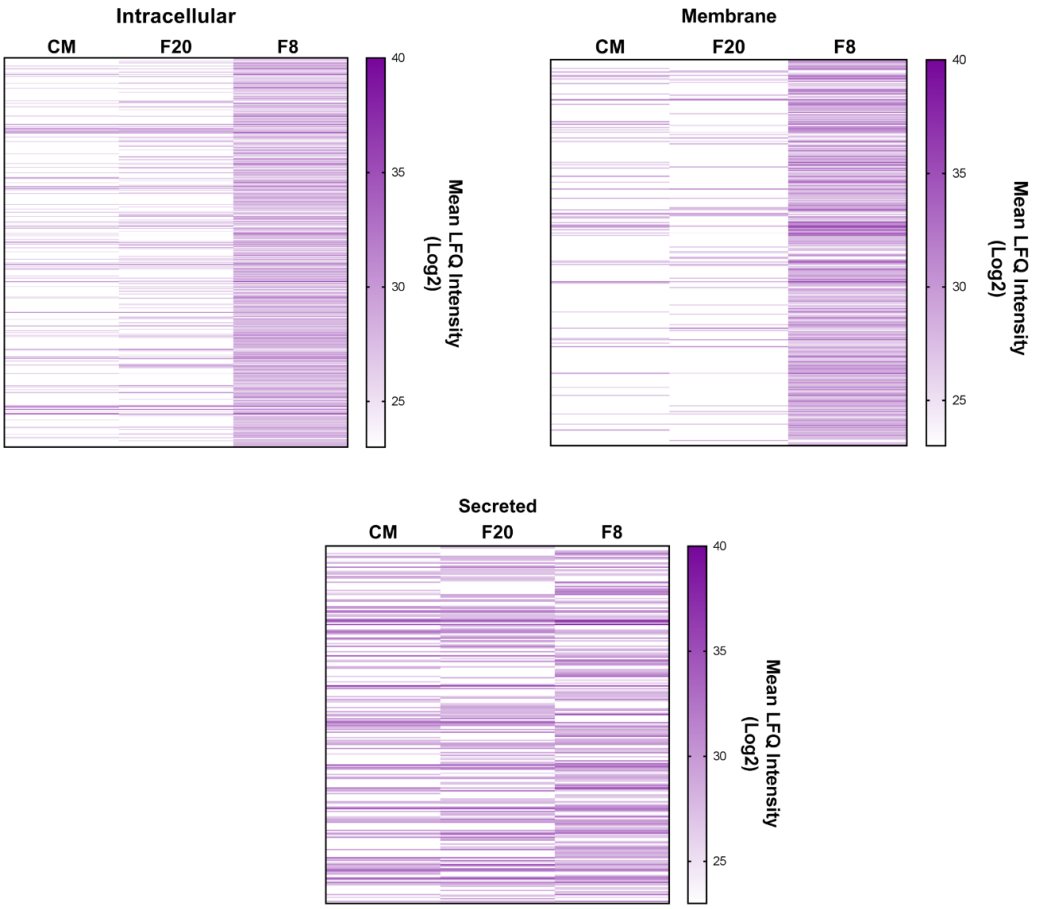

Figure 4.18: Heat maps showing Protein Atlas localisation data for conditioned media (CM), SEC Fraction 20 and SEC Fraction 8 from oncogene-induced senescent (OIS) IMR90s

Size-exclusion chromatography (SEC) was utilised as a means of EV isolation from OIS IMR90s according to the procedure described in section 2.8.2. SEC fractions 8 (EVs) and 20 (co-isolated protein) were analysed by mass spectrometry, along with conditioned media that was not subject to the EV isolation procedure. Protein localisations were then assessed via Protein Atlas (www.proteinatlas.org) for all proteins identified in each sample. Proteins were defined as either intracellular, membrane or secreted, with proteins able to receive multiple designations. For each localisation category, a heat map was produced that displays the mean LFQ intensity from three independent experimental replicates per sample for each protein. Proteins not identified in a sample appear white. N=3 independent experimental replicates (1 technical replicate per experiment).

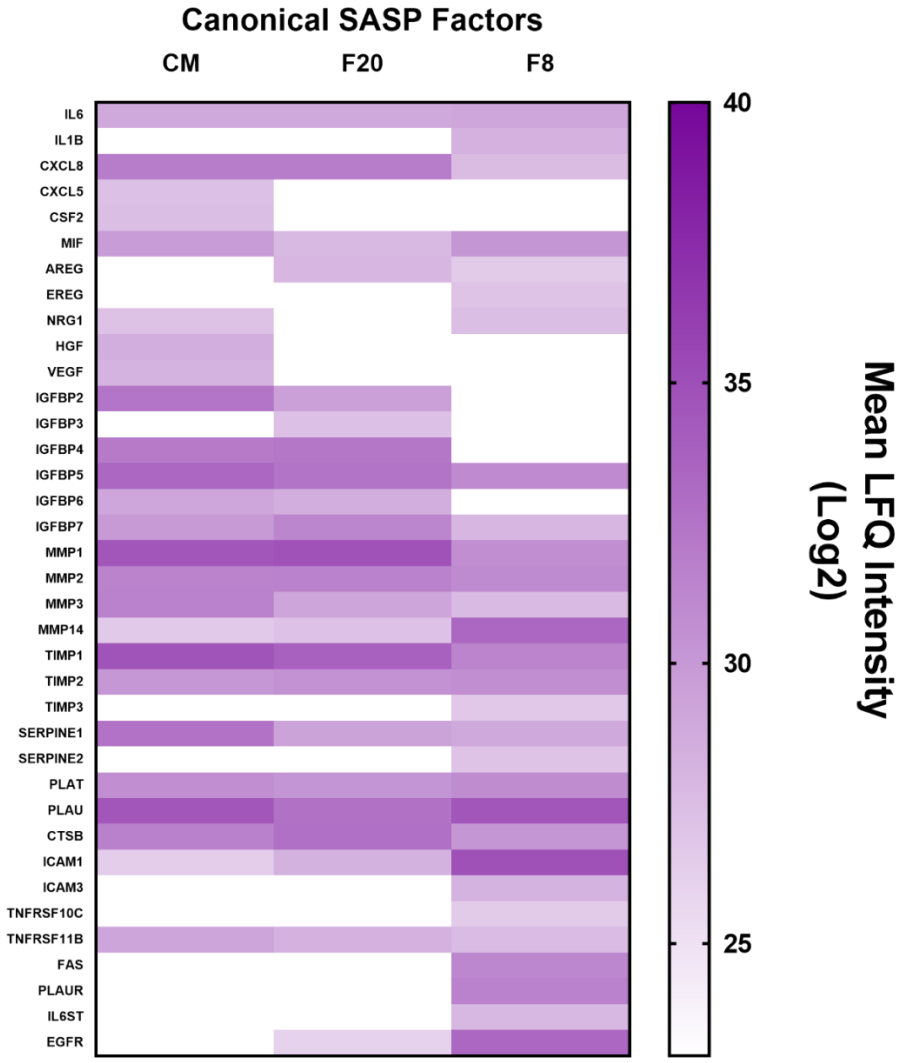

Figure 4.19: Canonical SASP Factors (and related) from (Coppé *et al.*, 2010)

Size-exclusion chromatography (SEC) was utilised as a means of EV isolation from OIS IMR90s according to the procedure described in section 2.8.2. SEC fractions 8 (EVs) and 20 (co-isolated protein) were analysed by mass spectrometry, along with conditioned media that was not subject to the EV isolation procedure. Proteins considered canonical SASP markers were identified based upon classification in (Coppé *et al*., 2010). Non-soluble extracellular-matrix components (collagens, laminins and fibronectin) were omitted. A heat map was produced that displays the mean LFQ intensity from three independent experimental replicates per sample for each protein. Proteins not identified in a sample appear white. N=3 independent experimental replicates (1 technical replicate per experiment). N=3 independent experimental replicates (1 technical replicate per experiment).

4.8 Proteomic Analysis 3: Size-Exclusion OIS and Vector (Conditioned Media, Fraction 8 and Fraction 20)

Following the establishment that SEC represented a more appropriate isolation methodology than differential centrifugation alone, a final round of proteomic analysis was employed in order to compare the conditioned media, Fraction 8 and Fraction 20 from both vector and OIS samples. Principal component analysis demonstrated that the different sample types were the primary determinant of protein expression. However, in all samples there was also distinct separation between the vector and OIS conditions along at least one principal component (Figure 4.20). Supporting this, hierarchical clustering analysis demonstrated that the soluble samples (CM and Fraction 20) had distinct expression profiles compared to the vesicular Fraction 8 samples (Figure 4.21). Here, the vector and OIS conditions also clustered separately, with the OIS samples demonstrating higher expression in many proteins. To explore this further, mean LFQ intensities were compared between vector and OIS conditions within each sample type (Figure 4.22). Differential expression was observed within all samples with increased abundance of 298, 144 and 374 proteins in OIS conditioned media, Fraction 20 and Fraction 8 respectively (Figure 4.23A). Of these, 256 were unique to Fraction 8 and GO analysis indicated that these comprised predominantly vesicular, membrane and cytosolic proteins (Figure 4.23B). These included the validated EV marker CD9 and the previously reported functional senescence cell-derived EV protein EphA2. This profile of Fraction 8 is not unexpected, as it would be anticipated to be enriched for EV proteins given the higher particle concentration compared to the vector identified by NTA. However, it is encouraging that those proteins with uniquely increased abundance in Fraction 8 appear predominantly vesicular, as this provides a clear distinction from the soluble Fraction 20 and CM. This list of 256 proteins (Appendix 4) represents a rich data set for probing any potential functional distinction between the vesicular and soluble SASP.

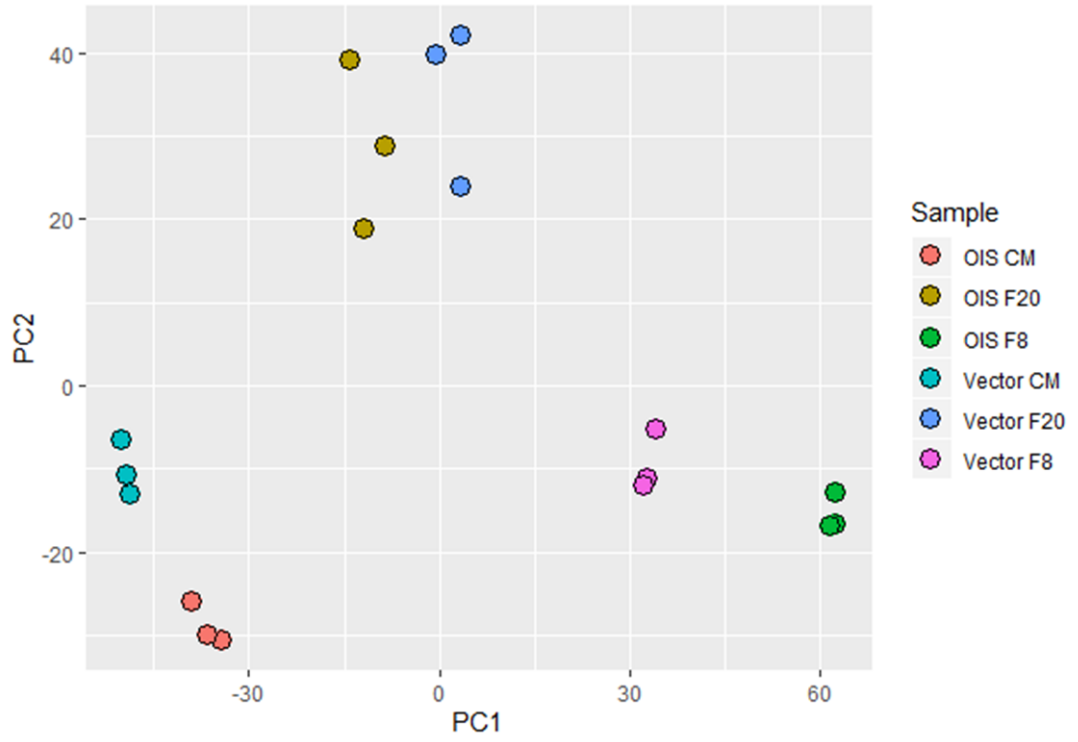

Figure 4.20: Principal component analysis (PCA) of conditioned media (CM), SEC Fraction 20 and SEC Fraction 8 from vector and oncogene-induced senescent (OIS) IMR90 fibroblasts

Conditioned media and size-exclusion chromatography (SEC) Fractions 8 and 20 from vector and OIS IMR90s were analysed by mass spectrometry. Principal component analysis was performed using mean LFQ intensity values for each identified protein within each sample. N=3 independent experimental replicates (1 technical replicate per experiment).

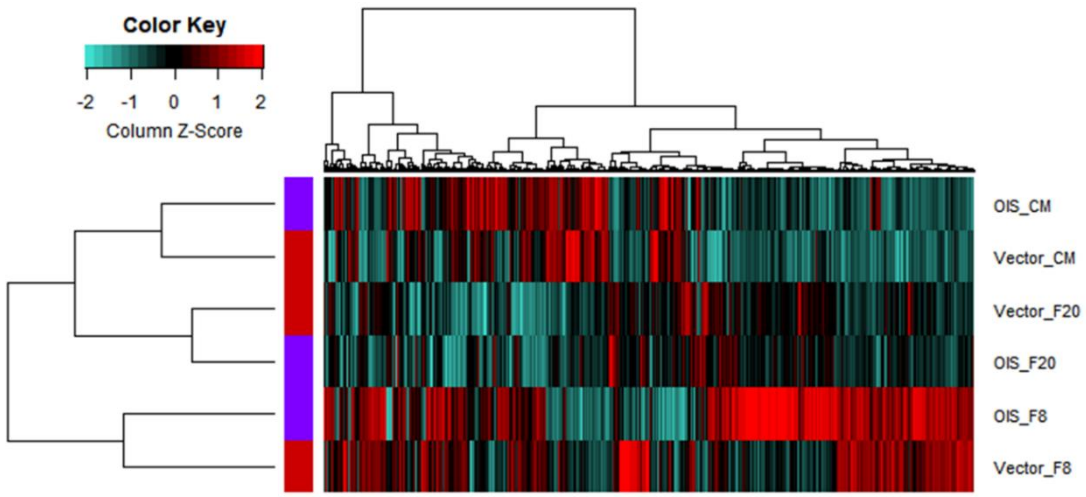

Figure 4.21: Hierarchical clustering analysis of conditioned media (CM), SEC Fraction 20 and SEC Fraction 8 from vector and oncogene-induced senescent (OIS) IMR90 fibroblasts

Conditioned media and size-exclusion chromatography (SEC) Fractions 8 and 20 from vector and OIS IMR90s were analysed by mass spectrometry. Hierarchical clustering analysis was performed using mean LFQ intensity values for each identified protein within each sample. Purple block identifies OIS samples and red block vector samples. N=3 independent experimental replicates (1 technical replicate per experiment).

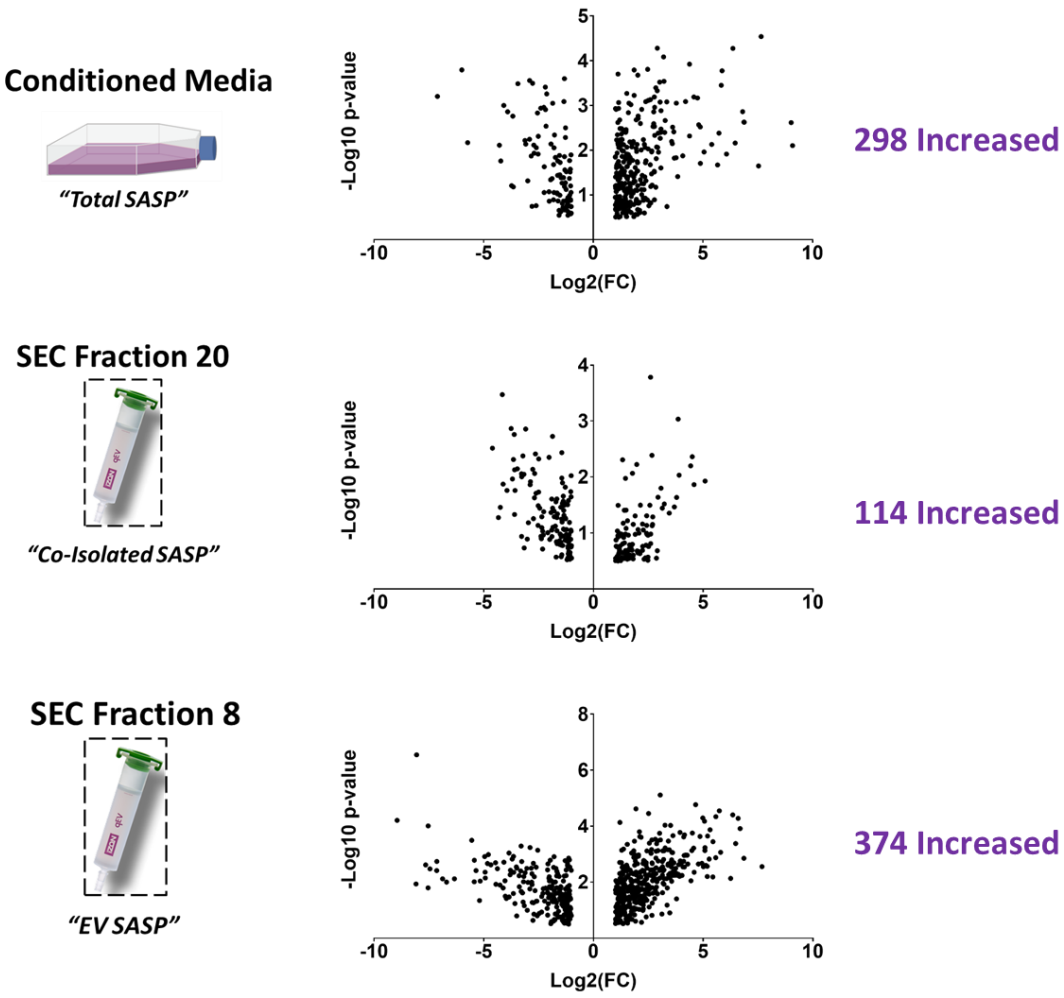

Figure 4.22: Volcano plots of conditioned media (CM), SEC Fraction 20 and SEC Fraction 8 from vector and oncogene-induced senescent (OIS) IMR90 fibroblasts

Conditioned media and size-exclusion chromatography (SEC) Fractions 8 and 20 from vector and OIS IMR90s were analysed by mass spectrometry. Volcano plots demonstrating Log2 fold change (Log2FC) in protein expression between OIS and vector conditions for each sample type were then prepared and the number of proteins present at increased levels highlighted. N=3 independent experimental replicates (1 technical replicate per experiment).

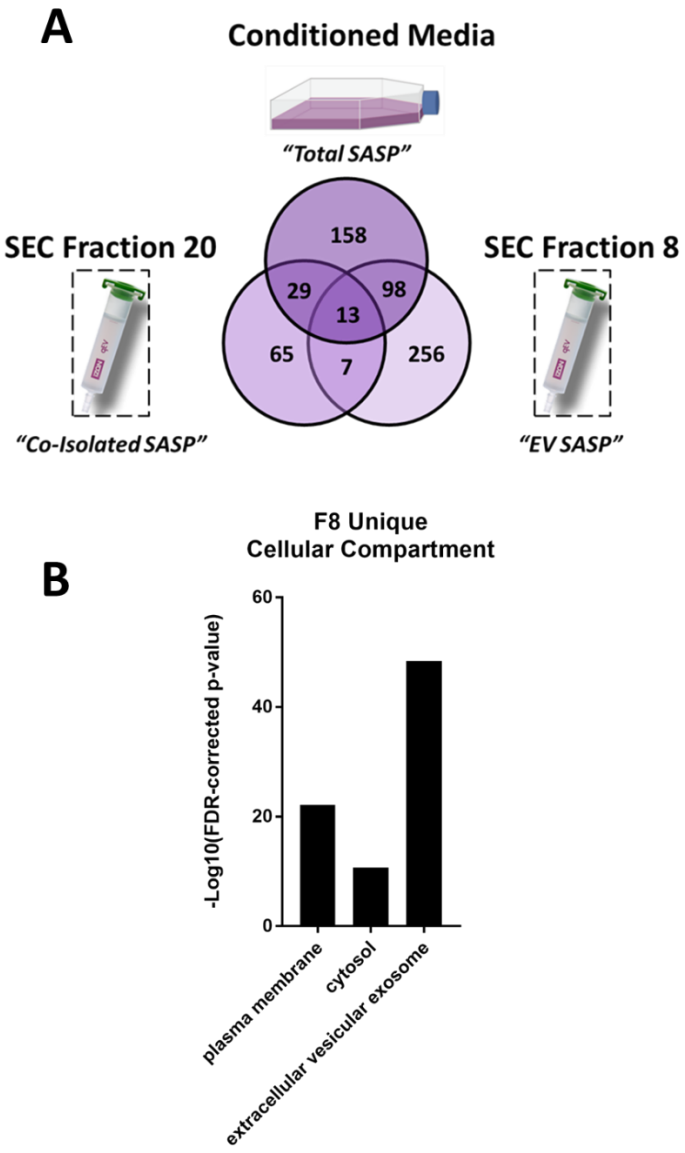

Figure 4.23: Schematic showing number of proteins with increased abundance in conditioned media (CM), SEC Fraction 20 and SEC Fraction 8 from oncogene-induced senescent (OIS) IMR90 fibroblasts and GO terms for those unique to OIS Fraction 8.

Conditioned media (CM), SEC Fraction 20 and SEC Fraction 8 samples from oncogene-induced senescent (OIS) and vector control IMR90 fibroblasts were assessed by mass spectrometry (MS). A) Proteins with increased abundance in OIS conditions were then identified (figure 4.22) within each sample type and are indicated in the Venn diagram. B) Gene Ontology cellular compartment terms were then assessed for proteins unique to OIS Fraction 8. N=3 independent experimental replicates (1 technical replicate per experiment).

4.9 Summary

EV research represents a burgeoning field, in which no single isolation technique or characterisation methodology has emerged as a universal gold standard. This is in part due to the ubiquity of EVs, which have been isolated and studied from a plethora of biological fluids and cell types, each of which require application of a context specific approach. Furthermore, the small size and lack of subset specific markers represent technical challenges that have hindered EV research, leading to attempts to achieve consensus and reporting standardisation (Lotvall *et al.*, 2014). However, this remains an issue within the field and in a senescence setting, a diverse set of isolation methodologies, characterisation methods and senescence models have been employed (Wallis, Mizen and Bishop, 2020). Therefore, it was important to establish that the isolation methodologies selected were appropriate and robust.

In this chapter, the process of setting up a rigorous workflow for EV isolation and characterisation from senescent cells has been described. This required numerous technical challenges to be overcome, simply to confidently isolate a population of EVs. Firstly, a solution was found to the issue of contaminating bovine EVs from FBS. Several alternatives were considered, but the use of a commercial “exosome” depleted FBS (ExoFBS) was demonstrated to produce negligible bovine EV contamination, whilst not compromising EP cellular proliferation. This was specifically aligned to the current isolation time-line, which subsequently underwent further optimisation. However, as the use of ExoFBS allowed interchange between multiple models of senescence, a balance between EV depletion, proliferation maintenance and logistical practicality justified its use. Similarly, investigations into the most appropriate storage conditions were made under the assumption that FBS derived EVs would behave in a similar manner to those from cultured cells. The decision to

store at -80°C was made by weighing the lack of experimentally observed degradation with literature recommended best practice. As with use of ExoFBS, this had to be considered alongside the practicality of working in multiple models of senescence. Therefore, whilst not conclusive, these initial experiments provided confidence that EV preparations could be produced which were free from contaminating bovine EVs and which could be stored long term without compromising integrity.

Having established these fundamentals, dUC was then used to isolate EVs from both the OIS and HMFs models. In both cases, the number of EVs produced increased in the senescent population (although the HMFs had yet to reach the point RS). This finding supports previous literature reports of EV production increasing in senescence (section 1.3.1). At this point, given the expediency of the OIS model, the decision was made to focus on EV isolation in OIS. This model was considered more appropriate for isolation methodology development, given the relative availability of senescent cells. As the project developed, the OIS model continued to facilitate research questions and the RS model was not explored further. However, given the context dependent nature of the SASP, recapitulating work in RS would support the conclusions drawn. Therefore, this has been included as a suggestion for follow up investigations (section 6.2).

Immunoblotting supported NTA data in validating that the dUC protocol isolated a population of EVs enriched for exosomes. MS was then applied in order to characterise the change in EV composition with the induction of OIS. One initial hypothesis was that EVs could act as “carriers” of SASP factors and potentially facilitate paracrine senescence. Therefore, the observation of multiple SASP factors within the more abundant proteins in OIS was encouraging. However, given the reported limitation of dUC in co-isolating soluble protein,

these could not be considered a true “cargo”. So far, achieving the maximum yield of isolated EVs had been a priority, as the required thresholds for each analysis technique had not been established. However, as these appeared robust, the purity of the isolated EV preparations began to take precedence and the use of PBS washes was initially considered as a purification step. However, whilst this may have diluted contamination due to relative centrifugation efficiencies, the potential for factors that had co-isolated once to do so again was considered too high (Coumans *et al.*, 2017). Therefore, SEC was selected as a complimentary technique.

Initial characterisation of Fraction 8 indicated that, whilst successfully able to isolate EVs, SEC was associated with a significant loss of yield. However, when all fractions were analysed, the potential advantages of SEC became evident. NTA and protein analysis indicated that a clear distinction could be made between fractions containing EVs and those containing the co-isolated soluble contaminating protein. This was further highlighted by the observation that the vast majority of IL-8 that had been associated with EV preparations generated by dUC was likely to constitute a contaminant rather than a cargo, as this was now primarily associated with the later SEC fractions. This made a compelling case for the use of SEC, as the SASP represented a potent source of potential contamination if dUC was employed alone. However, in order justify the compromised recovery yield a second round of MS was performed.

This second round of MS compared the CM, Fraction 8 and Fraction 20 from the OIS cells, in order to identify the relative composition of each sample type. Because this exercise compared fundamentally different samples, it was felt that normalising for protein or particle concentration would not be appropriate. As such, all proteins detected were included in the analysis, as opposed to only those that appeared in both samples, as in MS1. This highlighted

that there were many more proteins within the Fraction 8 samples, suggesting a more complex composition. GO analysis of the cellular compartments indicated that the CM and Fraction 20 samples were predominantly extracellular (i.e. secreted) whilst Fraction 8 contained enrichment for both membrane and cytosolic proteins. This was supported by localisation data from a second source (Protein Atlas), which indicated that secreted proteins were present across all samples, whereas membrane and intracellular proteins were enriched in Fraction 8. Overall, the MS analysis supported the previous data. Fraction 8 contained membrane bound vesicles that in turn contained cytosolic proteins. SEC allowed these to be separated from the predominantly soluble content of the conditioned media that is confined to Fraction 20. This major benefit of SEC was considered to outweigh the loss of yield when selecting the most appropriate isolation technique. Therefore, a final round of MS was performed to more accurately profile the change in EV composition with the induction of OIS.

MS3 was intended to represent a comprehensive characterisation of the change in EV composition with the onset of OIS, taking into account the considerations of isolation methodology discussed above. For completeness, the total CM, Fraction 8 and Fraction 20 was analysed from both vector and OIS cells. Principal component and hierarchical clustering analysis demonstrated that samples clustered according to sample type, with the soluble samples clustering away from the vesicular Fraction 8. Within the Fraction 8 clusters, distinction between the proliferating and senescent conditions could be made, emphasising that EVs are a reflection of their parental cell. In all samples, OIS was associated with differential protein expression, with proteins of increased abundance in each condition. Of these, 256 were uniquely present at increased levels in the OIS Fraction 8, representing the proteins most distinctly “vesicular” and thus of functional interest to the pursuit of

senescence cell derived EV mediated paracrine signalling. Interestingly, these included the EV marker CD9 and the previously reported senescence-associated functional EV cargo EphA2 (Takasugi *et al.*, 2017). In combination with the findings of MS2, MS3 facilitated the identification of functional leads for further mechanistic exploration. These are described in section 5.6 and further discussed in section 6.3.

Overall, this chapter highlights the technical challenges involved in the isolation and characterisation of EVs, as well as the particular considerations that are involved when bringing this into a senescence setting. dUC was demonstrated to be efficient at isolating EVs from the conditioned media of senescent cells, but limited through the co-isolation of secreted proteins. SEC provided a complimentary purification technique, which allowed separation of the soluble and vesicular components of the senescent secretome. This facilitated the characterisation of changes in EV cargo following the onset of senescence, providing potential candidates for investigation of functionally relevant pathways.

5 Results 3: Characterising the Role of Small Extracellular Vesicles to the Paracrine Signalling of the SASP

5.1 Introduction

One of the defining characteristics of senescence is the acquisition of an enhanced secretome – the SASP. As discussed above (sections 1.1.4), the composition of the SASP is dependent on both the cell type and specific trigger of senescence. The SASP has also been described as having a "bright" and "dark" side, with beneficial or detrimental effects based upon the specific cell context (Campisi and D'Adda Di Fagagna, 2007). Furthermore, the SASP can act paradoxically, having contradictory effects depending on the setting (for example being both pro- and anti-tumorigenic). Perhaps the most widely described role of the SASP is the process of paracrine senescence, the ability to confer senescence on proliferating cells in the local microenvironment. In this chapter, the contribution of EVs to the phenomenon of paracrine senescence is assessed in both IMR90 fibroblasts and MDA-MB-468 basal-like breast cancer cells (468s).

Initially, the SASP was investigated through conditioned media investigations, in order to establish the functional effect of the total senescence secretome. Next, building on the principles established in chapter 4, EV preparations isolated by SEC were used to investigate the specific contribution of EVs to the signalling of the SASP. Finally, preliminary investigations are carried out, with the aim of identifying pathways that may be functionally relevant to the EV mediated functions of the SASP.

5.2 Chapter Hypothesis and Aims

The aim of this chapter was to characterise the contribution of EVs to the signalling properties of the SASP. It was hypothesised that EVs represent discrete mediators of paracrine senescence, capable of inducing a secondary senescence response independent from that of the soluble SASP. This was investigated by first benchmarking the OIS paracrine senescence response through conditioned media investigations. EV treatment experiments were then performed with senescence induction characterised by high content analysis (HCA). Potential mechanistic targets were selected according to the proteomic profiling in Results 2, with the NOTCH1 and ADAM10/17 pathways hypothesised to be potential routes of EV mediated paracrine senescence.

The aims of this chapter are as follows:

- To characterise the paracrine senescence effect of the entire senescence secretome
    - To validate previously reported OIS paracrine senescence response through conditioned media investigations
    - To replicate paracrine senescence effect in a model of RS
    - To investigate the effect of OIS SASP on MDA-MB-468 basal-like breast cancer cells

- To characterise the contribution of EVs to the paracrine senescence effects of the SASP
    - To implement principles of SEC established in chapter 4 to explore the specific role of OIS cell derived EVs

- To explore potentially functional routes through which EVs may contribute to the paracrine senescence effects of the SASP
    - Investigate functional relevance of targets identified through proteomic assessment in chapter 4

5.3 Assessing the Paracrine Effects of the OIS SASP

The paracrine senescence effect of conditioned media from OIS IMR90s has been reported previously (Acosta *et al.*, 2013). It was important to reproduce this effect in order to provide a benchmark against which other paracrine senescence experiments could be assessed. Media was conditioned with OIS or vector control cells between day four and day eight, at which point it was collected, centrifuged at 2000 *x g* and supplemented with additional FBS and L-glutamine to ensure these would not be limiting (section 2.15). Vector control IMR90 fibroblasts were treated with this conditioned media (CM) one and four days post-seeding. The OIS CM produced a reduction in cell number compared to that from the vector cells (vector, 4504 ± 224.3; OIS, 1652 ± 73.2; Figure 5.1). This was accompanied by senescence-associated changes in a panel of morphological measures assessed by HCA, previously established in section 3.3. Taken together, this indicates that a paracrine senescence response from OIS CM was successfully produced.

The functional role of the SASP is highly context dependent and has been demonstrated to produce a variety of often-contradictory effects. This is particularly the case in cancer, where the SASP has been demonstrated to be both pro and anti-tumorigenic (Rao and Jackson, 2016; Saleh *et al.*, 2018). Therefore, the effect of the OIS CM in MDA-MB-468 basal-like breast cancer cells was investigated. These p16 positive cells have previously been extensively investigated within the lab, with a particular emphasis on the induction of senescence and phenotypic assessment using HCA morphological measures (Preprint:(Moore *et al.*, 2018)). The 468s are maintained in a different media to that used for the fibroblasts and so an alternative dosing regime was used. Rather than culture entirely in CM, 10µl conditioned fibroblast media was added per well, with standard 468 media making up the remaining volume. Here, it was identified that the OIS CM produced a reduction in

cellular proliferation compared to the vector control, demonstrated by a reduction in cell number (vector, 10606 ± 923.3; OIS, 7237 ± 593.2; Figure 5.2). Importantly, this was accompanied by potent morphological changes similar to those achieved by senescence induction through other means (Preprint:(Moore *et al.*, 2018)). Interestingly, the vector CM produced an increase in cellular proliferation compared to the unconditioned control media (8749 ± 378.7; Figure 5.2) and there was no difference between this control and the OIS. This may reflect heterogeneity within the SASP, with individual factors producing contradictory effects. However, the clear differences in response between vector and OIS CM indicates that the SASP from OIS has an inhibitory effect on cellular proliferation in the 468s.

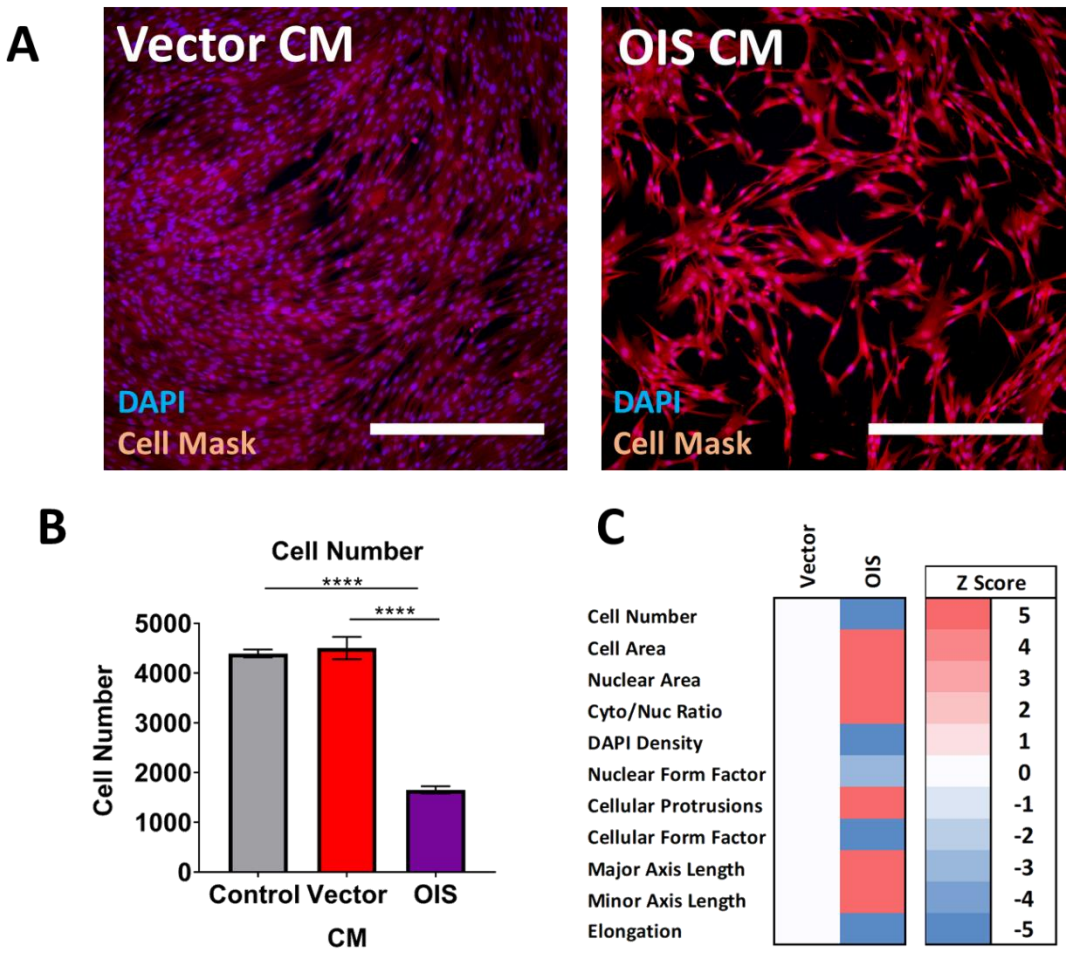

Figure 5.1: Immunofluorescence high-content analysis (HCA) of IMR90 fibroblasts treated with conditioned media from vector or oncogene-induced senescent (OIS) IMR90s

Vector IMR90 cells were treated with conditioned media (CM) collected from vector or OIS IMR90s and assessed by HCA. **A)** Representative immunofluorescence images for DAPI (blue) and Cell Mask (red) staining. **B)** Quantitation of HCA cell number. **C)** HCA morphology measures were converted to Z-scores according to the change from the vector control condition (see methods). Positive and negative modulation of each measure is demonstrated by a change of at least +/- one Z-score from the vector condition and indicated as red or blue respectively. White indicates no change from the control. N=3 independent experimental replicates (4 technical replicates per experiment). Statistical analysis performed via One-way ANOVA with Tukey's post-hoc test (section 2.17). Scale bars = 500µm. Four fields of view.

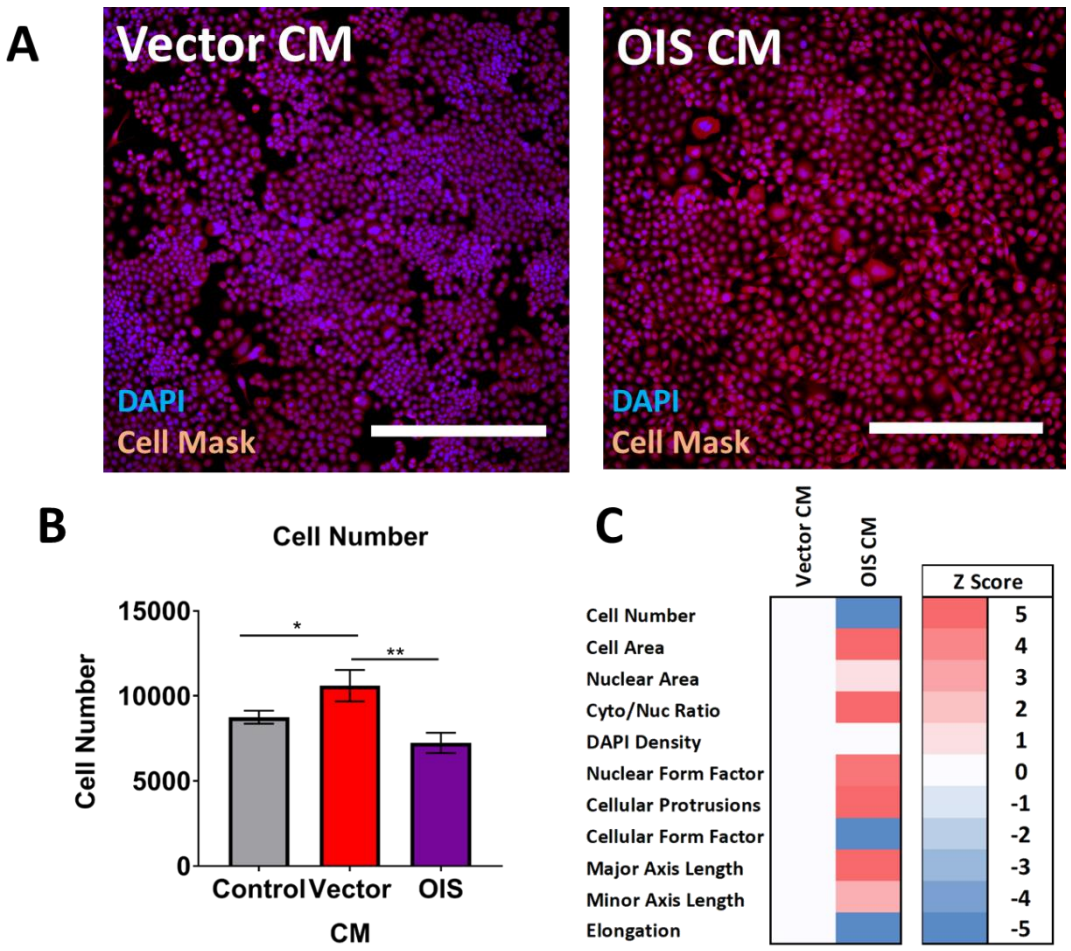

Figure 5.2: Immunofluorescence high-content analysis of MDA-MB-468 basal-like breast cancer cells treated with conditioned media from vector or oncogene-induced senescent (OIS) IMR90s

MDA-MB-468 cells were treated with conditioned media (CM) collected from vector or OIS IMR90s and assessed by HCA. **A)** Representative immunofluorescence images for DAPI (blue) and Cell Mask (red) staining. **B)** Quantitation of HCA cell number. **C)** HCA morphology measures were converted to Z-scores according to the change from the vector control condition (see methods). Positive and negative modulation of each measure is demonstrated by a change of at least +/- one Z-score from the vector condition and indicated as red or blue respectively. White indicates no change from the control. N=3 independent experimental replicates (4 technical replicates per experiment). Statistical analysis performed via One-way ANOVA with Tukey's post-hoc test (section 2.17). Scale bars = 500µm. Four fields of view.

5.4 Assessing the Paracrine Effects of the RS SASP

Having established that the OIS CM produced a potent paracrine senescence response, the RS model was then investigated. As previously, CM was collected from EP or DS cells, albeit here for 72 hours. This time-point was selected before the OIS experiment had been fully optimised and it would be an improvement to repeat this with a 96 hour conditioning time-point to allow for more accurate comparison. The CM was centrifuged at 2000 *x g* and supplements added. It is important to note that inter-experimental variability hindered statistical assessment, as final control cell numbers were variable. Therefore, proliferation data has been assessed using a block ANOVA (equivalent to a two-way ANOVA with experiment and treatment as factors) as described in (Lew, 2007). EP HMFs were then treated at day one and four post seeding and subsequently fixed on day six. The DS CM was demonstrated to produce a reduction in cell number compared to the EP CM (EP, 8110 ± 2742; DS, 5693 ± 1414; Figure 5.3). This was accompanied by modest changes in several components of the morphological panel. However, the effect of the RS media appeared less potent than that seen previously in the OIS investigations, which may be attributed to the reduced conditioning time. As with the EV investigations in section 4, in terms of workflow, the OIS model was prioritised in order to establish investigatory frameworks into which the RS model could then be taken.

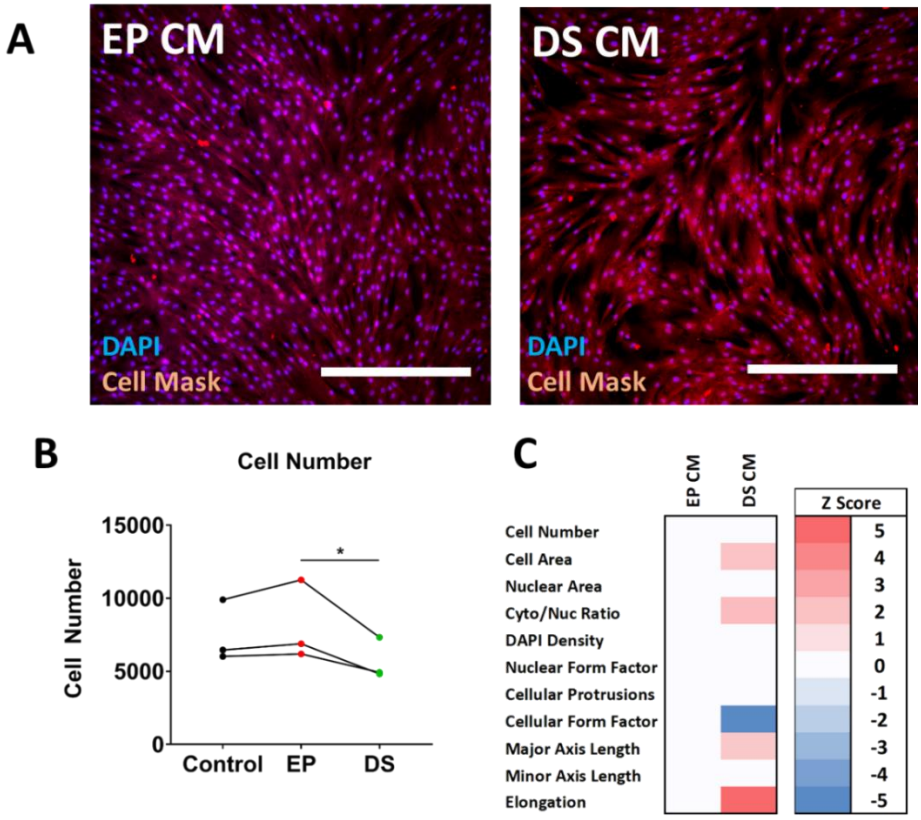

Figure 5.3: Immunofluorescence high-content analysis of proliferating human mammary fibroblasts (HMFs) treated with conditioned media from early proliferative (EP) or deeply senescent (DS) HMFs

Early proliferative (EP) human mammary fibroblasts were treated with conditioned media (CM) collected from EP or deeply senescent (DS) HMFs and assessed by HCA. **A)** Representative immunofluorescence images for DAPI (blue) and Cell Mask (red) staining. **B)** Quantitation of HCA cell number for Control (black), EP (red) and DS (green). **C)** HCA morphology measures were converted to Z-scores according to the change from the EP control condition (see methods). Positive and negative modulation of each measure is demonstrated by a change of at least +/- one Z-score from the EP condition and indicated as red or blue respectively. White indicates no change from the control. N=3 independent experimental replicates (4 technical replicates per experiment). Statistical analysis performed via Block ANOVA (equivalent to a two-way ANOVA with experiment and treatment as factors). Scale bars = 500µm. Four fields of view.

5.5 Assessing the Paracrine Effect of OIS EVs

Having established that the SASP from OIS cells produced a paracrine senescence response in both proliferating IMR90 fibroblasts and MDA-MB-468 cancer cells, the contribution of EVs to these effects was investigated. First, EVs were isolated using SEC, as this had been established to be crucial in dissecting the soluble and vesicular secretomes. 10µl treatments from PBS vehicle, vector Fraction 8, OIS Fraction 8 and OIS Fraction 20 were then administered to vector IMR90s on day one and four post seeding. It was demonstrated that whilst neither vector Fraction 8 or OIS Fraction 20 produced a change in cellular proliferation, OIS Fraction 8 produced a reduction in cell number compared to all other samples (Control, 3841 ± 112.7; Vector Fraction 8, 3683 ± 406.7; OIS Fraction 20, 3917 ± 168.6; OIS Fraction 8, 2805 ± 21.81; Figure 5.4). Importantly, this was accompanied by characteristic changes in cellular morphology, albeit notably less dramatic than those seen in previous investigations. Interestingly, OIS Fraction 20 appeared to be slightly pro-proliferative, causing inverse morphological changes to those typically seen with senescence induction. It is important to note that the vector Fraction 8 contains fewer EVs than the OIS Fraction 8 and so the observable differences may be driven by the "dose" of EV as opposed to a specific functional cargo. However, the differences in OIS Fractions 8 and 20 again emphasise the advantages of SEC as an isolation methodology.

Next, the same treatments were investigated in the 468 cancer cells. As in the RS CM investigation, inter-experimental variability necessitated use of block ANOVA analysis (Lew, 2007). With this caveat in mind, the OIS Fraction 8 reduced proliferation in comparison to the OIS Fraction 20 (OIS Fraction 8, 8567 ± 1482; OIS Fraction 20, 10569 ± 1847; Figure 5.5). Contrasting the IMR90 experiments, both OIS Fraction 20 and Fraction 8 produced morphological changes indicative of senescence, albeit more potently in Fraction 8.

However, OIS Fraction 20 once again produced a slight pro-proliferative effect compared to the PBS vehicle (9717 ± 1165; Figure 5.5). Ideally, this work would be repeated to produce replicates with more consistent final cell numbers in the control condition, thus allowing use of more standard statistical analysis. However, treatment with SEC fractions demonstrates a distinct role for senescence cell derived EVs in mediating the effects of the SASP.

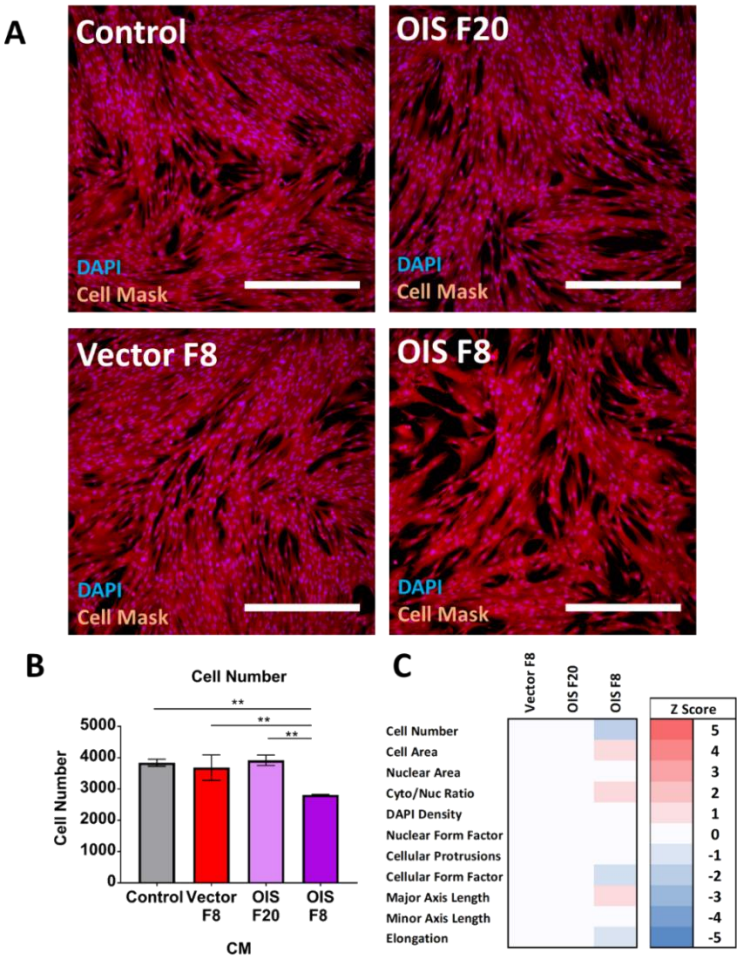

Figure 5.4: Immunofluorescence high-content analysis of IMR90 fibroblasts treated with EVs from vector or oncogene-induced senescent (OIS) IMR90s

Vector IMR90 cells were treated with size-exclusion chromatography (SEC) Fraction 8 or Fraction 20 collected from vector or OIS IMR90s and assessed by HCA. **A)** Representative immunofluorescence images for DAPI (blue) and Cell Mask (red) staining. **B)** Quantitation of HCA cell number. **C)** HCA morphology measures were converted to Z-scores according to the change from the vector control condition (see methods). Positive and negative modulation of each measure is demonstrated by a change of at least +/- one Z-score from the vector condition and indicated as red or blue respectively. White indicates no change from the control. N=3 independent experimental replicates (4 technical replicates per experiment). Statistical analysis performed via One-way ANOVA with Tukey's post-hoc test (section 2.17). Scale bars = 500µm. Four fields of view.

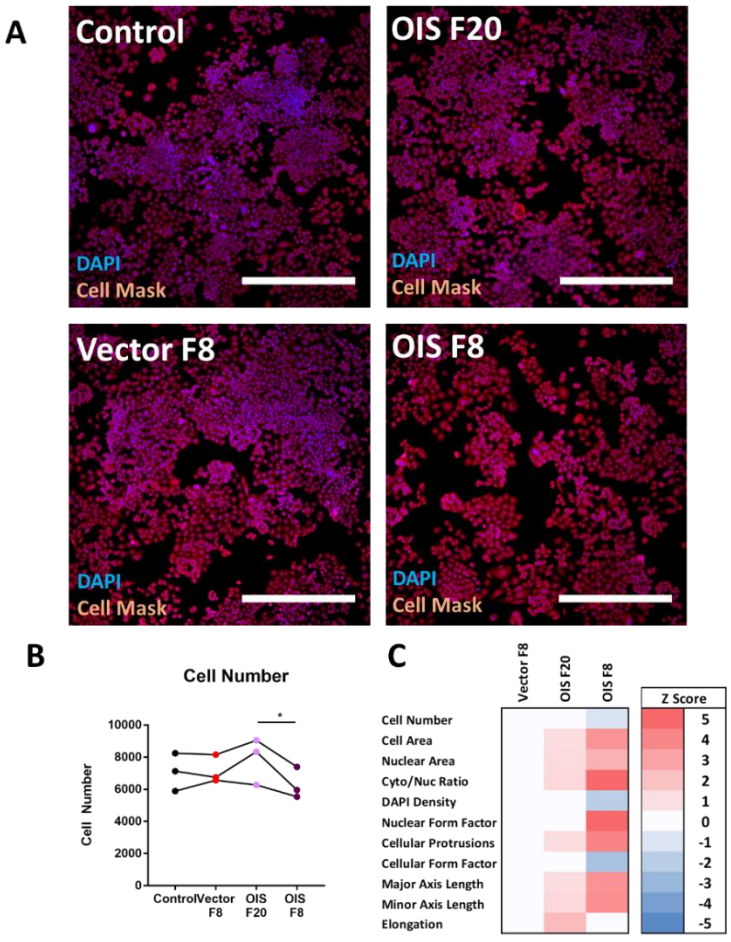

Figure 5.5: Immunofluorescence high-content analysis of MDA-MB-468 basal-like breast cancer cells treated with EVs from vector or oncogene-induced senescent (OIS) IMR90s

MDA-MB-468 cells were treated with size-exclusion chromatography (SEC) Fraction 8 or Fraction 20 collected from vector or OIS IMR90s and assessed by HCA. **A)** Representative immunofluorescence images for DAPI (blue) and Cell Mask (Red) staining. **B)** Quantitation of HCA cell number. **C)** HCA morphology measures were converted to Z-scores according to the change from the vector control condition (see methods). Positive and negative modulation of each measure is demonstrated by a change of at least +/- one Z-score from the vector condition and indicated as red or blue respectively. White indicates no change from the control. N=3 independent experimental replicates (4 technical replicates per experiment). Statistical analysis performed via Block ANOVA (equivalent to a two-way ANOVA with experiment and treatment as factors) (section 2.17). Scale bars = 500µm. Four fields of view.

5.6 Investigating Mechanistic Lead Candidates

Having established that OIS derived EVs could contribute to the paracrine senescence effects of the SASP, attention turned to exploring this on a mechanistic level. Importantly, understanding whether EVs act through a distinct mechanism from canonical soluble paracrine senescence was a key objective. Candidate pathways were selected by identifying leads from the proteomic assessments that also had a level of literature support for a feasible contribution to secondary senescence. PANTHER DB pathway analysis initially identified NOTCH1 signalling constituents within the OIS F8 EVs in MS2, including both the NOTCH1 receptor and the sheddase ADAM17. Importantly, both NOTCH1 and ADAM17 are membrane proteins, which were considered to represent a major compositional distinction of EVs from soluble factors (as emphasised in MS3 – section 4.8). NOTCH1 has recently been implicated in the induction of senescence in several ways. A juxtacrine senescence effect may be induced in proliferating cells through the display of NOTCH1 ligands on the surface of neighbouring senescent cells (section 1.1.7). These include DLL4 and JAG1, both of which were identified in the OIS Fraction 8 during the second round of proteomics (MS2). Secondly, ectopic expression of the cleaved intracellular NOTCH1 domain N1ICD, leads to induction of a senescence phenotype. As NOTCH1 was identified in the OIS F8 in both the second and third rounds of MS, the potential for transfer of NOTCH1 to recipient cells was of interest. Finally, the kinetics of NOTCH1 in OIS have not been fully elucidated. NOTCH1 expression increases in OIS up to day eight. However, expression of the functional cleaved intracellular domain is lost from day four. It was hypothesised that this crucial signalling domain could be packaged and released as an EV cargo, with potential for NOTCH1 induced responses in recipient cells. Overall, several canonical members of NOTCH signalling pathways were identified in the OIS EVs and, supported by a literature rationale, were pursued as a potential functionally relevant pathway (Figure 5.6).

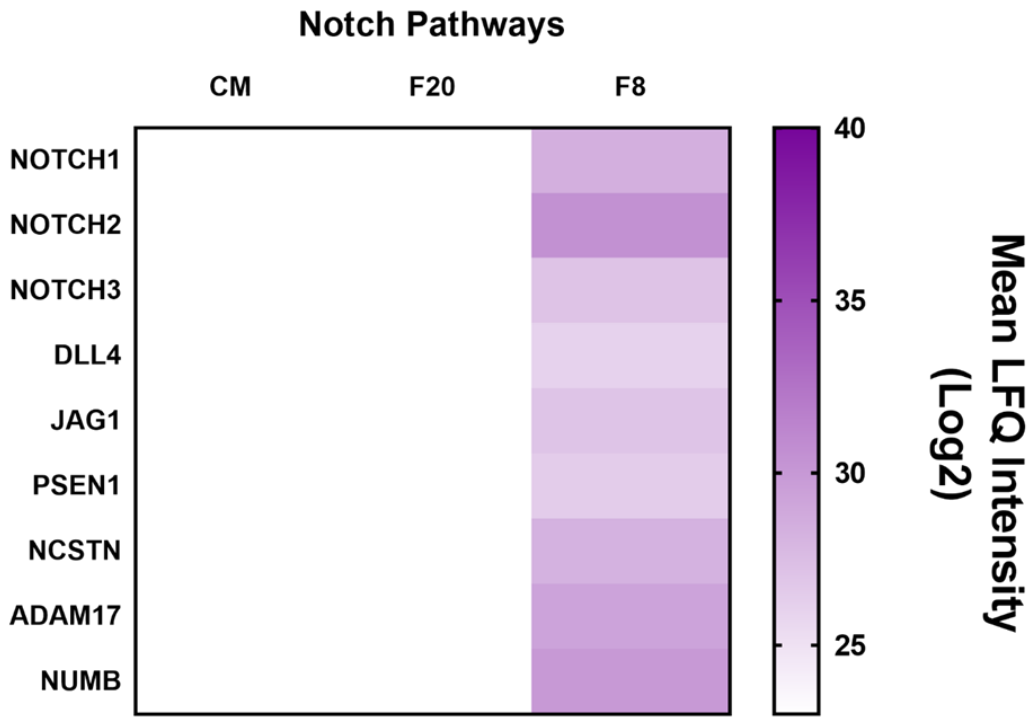

Figure 5.6: Heat Map Demonstrating Expression of NOTCH Pathway Associated Proteins in conditioned media, OIS SEC Fractions 20 and 8

Conditioned media and size-exclusion chromatography (SEC) Fractions 8 and 20 from OIS IMR90s were analysed by mass spectrometry. Genes related to NOTCH signalling pathways were identified by PANTHER DB pathway analysis. N=3 independent experimental replicates (1 technical replicate per experiment).

PANTHER DB pathway analysis of OIS F8 in MS2 identified numerous components of the NOTCH1 signalling pathway (described above). This included ADAM17, an important initiating enzyme in the NOTCH1 signalling cascade, mediating the cleavage and disengagement of NOTCH1 and its ligand following binding (section 1.1.7 – Figure 1.6). The presence of ADAM17 in OIS derived EVs led exploration of other ADAMs including the closely related family member ADAM10, which was strongly represented in all three rounds of MS, along with several other proteins associated with sheddase activity (Figure 5.7). ADAM10 has also previously been identified as a potential marker of EVs (Kowal *et al.*, 2016). However, there is has been limited research into the role of sheddases in a senescence setting. The role of shed ectodomains from the surface of senescent cells has also received relatively little research attention, although they have been described as components within the SASP (Coppe *et al.*, 2008). The potential identification of ADAMs within the composition of OIS EVs led to a broader consideration of the make-up of the senescence secretome. It was hypothesised that composition of the SASP could be broken down into three distinct parts: secreted soluble protein (secretome), secreted EVs (vesiculome) and shed ectodomains (sheddome). Of these, few studies have been conducted that focus on the functional contribution of these shed factors to the SASP. Furthermore, the presence of numerous ectodomains on the EV surface were hypothesised to represent a potential "reservoir" of these ectodomains, which could be mobilised by ADAMs on the EV. Therefore, the contribution of ADAM sheddases to both the composition of the SASP and the function of OIS EVs was investigated.

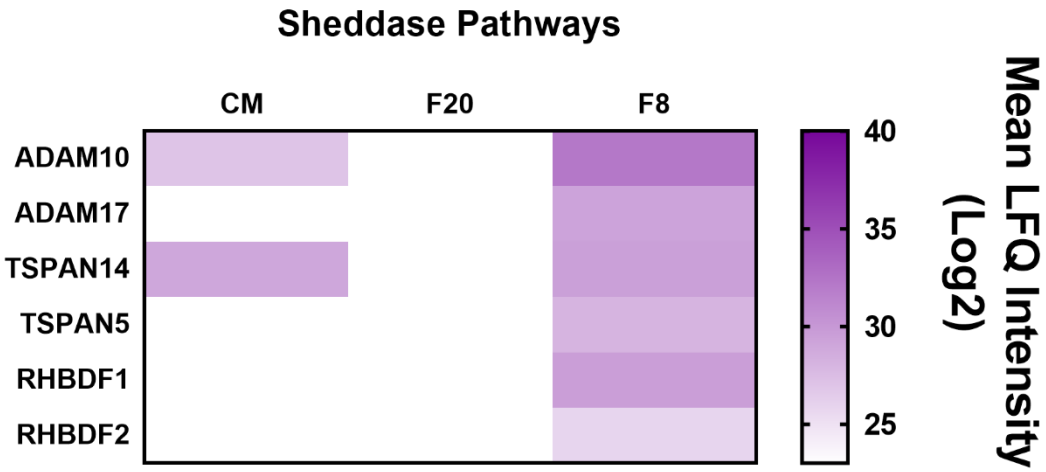

Figure 5.7: Heat Map Demonstrating Expression of ADAM10/17 Sheddase Pathway Associated Proteins in conditioned media, OIS SEC Fractions 20 and 8

Conditioned media and size-exclusion chromatography (SEC) Fractions 8 and 20 from OIS IMR90s were analysed by mass spectrometry. Genes related to ADAM10/17 sheddase pathways signalling pathways were identified. N=3 independent experimental replicates (1 technical replicate per experiment).

In order to investigate the potential for an EV mediated NOTCH1 driven signalling pathway, it was important to establish the presence of NOTCH1 in both the parental cell and the isolated EVs. This was carried out by immunoblotting, firstly in the WCL (Figure 5.9). It was established that NOTCH1 was present in both the vector and OIS cells. Interestingly, the cleaved intracellular domain N1ICD was detected in both vector and OIS WCL. This disputes previous reports in the literature, which have suggested that N1ICD expression is no longer present at day eight in OIS. It is important to note that whilst these western blots were loaded with the same amount of protein, they were intended as antibody validation blots and a loading control was not included. Therefore, despite indicating that NOTCH1 expression increases in OIS, that conclusion cannot be confidently supported based on these blots.

The presence of NOTCH1 was then assessed in SEC Fraction 8 samples form vector and OIS cells. As described in section 4, vector Fraction 8 contained insufficient vesicles to observe expression of the EV marker CD9. By contrast, CD9 was clearly expressed in the OIS EVs, as was NOTCH1 (Figure 5.10). The NOTCH1 antibody recognises both the full-length protein (300 kDa) as well as a "transmembrane" section (short transmembrane domain + intracellular domain; 120 kDa) both of which were observed in the OIS EVs (Figure 5.8). Attempts to detect the cleaved N1ICD protein in EVs via western blot were unsuccessful and it would represent useful follow up work to utilise increased amounts of EV protein and a form of loading control to more thoroughly explore this potential cargo. Therefore, this data indicated that NOTCH1 expression was present in the OIS cells and derived EVs, at least in the form of the full-length protein and "transmembrane" forms of the protein.

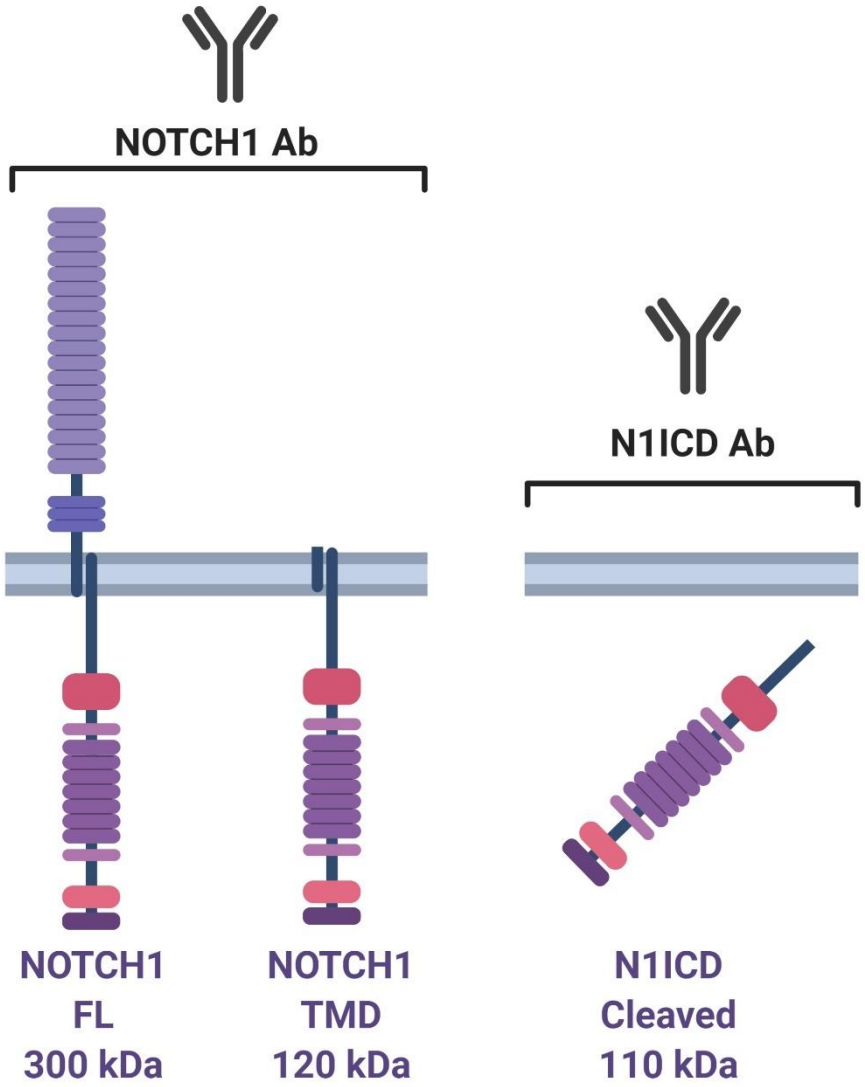

Figure 5.8: Schematic indicating epitopes detected by NOTCH1 and N1ICD Antibodies

The NOTCH1 antibody (4147, Cell Signalling UK) recognises both the full-length NOTCH1 protein (300 kDa) and a "transmembrane" section comprising a short transmembrane domain and the NOTCH1 intracellular domain (120Kda). The N1ICD antibody exclusively recognises the N1ICD domain following cleavage by the γ-secretase complex (110 kDa).

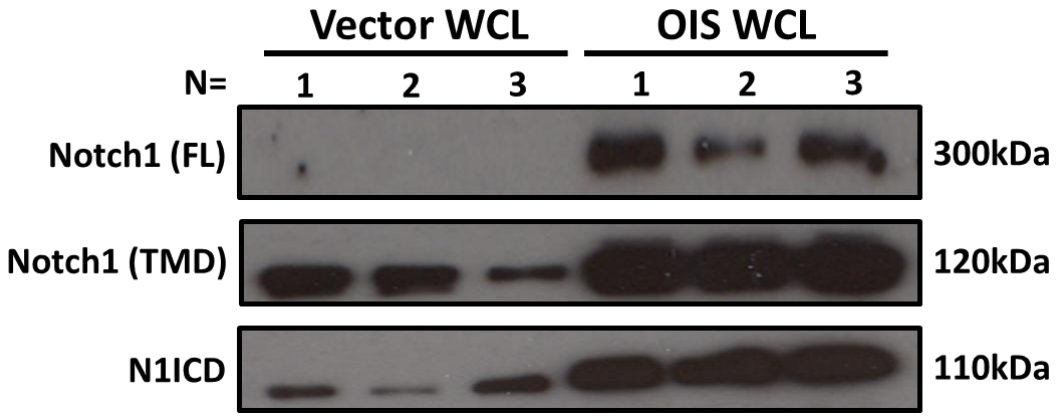

Figure 5.9: Western blot analysis of whole cell lysate (WCL) from vector or oncogene-induced senescent (OIS) IMR90 fibroblasts for Notch1 and cleaved NOTCH1 intracellular domain (N1ICD)

Immunoblot analysis of whole cell lysate (WCL) from vector and OIS IMR90s for NOTCH1 full length (FL), NOTCH1 transmembrane domain (TMD) and NOTCH1 intracellular domain (N1ICD). Each lane contains sample prepared during an individual experiment. N=3.

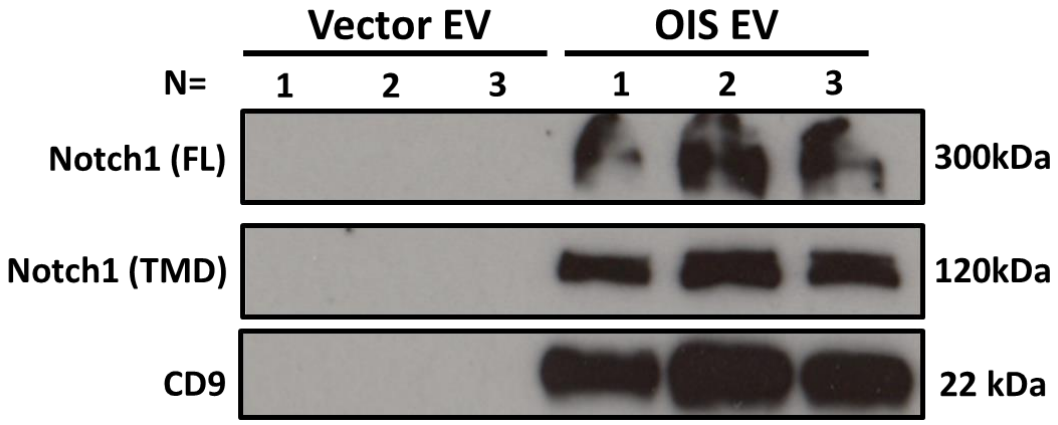

Figure 5.10: Western blot analysis of EVs from vector or oncogene-induced senescent (OIS) IMR90 fibroblasts for Notch1 and CD9

Immunoblot analysis of size-exclusion chromatography (SEC) Fraction 8 (EV) from vector and OIS IMR90s for NOTCH1 full length (FL), NOTCH1 transmembrane domain (TMD) and CD9. Each lane contains sample prepared during an individual experiment. N=3.

Mirroring the validation of NOTCH1 expression in OIS WCL and EVs, immunoblotting was also performed for ADAM10 and ADAM17. ADAM10 expression was observed in the WCL from OIS samples (Figure 5.11). Once again, direct comparisons to the vector WCL are difficult as loading based on cell number was also being investigated using these blots. Therefore, Lamin B1 was used as a loading control as it has previously been demonstrated to decrease in senescence and can thus serve as a proof of principle for demonstrating that lanes have not been overloaded (section 2.12). However, the anticipated decrease in Lamin B1 was not observed (possibly due to the day eight time point) and, as such, additional data is needed, with more conventional loading controls, to determine the change in ADAM10 expression with senescence. Next, OIS EV samples isolated by both dUC and SEC were assessed, with ADAM10 expression detected in both cases (Figure 5.12). Interestingly, ADAM10 expression was also observed in vector EV samples isolated by dUC, once again highlighting the loss of yield with SEC. Intriguingly, the observed band height in the WCL samples were at 90kDa, whilst in the EV samples were at 68kDa. The manufacturer's website indicated that the 90kDa band represented the pro- form of ADAM10, whilst the 68kDa band represented the active cleaved form. Therefore, this data indicates that ADAM10 is present in EVs from OIS cells but possibly predominantly in its active form.

ADAM17 was then assessed in Fraction 8 EVs and WCL from OIS and vector samples (Figure 5.13). Once again, this was observed in a pro- form in WCL samples from both vector and OIS cells. In the EVs, this was also seen in the OIS samples but the active form of ADAM17 appeared to be more extensively expressed. Overall, this data indicates that both ADAM10 and ADAM17 are present in OIS EVs, possibly in their active form.

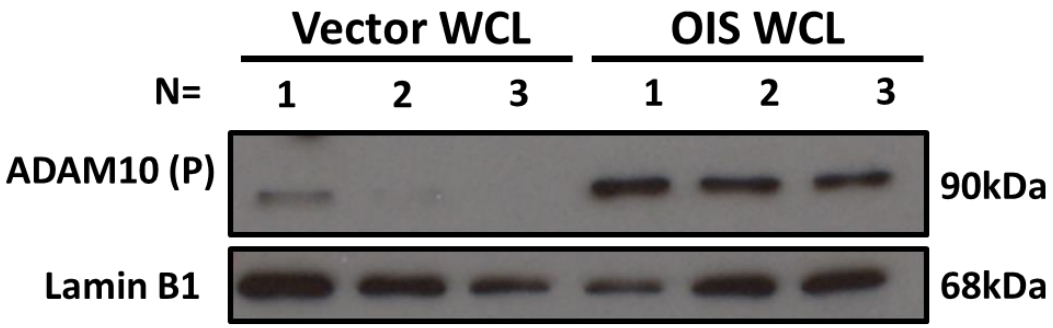

Figure 5.11: Western blot analysis of whole cell lysate (WCL) from vector or oncogene-induced senescent (OIS) IMR90 fibroblasts for ADAM10 and Lamin B1

Immunoblot analysis of whole cell lysate (WCL) from vector and OIS IMR90s for ADAM10 (P, precursor) and Lamin B1 as a loading control. Each lane contains sample prepared during an individual experiment. N=3.

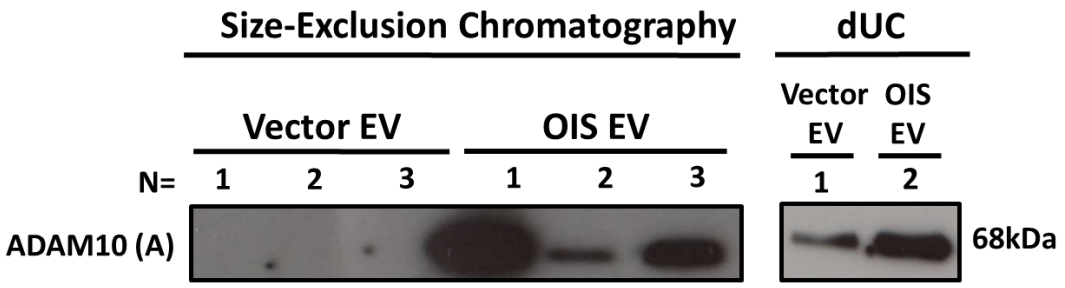

Figure 5.12: Western blot analysis of EVs from vector or oncogene-induced senescent (OIS) IMR90 fibroblasts for ADAM10

Immunoblot analysis of extracellular vesicles (EVs) isolated by size-exclusion chromatography (SEC) and differential ultracentrifugation (dUC) from vector and OIS IMR90s for ADAM10 (A, active). Each lane contains sample prepared during an individual experiment. SEC N=3, dUC N=1.

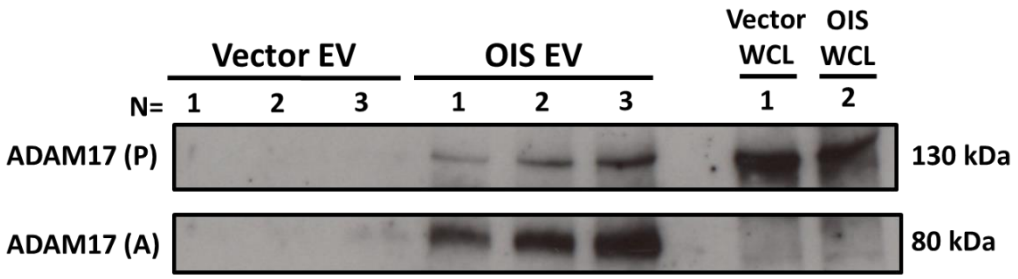

Figure 5.13: Western blot analysis of EVs from vector or oncogene-induced senescent (OIS) IMR90 fibroblasts for ADAM17

Immunoblot analysis of size-exclusion chromatography (SEC) Fraction 8 (EV) and whole cell lysate (WCL) from vector and OIS IMR90s for ADAM17 (P, precursor; A, active). Each lane contains sample prepared during an individual experiment. EV N=3, WCL N=1.

Having established that both NOTCH1 and ADAM10/17 were present in both the OIS cells and the derived EVs, the functional relevance of the pathways was then pursued. A preliminary experiment was carried out which investigated the effect of perturbing these pathways in cells from which conditioned media was then collected. This would allow assessment of the relative contribution of each pathway to the production of the SASP. DAPT, a γ-secretase inhibitor, was used to attenuate cleavage of the N1ICD domain and thus inhibit the NOTCH1 pathway. TMI005 was selected with the intention of inhibiting ADAM17, although it must be acknowledged that this compound also been reported to have an inhibitory effect on MMPs (Shu *et al.*, 2011; Richards *et al.*, 2012). Whilst DAPT appeared to have little effect on either vector or OIS CM, the TMI005 appeared to rescue the paracrine senescence effect of the OIS media. This was demonstrated through an observed increase in cell number (vector DMSO, 14407; vector TMI005,13435; OIS DMSO, 8831; OIS TMI005, 12114) with alterations in cell area (vector DMSO, 324.1 μm^2; vector TMI005,329.7 μm^2; OIS DMSO, 587.8 μm^2; OIS TMI005, 411.9 μm^2), nuclear area (vector DMSO, 142.4 μm^2; vector TMI005,141.5 μm^2; OIS DMSO, 200.3 μm^2; OIS TMI005, 164.7 μm^2), cytoplasmic/nuclear ratio (vector DMSO, 1.25; vector TMI005,1.28; OIS DMSO, 1.92; OIS TMI005, 1.45), DAPI density (vector DMSO, 9752 a.u.; vector TMI005, 9634 a.u.; OIS DMSO, 7981 a.u.; OIS TMI005, 9042 a.u.), Nuclear form factor (vector DMSO, 0.88; vector TMI005, 0.89; OIS DMSO, 0.92 OIS TMI005, 0.89), cellular protrusions (vector DMSO, 3.84; vector TMI005, 3.68; OIS DMSO, 5.52; OIS TMI005, 3.90), cellular form factor (vector DMSO, 0.74; vector TMI005, 0.74; OIS DMSO, 0.70; OIS TMI005, 0.74), Major axis length (vector DMSO, 23.3 μm; vector TMI005, 23.5 μm; OIS DMSO, 31.9 μm; OIS TMI005, 26.2 μm), minor axis length (vector DMSO, 16.06 μm; vector TMI005, 16.15 μm; OIS DMSO, 21.7 μm; OIS TMI005, 18.0 μm). However, there was no obvious change cellular elongation (vector DMSO, 0.69; vector TMI005, 0.69; OIS DMSO, 0.68; OIS TMI005, 0.68). It is important to note that this is a preliminary finding and replication is important. Furthermore, additional controls are

required to account for the transfer of drug along with the media. However, it indicates that of the two pathways selected, the sheddases may represent a more interesting mechanistic route to pursue. Additionally, the relative contribution of ADAM10/17 to the paracrine effects of the SASP could be investigated further via the use of other inhibitors including GI254023 (ADAM10) and GW280264X (ADAM10/17) in a similar manner to that described previously (Effenberger *et al.*, 2014).

A

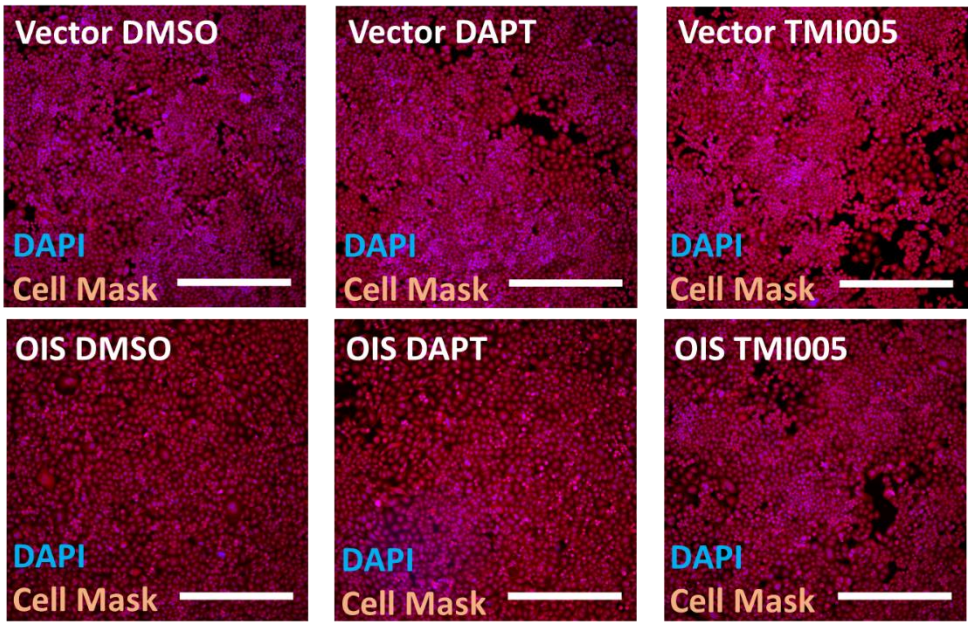

B

	Vector			OIS		
	DMSO	DAPT	TMI005	DMSO	DAPT	TMI005
Cell Number	14407.33	14408	13435.67	8831	8256.333	12114
Cell Area	324.117	321.1337	329.7703	587.816	633.5537	411.935
Nuclear Area	142.3587	142.2487	141.5477	200.265	204.8583	164.6577
Cyto/Nuc Ratio	1.248333	1.244667	1.282667	1.91633	2.068333	1.448333
DAPI Density	9752.608	9765.248	9634.821	7981.7	8056.781	9042.576
Nuclear Form Factor	0.884333	0.884	0.887667	0.91767	0.917	0.893667
Cellular Protrusions	3.835	3.929667	3.682667	5.52633	5.554	3.901333
Cellular Form Factor	0.738333	0.734	0.742	0.695	0.688667	0.740667
Major Axis Length	23.32467	23.279	23.492	31.8813	33.12633	26.22633
Minor Axis Length	16.06467	16.05133	16.14467	21.7167	22.49133	18.04067
Elongation	0.688742	0.68952	0.687241	0.68117	0.678956	0.687884

Figure 5.14: HCA of MDA-MB-468 basal-like breast cancer cells treated with conditioned from vector or oncogene-induced senescent (OIS) IMR90s following treatment with NOTCH1 pathway inhibitor (DAPT) or ADAM17 inhibitor (TMI005)

MDA-MB-468 cells were treated with conditioned media (CM) collected from vector or OIS IMR90s that had been treated with the γ-secretase inhibitor (DAPT), ADAM17 inhibitor (TMI005) or DMSO control and assessed by HCA. **A)** Representative immunofluorescence images for DAPI (blue) and Cell Mask (red) staining. **B)** Quantitation of HCA cell number and morphology measures. N=1 independent experimental replicates (4 technical replicates per experiment. Scale bars = 500µm.

5.7 Summary

The concept of the SASP has traditionally been associated with soluble factors and, as such, functional investigations have primarily focused on the use of conditioned media investigations in order to probe the associated functional effects. These conditioned media experiments have demonstrated that a secondary senescence effect can be initiated in treated proliferating cells through a mechanism of paracrine senescence. Recently, the role of EVs in this effect has been explored, but often not in combination with the highest levels of isolation rigor (Wallis, Mizen and Bishop, 2020). In this chapter, the advantages of SEC have been emphasised, with a particular focus on dissecting the relative contribution of soluble and vesicular constituents of the SASP to paracrine senescence.

Successful reproduction of OIS paracrine senescence conditioned media investigations from the literature was an important first step, as it provided a benchmark against which other models could be compared. This also demonstrated the advantages of the HCA morphological senescence characterisation, as a paracrine senescence response could be validated without extensive antibody staining. The use of complimentary senescence markers would have provided supporting evidence that a true “senescent” phenotype had been induced. However, this was considered to have more value as future work (section 6.5) to compliment the current objective, which was to demonstrate that senescent cell derived EVs produced a distinct functional effect from the soluble SASP, and that SEC allowed this to be more confidently determined than dUC alone. The use of dUC samples was not pursued, as the co-isolation of soluble factors would limit interpretation of the contribution of EVs. SEC provided confidence that Fraction 8 was primarily vesicular, and could thus be compared with the soluble Fraction 20. Given, the relative concentration of SASP factors between samples (section 4.6.2; Figure 4.15), it was intriguing that Fraction 8 and not Fraction 20

produced a paracrine response. However, the observable response in Fraction 8 suggests a mechanism distinct from canonical soluble factor signalling, hence the focus on membrane proteins. It is important to emphasise that the "dose" of EVs (10µl) was optimised based upon the volume of PBS vehicle which cells could tolerate without compromising final cell numbers. This also means that the difference in vector and OIS samples could be accounted for by the number of vesicles applied as much as any functionally relevant cargo. Therefore, comparisons between Fraction 8 and Fraction 20 are the most relevant to the work presented here, whilst dose responses would provide interesting complimentary data. However, the doses applied reflect the relative production of EVs that occur following OIS induction. Therefore, the experimental procedures are appropriate to describe the functional consequences of increased EV production in OIS and the capacity to illicit a paracrine senescence response.

Given the context dependent role of the SASP, the capacity of OIS EVs to produce paracrine senescence in additional cell types was also explored, given the paradoxical roles of the SASP reported previously. Here, the OIS SASP was demonstrated to inhibit the proliferation of 468 breast cancer cells, whilst inducing morphological changes indicative of senescence. This observation provided an additional model of paracrine senescence in which to assess the relative contribution of OIS EVs. However, further characterisation of the OIS paracrine effect in 468s (for example additional doses) would support this work. The observation that the OIS EVs recapitulate a paracrine senescence response in a second cell type supports their functional relevance within the SASP. However, the 468 EV experiments were hindered by inter-experimental variability and a block ANOVA statistical analysis approach was taken. This prevents the effects of each sample type from being masked by variability between experiments. Whilst this is an appropriate statistical approach, for consistency, additional

replicates would be useful support the conclusion that OIS EVs contribute to the paracrine effect of the OIS SASP on 468 cells. Overall, these functional experiments demonstrate that EVs derived from OIS can contribute to the paracrine signalling of the SASP and that SEC is an effective methodology for dissecting this effect from that of the soluble secretome.

The functional data described above suggests that EVs may contribute to paracrine senescence through a mechanism that is distinct from the soluble SASP. It was postulated that any alternative mechanism was likely to revolve around inherent compositional differences between the vesicular and soluble SASP. The presence of membrane proteins represent one such potential distinction, as these are fundamental to the structure of the EVs but would not be expected in the soluble SASP. This hypothesis was supported by MS2, which indicated enrichment in OIS Fraction 8 for membrane proteins and MS3, which indicated that those proteins uniquely present at increased levels in OIS Fraction 8 comprised a significant membrane component. Intracellular proteins derived from the cytoplasm of the parental cell could also represent a candidate route and would be interesting to explore during future work (Section 6.3). PANTHER pathway analysis identified NOTCH family proteins, as well as members of associated signalling cascades, as constituents of the OIS EVs. This was intriguing when combined with recent evidence for the role of NOTCH1 in secondary senescence. The ability of NOTCH1 ligands to elicit a juxtacrine senescence response in neighbouring cells was considered of interest, as the presence of these ligands on the surface of EVs may represent a potential route for “paracrine-juxtacrine” senescence induction (Sheldon *et al.*, 2010; Tan, Asada and Ge, 2018). Furthermore, NOTCH1 signalling is evidently important in both NIS and OIS, so the delivery of NOTCH1 and its intracellular domain to recipient cells represented another potential mechanistic route. However, JAG1 expression could not be validated by ELISA in either OIS WCL, CM or EV samples. Coupled

with the lack of observable change in OIS paracrine senescence with DAPT inhibition, preliminary data provides limited support to NOTCH1 (or its ligands) as a significant contributor to EV mediated paracrine senescence. However, it is important to note that DAPT inhibition was only used in CM experiments and thus not assessed directly in a vesicular context. Equally, NOTCH1 inhibition in treated cells rather than conditioning cells may should also be explored. These would be a useful additional experiment before discounting a NOTCH1 mediated role.

The decision to explore ADAM sheddases was a natural extension of the NOTCH1 investigations. ADAM10/17 facilitate cleavage of the N1ICD by γ-secretase and are thus essential in the activation of the NOTCH1 pathway (Bray, 2016). ADAM10 has also been previously reported as a specific marker of small EVs (Kowal *et al.*, 2016). The role of ADAMs within senescence has not been widely investigated but the presence in EVs would require expression in the producing cell. Interestingly, many ectodomains that are shed in ADAM dependent process have also been described as SASP factors (Coppé *et al.*, 2010; Morancho *et al.*, 2015). Coupled with EVs, this would represent an additional layer of complexity to the SASP that could be considered to comprise canonical soluble factors (secretome), EVs (vesiculome) and non-soluble shed ectodomains (sheddome). Given that EVs appear to have a distinct role within paracrine senescence, the relative contribution of the senescent sheddome was also explored. The potential for interplay between these two facets of the SASP is also worthy of investigation, as ectodomains on the EV surface may represent a potential "reservoir" which could be shed by EV-ADAMs. In order to explore this, the role of the sheddome within the composition of the SASP was explored though pharmacological inhibition of ADAM17 by TMI005. Although this experiment was only performed with one replicate, the OIS CM paracrine senescence effect appeared to be rescued by blocking

ADAM17 in the conditioning cells. This was an intriguing finding and suggests that shed ectodomains may be functionally important mediators within the SASP. Future work should explore the relative contribution of ADAM10/17 to this effect through use of inhibitors including GI254023 (ADAM10) and GW280264X (ADAM10/17). This would support preliminary findings and provide a clear rationale for exploring the sheddases as a mechanistic route. This could be achieved by using the same inhibitors to pharmacologically attenuate the EV mediated paracrine senescence response.

To conclude, in this chapter, the role of EVs within OIS paracrine senescence has been explored. The use of SEC allows distinction between the soluble and vesicular portions of the secretome, supporting the rationale for its use in Chapter 2. Whilst characterisation of the mechanisms underpinning this effect had proved beyond the scope of this project, preliminary investigations indicate that ADAM10/17 sheddases may represent a functionally relevant pathway that is worthy of further investigation.

6 Discussion and Future Work

The principal findings of the work set out here, regard demonstration of the technical challenges that underpin the study of EVs within a senescence setting, which have facilitated the thorough profiling of the change in EV composition following the induction of OIS. Whilst demonstrably evidenced to concentrate EVs from cell culture supernatant, dUC was also shown to be limited by the co-isolation of soluble SASP factors including IL-8. SEC served as a means by which to overcome this limitation, by providing separation between the vesicular and soluble divisions of the SASP. Through this process, it was demonstrated that EVs contribute to the phenomenon of paracrine senescence, in a process distinct from that of the soluble secretome. Interrogation of the senescent cell derived EV composition has provided avenues for future investigations to probe the functional role of the SASP, with preliminary results identifying the senescent "sheddome" as an unappreciated facet of the SASP. Therefore, through a dedication to isolation rigor, this work provides a framework in which to explore the potential mechanisms that underpin the EV mediated paracrine effects of senescent cells.

6.1 Overcoming the Technical Challenges of EV Isolation in Senescence

The study of EVs has long been hindered by the technical challenges of investigating these nanoscale sized mediators (Ramirez *et al.*, 2018). This includes a lack of utility for standard microscopy and flow cytometry techniques, the paucity of EV specific markers and shortfalls in the specificity of widely applied methods of EV characterisation (sections 1.2.5 and 1.2.6) (Coumans *et al.*, 2017). These issues are further compounded when studying EVs in a senescence setting, where considerations of yield and purity require an exceptionally careful balance.

The lack of efficiency in recovery yield is a widely described problem within EV research (Cvjetkovic *et al.*, 2014). This varies between different methods of EV isolation but generally sees techniques targeted towards either a high purity or high yield (Van Deun *et al.*, 2014; Mateescu *et al.*, 2017). Indeed, in this work, dUC was demonstrated to produce an approximately five-fold greater particle concentration than that observed with SEC. This was offset by the co-isolation of soluble factors alongside the final dUC pellet, limiting its value as an isolation technique upstream of proteomic or functional analysis. Therefore, this positioned dUC as a high-yield low-purity technique, whilst the opposite was true of SEC. In some settings, it could be possible to overcome the SEC-associated loss of yield by scaling up cell culture, increasing the number of cells and flasks used. However, the loss of cellular proliferation intrinsic to senescence induction restricts the feasibility of this solution, particularly in models of replicative senescence, where large numbers of flasks would have to be maintained for weeks or months depending on the associated Hayflick curves. An alternative solution is the application of bioreactor cell-culture systems, which have been successfully used generate higher concentrations of EVs than standard cell culture flasks (Webber and Clayton, 2013; Watson *et al.*, 2016). This would require optimisation of senescence induction within these systems, but may represent a useful technology to pair with SEC. Such a workflow would facilitate elaboration of the change in EV composition in further models of senescence, which is an important consideration given the heterogeneity between types of senescence. Furthermore, it could facilitate the exploration of the changes in EV composition in both the stages immediately preceding RS, and as the senescent phenotype matures to one of DS.

Alongside yield, the issue of purity is of particular concern when investigating EVs within senescence, due to the SASP, which represents a potent source of potential protein

contamination. Here, it was demonstrated that SASP factors were co-isolated with the final dUC product. This was overcome through use of SEC, where the majority of IL-8 was identified in fractions that did not contain EVs. However, it cannot be discounted that the modest amount of IL-8 still associated with the EV fractions may represent a limitation of SEC, as there may be incomplete removal of all soluble protein from the EV fractions. Regardless, SEC provides a significant advantage over dUC in terms of purity and should be considered a more appropriate isolation technique within a senescence setting. This extends beyond proteomic assessment of EV composition and into the challenges of more general EV characterisation approaches. In particular, NTA is a technique limited by its ability to detect non-vesicular material (Coumans *et al.*, 2017). It is feasible that a high level of SASP contamination within dUC preparations could produce an erroneously high concentration measurement, thus exacerbating the perceived loss of yield associated with SEC. However, the concurrent reduction in EV markers observed by immunoblotting suggest this to be a less important consideration. Finally, when determining SASP contamination of the EV products, it is important to acknowledge that IL-8 has been utilised as a surrogate marker of the OIS SASP throughout this work. It would represent a potential improvement to directly measure additional factors by ELISA, in order to demonstrate that the observed effects encompass a range of SASP components. However, the evidence presented in MS2 suggests that numerous proteins typically considered SASP factors are associated with the final OIS Fraction 20 samples (Coppé *et al.*, 2010). This provides evidence that the observed co-isolation is not IL-8 specific and can be considered associated with the senescent secretome more generally. It is also important to emphasise that due to the heterogeneity in SASP composition between models and cell types, the selection of any individual markers can be considered somewhat arbitrary. Therefore, IL-8 detection in the late SEC fractions served as justification for a more comprehensive assessment by mass spectrometry, than could be achieved by the analysis of several individual factors by ELISA. However, further validation

of MS2 could subsequently have been performed, with an emphasis on investigating the relative abundance of factors common between samples. This would reinforce the assertion that specific factors of the SASP were co-isolating during dUC and provide additional weight for the recommended use of SEC.

The presence of numerous SASP factors in OIS Fraction 20 is compelling evidence for the use of SEC within senescence, overcoming a major hurdle to accurate characterisation. It is important that these concerns become more widely appreciated, as there has been an apparent nescience within the field surrounding such considerations. This is emphasised in Figure 6.1, which depicts the relative usage of EV isolation techniques within the senescence and ageing literature (Introduction section 1.3). Use of dUC and precipitation based kits, widely considered the methodologies least weighted towards purity, have been the most popular techniques in the field, suggesting that much of the compositional and functional assessments of EVs may have been hindered by co-isolation of the SASP. Therefore, it is hoped that by explicitly investigating the importance of research methodology to the characterisation of senescent cell derived EVs, this work will contribute to the promotion of more rigorous senescence research.

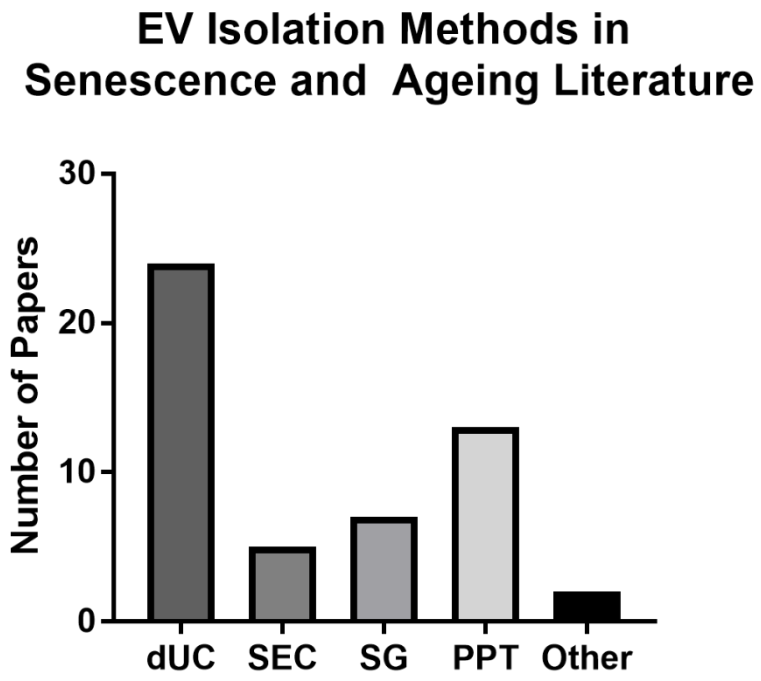

Figure 6.1: Use of EV Isolation Methodologies within senescence and ageing literature

Summary of the papers within section 1.3, which investigate extracellular vesicles (EVs) with senescence and ageing according to isolation methods. Isolation methods were included if they were utilised at any point within the publications. Abbreviations: differential ultracentrifugation (dUC), size-exclusion chromatography (SEC), sucrose gradient separation (SG), precipitation-based assays (PPT).

6.2 EV Heterogeneity – A Limitation Compounded in Senescence

It is important to emphasise some key limitations of the work presented here, in order to provide suggestion on where future investigations could build to support the conclusions drawn. One of the clearest limitations is the focus on a single model of senescence induction — OIS. Whilst RS was intended to serve as a complimentary model, as the focus of the project moved towards methodology comparisons, OIS emerged as the more appropriate setting due to the greater availability of senescent cells. Whilst the magnitude of EV production and the paracrine effect of conditioned media was examined in the RS model, further analysis of the RS derived EVs would be beneficial, in order to provide an insight into whether the observations made in OIS are consistent in other senescence models. This is an important consideration, as it is widely accepted that the SASP consists of a heterogeneous set of mediators, dependent on both cell type and senescence inducer. Indeed, the RS model was demonstrated to lack an IL-8 component and it may be anticipated that EV composition will also vary between models. Therefore, in order to probe the heterogeneity of EV composition between models of senescence, a round of proteomics similar to MS3 (performed in the RS model) would provide valuable interrogation of the composition of senescent cell derived EVs beyond the specific profiling of OIS presented here. Furthermore, investigation of senescence induction and EV composition in a cell type other than fibroblasts may also be beneficial, in order to improve the applicability of the work to senescence more generally. For example, investigation within TIS in cancer cells would be interesting, as the SASP has been proposed as a major limitation of this potential therapeutic strategy (section 1.1.10.2). Therefore, it would be prudent to explore any potentially deleterious effects of EVs within this setting, utilising the methodological considerations presented here. Additionally, further exploration of the kinetic development of the SASP and, in particular, its vesicular content, was not investigated in depth. Analysis of media collected regularly during the OIS induction schedule indicated that the SASP is far from a static phenotype. Indeed, it has previously

been demonstrated that the OIS SASP undergoes a NOTCH1 mediated switch, leading to its late inflammatory composition (Hoare *et al.*, 2016). There have been no reports to date describing a change in secretion of EVs across the course of senescence and it would be worthwhile to investigate whether the dynamic development of the SASP is reflected in a similar change in EV production. Furthermore, conditioned media and EV preparations collected across a time-course could be used in secondary senescence investigations, in order to understand how senescent cells modulate their microenvironment beyond a single time-point. Such investigations would only be worthwhile where confident attribution of EV dependent effects could be made, emphasising the value of the methodological development that was the focus of this work.

Another source of potential heterogeneity not explored here, is that between sub-types of EVs. This may occur between both classes of EV (i.e. MVs vs exosomes) or from heterogeneity within these broad classifications (e.g sub-populations of exosomes). Given the diverse set of potential functions indicated to occur through senescent cell derived EVs (section 1.3), understanding the heterogeneity of EV composition is essential to uncovering their contribution to the signalling of senescent cells. The current limitations in isolation methodology make this an ambitious goal. However, the emergence of new technologies, such as nanoFCM and ExoView, provide opportunities for characterisation of single EVs, as opposed to the bulk analysis provided by NTA and mass spectrometry. However, whilst these techniques provide single particle resolution, they must be tailored for predefined targets of interest and do not provide the “global profiling” offered by mass spectrometry. Therefore, it is feasible that a two-step workflow may be useful, with initial identification of potential targets by bulk proteomics, followed by a refined characterisation on a single vesicle level by either nanoFCM or ExoView. This approach could be applied in concert with the proteomic

investigations here, to explore the heterogeneity in NOTCH1 and sheddase expression within the SEC isolated EVs. Development of such experimental approaches represent the most likely avenue towards understanding the nuances and heterogeneity in EV composition and function. At present, it is important to acknowledge that all conclusions are drawn from a mixed population of EVs and that these may be contributing to the observed effects to varying degrees. Equally, individual isolation schedules will enrich for specific populations of EVs, which may confound comparisons of both function and composition. This is emphasised by the lack of IFITM3 identification in any proteomic assessment made here, despite it having previously been identified as a key mediator of EV driven paracrine senescence in OIS (Borghesan *et al.*, 2019). Interestingly, this particular factor was also not identified in the recent SASP Atlas investigation, emphasising the challenges of achieving standardisation within the field (Basisty *et al.*, 2020). Mirroring the approach of EV research more broadly, the most likely way to achieve consensus is to adhere to the MISEV guidelines and appreciate the potential sources of heterogeneity between studies, including final cell numbers, incubation times, senescence models, cell types and isolation schedules (Lotvall *et al.*, 2014; Théry *et al.*, 2018). Moreover, development of a system equivalent to the EV-TRACK initiative could provide value in the senescence field, by standardising reporting and ensuring details of the above sources of potential heterogeneity are explicitly described within publications (Van Deun *et al.*, 2017). This could be extended beyond an EV specific remit to a more general "SASP-Track" system, which would facilitate comprehensive reporting of experimental parameters and thus more straightforward comparison between investigations (Figure 6.2). Furthermore, this could be paired with a repository similar to ExoCarta, in order to develop an extensive database of SASP compositions within specific, well described, senescent contexts (Simpson, Kalra and Mathivanan, 2012). This seems to have been the broad aim of the SASP-Atlas, but that was limited (quite naturally) by the relatively few models that could be studied in a single publication. The value of such comparative databases relies on the

collation of a large number of data sets. Through a community driven approach, there is potential to develop an extensive database that may facilitate our understanding of the heterogeneity of the SASP, in terms of both its soluble and vesicular constituents. Overall, it is important to build on a firm foundation when assessing the role of EVs within senescence, which requires use stringent methodologies and an acknowledgment that even these are limited by the specificity of experimental parameters along with current technological constraints.

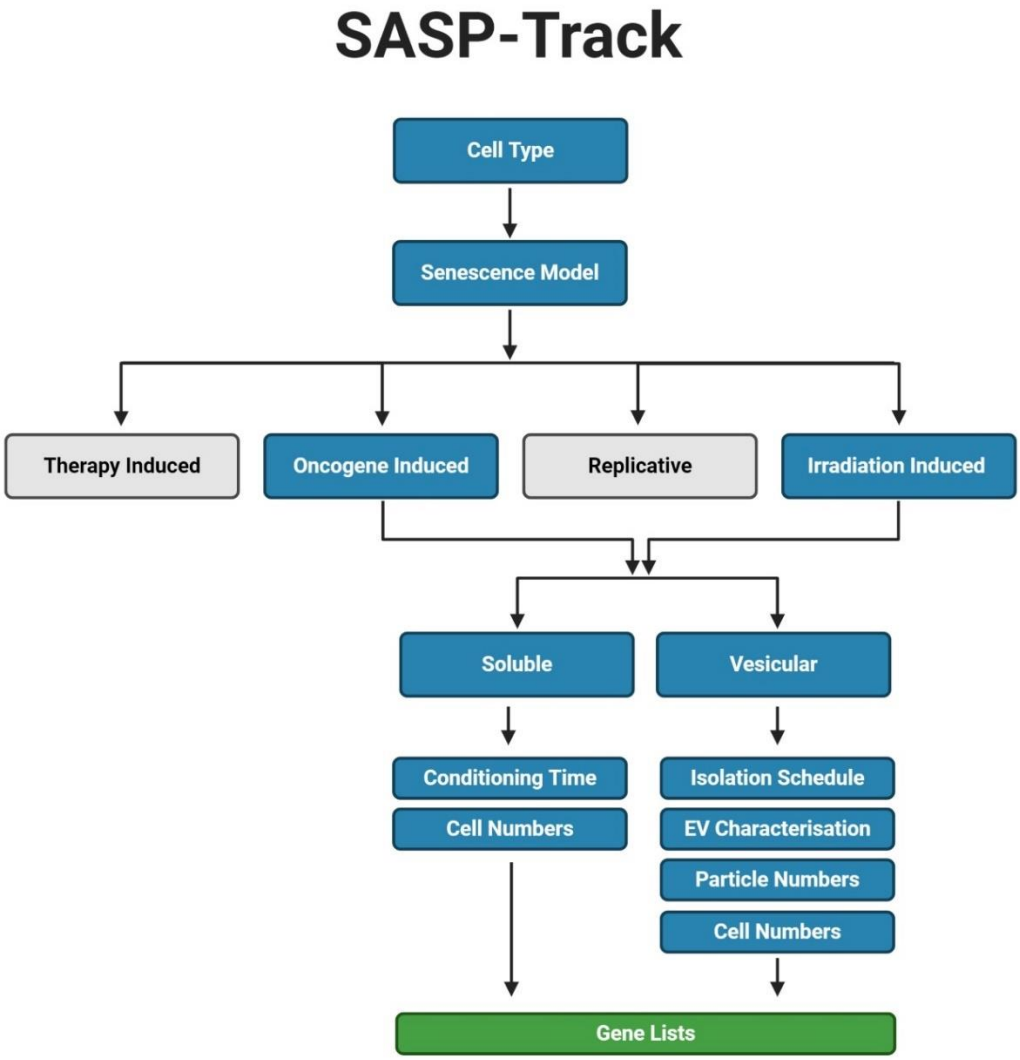

Figure 6.2: Proposal for Developing a SASP-Track Database

In order to develop a community driven database of context specific SASPs, a reporting interface would be useful within the field. This could facilitate standardisation of reporting, including parameters that underpin sources of heterogeneity in SASP composition. From a senescence perspective, clear identification of cell types, senescence models, cell numbers and conditioning times would be beneficial. From a vesicular outlook identification of isolation schedules, particles numbers and characterisation techniques would also be valuable. Collation of gene lists with the above experimental parameters clearly stated could help identify sources of heterogeneity and provide a rich database in which to explore the complex composition of the SASP.

6.3 Profiling the Composition of EVs in Senescence

Having established SEC as an appropriate technique for the isolation of EVs, in combination with an acknowledgment of the limitations inherent to studying senescence in one model at a single time point, the work set out here has mobilised the development of a rigorous isolation methodology to comprehensively characterise the composition of EVs derived from OIS IMR90 fibroblasts at day eight. The profiling performed in MS3, identified 374 proteins present at increased levels in the OIS EVs compared to those from the vector control. Of these, 256 were uniquely increased in the EVs, suggesting they may constitute functional candidates that could underpin a distinction from the soluble SASP. These included both NOTCH1 and ADAM10, which had been identified in the previous MS2 round of proteomic assessment, and had already been selected as candidates for functional exploration (sections 4.7 and 5.6). Additional validation included identification of increased levels of CD9, an EV marker that had been identified through immunoblotting, as well as EphA2, previously described as a functionally active component of senescent cell derived EVs (Takasugi *et al.*, 2017). These all represent membrane bound components, which account for a significant portion of those proteins uniquely present at increase levels in the OIS EVs. It is perhaps unsurprising that membrane proteins should be overexpressed within this data set, due to the higher particle numbers loaded (hence the abundance of CD9) and the inherent property of EVs as discrete membrane bound units, contrasting the soluble Fraction 20 and CM. Therefore, this dataset also provides a level of confidence that the preparations investigated were indeed EVs. This is corroborated further by the correspondingly high abundance of intracellular proteins, which should not be neglected in future work seeking to expand upon this initial profiling. Indeed, the diverse functional roles of EVs described previously in the literature have been have been demonstrated to occur through cargos with varied vesicular localisations (Wallis, Mizen and Bishop, 2020). In order to appreciate the broad range of potential EV mediated effects (described further below – section 6.4), it is crucial that

appreciation of all potential vesicular cargos be made. Therefore, whilst the MS3 proteomic assessment provides a rich source of data for future work to build upon, it should be acknowledged that it does not profile the entirety of EV composition. In particular, supporting such proteomic assessment with analysis of nucleic acid constituents would provide a more complete assessment of EV cargo and could reveal other avenues in which to explore the functional role of senescent cell derived EVs. However, within the scope of this work, the data within MS3 provides a thorough assessment of the proteomic cargo of OIS derived EVs and, in the context of SEC, serves as a demonstration of recommended practice when profiling EV proteomic composition within senescence.

6.4 Exploring the Contribution of EVs to Paracrine Senescence

One of the primary aims of this project has been to explore the contribution of EVs to the paracrine signalling of the SASP and, in particular, the induction of secondary senescence in proliferating cells. This is a crucial aspect of the SASP, as it has been widely hypothesised to contribute to the accumulation of senescent cells within ageing and age-related pathologies (section 1.3). Here, SEC was utilised to demonstrate that paracrine senescence could be facilitated through EVs in a manner distinct from that of the soluble SASP. This was evidenced by the reduced proliferation of IMR90 fibroblasts following OIS Fraction 8 treatment, which could not be recapitulated with Fraction 20. This was important, as it demonstrated that SEC did not preclude paracrine senescence investigation, which had been a possibility given the associated lack of yield. Furthermore, it supported literature evidence that EVs were important modulators of this secondary senescence effect (section 1.3.2.1). Most crucially, this effect could be confidently attributed to the EVs, due to the extensive compositional characterisation between Fraction 8 and Fraction 20. Together, this demonstrates that SEC

is a useful technique to apply in advance of EV treatment investigations, in order to convincingly demonstrate EV mediated outcomes.

This was utilised here to explore a novel role of OIS derived EVs to the induction of paracrine senescence in MDA-MB-468 breast cancer cells. This effect was demonstrated by both the EVs and total conditioned media. Interestingly, whilst senescence is predominantly considered an anti-tumorigenic effect, the SASP has been reported to promote the proliferation of cancer cells (Campisi and D'Adda Di Fagagna, 2007) in an effect recapitulated with senescent cell derived EVs (Takasugi *et al.*, 2017). By contrast, EVs derived from palbociclib-induced senescent cells have also been demonstrated to inhibit the proliferation of MCF-7 breast cancer cells (Borghesan *et al.*, 2019). Therefore, the classification of both the SASP and EVs as either pro- or anti-tumorigenic is currently uncertain (Rao and Jackson, 2016; Saleh *et al.*, 2018). In order to explore this further, some adjustment to the EV isolation experiments may be prudent. For example, use of a range of EV doses would facilitate a more compelling case for the observed loss of proliferation. Furthermore, use of co-culture or transwell experiments could be more representative of *in vivo* conditions than the discrete dose administrations utilised here. However, this work serves as a demonstration that the use of SEC may facilitate functional investigation of EVs in a senescence setting, providing a foundation for more comprehensive future investigation.

Whilst the work here has predominantly focused on the phenomenon of paracrine senescence, this is not the only function of the SASP, albeit one considered "dark" or detrimental within ageing (Wallis, Mizen and Bishop, 2020). As described in section 1.1.9, the SASP also contributes to homeostatic processes, including wound healing (Demaria *et al.*, 2014). Interestingly, EVs derived from senescent cells have also been implicated in a

similar role, suggesting they mediate some of the “bright” beneficial effects of senescence (Terlecki-Zaniewicz *et al.*, 2019). One underexplored role of EVs within senescence is the potential interaction with immune cells. Therefore, it would be interesting to utilise the methodologies optimised here, within experiments investigating the contribution of EVs to immune meditated responses. These could include investigations utilising NK cells, previously established as key effectors of senescent cell clearance via the SASP (section 1.1.9.2). In such investigations, it would be critical to minimise the contamination of EVs with SASP components, making a SEC based approach ideal. Furthermore, as described above, EVs have been implicated in a diverse set of functional roles, on both sides of the bright/dark dichotomy of the SASP. In order to uncover the relative contribution of EVs to these complex and contradictory functions, it is essential that effects can be convincingly credited to vesicles, emphasising the importance of diligence when selecting isolation methodologies.

6.5 Senescence Characterisation – A role for morphology

The characterisation of senescence has long been hindered by the lack of universally expressed markers with which to identify senescent cells. Consequently, best practice sees application of several markers, identifying hallmarks commonly observed following senescence induction (Hernandez-Segura, Nehme and Demaria, 2018). This requires significant optimisation, to find both markers and experimental conditions appropriate for the particular model and cell type under investigation. Therefore, there is significant research interest in identifying screening methods that may characterise senescence in a high-throughput manner, in a variety of cell types and models (Lahtela *et al.*, 2013; Sadaie *et al.*, 2015). Here, canonical markers of OIS were paired with a HCA based morphological panel in order to demonstrate the utility of this approach. Each individual morphology measure was selected in accordance with literature evidence that supported a potential senescence-

associated change. Cell number was assessed, in order to demonstrate the inherent reduction in proliferation that accompanies senescence induction (Munoz-Espin and Serrano, 2014). Additionally, cell area and axis lengths were measured in order to facilitate demonstration of the widely described increase in senescent cell size (Hwang, Yoon and Kang, 2009). Similarly, nuclear area was assessed, as identification of enlarged nuclei has been used successfully as a screening tool to characterise the induction of senescence (Sadaie *et al.*, 2015). Furthermore, measures assessing the uniformity of both cellular (cellular protrusions, cell form factor, cell elongation) and nuclear (nuclear form factor) morphology were also employed, as senescence has also been associated with irregularly shaped cells and nuclei (Hwang, Yoon and Kang, 2009; Sadaie *et al.*, 2015). Additionally, the ratio between cytoplasmic and nuclear areas was also measured, as cytoplasmic dilution resulting from a reduced DNA/cytoplasmic ratio has been demonstrated to occur in senescent cells previously (Goldstein, 1990; Neurohr *et al.*, 2019). Finally, assessment of DAPI intensity was made, as this has been successfully used to identify G1 arrested cells and as a screening tool for senescence assessment (Zhao *et al.*, 2010; Roukos *et al.*, 2015). Overall, the combination of these measures allowed a comprehensive assessment of OIS morphology to be made, supported by a panel of more conventional markers. This HCA approach was then applied to both replicative and secondary senescence investigations, emphasising its utility for characterising senescence in numerous settings.

However, it is important to acknowledge the limitations of utilising morphology as the sole method of senescence characterisation, as without the support of additional markers, it cannot conclusively be determined that senescence induction has occurred. Nevertheless, the context in which analysis has been performed is also relevant, as are the hypotheses being interrogated. Here, where morphological assessment has been employed in isolation,

it has not been done to characterise a previously unreported phenomenon, but rather to support the established principles of conditioned media and EV mediated paracrine senescence. HCA was used to provide distinction between treatments, rather than demonstrate a novel effect. Therefore, it has provided value by allowing exploration into the suitability of SEC as a method of EV isolation upstream of functional analysis. Future work characterising additional markers of senescence induction would further support the conclusions drawn. It would be prudent to begin by assessing markers previously associated with paracrine senescence (both in conditioned media and EV investigations), including p21, p16 and DNA damage foci (Acosta *et al.*, 2013; Borghesan *et al.*, 2019). However, HCA morphological analysis has merit as a first pass, proof of principle assessment, similar to that previously described for SA-β-gal (Gorgoulis *et al.*, 2019). It should be noted that selection of senescence markers always requires tailoring for the specific context. For example, SAHFs are predominately associated with OIS and thus would not be a suitable readout in the RS model (Di Micco *et al.*, 2011). Similarly, the p16 positive nature of MDA-MB-468 cells would limit the utility of this marker in secondary senescence investigations. This emphasises the more general challenges surrounding senescence characterisation, as well as the need for identification of novel senescence markers. The HCA based approach used here is well supported in the OIS model and has been employed to provide useful characterisation in several additional settings.

6.6 Senescence Reversal Investigations

In section 3.6, a protocol investigating the reversal of RS in HMFs was investigated. This has been extensively characterised in the lab previously, and presents a useful system in which to explore the phenotypes associated with senescence (Thesis:(Tyler, 2016)). In this work, a particular emphasis was placed on characterising the secretome of these reversed cells. IL-6

was demonstrated, through both qRT-PCR and immunoblotting, to be a major constituent of the RS SASP, whereas IL-8 was not. Following siRNA-induced reversal of RS, IL-6 was observed to decrease vs the siGLO control, albeit not to the level of EP cells. Interestingly, this was not recapitulated with the early SASP marker IL-1α, whilst IL-1β mRNA expression appeared to be dramatically increased following reversal. Together, this suggests that the secretome of reversed cells may be more complex than that of the EP counterparts. It may also indicate that the proliferative arrest associated with senescence may be uncoupled from the production of the SASP, as has been demonstrated elsewhere (Coppé *et al.*, 2011). The model of senescence reversal also presents the possibility to interrogate similar changes in EV production, which was demonstrated in this work to increase during RS. Whether this can be attenuated by the reversal protocol may provide an insight into the association of senescence with EV production, as the increased rate of production has been observed in all settings investigated (Section 1.3.1). However, some obstacles exist that preclude immediate exploration of this association, not least the transient nature of siRNA inhibition. This could be overcome through development of constitutive or inducible shRNA inhibitory systems, which would provide a stable knockdown in which to apply EV isolation protocols. Furthermore, exploration into compositional differences in EVs derived from EP, DS and reversed cells could provide insight into which cargos are of most functional significance within RS. Initial inquiries would focus on whether reversal attenuates RS-associated paracrine senescence, which would in turn lead to investigations pursing the EV mediated component of this response. Overall, whilst not the focus of this project, the senescence reversal investigations presented here, demonstrate the potential for further investigation into the pathways that underpin the phenotypes of RS.

6.7 Proposed Mechanisms of EV Mediated Paracrine Senescence

Having developed a robust workflow establishing isolation of EVs from OIS cells via SEC, the previously reported role of senescent cell derived EVs in mediating paracrine senescence was assessed. It was confirmed that EVs isolated by SEC contribute to paracrine senescence and, importantly, do so in way that appears distinct from that of the soluble SASP, given the lack of recapitulation with Fraction 20 treatments. It is possible that EVs may augment signalling of SASP factors previously demonstrated to contribute to senescence induction, in a similar manner to that of TGFβ1 and IFN-γ described previously (Cossetti *et al.*, 2014; Webber *et al.*, 2015). However, it is also feasible that components of the EV membrane may directly engage recipient cells in a manner reminiscent of IFITM3 and EphA2 (Takasugi *et al.*, 2017; Borghesan *et al.*, 2019). Alternatively, delivery of an EV cargo to the cytoplasm of a recipient cell could engage a distinct set of pathways inaccessible to the soluble factors of the SASP. Here, it was chosen to focus on the latter two scenarios, as the proteomic analysis performed in MS2/MS3 indicated that the EV preparations comprised heavy enrichment of membrane and cytosolic proteins, which were felt to possess more potential for engagement of distinct mechanisms compared to soluble factors.

6.7.1 NOTCH1 Investigations

One intriguing set of membrane constituents identified in MS2, were factors associated with NOTCH signalling, in particular NOTCH1 and its associated ligands JAG1 and DLL4. It was hypothesised that JAG1/DLL4 ligands on the surface of EVs may engage receptors on recipient cells, instigating a NOTCH1 dependent form of secondary senescence similar to that described between senescent and proliferating cells (Parry *et al.*, 2018; Teo *et al.*, 2019). This engagement of NOTCH signalling through ligands on the surface of EVs has been described elsewhere (Sheldon *et al.*, 2010; Sharghi-Namini *et al.*, 2014; Tan, Asada and Ge, 2018) and

would constitute an intriguing mechanism for a form of signalling traditionally considered juxtacrine. Additionally, the presence of NOTCH1 on EVs was also considered of functional interest, as a non-canonical form of NOTCH signalling facilitated by EV delivery has previously been described (Wang and Lu, 2017). Briefly, EVs are able to mediate the delivery of NOTCH to recipient cells, resulting in engagement of canonical NOTCH signalling cascades, whilst bypassing the requirement for binding of NOTCH ligands. Interestingly, this process has been demonstrated to require γ-secretase activity in the recipient cells, suggesting that the N1ICD is only cleaved following EV mediated delivery. It was considered that delivery of NOTCH1 and, in particular, the N1ICD intracellular domain, could facilitate similar signalling in the EV treatment experiments presented here, facilitating the instigation of a secondary senescence response. Furthermore, the previously reported loss of N1ICD expression from OIS cells after day four post-induction was also a source of interest (Hoare *et al.*, 2016). Whilst the previous report of non-canonical signalling suggested that N1ICD is not cleaved before incorporation into EVs, it was hypothesised that this could account for the observed loss in OIS. Alternatively, identification of critical components of the NOTCH signalling cascade within EVs, including members of the γ-secretase complex, as well as ADAM10 and 17, could account for reduced cleavage of the intracellular domain. Together, this provided a rationale for exploring the expression of NOTCH1 and N1ICD in OIS cells and EVs. NOTCH1 and N1ICD were both identified in the OIS cells, but only NOTCH1 was identified in the EVs. However, as the NOTCH1 antibody recognises an epitope also comprising N1ICD, this indicated that NOTCH1 was present within the EVs but had not been cleaved into its active form. Additionally, preliminary work investigating JAG1 by ELISA suggested it too was not present on OIS EVs. This could be accounted for by the change in OIS induction schedule, as JAG1 was also not observed in the MS3 round of proteomics. Overall, when coupled with the ineffectual DAPT treatment during preliminary conditioned media investigation, initial exploration of potential NOTCH1 mediated mechanisms provided minimal support for this

hypothesis. However, before entirely abandoning this line of investigation, it would be useful to utilise the DAPT inhibitor during EV treatment investigations, as this is would be a more appropriate scenario in which to assess modulation of an EV specific effect. Furthermore, treatment of recipient cells with DAPT may be a more prudent strategy for inhibition, given the previous report of EV delivered N1ICD cleavage only occurring in recipient cells (Wang and Lu, 2017).

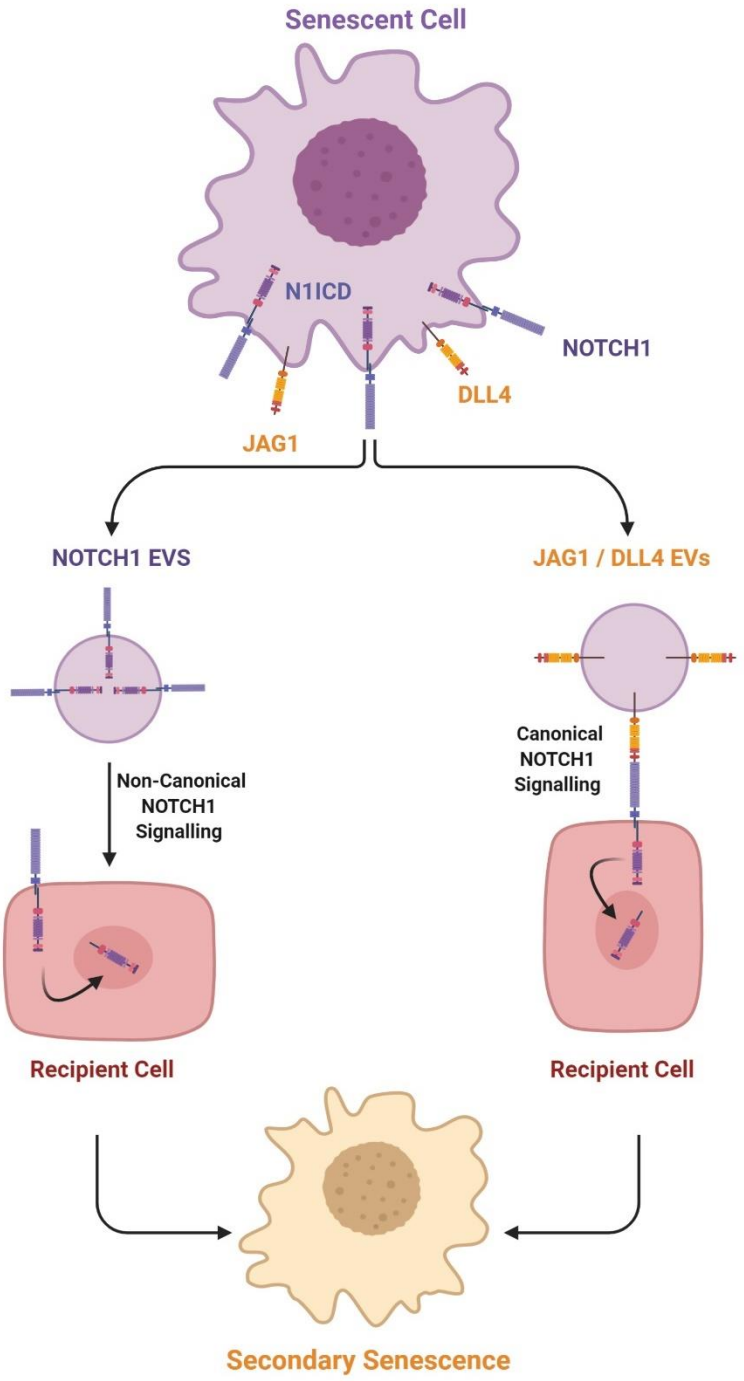

Figure 6.3: Hypotheses for routes of EV mediated paracrine senescence through NOTCH1

NOTCH1 and its ligands JAG1 and DLL4 were identified in OIS derived EVs by mass spectrometry (MS2). It is hypothesised that EVs may instigate a NOTCH1 mediated form of secondary senescence in proliferating cells through either binding NOTCH1 on the surface of recipient cells (canonical NOTCH1 signalling) or through delivery of NOTCH1 itself, which then may be cleaved in the recipient cell thus facilitating NOTCH signalling.

6.7.2 ADAM10/17 Sheddases

In the course of developing a rationale for the NOTCH1 mediated hypotheses discussed above, the sheddase ADAM17 was identified in the MS2 assessment of OIS Fraction 8. ADAM17, as well as the closely related ADAM10, are sheddases that mediate the initial cleavage events the follow NOTCH1 biding to it its ligands. Beyond this, these sheddases have a broad action, responsible for the shedding of membrane bound ectodomains, which subsequently come to comprise a significant part of the secretome. In senescence, shed ectodomains have been described to constitute around 10% of the total secreted factors (Morancho *et al.*, 2015). Furthermore, ADAM10 has been proposed as a marker of EVs, possibly serving as the elusive specific marker of small EVs (or exosomes) that has eluded the field (Kowal *et al.*, 2016). Therefore, it was decided to explore the role of both ADAM10 and ADAM17 within the development of the senescent secretome, particularly because the former appeared consistently present at increased levels in all three rounds of mass spectrometry. Immunoblotting demonstrated the presence of both sheddases in the OIS cells and derived EVs. However, for both proteins, epitopes of different sizes appeared to be identified depending on the type of sample examined. Communications from antibody manufacturers suggested that the lower molecular weight bands detected in the EVs represented cleaved, active forms of the sheddases, suggesting these forms to be preferentially trafficked during EV biogenesis or that EVs possessed the appropriate machinery to facilitate such activation. Additionally, proteomic data suggested that ADAM accessory proteins including IRHOM1, IRHOM2, TSPAN5 and TSPAN14 were also associated with the EVs. These proteins mediate the cleavage and shedding of specific ectodomains, tailoring the specificity of the sheddases (Matthews *et al.*, 2017). Together, these data suggested that further investigation of ADAM sheddases within senescence was worthwhile and, in particular, led to further consideration regarding the composition of the senescent secretome more broadly. It was hypothesised that alongside the canonical soluble SASP, and

the more recently accepted vesicular component, the less frequently described “sheddome” from senescent cells may represent an important and underexplored facet. Furthermore, it was considered that functionally active ADAMs on the surface of EVs could constitute a mechanism through which mobilisation of a “reservoir” of EV membrane ectodomains could occur, adding an additional layer of complexity (Effenberger *et al.*, 2014; Folkesson *et al.*, 2015; Schumacher *et al.*, 2015). In order to investigate this, modulation of both composition and function of the SASP could be investigated through use of ADAM inhibitors, including GW280264X (ADAM10/17), GI254023 (ADAM10) and TMI005 (ADAM17). The latter of these was the subject of preliminary investigation here, with modulation of OIS conditioning cells with TMI005 seeming to ablate the paracrine senescence effect of the collected media. Whilst a preliminary finding, this result suggests that further exploration of the role of sheddases in determining the composition of the SASP is worthwhile, along with further interrogation of potential activity of EV constituent sheddases. Overall, identification of this potentially underexplored dimension of the SASP was only feasible given the application of a high purity EV isolation workflow, reinforcing the primary finding of this work, that isolation methodology is essential to the evaluation of the extracellular vesicle component of the senescence-associated secretory phenotype.

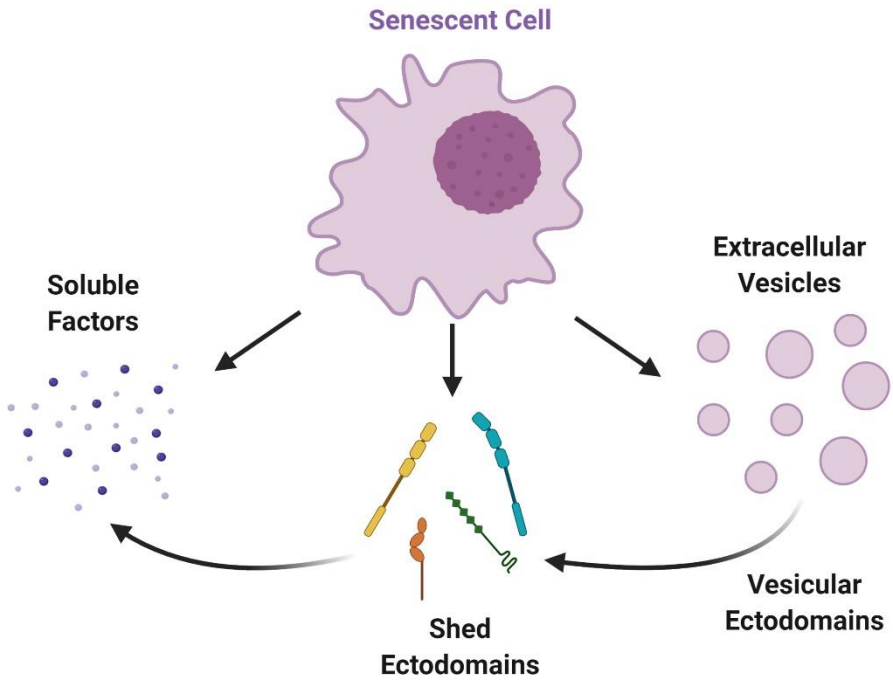

Figure 6.4: Composition of the Senescent Secretome

The secretome of senescent cells is complex, with the composition of the SASP dependent on both cell type and senescent inducing stimulus, as well as altering temporally within the course of senescence induction. The majority of studies investigating the SASP have focused on characterising the action of soluble factors but extracellular vesicles (EVs) are becoming widely appreciated a functionally relevant constituents. Whilst there have been investigations characterising the shedding of ectodomains from the surface of the senescent cells, which thus become part of the soluble SASP, their distinction from the rest of the secretome is not widely appreciated. Here, proteomic profiling of OIS derived EVs has led to the proposal that EVs possessive of the sheddases ADAM10/17 may be important contributors to the composition of the "sheddome". This may involve mobilisation of ectodomains from the surface of EVs, which, in turn, may contribute to the process of paracrine senescence.

7 Bibliography

Aaronson, S. *et al.* (1971) 'Ultrastructure of intracellular and extracellular vesicles, membranes, and myelin figures produced by Ochromonas danica', *Journal of Ultrasructure Research*. doi: 10.1016/S0022-5320(71)80003-5.

Abbas, M. *et al.* (2017) 'Endothelial Microparticles from Acute Coronary Syndrome Patients Induce Premature Coronary Artery Endothelial Cell Aging and Thrombogenicity: Role of the Ang II/AT1 Receptor/NADPH Oxidase-Mediated Activation of MAPKs and PI3-Kinase Pathways', *Circulation*, 135(3), pp. 280–296. doi: 10.1161/CIRCULATIONAHA.116.017513.

Acosta, J. C. *et al.* (2008) 'Chemokine Signaling via the CXCR2 Receptor Reinforces Senescence', *Cell*. Cell, 133(6), pp. 1006–1018. doi: 10.1016/j.cell.2008.03.038.

Acosta, J. C. *et al.* (2013) 'A complex secretory program orchestrated by the inflammasome controls paracrine senescence', *Nature Cell Biology*. doi: 10.1038/ncb2784.

Adan, A. *et al.* (2017) 'Flow cytometry: basic principles and applications', *Critical Reviews in Biotechnology*. doi: 10.3109/07388551.2015.1128876.

Alberro, A. *et al.* (2016) 'Inflammaging and frailty status do not result in an increased extracellular vesicle concentration in circulation', *International Journal of Molecular Sciences*. MDPI AG, 17(7). doi: 10.3390/ijms17071168.

Alcorta, D. A. *et al.* (1996) 'Involvement of the cyclin-dependent kinase inhibitor p16 (INK4a) in replicative senescence of normal human fibroblasts', *Biochemistry*, 93, pp. 13742–13747. Available at: http://www.pnas.org/content/pnas/93/24/13742.full.pdf (Accessed: 12 March 2018).

Alibhai, F. J. *et al.* (2020) 'Cellular senescence contributes to age-dependent changes in circulating extracellular vesicle cargo and function', *Aging Cell*. John Wiley & Sons, Ltd, 00, p. e13103. doi: 10.1111/acel.13103.

Alique, M. *et al.* (2018) 'Senescent Microvesicles: A Novel Advance in Molecular Mechanisms of Atherosclerotic Calcification.', *International journal of molecular sciences*. Multidisciplinary Digital Publishing Institute (MDPI), 19(7). doi: 10.3390/ijms19072003.

Assoian, R. K. and Zhu, X. (1997) 'Cell anchorage and the cytoskeleton as partners in growth factor dependent cell cycle progression', *Current Opinion in Cell Biology*. Elsevier Ltd, 9(1), pp. 93–98. doi: 10.1016/S0955-0674(97)80157-3.

Atha, D. H. and Inghamg, K. C. (1981) 'Mechanism of Precipitation of Proteins by Polyethylene Glycols', *THE JOURNAL OF BIOLOGICAL CHEMISTRY*.

Baar, M. P. *et al.* (2017) 'Targeted Apoptosis of Senescent Cells Restores Tissue Homeostasis in Response to Chemotoxicity and Aging', *Cell*. Cell Press, 169(1), pp. 132-147.e16. doi: 10.1016/j.cell.2017.02.031.

Bachurski, D. *et al.* (2019) 'Extracellular vesicle measurements with nanoparticle tracking analysis–An accuracy and repeatability comparison between NanoSight NS300 and ZetaView', *Journal of Extracellular Vesicles*. doi: 10.1080/20013078.2019.1596016.

Baietti, M. F. *et al.* (2012) 'Syndecan–syntenin–ALIX regulates the biogenesis of exosomes', *Nature Cell Biology*, 14(7), pp. 677–685. doi: 10.1038/ncb2502.

Baixauli, F., López-Otín, C. and Mittelbrunn, M. (2014) 'Exosomes and autophagy: Coordinated mechanisms for the maintenance of cellular fitness', *Frontiers in Immunology*, 5(AUG), p. 403. doi: 10.3389/fimmu.2014.00403.

Baker, B. M. and Chen, C. S. (2012) 'Deconstructing the third dimension-how 3D culture microenvironments alter cellular cues', *Journal of Cell Science*. doi: 10.1242/jcs.079509.

Baker, D. J. *et al.* (2011) 'Clearance of p16 Ink4a-positive senescent cells delays ageing-associated disorders', *Nature*. doi: 10.1038/nature10600.

Baker, D. J. *et al.* (2016) 'Naturally occurring p16Ink4a-positive cells shorten healthy lifespan', *Nature*. Nature Publishing Group, a division of Macmillan Publishers Limited. All Rights Reserved., 530(7589), pp. 184–189. doi: 10.1038/nature16932http://www.nature.com/nature/journal/v530/n7589/abs/nature16932.html#supplementary-information.

Bandu, R., Oh, J. W. and Kim, K. P. (2019) 'Mass spectrometry-based proteome profiling of extracellular vesicles and their roles in cancer biology', *Experimental and Molecular Medicine*. doi: 10.1038/s12276-019-0218-2.

Basisty, N. *et al.* (2020) 'A proteomic atlas of senescence-associated secretomes for aging biomarker development', *PLOS Biology*. Edited by M. Serrano, 18(1), p. e3000599. doi: 10.1371/journal.pbio.3000599.

Beauséjour, C. M. *et al.* (2003) 'Reversal of human cellular senescence: Roles of the p53 and p16 pathways', *EMBO Journal*. doi: 10.1093/emboj/cdg417.

Benedikter, B. J. *et al.* (2017) 'Ultrafiltration combined with size exclusion chromatography efficiently isolates extracellular vesicles from cell culture media for compositional and functional studies', *Scientific Reports*. doi: 10.1038/s41598-017-15717-7.

Bertoli, C., Skotheim, J. M. and De Bruin, R. A. M. (2013) 'Control of cell cycle transcription during G1 and S phases', *Nature Reviews Molecular Cell Biology*. doi: 10.1038/nrm3629.

Bhaumik, D. *et al.* (2009) 'MicroRNAs miR-146a/b negatively modulate the senescence-associated inflammatory mediators IL-6 and IL-8', *Aging*, 1(4), pp. 402–411. doi: 10.18632/aging.100042.

Biran, A. *et al.* (2017) 'Quantitative identification of senescent cells in aging and disease', *Aging Cell*. Blackwell Publishing Ltd, 16(4), pp. 661–671. doi: 10.1111/acel.12592.

Blackburn, E. H. (2001) 'Switching and signaling at the telomere', *Cell*. Cell Press, pp. 661–673. doi: 10.1016/S0092-8674(01)00492-5.

Blackburn, E. H. and Gall, J. G. (1978) 'A tandemly repeated sequence at the termini of the extrachromosomal ribosomal RNA genes in Tetrahymena', *Journal of Molecular Biology*. J Mol Biol, 120(1), pp. 33–53. doi: 10.1016/0022-2836(78)90294-2.

Bodnar, A. G. *et al.* (1998) 'Extension of life-span by introduction of telomerase into normal human cells', *Science*. American Association for the Advancement of Science, 279(5349), pp.

349–52. doi: 10.1126/science.279.5349.349.

Böing, A. N. *et al.* (2014) 'Single-step isolation of extracellular vesicles by size-exclusion chromatography', *J Extracell Vesicles*, 3. doi: 10.3402/jev.v3.23430.

Bonafè, M., Sabbatinelli, J. and Olivieri, F. (2020) 'Exploiting the telomere machinery to put the brakes on inflamm-aging', *Ageing Research Reviews*. Elsevier Ireland Ltd, p. 101027. doi: 10.1016/j.arr.2020.101027.

Boraschi, D. and Italiani, P. (2014) 'Immunosenescence and vaccine failure in the elderly: Strategies for improving response', *Immunology Letters*. doi: 10.1016/j.imlet.2014.06.006.

Borghesan, M. *et al.* (2019) 'Small Extracellular Vesicles Are Key Regulators of Non-cell Autonomous Intercellular Communication in Senescence via the Interferon Protein IFITM3', *CellReports*, 27, pp. 3956-3971.e6. doi: 10.1016/j.celrep.2019.05.095.

Boumendil, C. *et al.* (2019) 'Nuclear pore density controls heterochromatin reorganization during senescence', *Genes and Development*. doi: 10.1101/gad.321117.118.

Bray, S. J. (2016) 'Notch signalling in context', *Nature Reviews Molecular Cell Biology*. doi: 10.1038/nrm.2016.94.

Brennan, K. *et al.* (2020) 'A comparison of methods for the isolation and separation of extracellular vesicles from protein and lipid particles in human serum', *Scientific Reports*. doi: 10.1038/s41598-020-57497-7.

Brenner, A. J., Stampfer, M. R. and Aldaz, C. M. (1998) 'Increased p16 expression with first senescence arrest in human mammary epithelial cells and extended growth capacity with p16 inactivation', *Oncogene*. Nature Publishing Group, 17(2), pp. 199–205. doi: 10.1038/sj.onc.1201919.

Brownlee, Z. *et al.* (2014) 'A novel "salting-out" procedure for the isolation of tumor-derived exosomes', *J Immunol Methods*. 2014/04/17, 407, pp. 120–126. doi: 10.1016/j.jim.2014.04.003.

Buratta, S. *et al.* (2017) 'Extracellular vesicles released by fibroblasts undergoing H-Ras induced senescence show changes in lipid profile', *PLOS ONE*. Edited by G. Camussi, 12(11), p. e0188840. doi: 10.1371/journal.pone.0188840.

Campisi, J. (2001) 'Cellular senescence as a tumor-suppressor mechanism', *Trends in Cell Biology*. Elsevier Current Trends, pp. S27–S31. doi: 10.1016/S0962-8924(01)02151-1.

Campisi, J. and D'Adda Di Fagagna, F. (2007) 'Cellular senescence: When bad things happen to good cells', *Current Opinion in Genetics and Development*. doi: 10.1016/j.gde.2010.10.005.

Celeste, A. *et al.* (2002) 'Genomic instability in mice lacking histone H2AX', *Science*. Science, 296(5569), pp. 922–927. doi: 10.1126/science.1069398.

Chairoungdua, A. *et al.* (2010) 'Exosome release of β-catenin: a novel mechanism that antagonizes Wnt signaling', *The Journal of Cell Biology*, 190(6), pp. 1079–1091. doi: 10.1083/jcb.201002049.

Chang, J. *et al.* (2016) 'Clearance of senescent cells by ABT263 rejuvenates aged hematopoietic stem cells in mice', *Nature Medicine*. doi: 10.1038/nm.4010.

Chen, Q. and Ames, B. N. (1994) 'Senescence-like growth arrest induced by hydrogen peroxide in human diploid fibroblast F65 cells', *Proceedings of the National Academy of Sciences of the United States of America*. National Academy of Sciences, 91(10), pp. 4130–4134. doi: 10.1073/pnas.91.10.4130.

Chen, Q. M. *et al.* (2000) 'Involvement of Rb family proteins, focal adhesion proteins and protein synthesis in senescent morphogenesis induced by hydrogen peroxide', *Journal of Cell Science*.

Chen, Z. *et al.* (2005) 'Crucial role of p53-dependent cellular senescence in suppression of Pten-deficient tumorigenesis', *Nature*. Nature, 436(7051), pp. 725–730. doi: 10.1038/nature03918.

Cheng, M. (1999) 'The p21Cip1 and p27Kip1 CDK `inhibitors' are essential activators of cyclin D-dependent kinases in murine fibroblasts', *The EMBO Journal*. doi: 10.1093/emboj/18.6.1571.

Chien, Y. *et al.* (2011) 'Control of the senescence-associated secretory phenotype by NF-κB promotes senescence and enhances chemosensitivity.', *Genes & development*, 25(20), pp. 2125–36. doi: 10.1101/gad.17276711.

Choi, E.-J., Kil, I. S. and Cho, E.-G. (2020) 'Extracellular Vesicles Derived from Senescent Fibroblasts Attenuate the Dermal Effect on Keratinocyte Differentiation', *International Journal of Molecular Sciences*. MDPI AG, 21(3), p. 1022. doi: 10.3390/ijms21031022.

Chow, T. T. *et al.* (2012) 'Early and late steps in telomere overhang processing in normal human cells: The position of the final RNA primer drives telomere shortening', *Genes and Development*. Genes Dev, 26(11), pp. 1167–1178. doi: 10.1101/gad.187211.112.

Collado, M. *et al.* (2005) 'Tumour biology: Senescence in premalignant tumours', *Nature*. Nature, 436(7051), p. 642. doi: 10.1038/436642a.

Colombo, M., Raposo, G. and Thery, C. (2014) 'Biogenesis, secretion, and intercellular interactions of exosomes and other extracellular vesicles', *Annual Review of Cell and Developmental Biology*. United States, 30, pp. 255–289. doi: 10.1146/annurev-cellbio-101512-122326 [doi].

Coppé, J.-P. *et al.* (2010) 'The senescence-associated secretory phenotype: the dark side of tumor suppression', *Annu Rev Pathol*. 2010/01/19, 5, pp. 99–118. doi: 10.1146/annurev-pathol-121808-102144.

Coppé, J.-P. *et al.* (2011) 'Tumor Suppressor and Aging Biomarker p16 INK4a Induces Cellular Senescence without the Associated Inflammatory Secretory Phenotype * □ S'. doi: 10.1074/jbc.M111.257071.

Coppe, J. P. *et al.* (2008) 'Senescence-associated secretory phenotypes reveal cell-nonautonomous functions of oncogenic RAS and the p53 tumor suppressor', *PLoS Biol*. 2008/12/05, 6(12), pp. 2853–2868. doi: 10.1371/journal.pbio.0060301.

Cormenier, J. *et al.* (2018) 'The ATF6α arm of the Unfolded Protein Response mediates

replicative senescence in human fibroblasts through a COX2/prostaglandin E2 intracrine pathway', *Mechanisms of Ageing and Development*. Elsevier Ireland Ltd, 170, pp. 82–91. doi: 10.1016/j.mad.2017.08.003.

Cossetti, C. *et al.* (2014) 'Extracellular vesicles from neural stem cells transfer IFN-γ via Ifngr1 to activate Stat1 signaling in target cells', *Molecular Cell*. Europe PMC Funders, 56(2), pp. 193–204. doi: 10.1016/j.molcel.2014.08.020.

Coumans, F. A. W. *et al.* (2014) 'Reproducible extracellular vesicle size and concentration determination with tunable resistive pulse sensing', *Journal of Extracellular Vesicles*. doi: 10.3402/jev.v3.25922.

Coumans, F. A. W. W. *et al.* (2017) 'Methodological Guidelines to Study Extracellular Vesicles.', *Circulation research*. American Heart Association, Inc., 120(10), pp. 1632–1648. doi: 10.1161/CIRCRESAHA.117.309417.

Coverley, D., Laman, H. and Laskey, R. A. (2002) 'Distinct roles for cyclins E and A during DNA replication complex assembly and activation', *Nature Cell Biology*. Nature Publishing Group, 4(7), pp. 523–528. doi: 10.1038/ncb813.

Cox, J. and Mann, M. (2008) 'MaxQuant enables high peptide identification rates, individualized p.p.b.-range mass accuracies and proteome-wide protein quantification', *Nature Biotechnology*. doi: 10.1038/nbt.1511.

Cristofalo, V. J. and Kritchevsky, D. (1969) 'Cell size and nucleic acid content in the diploid human cell line WI-38 during aging', *Pharmacology*, 19(6), pp. 313–320. doi: 10.1159/000137216.

Cusanelli, E., Romero, C. A. P. and Chartrand, P. (2013) 'Telomeric Noncoding RNA TERRA Is Induced by Telomere Shortening to Nucleate Telomerase Molecules at Short Telomeres', *Molecular Cell*, 51(6), pp. 780–791. doi: 10.1016/j.molcel.2013.08.029.

Cvjetkovic, A. *et al.* (2014) 'The influence of rotor type and centrifugation time on the yield and purity of extracellular vesicles', *J Extracell Vesicles*. 2014/03/29, 3. doi: 10.3402/jev.v3.23111.

D'Adda Di Fagagna, F. *et al.* (2003) 'A DNA damage checkpoint response in telomere-initiated senescence', *Nature*. Nature, 426(6963), pp. 194–198. doi: 10.1038/nature02118.

Daaboul, G. G. *et al.* (2016) 'Digital Detection of Exosomes by Interferometric Imaging', *Scientific Reports*. doi: 10.1038/srep37246.

Davis, C. *et al.* (2017) 'MicroRNA-183-5p Increases with Age in Bone-Derived Extracellular Vesicles, Suppresses Bone Marrow Stromal (Stem) Cell Proliferation, and Induces Stem Cell Senescence.', *Tissue Engineering Part A*. Mary Ann Liebert, Inc. 140 Huguenot Street, 3rd Floor New Rochelle, NY 10801 USA, 23(21–22), pp. 1231–1240. doi: 10.1089/ten.tea.2016.0525.

Demaria, M. *et al.* (2014) 'An Essential Role for Senescent Cells in Optimal Wound Healing through Secretion of PDGF-AA', *Developmental Cell*, 31(6), pp. 722–733. doi: 10.1016/j.devcel.2014.11.012.

Deng, Q. *et al.* (2004) 'High Intensity ras Signaling Induces Premature Senescence by

Activating p38 Pathway in Primary Human Fibroblasts', *Journal of Biological Chemistry*. J Biol Chem, 279(2), pp. 1050–1059. doi: 10.1074/jbc.M308644200.

Van Deun, J. *et al.* (2014) 'The impact of disparate isolation methods for extracellular vesicles on downstream RNA profiling', *J Extracell Vesicles*, 3. doi: 10.3402/jev.v3.24858.

Van Deun, J. *et al.* (2017) 'EV-TRACK: Transparent reporting and centralizing knowledge in extracellular vesicle research', *Nature Methods*. Nature Publishing Group, pp. 228–232. doi: 10.1038/nmeth.4185.

van Deursen, J. M. (2014) 'The role of senescent cells in ageing', *Nature*. 2014/05/23, 509(7501), pp. 439–446. doi: 10.1038/nature13193.

Dewan, S. K. *et al.* (2012) 'Senescent remodeling of the immune system and its contribution to the predisposition of the elderly to infections', *Chinese Medical Journal*. doi: 10.3760/cma.j.issn.0366-6999.2012.18.023.

Dimri, G. P. *et al.* (1995) 'A biomarker that identifies senescent human cells in culture and in aging skin in vivo', *Cell Bioiogy*, 92, pp. 9363–9367. Available at: http://www.pnas.org/content/pnas/92/20/9363.full.pdf (Accessed: 12 March 2018).

Dirac, A. M. G. and Bernards, R. (2003) 'Reversal of senescence in mouse fibroblasts through lentiviral suppression of p53', *Journal of Biological Chemistry*. J Biol Chem, 278(14), pp. 11731–11734. doi: 10.1074/jbc.C300023200.

Doherty, G. J. and McMahon, H. T. (2009) 'Mechanisms of Endocytosis', *Annual Review of Biochemistry*. doi: 10.1146/annurev.biochem.78.081307.110540.

Dou, Z. *et al.* (2017) 'Cytoplasmic Chromatin Triggers Inflammation in Senescence and Cancer', *Nature*, 550(7676), pp. 402–406. doi: 10.1038/nature24050.

Dragovic, R. A. *et al.* (2011) 'Sizing and phenotyping of cellular vesicles using Nanoparticle Tracking Analysis', *Nanomedicine: Nanotechnology, Biology, and Medicine*. doi: 10.1016/j.nano.2011.04.003.

Druelle, C. *et al.* (2016) 'ATF6a regulates morphological changes associated with senescence in human fibroblasts', *Oncotarget*. Impact Journals LLC, 7(42), pp. 67699–67715. doi: 10.18632/oncotarget.11505.

Dyson, N. (1998) 'The regulation of E2F by pRB-family proteins', *Genes & Development*. Cold Spring Harbor Laboratory Press, 12(15), pp. 2245–2262. doi: 10.1101/gad.12.15.2245.

Effenberger, T. *et al.* (2014) 'Senescence-associated release of transmembrane proteins involves proteolytic processing by ADAM17 and microvesicle shedding', *FASEB Journal*. doi: 10.1096/fj.14-254565.

Eitan, E. *et al.* (2016) 'Impact of lysosome status on extracellular vesicle content and release', *Ageing Research Reviews*, 32, pp. 65–74. doi: 10.1016/j.arr.2016.05.001.

Eitan, E. *et al.* (2017) 'Age-Related Changes in Plasma Extracellular Vesicle Characteristics and Internalization by Leukocytes', *Scientific Reports*. Nature Publishing Group, 7(1), p. 1342. doi: 10.1038/s41598-017-01386-z.

Escrevente, C. *et al.* (2011) 'Interaction and uptake of exosomes by ovarian cancer cells', *BMC Cancer*. doi: 10.1186/1471-2407-11-108.

Espinosa, J. M., Verdun, R. E. and Emerson, B. M. (2003) 'p53 functions through stress- and promoter-specific recruitment of transcription initiation components before and after DNA damage', *Molecular Cell*. Cell Press, 12(4), pp. 1015–1027. doi: 10.1016/S1097-2765(03)00359-9.

Evangelou, K. *et al.* (2017) 'Robust, universal biomarker assay to detect senescent cells in biological specimens', *Aging Cell*. Blackwell Publishing Ltd, 16(1), pp. 192–197. doi: 10.1111/acel.12545.

Ewald, J. A. *et al.* (2010) 'Therapy-induced senescence in cancer', *Journal of the National Cancer Institute*. doi: 10.1093/jnci/djq364.

Fafián-Labora, J. A. and O'Loghlen, A. (2020) 'Classical and Nonclassical Intercellular Communication in Senescence and Ageing', *Trends in Cell Biology*. doi: 10.1016/j.tcb.2020.05.003.

Fafián-Labora, J. A., Rodríguez-Navarro, J. A. and O'Loghlen, A. (2020) 'Small Extracellular Vesicles Have GST Activity and Ameliorate Senescence-Related Tissue Damage', *Cell metabolism*. doi: 10.1016/j.cmet.2020.06.004.

Fagagna, F. d'Adda di *et al.* (2003) 'A DNA damage checkpoint response in telomere-initiated senescence', *Nature*, 426(6963), pp. 194–198. doi: 10.1038/nature02118.

Faget, D. V., Ren, Q. and Stewart, S. A. (2019) *Unmasking senescence: context-dependent effects of SASP in cancer*, *Nature Reviews Cancer*. Nature Publishing Group. doi: 10.1038/s41568-019-0156-2.

Filipe, V., Hawe, A. and Jiskoot, W. (2010) 'Critical evaluation of nanoparticle tracking analysis (NTA) by NanoSight for the measurement of nanoparticles and protein aggregates', *Pharmaceutical Research*. doi: 10.1007/s11095-010-0073-2.

Finn, R. S. *et al.* (2009) 'PD 0332991, a selective cyclin D kinase 4/6 inhibitor, preferentially inhibits proliferation of luminal estrogen receptor-positive human breast cancer cell lines in vitro', *Breast Cancer Research*. doi: 10.1186/bcr2419.

Finn, R. S. *et al.* (2016) 'Palbociclib and letrozole in advanced breast cancer', *New England Journal of Medicine*. doi: 10.1056/NEJMoa1607303.

Foers, A. D. *et al.* (2018) 'Enrichment of extracellular vesicles from human synovial fluid using size exclusion chromatography', *Journal of Extracellular Vesicles*. Taylor and Francis Ltd., 7(1). doi: 10.1080/20013078.2018.1490145.

Folkesson, M. *et al.* (2015) 'Proteolytically active ADAM10 and ADAM17 carried on membrane microvesicles in human abdominal aortic aneurysms', *Thrombosis and Haemostasis*. doi: 10.1160/TH14-10-0899.

Franceschi, C. (2007) 'Inflammaging as a Major Characteristic of Old People: Can It Be Prevented or Cured?', *Nutrition Reviews*. Nutr Rev, 65(SUPPL.3). doi: 10.1111/j.1753-4887.2007.tb00358.x.

Franceschi, C. and Campisi, J. (2014) 'Chronic inflammation (inflammaging) and its potential contribution to age-associated diseases.', *The journals of gerontology. Series A, Biological sciences and medical sciences*, 69 Suppl 1, pp. S4-9. doi: 10.1093/gerona/glu057.

Freund, A. *et al.* (2012) 'Lamin B1 loss is a senescence-associated biomarker', *Molecular Biology of the Cell*, 23(11), pp. 2066–2075. doi: 10.1091/mbc.E11-10-0884.

Freund, A., Patil, C. K. and Campisi, J. (2011) 'p38MAPK is a novel DNA damage response-independent regulator of the senescence-associated secretory phenotype.', *The EMBO journal*. European Molecular Biology Organization, 30(8), pp. 1536–48. doi: 10.1038/emboj.2011.69.

Fulzele, S. *et al.* (2019) 'Muscle-derived miR-34a increases with age in circulating extracellular vesicles and induces senescence of bone marrow stem cells.', *Aging*. Impact Journals, LLC, 11(6), pp. 1791–1803. doi: 10.18632/aging.101874.

Garbe, J. C. *et al.* (2009) 'Molecular distinctions between stasis and telomere attrition senescence barriers shown by long-term culture of normal human mammary epithelial cells', *Cancer Research*. doi: 10.1158/0008-5472.CAN-09-0270.

Garbe, J. C. *et al.* (2014) 'Immortalization of normal human mammary epithelial cells in two steps by direct targeting of senescence barriers does not require gross genomic alterations', *Cell Cycle*. Landes Bioscience, 13(21), pp. 3423–3435. doi: 10.4161/15384101.2014.954456.

Gardiner, C. *et al.* (2013) 'Extracellular vesicle sizing and enumeration by nanoparticle tracking analysis', *Journal of Extracellular Vesicles*. doi: 10.3402/jev.v2i0.19671.

Gardiner, C. *et al.* (2014) 'Measurement of refractive index by nanoparticle tracking analysis reveals heterogeneity in extracellular vesicles', *Journal of Extracellular Vesicles*. doi: 10.3402/jev.v3.25361.

Gardiner, C. *et al.* (2016) 'Techniques used for the isolation and characterization of extracellular vesicles: results of a worldwide survey', *Journal of Extracellular Vesicles*. Taylor and Francis Ltd., 5(1). doi: 10.3402/jev.v5.32945.

Georgakopoulou, E. A. *et al.* (2013) 'Specific lipofuscin staining as a novel biomarker to detect replicative and stress-induced senescence. A method applicable in cryo-preserved and archival tissues', *Aging*. Aging (Albany NY), 5(1), pp. 37–50. doi: 10.18632/aging.100527.

Ghosh, D. *et al.* (2020) 'Senescent mesenchymal stem cells remodel extracellular matrix driving breast cancer cells to more invasive phenotype', *Journal of Cell Science*. doi: 10.1242/jcs.232470.

Girard, F. *et al.* (1991) 'Cyclin a is required for the onset of DNA replication in mammalian fibroblasts', *Cell*, 67(6), pp. 1169–1179. doi: 10.1016/0092-8674(91)90293-8.

Gire, V. *et al.* (2004) 'DNA damage checkpoint kinase Chk2 triggers replicative senescence', *EMBO Journal*. doi: 10.1038/sj.emboj.7600259.

Gire, V. and Wynford-Thomas, D. (1998) 'Reinitiation of DNA Synthesis and Cell Division in Senescent Human Fibroblasts by Microinjection of Anti-p53 Antibodies', *Molecular and Cellular Biology*. American Society for Microbiology, 18(3), pp. 1611–1621. doi: 10.1128/mcb.18.3.1611.

Glück, S. *et al.* (2017) 'Innate Immune Sensing of Cytosolic Chromatin Fragments Through cGAS promotes Senescence', *Nature cell biology*, 19(9), pp. 1061–1070. doi: 10.1038/ncb3586.

Goldstein, S. (1990) 'Replicative senescence: The human fibroblast comes of age', *Science*. doi: 10.1126/science.2204114.

Gorgoulis, V. *et al.* (2019) 'Cellular Senescence: Defining a Path Forward', *Cell*, 179, pp. 813–827. doi: 10.1016/j.cell.2019.10.005.

Gould, S. J. and Raposo, G. (2013) 'As we wait: coping with an imperfect nomenclature for extracellular vesicles', *Journal of Extracellular Vesicles*, 2, p. 10.3402/jev.v2i0.20389. doi: 20389 [pii].

Greenberg, S. B., Grove, G. L. and Cristofalo, V. J. (1977) 'Cell size in aging monolayer cultures', *In Vitro*, 13(5), pp. 297–300. doi: 10.1007/BF02616174.

Greider, C. W. (1998) 'Telomeres and senescence: The history, the experiment, the future', *Current Biology*. Cell Press, pp. R178–R181. doi: 10.1016/s0960-9822(98)70105-8.

Guerrero, A. *et al.* (2019) 'Cardiac glycosides are broad-spectrum senolytics', *Nature Metabolism*. Nature Research, 1(11), pp. 1074–1088. doi: 10.1038/s42255-019-0122-z.

Hanahan, D. and Weinberg, R. A. (2011) 'Hallmarks of cancer: The next generation', *Cell*. doi: 10.1016/j.cell.2011.02.013.

Harashima, H., Dissmeyer, N. and Schnittger, A. (2013) 'Cell cycle control across the eukaryotic kingdom', *Trends in Cell Biology*. Elsevier Current Trends, pp. 345–356. doi: 10.1016/j.tcb.2013.03.002.

Harding, C., Heuser, J. and Stahl, P. (1983) 'Receptor-mediated endocytosis of transferrin and recycling of the transferrin receptor in rat reticulocytes', *The Journal of cell biology*. UNITED STATES, 97(2), pp. 329–339. Available at: http://jcb.rupress.org/content/jcb/97/2/329.full.pdf.

Hari, P. *et al.* (2019) 'The innate immune sensor Toll-like receptor 2 controls the senescence-associated secretory phenotype', *Science Advances*. American Association for the Advancement of Science, 5(6). doi: 10.1126/sciadv.aaw0254.

Harley, C. B., Futcher, A. B. and Greider, C. W. (1990) 'Telomeres shorten during ageing of human fibroblasts', *Nature*, 345(6274), pp. 458–460. doi: 10.1038/345458a0.

Harrison, D. E. *et al.* (2009) 'Rapamycin fed late in life extends lifespan in genetically heterogeneous mice.', *Nature*. NIH Public Access, 460(7253), pp. 392–5. doi: 10.1038/nature08221.

Harrison, P. and Gardiner, C. (2012) 'Invisible vesicles swarm within the iceberg', *Journal of Thrombosis and Haemostasis*. doi: 10.1111/j.1538-7836.2012.04711.x.

Hayflick, L. and Moorhead, P. S. (1961) 'The serial cultivation of human diploid cell strains', *Exp Cell Res*. 1961/12/01, 25, pp. 585–621.

Herbig, U. *et al.* (2004) 'Telomere shortening triggers senescence of human cells through a

pathway involving ATM, p53, and p21CIP1, but not p16INK4a', *Molecular Cell*. Mol Cell, 14(4), pp. 501–513. doi: 10.1016/S1097-2765(04)00256-4.

Hernandez-Segura, A., Nehme, J. and Demaria, M. (2018) 'Hallmarks of Cellular Senescence', *Trends in Cell Biology*. Elsevier Ltd, pp. 436–453. doi: 10.1016/j.tcb.2018.02.001.

Hickson, L. T. J. *et al.* (2019) 'Senolytics decrease senescent cells in humans: Preliminary report from a clinical trial of Dasatinib plus Quercetin in individuals with diabetic kidney disease', *EBioMedicine*. doi: 10.1016/j.ebiom.2019.08.069.

Hoare, M. *et al.* (2016) 'NOTCH1 mediates a switch between two distinct secretomes during senescence', *Nature Cell Biology*, 18(9), pp. 979–992. doi: 10.1038/ncb3397.

Hoare, M. and Narita, M. (2018) 'Notch and senescence', in *Advances in Experimental Medicine and Biology*. Springer New York LLC, pp. 299–318. doi: 10.1007/978-3-319-89512-3_15.

Hole, P. *et al.* (2013) 'Interlaboratory comparison of size measurements on nanoparticles using nanoparticle tracking analysis (NTA)', *Journal of Nanoparticle Research*. doi: 10.1007/s11051-013-2101-8.

Hsu, C. *et al.* (2010) 'Regulation of exosome secretion by Rab35 and its G... [J Cell Biol. 2010] - PubMed result', *The Journal of cell biology*, 189(2), pp. 223–32. doi: 10.1083/jcb.200911018.

Hui, R. *et al.* (2000) 'INK4a gene expression and methylation in primary breast cancer: Overexpression of p16(INK4a) messenger RNA is a marker of poor prognosis', *Clinical Cancer Research*.

Hurley, J. H. (2008) 'ESCRT complexes and the biogenesis of multivesicular bodies', *Current Opinion in Cell Biology*. doi: 10.1016/j.ceb.2007.12.002.

Hurley, J. H. (2015) ' ESCRT s are everywhere ', *The EMBO Journal*. EMBO, 34(19), pp. 2398–2407. doi: 10.15252/embj.201592484.

Hwang, E. S., Yoon, G. and Kang, H. T. (2009) 'A comparative analysis of the cell biology of senescence and aging', *Cellular and Molecular Life Sciences*. Cell Mol Life Sci, pp. 2503–2524. doi: 10.1007/s00018-009-0034-2.

Im, K. *et al.* (2018) 'The Comparison of Exosome and Exosomal Cytokines between Young and Old Individuals with or without Gastric Cancer', *International Journal of Gerontology*. No longer published by Elsevier, 12(3), pp. 233–238. doi: 10.1016/J.IJGE.2018.03.013.

Ipson, B. R. *et al.* (2018) 'Identifying Exosome-Derived MicroRNAs as Candidate Biomarkers of Frailty', *The Journal of frailty & aging*. NLM (Medline), 7(2), pp. 100–103. doi: 10.14283/jfa.2017.45.

Ivanov, A. *et al.* (2013) 'Lysosome-mediated processing of chromatin in senescence', *Journal of Cell Biology*, 202(1), pp. 129–143. doi: 10.1083/jcb.201212110.

Iwai, K. *et al.* (2016) 'Isolation of human salivary extracellular vesicles by iodixanol density gradient ultracentrifugation and their characterizations', *J Extracell Vesicles*, 5. doi: 10.3402/jev.v5.30829.

Janzen, V. *et al.* (2006) 'Stem-cell ageing modified by the cyclin-dependent kinase inhibitor p16 INK4a', *Nature*. doi: 10.1038/nature05159.

Jeon, O. H. *et al.* (2017) 'Local clearance of senescent cells attenuates the development of post-traumatic osteoarthritis and creates a pro-regenerative environment', *Nature Medicine*. doi: 10.1038/nm.4324.

Jeon, O. H. *et al.* (2019) 'Senescence cell–associated extracellular vesicles serve as osteoarthritis disease and therapeutic markers', *JCI Insight*, 4(7). doi: 10.1172/jci.insight.125019.

Johnstone, R. M. *et al.* (1987) 'Vesicle formation during reticulocyte maturation. Association of plasma membrane activities with released vesicles (exosomes)', *The Journal of biological chemistry*. UNITED STATES, 262(19), pp. 9412–9420. Available at: http://www.jbc.org/content/262/19/9412.full.pdf.

Johnstone, R. M. (1992) 'Maturation of reticulocytes: formation of exosomes as a mechanism for shedding membrane proteins', *Biochemistry and Cell Biology*, 70(3–4), pp. 179–190. doi: 10.1139/o92-028.

Jung, Y. S., Qian, Y. and Chen, X. (2010) 'Examination of the expanding pathways for the regulation of p21 expression and activity', *Cellular Signalling*. Pergamon, pp. 1003–1012. doi: 10.1016/j.cellsig.2010.01.013.

Justice, J. N. *et al.* (2019) 'Senolytics in idiopathic pulmonary fibrosis: Results from a first-in-human, open-label, pilot study', *EBioMedicine*, 40, pp. 554–563. doi: 10.1016/j.ebiom.2018.12.052.

Kang, C. *et al.* (2015) 'The DNA damage response induces inflammation and senescence by inhibiting autophagy of GATA4', *Science*. American Association for the Advancement of Science, 349(6255), p. aaa5612. doi: 10.1126/science.aaa5612.

Kang, T.-W. *et al.* (2011) 'Senescence surveillance of pre-malignant hepatocytes limits liver cancer development', *Nature*, 479(7374), pp. 547–551. doi: 10.1038/nature10599.

Karimi, N. *et al.* (2018) 'Detailed analysis of the plasma extracellular vesicle proteome after separation from lipoproteins', *Cellular and Molecular Life Sciences*. doi: 10.1007/s00018-018-2773-4.

Kavanagh, E. L. *et al.* (2017) 'Protein and chemotherapy profiling of extracellular vesicles harvested from therapeutic induced senescent triple negative breast cancer cells', *Oncogenesis*, 6(10), p. e388. doi: 10.1038/oncsis.2017.82.

Keerthikumar, S. *et al.* (2016) 'ExoCarta: A Web-Based Compendium of Exosomal Cargo', *Journal of Molecular Biology*. doi: 10.1016/j.jmb.2015.09.019.

Khayrullin, A. *et al.* (2019) 'Very Long-Chain C24:1 Ceramide Is Increased in Serum Extracellular Vesicles with Aging and Can Induce Senescence in Bone-Derived Mesenchymal Stem Cells.', *Cells*. Multidisciplinary Digital Publishing Institute (MDPI), 8(1). doi: 10.3390/cells8010037.

King, R. W., Jackson, P. K. and Kirschner, M. W. (1994) 'Mitosis in transition', *Cell*, pp. 563–571. doi: 10.1016/0092-8674(94)90542-8.

Kirkland, J. L. *et al.* (2017) 'The Clinical Potential of Senolytic Drugs', *Journal of the American Geriatrics Society*, 65(10), pp. 2297–2301. doi: 10.1111/jgs.14969.

Klumperman, J. and Raposo, G. (2014) 'The complex ultrastructure of the endolysosomal system', *Cold Spring Harbor Perspectives in Biology*. Cold Spring Harbor Laboratory Press, 6(10), p. a016857. doi: 10.1101/cshperspect.a016857.

Kocyłowski, M. K. *et al.* (2015) 'Ubiquitin-H2AX fusions render 53BP1 recruitment to DNA damage sites independent of RNF8 or RNF168', *Cell Cycle*. doi: 10.1080/15384101.2015.1010918.

Koh, Y. Q. *et al.* (2018) 'Exosome enrichment by ultracentrifugation and size exclusion chromatography', *Frontiers in Bioscience - Landmark*. doi: 10.2741/4621.

Kowal, J. *et al.* (2016) 'Proteomic comparison defines novel markers to characterize heterogeneous populations of extracellular vesicle subtypes', *Proceedings of the National Academy of Sciences*. doi: 10.1073/pnas.1521230113.

Krishnamurthy, J. *et al.* (2004) 'Ink4a/Arf expression is a biomarker of aging', *Journal of Clinical Investigation*, 114(9), pp. 1299–1307. doi: 10.1172/JCI22475.

Krizhanovsky, V. *et al.* (2008) 'Senescence of Activated Stellate Cells Limits Liver Fibrosis', *Cell*. Cell Press, 134(4), pp. 657–667. doi: 10.1016/j.cell.2008.06.049.

Krtolica, A. *et al.* (2001) 'Senescent fibroblasts promote epithelial cell growth and tumorigenesis: A link between cancer and aging', *Proceedings of the National Academy of Sciences of the United States of America*. Proc Natl Acad Sci U S A, 98(21), pp. 12072–12077. doi: 10.1073/pnas.211053698.

Kuilman, T. *et al.* (2008) 'Oncogene-induced senescence relayed by an interleukin-dependent inflammatory network.', *Cell*, 133(6), pp. 1019–31. doi: 10.1016/j.cell.2008.03.039.

Kuo, L. J. and Yang, L. X. (2008) 'γ-H2AX- A novel biomaker for DNA double-strand breaks', *In Vivo*.

Laberge, R. M. *et al.* (2015) 'MTOR regulates the pro-tumorigenic senescence-associated secretory phenotype by promoting IL1A translation', *Nature Cell Biology*. Nature Publishing Group, 17(8), pp. 1049–1061. doi: 10.1038/ncb3195.

Lahtela, J. *et al.* (2013) 'A high-content cellular senescence screen identifies candidate tumor suppressors, including EPHA3', *Cell Cycle*. doi: 10.4161/cc.23515.

Lamparski, H. G. *et al.* (2002) 'Production and characterization of clinical grade exosomes derived from dendritic cells', *Journal of Immunological Methods*. doi: 10.1016/S0022-1759(02)00330-7.

Lawless, C. *et al.* (2010) 'Quantitative assessment of markers for cell senescence', *Experimental Gerontology*. doi: 10.1016/j.exger.2010.01.018.

Lee, H. W. *et al.* (1998) 'Essential role of mouse telomerase in highly proliferative organs', *Nature*. doi: 10.1038/33345.

Lehmann, B. D. *et al.* (2008) 'Senescence-associated exosome release from human prostate cancer cells', *Cancer Research*. doi: 10.1158/0008-5472.CAN-07-6538.

Di Leonardo, A. *et al.* (1994) 'DNA damage triggers a prolonged p53-dependent G1 arrest and long-term induction of Cip1 in normal human fibroblasts', *Genes and Development*. Cold Spring Harbor Laboratory Press, 8(21), pp. 2540–2551. doi: 10.1101/gad.8.21.2540.

Lespagnol, A. *et al.* (2008) 'Exosome secretion, including the DNA damage-induced p53-dependent secretory pathway, is severely compromised in TSAP6/Steap3-null mice', *Cell Death & Differentiation*, 15(11), pp. 1723–1733. doi: 10.1038/cdd.2008.104.

Lew, M. (2007) 'Good statistical practice in pharmacology Problem 2', *British Journal of Pharmacology*, pp. 299–303. doi: 10.1038/sj.bjp.0707372.

Li, B. *et al.* (2012) 'RhoA triggers a specific signaling pathway that generates transforming microvesicles in cancer cells', *Oncogene*. Nature Publishing Group, 31(45), pp. 4740–4749. doi: 10.1038/onc.2011.636.

Lim, S. and Kaldis, P. (2013) 'Cdks, cyclins and CKIs: Roles beyond cell cycle regulation', *Development (Cambridge)*. Oxford University Press for The Company of Biologists Limited, pp. 3079–3093. doi: 10.1242/dev.091744.

Lin, A. W. *et al.* (1998) 'Premature senescence involving p53 and p16 is activated in response to constitutive MEK/MAPK mitogenic signaling.', *Genes & development*. Cold Spring Harbor Laboratory Press, 12(19), pp. 3008–19. Available at: http://www.ncbi.nlm.nih.gov/pubmed/9765203 (Accessed: 12 March 2018).

Livshits, M. A. *et al.* (2015) 'Isolation of exosomes by differential centrifugation: Theoretical analysis of a commonly used protocol', *Sci Rep*. 2015/12/01, 5, p. 17319. doi: 10.1038/srep17319.

Llorente, A. *et al.* (2013) 'Molecular lipidomics of exosomes released by PC-3 prostate cancer cells.', *Biochimica et biophysica acta*, 1831(7), pp. 1302–9. Available at: http://www.ncbi.nlm.nih.gov/pubmed/24046871 (Accessed: 12 March 2018).

Lobb, R. J. *et al.* (2015) 'Optimized exosome isolation protocol for cell culture supernatant and human plasma', *Journal of Extracellular Vesicles*. doi: 10.3402/jev.v4.27031.

López-Otín, C. *et al.* (2013) 'The hallmarks of aging', *Cell*. Cell Press, p. 1194. doi: 10.1016/j.cell.2013.05.039.

Lotvall, J. *et al.* (2014) 'Minimal experimental requirements for definition of extracellular vesicles and their functions: a position statement from the International Society for Extracellular Vesicles', *Journal of Extracellular Vesicles*. Co-Action Publishing, 3(2001-3078 (Linking)). doi: D - NLM: PMC4275645 OTO - NOTNLM.

Lowe, R. *et al.* (2015) 'The senescent methylome and its relationship with cancer, ageing and germline genetic variation in humans', *Genome Biology*. London: BioMed Central, 16(1), p. 194. doi: 10.1186/s13059-015-0748-4.

Maciel-Barón, L. A. *et al.* (2016) 'Senescence associated secretory phenotype profile from primary lung mice fibroblasts depends on the senescence induction stimuli', *Age*. Springer Netherlands, 38(1), pp. 1–14. doi: 10.1007/s11357-016-9886-1.

Malumbres, M. and Barbacid, M. (2001) 'To cycle or not to cycle: A critical decision in cancer', *Nature Reviews Cancer*. Nature Publishing Group, 1(3), pp. 222–231. doi: 10.1038/35106065.

Massagué, J. (2004) 'G1 cell-cycle control and cancer', *Nature*. Nature Publishing Group, pp. 298–306. doi: 10.1038/nature03094.

Mateescu, B. *et al.* (2017) 'Obstacles and opportunities in the functional analysis of extracellular vesicle RNA - An ISEV position paper', *Journal of Extracellular Vesicles*. doi: 10.1080/20013078.2017.1286095.

Mathivanan, S. *et al.* (2012) 'ExoCarta 2012: Database of exosomal proteins, RNA and lipids', *Nucleic Acids Research*. doi: 10.1093/nar/gkr828.

Matthews, A. L. *et al.* (2017) 'Regulation of A disintegrin and metalloproteinase (ADAM) family sheddases ADAM10 and ADAM17: The emerging role of tetraspanins and rhomboids', *Platelets*. doi: 10.1080/09537104.2016.1184751.

Mehta, I. S. *et al.* (2007) 'Alterations to nuclear architecture and genome behavior in senescent cells', in *Annals of the New York Academy of Sciences*. Blackwell Publishing Inc., pp. 250–263. doi: 10.1196/annals.1395.027.

Mensà, E. *et al.* (2020) 'Small extracellular vesicles deliver miR-21 and miR-217 as pro-senescence effectors to endothelial cells', *Journal of Extracellular Vesicles*. Taylor and Francis Ltd., 9(1), p. 1725285. doi: 10.1080/20013078.2020.1725285.

Di Micco, R. *et al.* (2011) 'Interplay between oncogene-induced DNA damage response and heterochromatin in senescence and cancer', *Nature Cell Biology*. doi: 10.1038/ncb2170.

Mitsuhashi, M. *et al.* (2013) 'Aging Enhances Release of Exosomal Cytokine mRNAs by Aβ1-42-stimulated Macrophages', *FASEB Journal*, 27(12), pp. 5141–5150. doi: 10.1096/fj.13-238980.

Möbius, W. *et al.* (2003) 'Recycling compartments and the internal vesicles of multivesicular bodies harbor most of the cholesterol found in the endocytic pathway.', *Traffic (Copenhagen, Denmark)*, 4(4), pp. 222–31. Available at: http://www.ncbi.nlm.nih.gov/pubmed/12694561 (Accessed: 12 March 2018).

Moore, M. *et al.* (2018) 'Ribosomal stress-induced senescence as a novel pro-senescence strategy for p16 positive basal-like breast cancer', *bioRxiv*. Cold Spring Harbor Laboratory. doi: 10.1101/469445.

Morancho, B. *et al.* (2015) 'Role of ADAM17 in the non-cell autonomous effects of oncogene-induced senescence', *Breast Cancer Research*. BioMed Central Ltd., 17(1), p. 106. doi: 10.1186/s13058-015-0619-7.

Morelli, A. E. *et al.* (2004) 'Endocytosis, intracellular sorting, and processing of exosomes by dendritic cells', *Blood*, 104(10), pp. 3257–3266. doi: 10.1182/blood-2004-03-0824.

Moser, J. *et al.* (2018) 'Control of the restriction point by rb and p21', *Proceedings of the National Academy of Sciences of the United States of America*. doi: 10.1073/pnas.1722446115.

Mu, X.-C. and Higgins, P. J. (1995) 'Differential growth state-dependent regulation of plasminogen activator inhibitor type-1 expression in senescent IMR-90 human diploid fibroblasts', *Journal of Cellular Physiology*. John Wiley & Sons, Ltd, 165(3), pp. 647–657. doi: 10.1002/jcp.1041650324.

Mulcahy, L. A., Pink, R. C. and Carter, D. R. F. (2014) 'Routes and mechanisms of extracellular vesicle uptake', *Journal of Extracellular Vesicles*. doi: 10.3402/jev.v3.24641.

Muñoz-Espín, D. *et al.* (2013) 'Programmed cell senescence during mammalian embryonic development', *Cell*. Cell Press, 155(5), p. 1104. doi: 10.1016/j.cell.2013.10.019.

Munoz-Espin, D. and Serrano, M. (2014) 'Cellular senescence: from physiology to pathology', *Nat Rev Mol Cell Biol*. 2014/06/24, 15(7), pp. 482–496. doi: 10.1038/nrm3823.

Nabhan, J. F. *et al.* (2012) 'Formation and release of arrestin domain-containing protein 1-mediated microvesicles (ARMMs) at plasma membrane by recruitment of TSG101 protein', *Proceedings of the National Academy of Sciences of the United States of America*. Proc Natl Acad Sci U S A, 109(11), pp. 4146–4151. doi: 10.1073/pnas.1200448109.

Nacher, V. *et al.* (2006) 'The Quail Mesonephros: A New Model for Renal Senescence?', *Journal of Vascular Research*. Karger Publishers, 43(6), pp. 581–586. doi: 10.1159/000096076.

Narita, Masashi *et al.* (2003) 'Rb-mediated heterochromatin formation and silencing of E2F target genes during cellular senescence', *Cell*. Cell Press, 113(6), pp. 703–716. doi: 10.1016/S0092-8674(03)00401-X.

Nelson, G. *et al.* (2012) 'A senescent cell bystander effect: Senescence-induced senescence', *Aging Cell*. Wiley-Blackwell, pp. 345–349. doi: 10.1111/j.1474-9726.2012.00795.x.

Neurohr, G. E. *et al.* (2019) 'Excessive Cell Growth Causes Cytoplasm Dilution And Contributes to Senescence', *Cell*, 176, pp. 1083-1097.e18. doi: 10.1016/j.cell.2019.01.018.

van Niel, G. *et al.* (2011) 'The Tetraspanin CD63 Regulates ESCRT-Independent and -Dependent Endosomal Sorting during Melanogenesis', *Developmental Cell*. Elsevier, 21(4), pp. 708–721. doi: 10.1016/j.devcel.2011.08.019.

van Niel, G., D'Angelo, G. and Raposo, G. (2018) 'Shedding light on the cell biology of extracellular vesicles', *Nature Reviews Molecular Cell Biology*. Nature Publishing Group. doi: 10.1038/nrm.2017.125.

Nielsen, G. P. *et al.* (1999) 'Immunohistochemical survey of p16INK4A expression in normal human adult and infant tissues.', *Laboratory investigation; a journal of technical methods and pathology*, 79(9), pp. 1137–43. Available at: http://www.ncbi.nlm.nih.gov/pubmed/10496532 (Accessed: 12 March 2018).

Nikolich-Žugich, J. (2008) 'Ageing and life-long maintenance of T-cell subsets in the face of latent persistent infections', *Nature Reviews Immunology*. doi: 10.1038/nri2318.

Nishio, K. *et al.* (2001) 'Senescence and cytoskeleton: Overproduction of vimentin induces senescent-like morphology in human fibroblasts', *Histochemistry and Cell Biology*. Histochem Cell Biol, 116(4), pp. 321–327. doi: 10.1007/s004180100325.

Nishio, K. and Inoue, A. (2005) 'Senescence-associated alterations of cytoskeleton: Extraordinary production of vimentin that anchors cytoplasmic p53 in senescent human fibroblasts', *Histochemistry and Cell Biology*. Histochem Cell Biol, 123(3), pp. 263–273. doi: 10.1007/s00418-005-0766-5.

Nordin, J. Z. *et al.* (2015) 'Ultrafiltration with size-exclusion liquid chromatography for high yield isolation of extracellular vesicles preserving intact biophysical and functional properties', *Nanomedicine: Nanotechnology, Biology, and Medicine*. doi: 10.1016/j.nano.2015.01.003.

Nowakowski, R. S., Lewin, S. B. and Miller, M. W. (1989) 'Bromodeoxyuridine immunohistochemical determination of the lengths of the cell cycle and the DNA-synthetic phase for an anatomically defined population', *Journal of Neurocytology*. Kluwer Academic Publishers, 18(3), pp. 311–318. doi: 10.1007/BF01190834.

Nyunoya, T. *et al.* (2006) 'Cigarette smoke induces cellular senescence', *American Journal of Respiratory Cell and Molecular Biology*, 35(6), pp. 681–688. doi: 10.1165/rcmb.2006-0169OC.

Ogrodnik, M. *et al.* (2019) 'Obesity-Induced Cellular Senescence Drives Anxiety and Impairs Neurogenesis', *Cell Metabolism*. Cell Press, 29(5), pp. 1061-1077.e8. doi: 10.1016/j.cmet.2018.12.008.

Ohtsubo, M. *et al.* (1995) 'Human cyclin E, a nuclear protein essential for the G1-to-S phase transition.', *Molecular and Cellular Biology*. American Society for Microbiology, 15(5), pp. 2612–2624. doi: 10.1128/mcb.15.5.2612.

Olovnikov, A. M. (1971) '[Principle of marginotomy in template synthesis of polynucleotides].', *Doklady Akademii nauk SSSR*.

Olovnikov, A. M. (1973) 'A theory of marginotomy. The incomplete copying of template margin in enzymic synthesis of polynucleotides and biological significance of the phenomenon', *Journal of Theoretical Biology*. doi: 10.1016/0022-5193(73)90198-7.

Olovnikov, A. M. (1996) 'Telomeres, telomerase, and aging: Origin of the theory', *Experimental Gerontology*. Elsevier Inc., 31(4), pp. 443–448. doi: 10.1016/0531-5565(96)00005-8.

Onódi, Z. *et al.* (2018) 'Isolation of high-purity extracellular vesicles by the combination of iodixanol density gradient ultracentrifugation and bind-elute chromatography from blood plasma', *Frontiers in Physiology*. doi: 10.3389/fphys.2018.01479.

Orjalo, A. V. *et al.* (2009) 'Cell surface-bound IL-1 is an upstream regulator of the senescence-associated IL-6/IL-8 cytokine network', *Proceedings of the National Academy of Sciences*, 106(40), pp. 17031–17036. doi: 10.1073/pnas.0905299106.

Ostrowski, M. *et al.* (2010) 'Rab27a and Rab27b control different steps of the exosome secretion pathway', *Nature Cell Biology*. Nat Cell Biol, 12(1), pp. 19–30. doi: 10.1038/ncb2000.

Overhoff, M. G. *et al.* (2014) 'Cellular senescence mediated by p16INK4A-coupled miRNA pathways', *Nucleic Acids Research*, 42(3), pp. 1606–1618. doi: 10.1093/nar/gkt1096.

Pagano, M. *et al.* (1992) 'Cyclin A is required at two points in the human cell cycle.', *The EMBO Journal*. Wiley, 11(3), pp. 961–971. doi: 10.1002/j.1460-2075.1992.tb05135.x.

Pan, B. T. and Johnstone, R. M. (1983) 'Fate of the transferrin receptor during maturation of sheep reticulocytes in vitro: selective externalization of the receptor', *Cell*. UNITED STATES, 33(3), pp. 967–978. doi: 0092-8674(83)90040-5 [pii].

Panier, S. and Boulton, S. J. (2014) 'Double-strand break repair: 53BP1 comes into focus', *Nature Reviews Molecular Cell Biology*. Nat Rev Mol Cell Biol, pp. 7–18. doi: 10.1038/nrm3719.

Pardee, A. B. (1974) *A Restriction Point for Control of Normal Animal Cell Proliferation (growth control/cell survival/cancer)*.

Parolini, I. *et al.* (2009) 'Microenvironmental pH is a key factor for exosome traffic in tumor cells', *Journal of Biological Chemistry*. doi: 10.1074/jbc.M109.041152.

Parry, A. J. *et al.* (2018) 'NOTCH-mediated non-cell autonomous regulation of chromatin structure during senescence', *Nature Communications*. Nature Publishing Group, 9(1), pp. 1–15. doi: 10.1038/s41467-018-04283-9.

Parry, A. J. and Narita, M. (2016) 'Old cells, new tricks: chromatin structure in senescence', *Mammalian Genome*. doi: 10.1007/s00335-016-9628-9.

Passos, J. F. *et al.* (2007) 'Mitochondrial dysfunction accounts for the stochastic heterogeneity in telomere-dependent senescence', *PLoS Biology*. PLoS Biol, 5(5), pp. 1138–1151. doi: 10.1371/journal.pbio.0050110.

Passos, J. F. *et al.* (2010) 'Feedback between p21 and reactive oxygen production is necessary for cell senescence', *Molecular Systems Biology*. doi: 10.1038/msb.2010.5.

Pegtel, D. M. *et al.* (2010) 'Functional delivery of viral miRNAs via exosomes', *Proc Natl Acad Sci U S A*. 2010/03/23, 107(14), pp. 6328–6333. doi: 10.1073/pnas.0914843107.

Pernas, S. *et al.* (2018) 'CDK4/6 inhibition in breast cancer: current practice and future directions', *Therapeutic Advances in Medical Oncology*. doi: 10.1177/1758835918786451.

Peters, J. M. (2006) 'The anaphase promoting complex/cyclosome: A machine designed to destroy', *Nature Reviews Molecular Cell Biology*. Nature Publishing Group, pp. 644–656. doi: 10.1038/nrm1988.

Petrova, N. V. *et al.* (2016) 'Small molecule compounds that induce cellular senescence', *Aging Cell*. Blackwell Publishing Ltd, pp. 999–1017. doi: 10.1111/acel.12518.

Picca, A. *et al.* (2019) 'Molecular Sciences Review Mitochondrial Dysfunction and Aging: Insights from the Analysis of Extracellular Vesicles'. doi: 10.3390/ijms20040805.

Piccin, A., Murphy, W. G. and Smith, O. P. (2007) 'Circulating microparticles: pathophysiology and clinical implications', *Blood Reviews*. Churchill Livingstone, 21(3), pp. 157–171. doi: 10.1016/j.blre.2006.09.001.

van der Pol, E. *et al.* (2014) 'Particle size distribution of exosomes and microvesicles determined by transmission electron microscopy, flow cytometry, nanoparticle tracking

analysis, and resistive pulse sensing', *Journal of Thrombosis and Haemostasis*. doi: 10.1111/jth.12602.

Van Der Pol, E. *et al.* (2012) 'Single vs. swarm detection of microparticles and exosomes by flow cytometry', *Journal of Thrombosis and Haemostasis*. doi: 10.1111/j.1538-7836.2012.04683.x.

Ramirez, M. I. *et al.* (2018) 'Technical challenges of working with extracellular vesicles.', *Nanoscale*, 10(3), pp. 881–906. doi: 10.1039/c7nr08360b.

Rao, S. G. and Jackson, J. G. (2016) 'SASP: Tumor Suppressor or Promoter? Yes!', *Trends in Cancer*. Cell Press, pp. 676–687. doi: 10.1016/j.trecan.2016.10.001.

Raposo, G. *et al.* (1996) 'B lymphocytes secrete antigen-presenting vesicles', *Journal of Experimental Medicine*. doi: 10.1084/jem.183.3.1161.

Rauser, C. L., Mueller, L. D. and Rose, M. R. (2006) 'The evolution of late life', *Ageing Research Reviews*. Elsevier, 5(1), pp. 14–32. doi: 10.1016/J.ARR.2005.06.003.

Ressler, S. *et al.* (2006) 'p16INK4A is a robust in vivo biomarker of cellular aging in human skin', *Aging Cell*. Aging Cell, 5(5), pp. 379–389. doi: 10.1111/j.1474-9726.2006.00231.x.

Reuter, J. A. and Khavari, P. A. (2006) 'Use of Conditionally Active Ras Fusion Proteins to Study Epidermal Growth, Differentiation, and Neoplasia', *Methods in Enzymology*. doi: 10.1016/S0076-6879(05)07054-0.

Richards, F. M. *et al.* (2012) 'Anti-tumour effects of a specific anti-ADAM17 antibody in an ovarian cancer model in vivo', *PLoS ONE*. doi: 10.1371/journal.pone.0040597.

Rider, M. A., Hurwitz, S. N. and Meckes Jr., D. G. (2016) 'ExtraPEG: A Polyethylene Glycol-Based Method for Enrichment of Extracellular Vesicles', *Sci Rep*. 2016/04/14, 6, p. 23978. doi: 10.1038/srep23978.

Rikkert, L. G. *et al.* (2019) 'Quality of extracellular vesicle images by transmission electron microscopy is operator and protocol dependent', *Journal of Extracellular Vesicles*. Taylor and Francis Ltd., 8(1). doi: 10.1080/20013078.2018.1555419.

Rink, J. *et al.* (2005) 'Rab conversion as a mechanism of progression from early to late endosomes', *Cell*. Cell, 122(5), pp. 735–749. doi: 10.1016/j.cell.2005.06.043.

Riquelme, J. A. *et al.* (2020) 'Increased production of functional small extracellular vesicles in senescent endothelial cells.', *Journal of cellular and molecular medicine*. John Wiley & Sons, Ltd, p. jcmm.15047. doi: 10.1111/jcmm.15047.

Rocha, S. *et al.* (2019) '3D Cellular Architecture Affects MicroRNA and Protein Cargo of Extracellular Vesicles', *Advanced Science*. doi: 10.1002/advs.201800948.

Rodier, F. *et al.* (2009) 'Persistent DNA damage signalling triggers senescence-associated inflammatory cytokine secretion.', *Nature cell biology*. NIH Public Access, 11(8), pp. 973–9. doi: 10.1038/ncb1909.

Romanov, S. R. *et al.* (2001) 'Normal human mammary epithelial cells spontaneously escape senescence and acquire genomic changes', *Nature*. Nature, 409(6820), pp. 633–637. doi:

10.1038/35054579.

Roukos, V. *et al.* (2015) 'Cell cycle staging of individual cells by fluorescence microscopy', *Nature Protocols*. Nature Publishing Group, 10(2), pp. 334–348. doi: 10.1038/nprot.2015.016.

Sadaie, M. *et al.* (2015) 'Cell-based screen for altered nuclear phenotypes reveals senescence progression in polyploid cells after Aurora kinase B inhibition', *Molecular Biology of the Cell*. American Society for Cell Biology, 26(17), pp. 2971–2985. doi: 10.1091/mbc.E15-01-0003.

Sage, J. *et al.* (2003) 'Acute mutation of retinoblastoma gene function is sufficient for cell cycle re-entry', *Nature*. doi: 10.1038/nature01764.

Sagini, K. *et al.* (2018) 'Oncogenic H-Ras Expression Induces Fatty Acid Profile Changes in Human Fibroblasts and Extracellular Vesicles.', *International journal of molecular sciences*. Multidisciplinary Digital Publishing Institute (MDPI), 19(11). doi: 10.3390/ijms19113515.

Salama, R. *et al.* (2014) 'Cellular senescence and its effector programs', *Genes and Development*, pp. 99–114. doi: 10.1101/gad.235184.113.

Saleem, S. N. and Abdel-Mageed, A. B. (2015) 'Tumor-derived exosomes in oncogenic reprogramming and cancer progression', *Cellular and Molecular Life Sciences*. Birkhauser Verlag AG, pp. 1–10. doi: 10.1007/s00018-014-1710-4.

Saleh, T. *et al.* (2018) 'Non-cell autonomous effects of the senescence-associated secretory phenotype in cancer therapy', *Frontiers in Oncology*. doi: 10.3389/fonc.2018.00164.

Satyanarayana, A. and Kaldis, P. (2009) 'Mammalian cell-cycle regulation: Several cdks, numerous cyclins and diverse compensatory mechanisms', *Oncogene*. doi: 10.1038/onc.2009.170.

Savina, A., Vidal, M. and Colombo, M. I. (2002) 'The exosome pathway in K562 cells is regulated by Rab11', *Journal of Cell Science*, 115(12), pp. 2505–2515.

Schafer, K. A. (1998) 'The Cell Cycle: A Review', *Veterinary Pathology*. SAGE PublicationsSage CA: Los Angeles, CA, 35(6), pp. 461–478. doi: 10.1177/030098589803500601.

Schafer, M. J. *et al.* (2017) 'Cellular senescence mediates fibrotic pulmonary disease', *Nature Communications*. doi: 10.1038/ncomms14532.

Schumacher, N. *et al.* (2015) 'Shedding of endogenous interleukin-6 receptor (IL-6R) is governed by a disintegrin and metalloproteinase (ADAM) proteases while a full-length IL-6R isoform localizes to circulating microvesicles', *Journal of Biological Chemistry*. doi: 10.1074/jbc.M115.649509.

Serrano, M. *et al.* (1997) 'Oncogenic ras provokes premature cell senescence associated with accumulation of p53 and p16(INK4a)', *Cell*. Cell Press, 88(5), pp. 593–602. doi: 10.1016/S0092-8674(00)81902-9.

Sharghi-Namini, S. *et al.* (2014) 'Dll4-containing exosomes induce capillary sprout retraction in a 3D microenvironment', *Scientific Reports*. doi: 10.1038/srep04031.

Sharpless, N. E. and Sherr, C. J. (2015) 'Forging a signature of in vivo senescence', *Nat Rev Cancer*. 2015/06/25, 15(7), pp. 397–408. doi: 10.1038/nrc3960.

Sheldon, H. *et al.* (2010) 'New mechanism for Notch signaling to endothelium at a distance by delta-like 4 incorporation into exosomes', *Blood*. doi: 10.1182/blood-2009-08-239228.

Sherr, C. J. (2000) 'The pezcoller lecture: Cancer cell cycles revisited', in *Cancer Research*, pp. 3689–3695.

Sherr, C. J. (2001) 'The INK4a/ARF network in tumour suppression', *Nature Reviews Molecular Cell Biology*. Nature Publishing Group, pp. 731–737. doi: 10.1038/35096061.

Sherr, C. J. and McCormick, F. (2002) 'The RB and p53 pathways in cancer', *Cancer Cell*. Cell Press, pp. 103–112. doi: 10.1016/S1535-6108(02)00102-2.

Sherr, C. J. and Roberts, J. M. (1999) 'CDK inhibitors: Positive and negative regulators of G1-phase progression', *Genes and Development*. Cold Spring Harbor Laboratory Press, pp. 1501–1512. doi: 10.1101/gad.13.12.1501.

Shu, C. *et al.* (2011) 'Pharmacokinetic-pharmacodynamic modeling of apratastat: A population-based approach', *Journal of Clinical Pharmacology*. doi: 10.1177/0091270010372389.

Simpson, R. J., Kalra, H. and Mathivanan, S. (2012) 'ExoCarta as a resource for exosomal research', *Journal of Extracellular Vesicles*. Co-Action Publishing, 1(1), p. 18374. doi: 10.3402/jev.v1i0.18374.

Stampfer, M. R. *et al.* (1981) 'Metabolism of benzo[a]pyrene by human mammary epithelial cells: toxicity and DNA adduct formation.', *Proceedings of the National Academy of Sciences of the United States of America*. National Academy of Sciences, 78(10), pp. 6251–5. Available at: http://www.ncbi.nlm.nih.gov/pubmed/6273860 (Accessed: 14 March 2018).

Stoorvogel, W. *et al.* (1991) 'Late endosomes derive from early endosomes by maturation', *Cell*. doi: 10.1016/0092-8674(91)90459-C.

Storer, M. *et al.* (2013) 'Senescence is a developmental mechanism that contributes to embryonic growth and patterning', *Cell*. Cell Press, 155(5), p. 1119. doi: 10.1016/j.cell.2013.10.041.

Studencka, M. and Schaber, J. (2017) 'Senoptosis: Non-lethal DNA cleavage as a route to deep senescence', *Oncotarget*. Impact Journals LLC, 8(19), pp. 30656–30671. doi: 10.18632/oncotarget.15693.

Stuffers, S. *et al.* (2009) 'Multivesicular endosome biogenesis in the absence of ESCRTs', *Traffic (Copenhagen, Denmark)*. Denmark, 10(7), pp. 925–937. doi: 10.1111/j.1600-0854.2009.00920.x [doi].

Tai, H. *et al.* (2017) 'Autophagy impairment with lysosomal and mitochondrial dysfunction is an important characteristic of oxidative stress-induced senescence', *Autophagy*. doi: 10.1080/15548627.2016.1247143.

Takahashi, A. *et al.* (2017) 'Exosomes maintain cellular homeostasis by excreting harmful DNA from cells', *Nature Communications*. Nature Publishing Group, 8(1), pp. 1–16. doi:

10.1038/ncomms15287.

Takahashi, A. *et al.* (2018) 'Downregulation of cytoplasmic DNases is implicated in cytoplasmic DNA accumulation and SASP in senescent cells', *Nature Communications*. Nature Publishing Group, 9(1). doi: 10.1038/s41467-018-03555-8.

Takasugi, M. *et al.* (2017) 'Small extracellular vesicles secreted from senescent cells promote cancer cell proliferation through EphA2', *Nature Communications*. Nature Publishing Group, 8(1), pp. 1–11. doi: 10.1038/ncomms15728.

Takasugi, M. (2018) 'Emerging roles of extracellular vesicles in cellular senescence and aging', *Aging Cell*, 17(2), p. e12734. doi: 10.1111/acel.12734.

Tan, D. B. A. *et al.* (2017) 'Elevated levels of circulating exosome in COPD patients are associated with systemic inflammation', *Respiratory Medicine*. W.B. Saunders Ltd, 132, pp. 261–264. doi: 10.1016/j.rmed.2017.04.014.

Tan, E., Asada, H. H. and Ge, R. (2018) 'Extracellular vesicle-carried Jagged-1 inhibits HUVEC sprouting in a 3D microenvironment', *Angiogenesis*. doi: 10.1007/s10456-018-9609-6.

Tauro, B. J. *et al.* (2012) 'Comparison of ultracentrifugation, density gradient separation, and immunoaffinity capture methods for isolating human colon cancer cell line LIM1863-derived exosomes', *Methods*. doi: 10.1016/j.ymeth.2012.01.002.

Taylor, D. D. and Shah, S. (2015) 'Methods of isolating extracellular vesicles impact down-stream analyses of their cargoes', *Methods*. doi: 10.1016/j.ymeth.2015.02.019.

Teo, Y. V. *et al.* (2019) 'Notch Signaling Mediates Secondary Senescence', *Cell Reports*, 27, pp. 997–1007. doi: 10.1016/j.celrep.2019.03.104.

Terlecki-Zaniewicz, L. *et al.* (2018) 'Small extracellular vesicles and their miRNA cargo are anti-apoptotic members of the senescence-associated secretory phenotype', *Aging*, 10(5), pp. 1103–1132. doi: 10.18632/aging.101452.

Terlecki-Zaniewicz, L. *et al.* (2019) 'Extracellular vesicles in human skin: cross-talk from senescent fibroblasts to keratinocytes by miRNAs', *Journal of Investigative Dermatology*. Elsevier. doi: 10.1016/J.JID.2019.05.015.

Terman, A. *et al.* (2010) 'Mitochondrial Turnover and aging of long-lived postmitotic cells: The mitochondrial-lysosomal axis theory of aging', *Antioxidants and Redox Signaling*, pp. 503–535. doi: 10.1089/ars.2009.2598.

Théry, C. *et al.* (2001) 'Proteomic Analysis of Dendritic Cell-Derived Exosomes: A Secreted Subcellular Compartment Distinct from Apoptotic Vesicles', *The Journal of Immunology*. doi: 10.4049/jimmunol.166.12.7309.

Théry, C. *et al.* (2006) 'Isolation and Characterization of Exosomes from Cell Culture Supernatants and Biological Fluids', *Current Protocols in Cell Biology*. doi: 10.1002/0471143030.cb0322s30.

Théry, C. *et al.* (2018) 'Minimal information for studies of extracellular vesicles 2018 (MISEV2018): a position statement of the International Society for Extracellular Vesicles and update of the MISEV2014 guidelines.', *Journal of extracellular vesicles*, 7(1), p. 1535750. doi:

10.1080/20013078.2018.1535750.

Thippabhotla, S., Zhong, C. and He, M. (2019) '3D cell culture stimulates the secretion of in vivo like extracellular vesicles', *Scientific Reports*. doi: 10.1038/s41598-019-49671-3.

Tian, Y. *et al.* (2018) 'Protein Profiling and Sizing of Extracellular Vesicles from Colorectal Cancer Patients via Flow Cytometry', *ACS Nano*. doi: 10.1021/acsnano.7b07782.

Tian, Y. *et al.* (2020) 'Quality and efficiency assessment of six extracellular vesicle isolation methods by nano-flow cytometry', *Journal of Extracellular Vesicles*. doi: 10.1080/20013078.2019.1697028.

Tibbitt, M. W. and Anseth, K. S. (2009) 'Hydrogels as extracellular matrix mimics for 3D cell culture', *Biotechnology and Bioengineering*. doi: 10.1002/bit.22361.

Tilstra, J. S. *et al.* (2012) 'NF-κB inhibition delays DNA damage - Induced senescence and aging in mice', *Journal of Clinical Investigation*. doi: 10.1172/JCI45785.

Tosar, J. P. *et al.* (2017) 'Ribonucleic artefacts: Are some extracellular RNA discoveries driven by cell culture medium components?', *Journal of Extracellular Vesicles*. doi: 10.1080/20013078.2017.1272832.

Trajkovic, K. *et al.* (2008) 'Ceramide Triggers Budding of Exosome Vesicles into Multivesicular Endosomes', *Science*, 319(5867), pp. 1244–1247. doi: 10.1126/science.1153124.

Trams, E. G. *et al.* (1981) 'Exfoliation of membrane ecto-enzymes in the form of micro-vesicles', *Biochimica et biophysica acta*. NETHERLANDS, 645(1), pp. 63–70.

Triana-Martínez, F. *et al.* (2019) 'Identification and characterization of Cardiac Glycosides as senolytic compounds', *Nature Communications*. Nature Publishing Group, 10(1), pp. 1–12. doi: 10.1038/s41467-019-12888-x.

Tyanova, S. *et al.* (2016) 'The Perseus computational platform for comprehensive analysis of (prote)omics data', *Nature Methods*. doi: 10.1038/nmeth.3901.

Tyler, E. J. (2016) *Understanding the molecular interplay between senescence, rejuvenation, and healthy ageing*. Queen Mary University of London. Available at: https://qmro.qmul.ac.uk/xmlui/handle/123456789/25981.

Valadi, H. *et al.* (2007) 'Exosome-mediated transfer of mRNAs and microRNAs is a novel mechanism of genetic exchange between cells', *Nature cell biology*. England, 9(6), pp. 654–659. doi: ncb1596 [pii].

Vasileiou, P. *et al.* (2019) 'Mitochondrial Homeostasis and Cellular Senescence', *Cells*. doi: 10.3390/cells8070686.

Vega, L. R., Mateyak, M. K. and Zakian, V. A. (2003) 'Getting to the end: Telomerase access in yeast and humans', *Nature Reviews Molecular Cell Biology*. Nature Publishing Group, pp. 948–959. doi: 10.1038/nrm1256.

Vermeulen, K., Van Bockstaele, D. R. and Berneman, Z. N. (2003) 'The cell cycle: A review of regulation, deregulation and therapeutic targets in cancer', *Cell Proliferation*. Wiley-Blackwell, pp. 131–149. doi: 10.1046/j.1365-2184.2003.00266.x.

Villarroya-Beltri, C. *et al.* (2016) 'ISGylation controls exosome secretion by promoting lysosomal degradation of MVB proteins', *Nature Communications*. doi: 10.1038/ncomms13588.

Walker, D. H. and Maller, J. L. (1991) 'Role for cyclin A in the dependence of mitosis on completion of DMA replication', *Nature*, 354(6351), pp. 314–317. doi: 10.1038/354314a0.

Wallis, R., Mizen, H. and Bishop, C. L. (2020) 'The Bright and Dark Side of Extracellular Vesicles in the Senescence-Associated Secretory Phenotype', *Mechanisms of Ageing and Development*. Elsevier, p. 111263. doi: 10.1016/j.mad.2020.111263.

Wang, C. *et al.* (2019) 'Inducing and exploiting vulnerabilities for the treatment of liver cancer', *Nature*. Nature Publishing Group, 574(7777), pp. 268–272. doi: 10.1038/s41586-019-1607-3.

Wang, E. and Gundersen, D. (1984) 'Increased organization of cytoskeleton accompanying the aging of human fibroblasts in vitro', *Experimental Cell Research*, 154(1), pp. 191–202. doi: 10.1016/0014-4827(84)90679-7.

Wang, Q. and Lu, Q. (2017) 'Plasma membrane-derived extracellular microvesicles mediate non-canonical intercellular NOTCH signaling', *Nature Communications*. doi: 10.1038/s41467-017-00767-2.

Wang, W. *et al.* (2002) 'Sequential Activation of the MEK-Extracellular Signal-Regulated Kinase and MKK3/6-p38 Mitogen-Activated Protein Kinase Pathways Mediates Oncogenic ras-Induced Premature Senescence', *Molecular and Cellular Biology*. American Society for Microbiology, 22(10), pp. 3389–3403. doi: 10.1128/mcb.22.10.3389-3403.2002.

Wang, Z. *et al.* (2015) 'Telomeric repeat-containing RNA (TERRA) constitutes a nucleoprotein component of extracellular inflammatory exosomes', *Proceedings of the National Academy of Sciences*. National Academy of Sciences, 112(46), pp. E6293–E6300. doi: 10.1073/pnas.1505962112.

Wang, Z. and Lieberman, P. M. (2016) 'The crosstalk of telomere dysfunction and inflammation through cell-free TERRA containing exosomes', *RNA Biology*, 13(8), pp. 690–695. doi: 10.1080/15476286.2016.1203503.

Watson, D. C. *et al.* (2016) 'Efficient production and enhanced tumor delivery of engineered extracellular vesicles', *Biomaterials*. doi: 10.1016/j.biomaterials.2016.07.003.

Watson, J. (1972) 'Origin of Concatemeric T7DNA', *Nature*. doi: 10.1038/10.1038/newbio239197a0.

Webber, J. and Clayton, A. (2013) 'How pure are your vesicles?', *Journal of extracellular vesicles*. Taylor & Francis, 2. doi: 10.3402/jev.v2i0.19861.

Webber, J. P. *et al.* (2015) 'Differentiation of tumour-promoting stromal myofibroblasts by cancer exosomes', *Oncogene*. Nature Publishing Group, 34(3), pp. 319–333. doi: 10.1038/onc.2013.560.

Wehman, A. M. *et al.* (2011) 'The P4-ATPase TAT-5 inhibits the budding of extracellular vesicles in C. elegans embryos', *Current Biology*. Elsevier, 21(23), pp. 1951–1959. doi: 10.1016/j.cub.2011.10.040.

Weilner, S., Schraml, E., *et al.* (2016) 'Secreted microvesicular miR-31 inhibits osteogenic differentiation of mesenchymal stem cells', *Aging cell*, 15(4), pp. 744–54. doi: 10.1111/acel.12484.

Weilner, S., Keider, V., *et al.* (2016) 'Vesicular Galectin-3 levels decrease with donor age and contribute to the reduced osteo-inductive potential of human plasma derived extracellular vesicles', *Aging*, 8(1), pp. 16–30. doi: 10.18632/aging.100865.

Weiner-Gorzel, K. *et al.* (2015) 'Overexpression of the microRNA miR-433 promotes resistance to paclitaxel through the induction of cellular senescence in ovarian cancer cells', *Cancer Medicine*, 4(5), pp. 745–758. doi: 10.1002/cam4.409.

Wieser, S. and Pines, J. (2015) 'The biochemistry of mitosis', *Cold Spring Harbor Perspectives in Biology*. Cold Spring Harbor Laboratory Press, 7(3). doi: 10.1101/cshperspect.a015776.

Wiley, C. D. *et al.* (2016) 'Mitochondrial dysfunction induces senescence with a distinct secretory phenotype', *Cell Metabolism*. Cell Press, 23(2), pp. 303–314. doi: 10.1016/j.cmet.2015.11.011.

Willms, E. *et al.* (2016) 'Cells release subpopulations of exosomes with distinct molecular and biological properties', *Scientific Reports*. doi: 10.1038/srep22519.

Witwer, K. W. *et al.* (2013) 'Standardization of sample collection, isolation and analysis methods in extracellular vesicle research', *Journal of Extracellular Vesicles*. Taylor & Francis, 2(1), p. 20360. doi: 10.3402/jev.v2i0.20360.

Witwer, K. W. and Théry, C. (2019) 'Extracellular vesicles or exosomes? On primacy, precision, and popularity influencing a choice of nomenclature', *Journal of Extracellular Vesicles*. Informa UK Limited, 8(1), p. 1648167. doi: 10.1080/20013078.2019.1648167.

Wollert, T. *et al.* (2009) 'Membrane scission by the ESCRT-III complex', *Nature*. doi: 10.1038/nature07836.

Wollert, T. and Hurley, J. H. (2010) 'Molecular mechanism of multivesicular body biogenesis by ESCRT complexes', *Nature*. doi: 10.1038/nature08849.

Woo, R. A. and Poon, R. Y. C. (2003) 'Cyclin-dependent kinases and S phase control in mammalian cells.', *Cell cycle (Georgetown, Tex.)*, pp. 315–323. doi: 10.4161/cc.2.4.468.

Xu, M. *et al.* (2015) 'JAK inhibition alleviates the cellular senescence-associated secretory phenotype and frailty in old age', *Proceedings of the National Academy of Sciences of the United States of America*. doi: 10.1073/pnas.1515386112.

Xu, M. *et al.* (2018) 'Senolytics improve physical function and increase lifespan in old age', *Nature Medicine*, 24(8), pp. 1246–1256. doi: 10.1038/s41591-018-0092-9.

Xu, S. *et al.* (2019) 'The p53/miRNAs/Ccna2 pathway serves as a novel regulator of cellular senescence: Complement of the canonical p53/p21 pathway', *Aging Cell*, 18(3), p. e12918. doi: 10.1111/acel.12918.

Xue, W. *et al.* (2007) 'Senescence and tumour clearance is triggered by p53 restoration in murine liver carcinomas', *Nature*, 445(7128), pp. 656–660. doi: 10.1038/nature05529.

Yamakuchi, M. and Lowenstein, C. J. (2009) 'MiR-34, SIRT1 and p53: The feedback loop', *Cell Cycle*. Taylor and Francis Inc., pp. 712–715. doi: 10.4161/cc.8.5.7753.

Yang, N. C. and Hu, M. L. (2005) 'The limitations and validities of senescence associated-β-galactosidase activity as an aging marker for human foreskin fibroblast Hs68 cells', *Experimental Gerontology*. Pergamon, 40(10), pp. 813–819. doi: 10.1016/j.exger.2005.07.011.

Yosef, R. *et al.* (2016) 'Directed elimination of senescent cells by inhibition of BCL-W and BCL-XL', *Nature Communications*. Nature Publishing Group, 7(1), pp. 1–11. doi: 10.1038/ncomms11190.

Yoshida, M. *et al.* (2019) 'Extracellular Vesicle-Contained eNAMPT Delays Aging and Extends Lifespan in Mice', *Cell Metabolism*, 30, pp. 1–14. doi: 10.1016/j.cmet.2019.05.015.

Yu, X., Harris, S. L. and Levine, A. J. (2006) 'The regulation of exosome secretion: A novel function of the p53 protein', *Cancer Research*. Cancer Res, 66(9), pp. 4795–4801. doi: 10.1158/0008-5472.CAN-05-4579.

Zech, D. *et al.* (2012) 'Tumor-exosomes and leukocyte activation: An ambivalent crosstalk', *Cell Communication and Signaling*. doi: 10.1186/1478-811X-10-37.

Zhao, H. *et al.* (2010) 'New biomarkers probing depth of cell senescence assessed by laser scanning cytometry', *Cytometry Part A*, (11), pp. 999–1007. doi: 10.1002/cyto.a.20983.

Zhao, H. and Darzynkiewicz, Z. (2013) 'Biomarkers of cell senescence assessed by imaging cytometry', *Methods in Molecular Biology*. Humana Press Inc., 965, pp. 83–92. doi: 10.1007/978-1-62703-239-1_5.

Zhu, J. *et al.* (1998) 'Senescence of human fibroblasts induced by oncogenic Raf.', *Genes & development*. Cold Spring Harbor Laboratory Press, 12(19), pp. 2997–3007. Available at: http://www.ncbi.nlm.nih.gov/pubmed/9765202 (Accessed: 12 March 2018).

Zhu, Y. *et al.* (2015) 'The Achilles' heel of senescent cells: From transcriptome to senolytic drugs', *Aging Cell*. Blackwell Publishing Ltd, 14(4), pp. 644–658. doi: 10.1111/acel.12344.

Zhu, Y. *et al.* (2016) 'Identification of a novel senolytic agent, navitoclax, targeting the Bcl-2 family of anti-apoptotic factors', *Aging Cell*. Blackwell Publishing Ltd, 15(3), pp. 428–435. doi: 10.1111/acel.12445.

Zhu, Y. *et al.* (2017) 'New agents that target senescent cells: The flavone, fisetin, and the BCL-XL inhibitors, A1331852 and A1155463', *Aging*. doi: 10.18632/aging.101202.

8 Appendix

8.1 Mass Spectrometry 1: Proteomic assessment of EVs isolated by dUC from vector and OIS IMR90s

This data forms the basis of section 4.5 and is referred to throughout as MS1. EV samples were isolated in triplicate by dUC from vector and OIS IMR90s. These were analysed by mass spectrometry through collaboration with the CECAD proteomic facility (University of Cologne). Gene lists detailing the label-free quantitation intensities (LFQ) for each sample were produced and analysed according to section 2.13.2. Mean LFQ intensity values (Mean LFQ) from vector (orange) and OIS (purple) replicates are detailed, along with positive or negative fold change (FC). Unpaired Student's t-tests were also performed, with the p-value described in the final column for each gene (-Log10 p-value).

Gene names	Vector dUC Mean LFQ (Log2)	OIS dUC Mean LFQ (Log2)	FC Mean LFQ (Log2)	-Log10 p-value
HRAS	25.70	32.51	6.81	3.00359
PLAT	24.92	30.18	5.26	3.16908
STC1	24.94	29.84	4.90	1.71936
SLC16A6	23.83	28.58	4.75	2.95297
PLAU	27.21	31.96	4.75	2.08836
ESR1	25.09	29.47	4.38	1.16622
NRG1	23.84	28.18	4.33	2.29246
ANPEP	26.85	31.07	4.22	1.68092
ITGA6	25.28	29.45	4.17	1.77055
CDCP1	24.02	28.14	4.12	2.85444
FAT1	24.66	28.71	4.05	1.58854
ANGPTL4	23.94	27.94	4.01	1.48653
CXCL8	24.17	28.09	3.92	1.09485
ITGB5	23.94	27.83	3.89	2.1631
CD81	28.19	32.05	3.86	0.697259
ITGA2	29.87	33.58	3.71	2.7326
ADAM10	26.88	30.58	3.70	0.969503
SRPX	25.00	28.58	3.58	2.3039
AREG	23.67	27.19	3.52	1.93028
CD9	29.96	33.47	3.51	1.92014
MMP1	29.60	33.09	3.49	3.63488
MMP14	26.19	29.59	3.39	1.30072

ICAM1	24.61	27.83	3.23	1.34471
ITGA5	26.03	29.25	3.22	1.35397
CD82	24.34	27.56	3.21	0.844971
NT5E	29.90	33.11	3.21	2.29579
VGF	23.83	27.04	3.21	1.60946
TSPAN9	23.88	27.06	3.17	1.08192
EPHB2	23.95	27.12	3.17	1.36677
ANTXR2	24.03	27.12	3.09	1.72921
F3	24.97	28.04	3.08	1.91424
CD46	23.98	26.91	2.94	2.20242
ATP1A1	27.55	30.48	2.93	1.57059
MARCKSL1	25.39	28.27	2.89	1.64189
EPHA2	25.40	28.27	2.87	1.28975
INHBA	24.50	27.24	2.74	0.836981
IGSF8	26.04	28.77	2.73	0.821364
PSMA1	24.51	27.22	2.71	1.17663
TFPI2	24.12	26.82	2.70	1.75395
SERPINB2	24.03	26.73	2.69	2.0259
PRSS23	25.76	28.44	2.68	1.49614
ITGB3	24.81	27.45	2.64	1.78118
ITGA3	27.79	30.37	2.58	1.68267
GPX3;GPX6;GPX5	23.99	26.55	2.55	3.12507
AKAP12	24.32	26.86	2.54	1.4676
SERPINE2	24.10	26.63	2.53	1.32185
TPBG	24.40	26.92	2.51	1.37937
EMILIN1	25.15	27.66	2.51	1.23251
CD276	24.00	26.51	2.50	1.92512
TPP2	26.91	29.35	2.44	0.685864
GNB1	25.89	28.33	2.44	0.871749
GNAI3	24.06	26.43	2.36	1.04047
CD151	26.02	28.37	2.35	1.21775
MAP4K4;TNIK;MINK1	24.11	26.46	2.35	1.39218
WNT5A	26.93	29.27	2.34	1.8858
PTGES3	26.79	29.13	2.34	0.499642
SCUBE3	24.23	26.55	2.32	0.902257
S100A13	26.15	28.37	2.22	0.735764
ITGAV	26.64	28.85	2.21	1.30962
SLC39A10	23.53	25.73	2.21	2.56138
HGF	27.03	29.23	2.20	1.00574
SDCBP	26.24	28.42	2.18	0.545436
SEMA7A	25.10	27.27	2.17	0.829803
GNG5	23.40	25.57	2.17	1.9908
ITGB1	31.47	33.59	2.12	2.16295
GNG2	24.18	26.22	2.05	1.1095
TGM2	27.52	29.54	2.02	2.7114
PSMC2	24.25	26.27	2.02	0.846803

PLXNB2	25.28	27.29	2.01	1.26521
COLEC10	24.19	26.19	2.00	2.2834
RAB13	24.97	26.95	1.98	0.961604
MME	24.82	26.79	1.96	1.36464
PAPPA	27.11	29.07	1.96	1.00374
PSMC6	24.29	26.25	1.96	0.814239
RALA	24.99	26.94	1.95	0.930667
PDCD6IP	27.73	29.68	1.95	0.511703
POSTN	25.26	27.20	1.94	0.590062
EGFR	26.74	28.66	1.91	1.96907
TIMP1	29.50	31.40	1.90	1.78323
ANP32B	24.34	26.19	1.85	0.786356
PSMA5	26.64	28.48	1.84	1.34325
BSG	26.21	28.05	1.84	1.86716
GSTO1	25.73	27.56	1.82	0.483914
ITGA1	25.00	26.81	1.82	0.576688
HMGB2	28.26	30.07	1.81	0.66992
CD59	29.91	31.72	1.81	1.0804
PHLDA1	24.00	25.78	1.78	0.873278
PSMA6	25.45	27.20	1.75	0.810143
COL6A3	34.52	36.27	1.75	1.30193
COL6A2	32.11	33.84	1.73	1.55027
GNAI2	27.88	29.57	1.69	1.00008
FAM129B	25.04	26.71	1.67	0.68106
CD44	29.63	31.30	1.67	2.36033
GNAS	24.21	25.87	1.66	1.21263
CCT8	27.58	29.24	1.66	0.951109
NRP1	26.57	28.22	1.65	0.848592
TFRC	26.54	28.18	1.64	0.293772
PLOD3	25.06	26.65	1.59	0.827253
EIF3I	24.37	25.96	1.59	0.579586
CTNNA1	26.56	28.13	1.57	0.717302
BZW1	24.17	25.73	1.56	0.465704
THBS1	32.97	34.52	1.55	1.26771
SLC16A3	25.24	26.73	1.48	1.17785
FARP1	23.96	25.44	1.48	0.592974
GDF15	24.27	25.73	1.45	0.950164
PSMD3	24.93	26.35	1.42	1.35659
CCT3	26.12	27.53	1.41	0.459598
EPRS	25.71	27.09	1.39	0.440838
DYNC1H1	28.02	29.40	1.37	0.569275
FASN	25.78	27.15	1.37	0.469999
PSMD11	25.22	26.59	1.37	0.589214
RAB5C	25.41	26.77	1.36	0.844313
HINT1	24.58	25.93	1.35	0.474625
ACTR1B	24.15	25.49	1.34	0.48229

APOB	25.07	26.41	1.34	0.575553
COL6A1	33.31	34.63	1.33	1.28906
SRSF1	24.48	25.80	1.32	0.462412
PSMD2	25.44	26.75	1.32	0.49747
LRP1	29.51	30.83	1.32	0.93725
DNAJA1	24.34	25.65	1.31	0.915416
ILK	24.52	25.82	1.31	0.850565
ARF1;ARF3	25.28	26.57	1.30	0.912451
PSMA7	26.08	27.37	1.29	0.887924
RPS9	25.65	26.94	1.29	0.424107
CST3	26.10	27.38	1.28	0.524208
PPP2CA;PPP2CB	23.78	25.05	1.28	1.4527
DCTN2	24.50	25.76	1.26	0.509573
TUBB4B;TUBB4A	25.16	26.41	1.24	0.376553
HTRA1	28.27	29.49	1.22	0.681053
PTMA	26.76	27.98	1.22	0.211827
CTNND1	24.93	26.15	1.22	0.522061
NPTN	25.53	26.74	1.22	1.09229
CCT4	27.63	28.84	1.21	0.650055
PSMA2	26.58	27.77	1.20	0.418715
HLA-A	28.13	29.32	1.19	2.40925
CDH13	27.75	28.93	1.18	1.32598
AHCY	28.43	29.59	1.16	0.789628
LGALS3BP	31.04	32.21	1.16	0.429142
WNT5B	25.21	26.36	1.15	0.480317
IGF2R	26.76	27.91	1.15	0.668061
TNFRSF10D	24.43	25.57	1.14	0.633442
COL4A2	25.67	26.80	1.13	0.398245
SOD1	26.86	27.99	1.13	0.361085
HSPH1	25.27	26.39	1.12	0.428672
SLC3A2	29.01	30.12	1.11	0.669216
TUBA4A	27.24	28.33	1.09	0.894038
EIF3C;EIF3CL	24.92	25.98	1.06	0.577071
ST13;ST13P4;ST13P5	25.90	26.95	1.05	0.316926
CTTN	24.53	25.57	1.05	0.347846
S100A16	26.78	27.83	1.05	0.801921
PPP1R12A	25.39	26.44	1.04	0.266924
PLEK	27.76	28.77	1.02	0.640661
PLOD1	27.20	28.21	1.01	0.693833
RAC1;RAC3	28.34	29.34	1.00	0.612795
PXDN	31.12	32.10	0.98	1.00496
PSMC3	25.78	26.73	0.96	0.531628
EHD1	27.11	28.07	0.95	0.439226
CORO1C	25.07	26.00	0.93	0.212913
RFTN1	25.47	26.40	0.93	0.383035
TCP1	27.64	28.55	0.91	0.615714

SSC5D	25.78	26.68	0.90	0.284664
TOP1	25.94	26.83	0.89	0.183879
THBS2	24.21	25.10	0.89	1.4964
SLC1A5	27.80	28.69	0.89	0.543108
GREM1	28.40	29.27	0.87	0.749457
WARS	24.54	25.41	0.87	0.264027
SUB1	25.37	26.24	0.86	0.246806
MAPRE2	26.14	27.00	0.86	0.638382
LAMA2	25.94	26.79	0.85	0.224028
ABCA1	24.50	25.35	0.84	0.625254
SARS	25.48	26.32	0.84	0.388223
HGFAC	27.01	27.85	0.84	0.291945
EEF1D	25.36	26.19	0.83	0.204186
TNFRSF11B	25.13	25.95	0.82	0.502863
CCT2	27.88	28.70	0.82	0.632221
CDC42	27.52	28.33	0.81	0.970418
CCT5	27.88	28.69	0.81	0.659863
RP2	25.72	26.52	0.80	0.314374
PSMC4	24.46	25.25	0.79	0.509526
HSPA4	25.20	25.98	0.79	0.773002
SET	27.11	27.88	0.76	0.16743
RAP1B	28.85	29.61	0.76	0.311871
CSPG4	25.89	26.65	0.76	1.41211
HMGB1;HMGB1P1	30.04	30.79	0.75	0.645217
CACNA2D1	26.65	27.40	0.75	1.15293
EPB41L3	25.79	26.54	0.75	0.250794
LTBP1	27.68	28.43	0.75	1.85941
CCT7	26.90	27.64	0.74	0.511763
HEXB	25.38	26.11	0.73	0.209121
ARPC1B	25.52	26.25	0.73	0.237469
ACLY	26.95	27.67	0.73	0.568308
CCT6A	27.49	28.22	0.73	0.876551
ATP2B1	26.49	27.21	0.72	0.219917
PSMD13	25.13	25.83	0.70	0.369156
BMP1	25.91	26.60	0.69	0.501979
TGFBI	31.14	31.82	0.68	0.439882
PSMD12	25.57	26.24	0.67	0.495602
SDF4	25.20	25.87	0.67	0.214607
RAB7A	27.63	28.30	0.67	0.36919
STIP1	26.33	26.99	0.67	0.379733
CD99	25.91	26.58	0.67	0.204738
GDI2	28.82	29.48	0.66	0.580201
C1QTNF3	28.91	29.57	0.65	0.217595
ANXA11	24.72	25.37	0.65	0.295833
CAND1	26.43	27.05	0.63	0.248474
ATIC	26.86	27.49	0.63	0.60159

RPS27	24.97	25.58	0.61	0.212732
AKR1B1	25.55	26.16	0.61	0.315674
PAFAH1B1	26.38	26.98	0.60	0.233236
RPLP2	28.10	28.70	0.60	0.67797
SPON2	27.94	28.52	0.58	0.351167
RPS5	25.48	26.03	0.56	0.161835
HABP2	26.12	26.66	0.54	0.683673
CAPZA1	25.95	26.48	0.53	0.314111
RPL22	25.30	25.83	0.53	0.133922
RAB11B;RAB11A	27.52	28.05	0.53	1.2255
BASP1	30.26	30.79	0.52	0.229193
ALDOA	30.35	30.87	0.52	0.440168
RPL14	26.21	26.72	0.52	0.132009
RPSA	25.48	25.99	0.51	0.176139
YWHAG	29.24	29.75	0.51	0.435627
CA2	24.80	25.31	0.51	0.367952
DBN1	24.46	24.96	0.51	0.129592
HSPA8	31.61	32.12	0.51	0.417437
RPL8	26.75	27.25	0.50	0.11295
CTSB	29.19	29.68	0.49	0.282859
FKBP1A	26.67	27.15	0.48	1.74158
YWHAZ	30.01	30.48	0.47	0.543776
ARPC3	25.89	26.36	0.47	0.186757
EIF3A	26.26	26.72	0.46	0.128273
TPM3	25.43	25.89	0.46	0.124284
ARHGDIA	28.07	28.53	0.46	0.318973
RPL29	25.90	26.35	0.45	0.105135
PGK1	29.94	30.39	0.45	0.632015
AP2B1;AP1B1	25.84	26.28	0.44	0.227905
RPLP1	25.82	26.25	0.43	0.208585
SRSF3	25.49	25.91	0.42	0.163422
STRAP	24.51	24.93	0.42	0.174418
COPB2	25.08	25.50	0.42	0.135874
FN1	34.95	35.36	0.42	0.336002
IARS	25.10	25.51	0.41	0.184804
CLIC1	28.97	29.38	0.41	0.576218
MYO1C	26.03	26.43	0.40	0.0820101
RHOA	27.17	27.57	0.40	0.270317
ANXA1	30.46	30.86	0.40	0.271405
RPLP0P6;RPLP0	28.14	28.53	0.40	0.130873
RPS16	26.41	26.80	0.39	0.152499
TPT1	26.89	27.28	0.39	0.356123
YWHAH	25.82	26.20	0.38	0.138328
OTUB1	24.81	25.17	0.36	0.542483
RAB1A	28.36	28.72	0.36	0.265624
GPI	27.30	27.65	0.35	0.394229

GDI1	23.93	24.27	0.34	0.472831
UCHL1	27.97	28.30	0.32	0.194818
MSN	31.54	31.85	0.31	0.384454
NAP1L1	27.02	27.33	0.31	0.172464
ATP2B4	26.56	26.87	0.31	0.183344
PKM	30.88	31.18	0.30	0.239856
ECE1	25.44	25.74	0.30	0.115338
ACTR2	26.81	27.11	0.30	0.158494
YWHAB	28.19	28.48	0.29	0.288171
TNC	30.26	30.55	0.29	0.245831
S100A11	29.64	29.93	0.29	0.256068
LDHA	28.60	28.88	0.28	0.134582
PRPS1;PRPS1L1	24.31	24.58	0.26	0.147803
LGALS1	30.17	30.42	0.24	0.227005
LAMA4	30.18	30.42	0.24	0.0795321
NPTX1	28.97	29.21	0.24	0.0909086
CAP1	28.85	29.09	0.24	0.106257
RPL5	29.00	29.23	0.23	0.0772643
PABPC1;PABPC3	26.85	27.08	0.23	0.136421
ANXA6	29.97	30.21	0.23	0.131209
RPL10	26.97	27.19	0.23	0.0595955
WDR1	28.84	29.07	0.22	0.224048
RPL19	26.04	26.25	0.21	0.0693246
LRRC17	28.71	28.92	0.20	0.0704307
DCD	29.90	30.10	0.20	0.0934322
TLN1	30.78	30.98	0.20	0.207952
TWF2	24.25	24.45	0.20	0.0783927
GAPDH	31.73	31.93	0.20	0.121278
CDH6	26.18	26.36	0.18	0.300873
YWHAE	30.34	30.50	0.16	0.0946144
ACTR3	26.46	26.62	0.16	0.0816506
NME2;NME2P1	26.13	26.29	0.16	0.0601313
ADK	26.07	26.23	0.16	0.0847547
RPS4X	28.07	28.22	0.15	0.100176
RPS23	27.18	27.32	0.14	0.0562509
ACTR1A	25.94	26.08	0.14	0.106344
TPI1	29.96	30.09	0.13	0.140454
SH3BGRL3	28.40	28.53	0.13	0.114869
F10	28.93	29.06	0.12	0.0862334
ECM1	29.23	29.35	0.12	0.0680848
RPS11	27.11	27.23	0.12	0.0671045
HSP90AB1	31.44	31.55	0.11	0.0519229
GNB2L1	27.06	27.17	0.11	0.0228686
STOM	26.38	26.49	0.11	0.0279364
ERP29	26.07	26.17	0.10	0.03449
NPC2	25.59	25.67	0.08	0.0207312

TUBB3	26.60	26.66	0.06	0.0375343
EIF4A1	26.73	26.79	0.06	0.0210235
ANXA2;ANXA2P2	32.76	32.82	0.06	0.0333452
EEF2	29.91	29.96	0.05	0.0307063
HSP90AA1	30.73	30.76	0.04	0.020694
TFPI	26.44	26.47	0.04	0.0290542
RPS6	28.97	28.99	0.02	0.00851102
PARK7	27.41	27.43	0.02	0.0121102
THY1	28.66	28.67	0.02	0.00990806
RPS21	26.32	26.33	0.01	0.00291367
ENO1	30.85	30.85	0.00	0.000354674
CCDC66	26.87	26.87	0.00	0.00428466
NCL	28.94	28.93	-0.01	0.00368642
IGFBP2	29.40	29.37	-0.02	0.0112548
HSPE1	27.95	27.93	-0.02	0.00556022
RSU1	26.91	26.87	-0.05	0.0772534
RPS20	26.52	26.47	-0.05	0.0177527
EEF1G	27.33	27.28	-0.05	0.0237647
RPS28	26.28	26.22	-0.05	0.0139397
RPL7A	27.38	27.33	-0.06	0.0176945
RPL24	25.54	25.49	-0.06	0.0172507
TUBA1B	31.32	31.27	-0.06	0.0440691
CLSTN1	26.74	26.68	-0.06	0.0530084
RPS15	24.62	24.55	-0.07	0.0179801
RPS15A	24.47	24.40	-0.08	0.0213376
RARS	24.61	24.53	-0.08	0.0485728
RPL26;RPL26L1	27.99	27.91	-0.08	0.0256395
S100A6	28.06	27.97	-0.09	0.0174966
IGF2	27.70	27.61	-0.09	0.0599356
NCAM1	25.37	25.28	-0.09	0.0586614
RPL17	27.84	27.74	-0.10	0.0262326
RPS8	29.20	29.09	-0.11	0.0450309
PRDX1	30.13	30.00	-0.13	0.0893899
NACA	25.40	25.27	-0.13	0.0405686
CALM3	28.93	28.81	-0.13	0.0531057
MARCKS	29.21	29.08	-0.13	0.0640214
HSPB1	28.00	27.85	-0.14	0.107225
GSTP1	27.84	27.69	-0.15	0.0691929
PFN1	30.34	30.19	-0.15	0.105744
S100A10	28.09	27.93	-0.16	0.109671
CFL1	31.01	30.85	-0.16	0.170014
LDHB	29.09	28.92	-0.17	0.19321
VIM	32.33	32.16	-0.17	0.0586126
CSRP1	27.43	27.25	-0.17	0.109845
VCP	29.64	29.47	-0.17	0.0785448
SEPT7	25.87	25.69	-0.18	0.0505022

COL5A1	29.43	29.24	-0.18	0.187057
PFKP	26.89	26.70	-0.19	0.180536
MYDGF	26.40	26.21	-0.19	0.0515471
PHGDH	27.86	27.67	-0.20	0.225723
EEF1A1;EEF1A1P5	32.01	31.80	-0.21	0.302323
LOXL2	29.27	29.06	-0.21	0.395992
RPS3	26.64	26.43	-0.21	0.0989594
TXN	30.02	29.80	-0.22	0.227291
VCL	29.96	29.74	-0.22	0.395569
GSN	26.12	25.89	-0.23	0.374697
RPL27	26.27	26.03	-0.24	0.0556283
LAMB1	32.06	31.82	-0.24	0.103977
FABP5	28.51	28.26	-0.25	0.106413
RBP4	28.56	28.31	-0.25	0.0984198
CNTN1	24.93	24.66	-0.27	0.2489
G6PD	25.76	25.48	-0.28	0.335083
CLTC	29.91	29.63	-0.28	0.222965
PSAP	28.82	28.53	-0.29	0.132761
TKT	28.05	27.75	-0.30	0.139845
RPL23A	25.97	25.67	-0.30	0.0818649
ACTN4	30.96	30.65	-0.31	0.238159
RPS17	25.46	25.14	-0.32	0.296155
NPM1	29.01	28.68	-0.32	0.159817
FBN1	28.63	28.30	-0.33	0.619871
BGN	28.93	28.59	-0.34	0.69703
RPL13	27.44	27.09	-0.35	0.165452
VPS35	25.28	24.93	-0.35	1.14024
COL12A1	34.19	33.84	-0.35	0.267216
PPP2R1A	26.69	26.34	-0.35	0.478132
EIF5A;EIF5AL1;EIF5A2	28.20	27.84	-0.36	0.534278
RPL15	27.79	27.43	-0.36	0.165221
HSPA1B;HSPA1A	28.25	27.89	-0.36	0.152895
APP	26.35	25.98	-0.37	0.321732
UBA1	26.51	26.11	-0.40	0.25028
PLEC	27.87	27.46	-0.41	0.104266
PTK7	25.46	25.04	-0.42	0.143122
RPS3A	28.30	27.88	-0.42	0.223698
NID1	33.55	33.13	-0.42	0.149754
TUFM	25.67	25.25	-0.42	0.133356
PDAP1	25.59	25.16	-0.42	0.182493
SEPT9	26.67	26.24	-0.42	0.258776
PGAM1	27.65	27.22	-0.43	0.541
HPX	27.12	26.69	-0.43	0.330433
LAMC1	32.53	32.09	-0.43	0.241862
MAMDC2	26.11	25.67	-0.44	0.205415
SFRP1	27.39	26.95	-0.44	0.178272

RPS2	28.73	28.28	-0.45	0.287787
VAT1	28.81	28.35	-0.46	0.416918
RPL10A	27.52	27.04	-0.49	0.304784
ARPC2	25.52	25.03	-0.49	0.145361
TUBB	31.76	31.27	-0.49	0.319678
COTL1	28.98	28.49	-0.49	0.550463
DSTN	27.01	26.52	-0.49	0.74662
BANF1	28.59	28.09	-0.51	0.230091
TXNDC17	26.78	26.27	-0.51	0.98271
SDC4	28.17	27.67	-0.51	0.337291
ACTB	33.90	33.39	-0.51	0.809917
YWHAQ	28.47	27.95	-0.52	0.313292
FKBP7	24.16	23.64	-0.52	0.186681
RPL12	26.48	25.96	-0.52	0.189623
GPC1	27.97	27.45	-0.52	0.893542
RRBP1	25.92	25.40	-0.52	0.116676
H2AFY	26.82	26.30	-0.53	0.0941237
TAGLN2	26.70	26.17	-0.53	0.334707
ALCAM	28.91	28.38	-0.53	0.550014
RPS14	27.52	26.98	-0.54	0.296766
RPS18	27.19	26.64	-0.55	0.240855
YBX1;YBX3	26.80	26.24	-0.56	0.272284
MDH1	26.75	26.19	-0.56	0.522118
CLIC4	29.17	28.60	-0.57	0.867111
RPL11	27.80	27.21	-0.59	0.469115
RPL31	25.19	24.60	-0.60	0.149902
RPS27A;UBA52;UBB;UBC	29.52	28.92	-0.60	0.236872
DNAH17	28.00	27.39	-0.61	0.595612
EDIL3	31.02	30.41	-0.61	0.298768
ACTN1	29.70	29.08	-0.62	0.665388
RPL36AL;RPL36A	26.55	25.93	-0.63	0.387084
ACTC1;ACTA1	30.52	29.89	-0.63	0.309281
SEPT2	27.10	26.47	-0.63	0.317794
LAMP1	27.28	26.65	-0.64	0.162332
AGRN	30.30	29.67	-0.64	0.274315
RPL6	29.39	28.75	-0.64	0.382132
FSCN1	26.86	26.23	-0.64	0.461361
KIF5B	27.30	26.66	-0.64	1.4221
RPS25	26.38	25.72	-0.65	0.173257
NUCB1	28.38	27.72	-0.66	0.898929
B2M	32.09	31.42	-0.67	0.766374
HNRNPC	26.95	26.27	-0.68	0.18452
PEBP1	28.80	28.11	-0.69	2.03048
FABP1	28.86	28.16	-0.70	0.620114
MMP2	31.27	30.56	-0.71	1.65032
PDIA4	28.66	27.93	-0.73	0.209006

LASP1	28.22	27.48	-0.74	0.506788
ANXA5	32.22	31.46	-0.76	0.751591
RPS12	27.52	26.77	-0.76	0.396355
VNN2	26.72	25.96	-0.76	0.595204
DBI	26.92	26.16	-0.77	0.447709
TMSB4X	31.15	30.38	-0.77	1.10001
THBS4	27.51	26.74	-0.77	0.27164
RPL18	27.28	26.50	-0.78	0.263544
IGFBP5	33.13	32.35	-0.78	0.727898
BCAP31	25.34	24.55	-0.79	0.525449
RCN1	28.81	28.02	-0.79	0.410211
RPL27A	26.85	26.05	-0.80	0.288423
DSG1	27.45	26.64	-0.81	0.157441
RPL4	28.72	27.91	-0.81	0.28423
PCOLCE	29.70	28.86	-0.83	0.619049
CALML5	27.38	26.55	-0.83	0.111215
AHNAK	30.21	29.38	-0.84	0.484195
HSPD1	29.44	28.60	-0.84	0.255136
RPL3	28.50	27.66	-0.84	0.286434
DSC1	26.51	25.66	-0.85	0.124729
PSMB3	24.29	23.43	-0.85	0.721641
IQGAP1	25.99	25.14	-0.85	0.269007
MDH2	27.77	26.91	-0.85	0.194684
CSTA	26.25	25.40	-0.85	0.172933
RPS19	25.61	24.74	-0.87	0.199427
RPS7	26.36	25.48	-0.88	0.431883
VDAC1	26.06	25.18	-0.88	0.79143
FLNA	31.08	30.20	-0.88	0.861366
TXNDC5	27.21	26.32	-0.89	0.260203
FLNC	29.14	28.23	-0.90	0.75825
SEC13	24.33	23.43	-0.91	0.592841
IGFBP4	29.73	28.82	-0.91	0.56565
COL5A2	27.77	26.85	-0.92	2.42653
COL11A1	29.40	28.48	-0.92	1.17939
IGFBP7	29.08	28.14	-0.93	0.638886
SERPINE1	27.41	26.46	-0.94	0.513643
MVP	30.19	29.23	-0.96	0.690925
SPARC	31.89	30.93	-0.96	0.707015
RPL7	27.55	26.55	-1.00	0.313476
PA2G4	24.04	23.02	-1.01	0.298036
TIMP2	29.58	28.57	-1.01	1.88152
VCAN	32.60	31.56	-1.04	0.323094
PAICS	26.21	25.16	-1.05	0.569732
PRKCSH	28.36	27.31	-1.05	0.66318
FST	26.82	25.76	-1.06	0.875112
SH3BGRL	24.66	23.61	-1.06	1.05193

P4HB	31.08	30.02	-1.06	0.431898
FLNB	25.72	24.65	-1.07	0.284411
MRC2	26.68	25.61	-1.07	0.494651
HIST1H2BC;HIST1H2BM;HIST1H2BN;HIST1H2BH;HIST2H2BF;HIST1H2BD	31.78	30.68	-1.10	0.328476
PDIA3	30.81	29.71	-1.10	0.39672
SUMO2	26.32	25.22	-1.10	1.7321
GARS	26.61	25.47	-1.14	0.326518
APOM	27.38	26.24	-1.14	0.366223
PTMS	27.58	26.42	-1.15	0.513706
NCAPG	27.72	26.56	-1.16	1.08891
CALD1	28.26	27.09	-1.17	0.592184
KPNB1	25.88	24.71	-1.17	0.620067
MYH9	33.19	32.00	-1.20	0.619931
GANAB	25.94	24.74	-1.20	0.320315
MFGE8	33.28	32.04	-1.25	0.787162
HSPA5	31.00	29.75	-1.25	0.53124
CALU	30.64	29.38	-1.27	0.919994
CAT	25.92	24.64	-1.28	0.521895
AHCTF1	31.79	30.50	-1.30	0.732242
PLS3	27.11	25.81	-1.30	1.0909
QSOX1	27.96	26.65	-1.32	0.851985
SPTAN1	27.65	26.32	-1.33	0.665678
SERPINF1	27.45	26.11	-1.34	1.15211
HSP90B1	30.52	29.16	-1.36	0.515026
CALR	31.24	29.86	-1.38	0.756862
PRDX2	27.12	25.72	-1.40	0.611713
NID2	30.96	29.55	-1.41	1.40788
MAP4	25.31	23.89	-1.42	0.39227
LAMA5	27.41	25.98	-1.43	0.595859
MYL6	29.86	28.40	-1.46	0.799571
EZR	26.93	25.44	-1.49	0.730255
NUCB2	25.16	23.61	-1.55	1.37034
PPIB	29.66	28.11	-1.55	0.816317
HNRNPD	25.66	24.08	-1.58	0.514541
HIST1H4A	30.37	28.77	-1.59	0.490569
GLUD1;GLUD2	26.65	25.05	-1.60	0.77539
HSPG2	28.40	26.77	-1.63	0.88396
MYL12A;MYL12B	27.38	25.75	-1.64	1.15024
HNRNPA3	25.70	24.05	-1.65	0.50447
ATP5B	28.42	26.77	-1.66	0.582229
HIST3H2A;HIST1H2AD;HIST1H2AB	31.76	30.07	-1.69	0.673113
CAV1	26.47	24.74	-1.73	0.898265
HNRNPA1;HNRNPA1L2	27.26	25.53	-1.73	0.631412
CLU	30.76	29.02	-1.74	1.65262
XRCC6	26.79	25.01	-1.78	0.844014

ATP5A1	27.72	25.93	-1.79	0.551468
MYOF	27.45	25.63	-1.82	0.817158
PDIA6	27.01	25.16	-1.84	0.621581
TPM4	32.05	30.19	-1.85	1.48177
MDK	26.49	24.63	-1.86	1.24158
RPN1	26.69	24.82	-1.86	0.789321
LRRC59	25.84	23.98	-1.87	0.868473
DSP	33.47	31.60	-1.87	1.27375
PTX3	28.74	26.86	-1.88	0.321278
HIST2H3A	29.64	27.75	-1.89	0.628059
HNRNPU	26.68	24.75	-1.92	0.621967
HNRNPA2B1	28.41	26.49	-1.92	0.660663
LAMA1	30.30	28.38	-1.93	0.775132
SERPINH1	29.45	27.50	-1.95	1.13188
COL1A1	34.69	32.74	-1.95	2.07079
GAS6	27.50	25.54	-1.96	0.956109
HYOU1	25.51	23.54	-1.97	0.585456
STMN1	27.52	25.48	-2.04	0.901188
FSTL1	30.83	28.76	-2.07	2.15666
COL3A1	31.03	28.91	-2.12	2.04479
LMNA	28.96	26.84	-2.13	1.09973
COL1A2	33.65	31.46	-2.19	2.63217
CANX	28.69	26.43	-2.26	1.0445
JUP	26.54	24.22	-2.32	0.357823
LUM	26.34	23.91	-2.43	1.17689
HIST1H1B	30.14	27.69	-2.45	0.824482
HP1BP3	25.66	23.03	-2.63	0.801125
CCBE1	26.69	24.04	-2.65	2.7338
CKAP4	29.38	26.71	-2.67	0.804589
MYH10	26.28	23.53	-2.75	0.623494
C2orf16	29.03	26.27	-2.76	0.795121
TAGLN	26.93	24.15	-2.78	1.73403
C1R	29.79	26.95	-2.85	1.78667
H2AFV;H2AFZ	26.31	23.46	-2.85	1.44313
RELN	27.66	24.28	-3.37	1.3837
C1S	29.62	26.20	-3.42	2.3826
HIST1H1C	31.45	28.03	-3.42	1.23882
ESYT1	28.27	24.24	-4.03	3.53476
TPM1	27.71	23.66	-4.05	1.20751
FBLN1	28.85	24.22	-4.63	1.42214
SVEP1	29.50	24.26	-5.23	3.19075
DCN	31.85	23.59	-8.27	4.08279

8.2 Mass Spectrometry 2: Proteomic assessment of Conditioned Media and EVs isolated by SEC from OIS IMR90s

This data forms the basis of section 4.7 and is referred to throughout as MS2. Conditioned media (CM) and SEC fractions 8 (F8) and 20 (F20) were collected in triplicate from OIS IMR90s. These were analysed by mass spectrometry through collaboration with the CECAD proteomic facility (University of Cologne). Gene lists detailing the label-free quantitation intensities (LFQ) for each sample were produced and analysed according to section 2.13.2. Mean LFQ intensity values (Mean LFQ) from CM (blue), F20 (orange) and F8 (yellow) replicates are detailed. Localisation data designating each gene as intracellular (IC), membrane (M) or secreted (S) was determined via Protein Atlas (www.proteinatlas.org) with genes able to receive multiple designations.

Gene names	Localisation	OIS CM Mean LFQ (Log2)	OIS F20 Mean LFQ (Log2)	OIS F8 Mean LFQ (Log2)
AAMDC	IC			24.98371
ABCA1	IC/M			29.68345
ABCB1	IC/M			25.95742
ABCC1	M			29.13849
ABCC4	M			30.46293
ABI1	IC			30.12145
ABI2	IC			26.66569
ABLIM3	IC			25.08053
ABRACL	IC	25.4159		25.28334
ACAT2	IC	26.48094		27.13531
ACE	IC/M/S			27.38164
ACO1	IC	26.53025		29.09845
ACSL4	IC/M			30.85085
ACVR1	IC/M/S			28.48284
ADAM10	M/S		26.97185	32.19276
ADAM17	M/S			29.22058
ADAM19	M	26.90319		
ADAM9	M/S	27.90273	29.07207	
ADCY9	IC/M			25.57121
ADGRL2;LPHN2	M			26.31223
ADH5	IC			29.32701
ADSS	IC			28.22857
AGRN	IC/M/S	27.9858	28.53762	30.96894

AHCYL1;AHCYL2	IC			26.969
AHSA1	IC			25.69364
AIDA	IC			29.13232
AK1	IC			29.14786
AKAP12	IC		25.9627	31.61564
AKR1B1	IC	29.26335	28.62211	31.46519
AKR7A2	IC			26.24693
AKT1	IC			27.33822
AKT2	IC			25.59523
AKT3	IC			25.54323
ALCAM	M		27.83661	31.61411
AMPD3	IC			25.80188
ANGPTL3	S	27.08665		
ANGPTL4	IC/S	27.83144		27.25433
ANO6	M			29.60783
ANPEP	M	24.66107	26.83289	33.60273
ANTXR1	IC/M/S	27.02419		
ANTXR2	M			30.11047
ANXA11	IC		25.948	32.23455
ANXA3	IC			26.85678
ANXA4	IC		26.9667	31.68801
ANXA6	IC	27.77959	32.0543	35.55463
ANXA7	IC			29.89894
AOC3;AOC2	IC/S		24.82403	
AP3M1;AP3M2	IC			24.12766
APOB	S	26.47176		
APOM	IC/S	29.55682	28.30869	28.67931
APP	IC/M	26.3001		
APPL1	IC			25.77723
APPL2	IC			25.94381
ARAF	IC			27.03641
ARCN1	IC/S			26.36757
AREG	M		27.94792	26.58249
ARF6	IC			25.35626
ARHGAP1	IC/M			26.34283
ARHGAP17	IC			24.71077
ARHGAP18	IC			26.78504
ARHGEF7	IC			26.29087
ARL3	IC			28.1471
ARMT1	IC			25.87171
ARPC1B	IC	28.17091		29.08967
ARPC1B	IC	26.79546	25.70912	30.78283
ARPC5	IC			29.14601
ARPC5L	IC			27.55116
ARRB1	IC			25.02663
ARVCF	IC			27.14921

ASPH	IC/M			26.47689
ASS1	IC			25.03871
ATOX1	IC			28.73419
ATP10D	M			24.19031
ATP13A3	M			25.47157
ATP1B1	IC/M			31.61045
ATP1B3	IC/M			31.12847
ATP2B1	M			31.25346
ATP2B3	M			27.16579
ATP2B4	IC/M		26.91019	33.17017
ATP6AP2	IC/M/S	27.61471		
ATP6V0D1	IC			27.50479
ATP6V1C1	IC			26.4347
ATP6V1D	IC			25.71886
ATP6V1E1	IC			26.16209
ATP6V1G1	IC			28.94606
ATP6V1H	IC			25.24715
ATP7A	M			27.24007
ATRN	M			26.68793
AXL	M	26.14645		
B2M	M/S	32.31861	32.08738	32.72649
B3GAT3;B3GAT2	IC/S	26.50131		
B4GAT1	S	27.39915		28.60696
BAG3	IC/M			26.40843
BAIAP2	IC			27.50806
BAX	IC			27.61296
BCR;BCR/ABL fusion	IC			25.98291
BDKRB2	M			29.16384
BGN	S	26.82017	25.97856	25.41406
BHMT	IC			
BICD2	IC			24.50211
BLVRA	IC			25.68802
BMP1	S	26.94628	27.91903	
BMP2	S	27.29726	27.68412	27.15996
BPGM	IC			29.54921
BPNT1	IC			26.69035
BRCC3	IC			24.49995
BRK1	IC			29.78575
BTN2A1	IC/M			31.14343
BZW1	IC			25.88027
C12orf10	IC/S			26.30164
C12orf57	IC			26.579
C12orf75;OCC1	IC			28.03858
C1QTNF3-AMACR;C1QTNF3	S	26.04894	29.65673	
C1S	IC/S	27.7316	27.42667	
C3	IC/S	27.4315		

C8B	IC/S	26.36645		
CA2	IC	28.85286		
CAB39	IC	27.85318		27.90122
CACNA2D1	IC/M/S		27.82248	32.12043
CADM1	IC/M			30.22755
CALML5	IC			25.05173
CAMK2D	IC/M/S			26.7242
CAPG	IC			26.87971
CAPN1	IC			28.18003
CAPN5	IC			29.71995
CAPNS1	IC	28.01178	27.45631	29.45722
CARS	IC	26.78809		
CASK	IC/M			29.41138
CASP3	IC			26.14507
CASP7	IC			24.45428
CAST	IC			28.13098
CAT	IC	25.85399		
CAV1	M			27.8812
CAV1	M			29.67712
CCDC22	IC			23.41023
CCDC50	IC			28.46891
CCDC6	IC			25.80933
CCM2	IC			27.58504
CCNYL1	IC			24.53658
CCS	IC			25.64502
CD109	M			26.30211
CD151	M			32.04515
CD248	M	26.57525		
CD276	M/S			30.92165
CD4	IC/M/S			25.8651
CD46	M			28.17717
CD46	M			26.84842
CD47	IC/M			28.91376
CD63	M			26.86543
CD81	M		31.23326	31.32081
CD82	IC/M			28.26552
CD9	M		30.90094	34.0278
CD93	M	25.48963		
CD97	IC/M/S			30.23927
CD99	M/S		27.02464	30.67723
CDC42SE1	IC			27.39194
CDCP1	M/S			32.29887
CDH11	IC/M/S		25.79525	30.59884
CDH13	IC/S	27.82877	26.9097	32.55167
CDH2	IC/M			30.37734
CDH6	M	24.18246	26.34989	29.43752

CDK4	IC			27.14127
CDKN1A	IC			24.4423
CDV3	IC			27.09979
CFD	S	29.24857		
CFHR5	S	27.69297		
CHMP1A	IC			28.27383
CHMP1B	IC			28.47134
CHMP2A	IC			26.77649
CHMP2B	IC			25.517
CHMP3	IC			27.12865
CHMP4A	IC			27.40682
CHMP4B	IC			30.12222
CHMP5	IC			30.144
CHMP6	IC			27.07033
CHORDC1	IC			25.0647
CHRM2	M			26.67278
CHST3	M	25.78254		
CLDND1	IC/M/S			25.95879
CLEC11A	S	29.52895	29.00702	
CLIC1	IC	29.66686	29.38579	33.06066
CLIC4	IC	29.57108	29.56432	32.71655
CLIP1	IC			24.55666
CLIP2	IC			26.90825
CLMP	M			27.93701
CLSTN1	M	30.7713	29.12313	
CLTB	IC	25.72156		28.73788
CLU	IC/S	28.04072	28.73055	27.63376
CMPK1	S			29.15157
CNDP2	IC			28.17757
CNNM4;CNNM3	M			24.39897
CNPY2	IC/S			24.70247
CNTN1	S	23.99595		
COL11A1	IC/S	27.33434	29.74854	
COL12A1	IC/S	30.65987	30.13416	30.21902
COL18A1	IC/S	25.66949		
COL1A1	IC/S	32.15053	32.41099	31.33486
COL1A2	S	30.91824	31.24826	30.00484
COL2A1	S	25.5726		
COL3A1	IC/S	27.23291	27.37475	25.16726
COL4A1	IC/S	27.35603	27.86335	27.80506
COL4A2	IC/S	27.19336		27.0645
COL5A1	IC/S	28.83933	30.584	26.08256
COL6A1	S	34.07177	34.56767	36.72612
COL6A2	IC/S	31.98974	33.15217	36.21564
COL6A3	IC/S			28.05809
COL6A3	IC/S	34.28388	35.57797	38.27821

COLEC10	S	27.7668		
COMT	IC/M			26.68445
COPS3	IC			25.50543
COPS4	IC			26.2468
COPS5	IC			25.55175
COPZ1	IC			26.36827
CORO2B	IC			26.65162
COTL1	IC	29.32716	28.88078	30.57866
CPNE3	IC			30.27408
CRIP2	IC	29.27649		
CRYZ	IC			26.81033
CSDE1	IC			26.1773
CSF2	S	27.41924		
CSNK1E	IC			25.76321
CSPG4	M	25.07481	26.58626	31.97827
CST1	S	30.76601	28.96765	27.69106
CST3	S	30.87573	32.36263	28.28488
CST4	S	30.79638	31.53749	28.79743
CTGF	S		27.61956	27.06057
CTHRC1	IC/S	26.39175		
CTNNA2	IC			25.66694
CTSA	IC/S	28.98934		
CTSB	S	31.65713	32.75062	30.14217
CTSC	IC/S		27.98556	
CTSD	IC/S	30.6346		27.28583
CTSL	S	26.4262		
CTSV	S		26.80951	
CUL1	IC			26.58388
CUL3	IC			26.93611
CUL5	IC			27.47835
CXCL5	S	27.23754		
CXCL8	S	31.8142	31.91948	27.57283
CYBRD1	M			26.91006
CYFIP1	IC			30.38793
CYFIP2	IC			25.47448
DAB2	IC			24.96796
DAG1	IC/M/S	28.25213		
DAP	IC			29.47527
DBI	IC	28.72885		
DBNL	IC/S			28.22904
DCBLD1	M			27.99954
DCBLD2	IC/M			30.29365
DCC	IC/M			24.69239
DCTN3	IC			26.45367
DCTN4	IC			25.88731
DCUN1D3	IC			28.07937

DDAH1	IC	27.30423		27.39142
DDAH2	IC			28.64048
DDR2	IC/M/S			28.17837
DDX19A;DDX19B	IC			24.77679
DIAPH1	IC			24.77697
DIP2B	IC			30.2913
DIP2C	IC/M			26.62871
DKFZp566H1924;NPTN	IC/M			31.68294
DKFZp686J1372	IC		27.49322	28.75377
DKK3	S	30.00006	28.31207	
DLG5	IC			25.5255
DLGAP4	IC			26.80046
DLL4	M			26.02678
DMBT1	S			26.84736
DMD	IC			26.58968
DNAJB1	IC			25.7483
DNAJC13	M			26.17971
DNAJC5	M			26.61899
DNM2	IC			27.84312
DOCK10	IC	34.13003		
DOCK11	IC			24.30023
DOCK9	IC			24.96935
DOS	M/S			27.33366
DPP3	IC			27.59288
DPP4	IC/M			32.28726
DPYSL2	IC	26.96145		29.25552
DPYSL3	IC	27.46801		27.55248
DTNA;DTNB	IC/M			26.81714
DUSP3	IC			26.29814
DYNC1LI2	IC			26.16198
ECE1	IC/M			30.21763
ECM1	S	31.82385	32.79427	28.90761
EDIL3	S			31.03648
EEA1	IC			28.12463
EFEMP1	IC/S	26.0604		
EFNB1	M			29.03488
EFNB2	M			26.83809
EGFR	IC/M/S		26.03454	33.31243
EHD1	IC	26.32652	24.69603	33.23429
EHD2	IC	25.92414		30.64911
EHD3	IC			28.25187
EHD4	IC			29.62248
EIF2B3	IC			24.95084
EIF5	IC			25.77345
ELFN2	M			27.5582
ELMO2	IC			26.27871

EMILIN1	IC/S	29.66984	27.77475	31.03605
ENG	M		25.97461	32.00021
ENOPH1	IC	26.21552		
ENPP1	M			30.42673
ENPP2	IC/M	28.51252		
ENSA	IC			27.07527
EPB41L1	IC			26.91504
EPB41L1	IC			26.38871
EPB41L2	IC			30.713
EPB41L5	IC			26.53978
EPHA2	M		27.98501	32.92589
EPHA4	IC/M/S			28.01286
EPHB2	M/S			30.9764
ERBB2	IC/M			24.61912
EREG	M			27.04767
ERP44	S			26.65347
ESD	IC			28.90047
ESR1	IC	30.8498	27.2496	31.78582
ETF1	IC			26.77803
ETHE1	IC			27.39024
EVA1A	IC			25.83162
EVA1B	IC			31.68921
EXOC4	IC			26.56224
EXOC5	IC			25.73983
EXOC7	IC			26.10321
EXOC8	IC			27.47053
F10	S	27.06094	28.18829	
F11	IC/S		28.71773	
F2R	M/S			27.74002
F2RL1	M			25.44823
F3	IC/M		29.05341	31.56602
FABP1	IC	27.43231	28.40578	
FABP5	IC		26.08082	30.12982
FAH	IC	25.50598		
FAM114A1	IC			27.76194
FAM126A	IC			26.0311
FAM129B	IC	25.99097		30.59549
FAM171A1	M/S			27.24642
FAM171A2	M			26.09137
FAM171B	M/S			28.5339
FAM49B	IC			29.78369
FAM65A	IC			26.51711
FAP	IC/S			30.30211
FAS	M/S			31.19182
FAT1	IC/M/S		26.36902	33.41288
FAT4	M			28.47469

FBN1	S	28.3583		
FERMT2	IC			29.37856
FGFR1	IC/M/S			24.34287
FGG	IC/S			25.62035
FGL2	S		26.36622	
FH	IC			25.32206
FHL2	IC	28.6511		30.34355
FKBP10	IC/S			26.56547
FLRT3	M			29.59927
FMNL3	IC			29.54856
FMOD	S	28.17123		
FN1	IC/S	35.76691	36.59223	34.29031
FN3KRP	IC			25.52515
FRMD6	IC			26.70631
FST	IC/S		27.39367	
FSTL1	IC/S	30.69041	30.98313	28.16377
FTH1	IC		27.73032	28.87451
FTL	IC			27.46605
FZD6	M			26.94536
G6PD	IC	27.37021	25.97207	31.64911
GABARAP	IC			25.7994
GALK1	IC			28.01353
GALNT2	S			24.48103
GAP43	IC			24.4749
GBE1	IC	27.57513		28.23225
GCLC	IC/M			26.39736
GDF15	IC/M	31.68923	30.19443	31.41039
GFPT1	IC/M			28.53562
GFPT2	IC/M/S			25.9191
GGT1;GGT3P;GGT2	IC/M/S			28.74391
GIT2	IC			26.32463
GJA1	M			30.66711
GLG1	IC/M/S			27.39026
GLIPR1	IC/M/S			27.65705
GLIPR2	IC			30.11239
GLOD4	IC			28.05197
GLRX	IC			28.92269
GLRX3	IC			28.45656
GMFB	IC			27.19947
GMPPA	IC			26.20434
GMPR2	IC			25.71238
GNA12	IC			26.07672
GNA13	IC			30.48645
GNG10	IC			27.85776
GNG11	IC			27.49076
GNG2	IC			30.39266

GNL1	IC			24.38264
GOLGA7	IC			27.40664
GOLIM4	M			26.83744
GOT1	IC			27.85935
GPC1	IC/M/S	26.92725	27.71591	27.74539
GPR68	M			25.64909
GPRIN1	IC			29.59752
GPS1	IC			25.49782
GPSM1	IC			26.21096
GPX1	IC			26.72293
GPX3;GPX6;GPX5	IC/S	28.1914		26.03492
GRB2	IC			26.98962
GREM1	S		28.83923	31.2571
GRHPR	IC			27.21482
GRK5	IC			28.3494
GRN	IC/S		26.4658	26.17801
GSK3A	IC			25.45356
GSK3B	IC			26.50201
GSR	IC			26.69868
GSS	IC			26.57943
GSTA3	IC	25.82863		
HABP2	IC/S		26.19092	
HAGH	IC	27.98749	27.1981	28.23525
hCG_2004507;CSNK1G1	IC/M			28.07493
HEBP1	IC			26.7726
HEBP2	IC	28.03107		27.96101
HERC4	IC/M			25.60331
HEXA	S	25.66427		
HEXB	IC/S	27.12904		
HGF	IC/S	28.51953		
HGFAC	S	29.46615	28.38275	
HGS	IC	27.19999		27.67898
HINT1	IC	29.27498	27.14992	30.67472
HINT3	IC			27.12627
HLA-B	IC/M			28.97657
HLA-B	IC/M			28.61584
HLA-B	IC/M			31.19205
HLA-B	IC/M			28.87998
HLA-C	M/S	27.92785		28.24611
HLA-C	M/S	27.48148		30.023
HN1	IC			26.94596
HPCAL1;HPCA	IC	27.27584		27.26928
HPD	IC			
HSP90AB2P	IC			27.73611
HSPB1	IC	28.80611	27.57506	30.95106
HSPB6	IC			27.55946

HSPG2	IC/S	27.91846	28.57577	
HTRA1	IC/S	28.15631		27.53752
ICAM1	M/S	26.37607	28.24003	34.83569
ICAM5	IC/M			28.18847
IDH1	IC	27.08106		27.89192
IDI1	IC			26.53806
IGF1R	IC/M			25.83639
IGF2	M/S	28.53118	29.47018	
IGF2R	IC/M	28.78364	28.33133	28.24068
IGFALS	IC/M/S	27.59734		
IGFBP2	IC/S	32.40348	29.41945	
IGFBP3	IC/S		27.27775	
IGFBP4	S	32.04973	32.30362	
IGFBP5	S	33.34144	32.44885	30.93588
IGFBP6	S	29.00944	28.49255	
IGFBP7	S	29.87992	31.20537	27.90544
IGSF8	M/S		28.27907	31.6957
IL1B	IC			28.28831
IL1RAP	IC/M/S		26.89943	26.65693
IL6	IC/S	28.80475	28.81594	29.03625
IL6ST	M/S			27.84342
ILK	IC			30.57864
IMPA1	IC			26.6741
IMPAD1	IC/M			25.22971
INHBA	S	31.73799	30.12643	27.19543
INPP5A	IC/S			27.85168
IRGQ	IC			27.2548
ISG15	IC	24.76273		
IST1	IC			29.633
ITCH	IC			27.01664
ITFG3	IC/M			29.72018
ITGA1	M		26.9212	33.60386
ITGA11	M			29.91783
ITGA2	M		28.09908	30.9677
ITGA2	M	28.438	31.33204	36.067
ITGA3	IC/M		27.24644	33.6525
ITGA4	M/S			29.6861
ITGA5	M		27.72002	32.4898
ITGA6	IC/M			32.19271
ITGA7	IC/M			27.39176
ITGAV	IC/M	23.42509	26.80322	33.61011
ITGB1BP1	IC			25.6733
ITGB3	M/S			32.75568
ITGB5	IC/M		26.51773	32.67752
ITGB8	M			28.02858
ITPA	IC			25.47015

JAG1	IC/M			26.97356
JAM3	IC/M			27.66632
KIDINS220	IC/M			26.89654
KIRREL	M			29.56005
KLC1	IC			29.06334
KLC2	IC			26.79641
KLKB1	IC/S		27.03479	
KPNA3	IC			25.42527
KRIT1	IC			26.83184
L1CAM	IC/M/S			27.54319
LAMA4	IC/S	26.85994	27.91092	28.43366
LAMA5	IC/S		26.91411	28.55402
LAMB1	IC/S	28.98191	28.48797	29.95112
LAMC1	IC/S	29.55868	29.01692	29.93747
LAMP1	M			29.20407
LAMP2	M			26.10976
LAMTOR1	IC			26.16793
LAP3	IC	25.26046	25.65875	29.9574
LASP1	IC	25.96213	27.67939	30.7955
LGALS3	IC	29.00945		29.59699
LHFPL2	M			27.45256
LIF	IC/S	29.03465		
LIMS1	IC			29.17086
LIN7C	IC			30.24314
LLGL1	IC			27.64139
LMAN2	IC/M/S	27.05191		
LOXL2	IC/S	30.13479	30.89556	28.46527
LPAR1	IC/S			27.45228
LPP	IC	27.09394		
LPXN	IC			26.55418
LRPAP1	S			26.26091
LRRC17	S	28.29987		30.65916
LRRC47	IC			26.05596
LRRC57	IC			29.06475
LRRC8C	M			26.21609
LRRFIP1	IC			25.71015
LRSAM1	IC			25.70578
LTBP2	IC/S		26.09978	
LTBR	IC/M			27.34736
LXN	IC			28.4361
LYPLA1	IC/M			26.91693
LYPLA2	IC			27.87896
LYZ	S	28.8453		
MAMDC2	S			27.23568
MAN1A1	M	26.46734		
MAN2A1	M	25.75539		

MAN2B1	S	25.99174		
MANBA	S	26.64081		
MAP2K1	IC			28.29473
MAP2K2	IC			27.36154
MAP3K9	IC/S			30.37108
MAP4K4	IC			31.46298
MAPK1	IC	27.88615		
MAPK3	IC			26.76223
MAPRE2	IC	26.27651		
MARK2	IC			28.00038
MARK3	IC/M			26.9612
MCAM	M			30.49765
MCFD2	IC/S	27.67528		
MDH1	IC	27.18726	27.368	30.75037
ME1	IC			25.80486
MEMO1	IC/M			27.21466
METTL2B	IC/M	28.13901		
MFGE8	S	27.74061		32.80285
MGAT5	M	26.92599		
MGLL	IC			28.12644
MGRN1	IC			24.9537
MICA	M			27.15788
MICAL1	IC			25.50143
MIF	IC	29.71797	27.77607	30.11083
MINK1	IC			29.27495
MME	IC/M		26.14485	32.59869
MMP1	S	34.51389	34.7442	30.61922
MMP14	M/S	26.61133	27.17589	33.32472
MMP2	IC/S	31.43456	31.55919	30.86856
MMP3	IC/S	31.50699	29.1156	27.66794
MOB1A;MOB1B	IC			28.60301
MPZL1	M/S			29.77025
MRAS	IC			27.38729
MRC2	IC/M	27.96275	27.662	27.30278
MSRA	IC/S			26.08895
MST1	IC/S	25.72193		
MT1F	IC			26.14225
MT2A	IC	27.96712	31.34174	32.20433
MVB12A	IC			26.35701
MVP	IC	26.80424	26.65349	33.26288
MXRA8	M	26.79608		
MYADM	M			27.39237
MYDGF	IC/S		27.11068	27.77214
MYLK	IC/M			24.69938
MYO10	IC			27.59087
MYOF	IC/M			32.58382

NAGK	IC			26.00601
NANS	IC			27.46246
NAPA	IC			29.2588
NAPG	IC			28.75444
NCKAP1	M			29.54234
NCS1	IC			26.00949
NCSTN	IC/M/S			28.21193
NDRG1	IC			29.62173
NDRG3	IC			26.39334
NEDD4	IC			25.49854
NEDD8;NEDD8-MDP1	IC		27.32939	30.13923
NEO1	M			27.73109
NES	IC			27.45899
NF2	IC			28.93109
NFKB2	IC			25.8123
NID1	S	28.82867	29.00822	29.22574
NID2	IC/S	28.96072	28.61428	28.15737
NINJ1	M			27.812
NIT2	IC			26.33196
NOTCH1	M			28.4551
NOTCH2	IC/M			30.49876
NOTCH3	IC/M/S			27.07502
NPC2	IC/S			26.22055
NPTX1	S	27.10634		
NRG1	IC/M/S	27.16077		27.38026
NRP1	IC/M/S			31.72999
NRP2	M/S			28.84191
NT5E	IC/M/S	28.30493	31.75785	35.61343
NTM	IC/M/S		27.4291	29.63415
NTSR1	M			27.61587
NUCB1	S	31.42384	28.97977	26.32567
NUCB2;Nucb2;HEL-S-109	IC/S			
NUDT5	IC	27.2056		28.00582
NUMB	IC			29.93208
NUTF2	IC	27.19489		28.13441
OGFR	IC			23.93844
OMD	S		27.81899	
OPTN	IC			25.54466
ORAI1	M/S			27.77308
OSBP	IC			26.71679
OSMR	IC/M/S			26.58643
OTUB1	IC	27.34647	26.0344	28.05048
OXSR1	IC			27.14431
P4HA1	S			26.31968
PACSIN2	IC			29.84604
PAFAH1B1	IC	27.99133		27.85709

PAFAH1B2	IC	26.55805		
PAFAH1B3	IC			24.91975
PAG1	IC			29.32336
PAK2	IC			28.41676
PALLD	IC			26.83318
PAM	IC/M/S	26.92196		
PAMR1	IC/S	26.62846		
PAPPA	S	27.62469	28.62732	27.87462
PAPSS2	IC			27.40706
PARP4	IC			28.48363
PARVA	IC/M			29.03739
PBXIP1	IC/M			29.22529
PCBD1	IC	27.56312		
PCDH18	IC/M			27.61936
PCDH7	IC/M			26.54544
PCDH9	M			27.44591
PCDHGA4;PCDHGA7	M			25.04758
PCDHGB4	M			25.51563
PCDHGB5	M			28.72165
PCDHGC3	IC/M			26.52571
PCOLCE	S	28.19793	27.41966	
PDCD10	IC			28.59111
PDCD6	IC			28.36998
PDCD6IP	IC		27.80326	33.89684
PDGFC	S			26.56183
PDGFRB	IC/S			30.66343
PDLIM1	IC	28.42627	27.91281	30.79498
PDLIM4	IC	27.32045		29.71059
PDLIM5	IC/M			27.21206
PDPK1;PDPK2P	IC			26.58039
PDXK	IC			27.06145
PEA15	IC			27.54073
PFDN1	IC/M			28.46684
PFDN2	IC			28.81587
PFDN6	IC			28.67132
PFKL	IC			27.53484
PFKM	IC			25.70935
PFN2	IC/M			29.62106
PGLS	IC	26.66479		27.80562
PGM1	IC			26.22002
PGM3	IC	27.98317		
PGRMC2	IC/M			25.37246
PHLDA1	IC			29.58839
PHLDA2	IC			29.27095
PHLDA3	IC			27.76765
PHLDB1	IC			30.4321

PHPT1	IC	27.1898		28.28097
PI4K2A	IC			25.50851
PICALM	IC			26.44003
PIN1	IC			27.57633
PIP4K2A	IC			25.99935
PIP4K2B	IC			28.50235
PIP5K1A	IC			26.77896
PITPNA	IC			26.84418
PITPNB	IC			27.6188
PLAT	S	30.8295	30.04223	30.20124
PLAU	IC/S	34.51733	34.50888	32.6261
PLAUR	S			31.49907
PLCB1	IC			24.80887
PLCB3	IC			28.04281
PLCB4	IC			26.73405
PLCD1	IC			26.04067
PLCD3	IC			26.41027
PLD1	IC			25.90699
PLD3	IC/M			25.81915
PLEKHO2	IC			29.21452
PLIN3	IC	28.00106		29.62529
PLOD1	S	31.51486	28.23882	27.85483
PLOD2	IC/M/S	26.52342		
PLOD3	IC/S	28.68864		
PLSCR3;TMEM256-PLSCR3	IC/M			29.20232
PLTP	IC/S	26.64294		26.86514
PLXDC2	M			
PLXNA1	M			30.59561
PLXNA3	M			26.975
PLXNB1	M			27.50933
PLXNB2	IC/M/S		26.22972	33.11894
PMM2	IC			26.47054
POSTN	S	26.90807	27.09157	
POSTN	S	32.02559	28.925	27.70921
PPFIA1	IC/M			26.24058
PPFIBP1	IC			29.24074
PPP1R7	IC			27.55985
PPP5C	IC			27.28061
PPP6C	IC			25.31343
PRDX5	IC	28.0387		28.58629
PRKAA1	IC			28.63019
PRKACA;PRKACB;KIN27	IC			26.34648
PRKCA	IC			29.74905
PRKCDBP	IC			26.97614
PROCR	IC/M	26.9131		
PRSS23	IC/S	28.30412	28.5858	30.29482

PSAP	IC/S	30.5568	29.66366	29.05495
PSD3	IC			26.94085
PSEN1	IC/M			26.41718
PSMD10	IC			27.91199
PSMD5	IC			25.46802
PSMD9	IC			27.94733
PSME1	IC	26.40553		26.27871
PTGFRN	M			27.18141
PTGR1	IC			26.71171
PTK7	IC/M/S			31.0224
PTMS	IC		28.78505	25.49135
PTP4A2	IC			28.08814
PTPN11	IC			26.9426
PTPRA	M/S			29.23386
PTPRD;PTPRS;PTPRF	M/S			25.22142
PTPRJ	M/S			27.31277
PTPRK	IC/M			29.47702
PTRF	IC		29.44804	30.12986
PTRHD1	IC			25.79263
PTTG1IP	M/S			27.63104
PTX3	S	29.16739	30.04007	31.0676
PVR	IC/M/S	25.90889		30.49625
PVRL2	IC/M			29.65869
PVRL3	IC/M			28.3468
PXDN	IC/S	33.03299	30.29812	33.43946
PXN	IC			28.54941
QDPR	IC			26.81043
QSOX1	IC/M/S	31.9553	27.79634	25.95287
RAB10	IC			29.59976
RAB11B;RAB11A	IC	25.70887		31.50569
RAB12	IC			25.12749
RAB13	IC			31.56341
RAB18	IC/M			26.25745
RAB21	IC			27.87566
RAB22A	IC			28.12421
RAB23	IC			28.39584
RAB2A	IC			28.48587
RAB34	IC			28.25073
RAB35	IC			30.301
RAB3A	IC			26.86904
RAB3B	IC			26.34081
RAB6A	IC			28.98685
RAB8A	IC			29.73833
RAB8B	IC			29.27504
RAB9A;RAB9B	IC			25.81714
RAC2	IC			30.96855

RAD23B	IC			28.3111
RAF1	IC			27.55069
RAP2B	IC			28.08048
RAP2C	IC			29.61823
RASA1	IC			24.14095
RASA2	S			26.59295
RASA3	IC			29.45251
RBP4	IC/S	32.01303	30.53825	26.99356
RCN3	IC/M/S	27.86834		
RECK	M			28.61125
REEP5	M			26.59033
RELB	IC	31.31446	31.70667	
RELL1	M			28.18362
REPS1	IC			27.79677
RGN	IC	27.09418		
RGS17	IC			28.07308
RHBDF1	IC/M			29.56479
RHBDF2	IC/M			25.86072
RHOG	IC			32.07817
RIN1	IC			27.42455
RIT1	IC			25.95516
RNASE4	S	29.72282		
RND3	IC			29.90227
RNH1	IC	26.50662		28.76448
RNPEP	IC/S			26.10546
ROBO1	IC/M			28.99611
RTN4	IC/M		26.90816	28.92491
S100A10	M	29.5999	27.19331	32.44305
S100A13	IC	29.24237	29.64687	33.30081
S100A16	IC		26.7179	31.56861
S100A4	IC			24.86462
S100A6	IC	31.42528	31.02325	32.75807
SARS	IC	26.60463		28.40783
SBDS	IC			26.08909
SCAMP1	IC/M			25.34653
SCRN1	IC			28.78911
SDC2	M			27.06735
SDC4	M		26.17773	26.2302
SDCBP	IC		28.12719	32.3221
SEC13	IC			27.39036
SEC22B	IC/M			25.284
SEC24C	IC			26.65125
SEC24D	IC			26.3614
SEC31A	IC/S			28.63002
SEMA3A	IC/S	28.08983		
SEMA6D	IC/M/S			25.54213

SEMA7A	IC/M	30.38024	29.70479	28.13664
SEPT11	IC	28.33396		29.56581
SEPT2	IC	28.14288		28.83201
SEPT7	IC	27.39129		29.66791
SEPT9	IC/S	26.55942		29.86548
SERPINB2;SERPINB10	S	26.31261		30.50017
SERPINB6	IC	26.49354		27.30097
SERPINB8	IC	25.98022		26.61186
SERPINE1	S	32.54554	29.23792	28.82729
SERPINE2	S			27.0296
SGCD	M			29.54357
SGCE	M			25.72324
SGTA	IC			27.48779
SH3BGRL	IC			27.97101
SH3BP4	IC			29.36881
SH3GL1	IC			29.75113
SH3KBP1	IC			28.298
SH3PXD2B	IC			25.2054
SHC1;SHC2	IC			25.82522
SIRPA	M			26.74977
SLC12A2	M			28.83066
SLC12A4	M			28.35339
SLC12A7	M			26.60083
SLC14A1	IC/M			26.55696
SLC16A3	M			31.47539
SLC16A6	M			31.15539
SLC16A7	M			25.19583
SLC1A3	M			26.3604
SLC1A4	M			26.025
SLC20A1	M			31.0752
SLC20A2	M			27.76431
SLC26A2	IC/M			26.74483
SLC2A3;SLC2A14	M			31.1226
SLC30A1	M			28.96439
SLC38A1	IC/M			28.88247
SLC38A2	M			30.95973
SLC39A10	M/S			28.85957
SLC39A14	M/S			28.83616
SLC39A6	M			27.78814
SLC3A2	IC/M	24.79139	29.06569	33.15626
SLC3A2	IC/M			27.12538
SLC44A1	M			28.43412
SLC44A2	IC/M			27.34744
SLC4A2	IC/M			25.51587
SLC4A4	IC/M			28.65312
SLC4A7	M			29.12876

SLC4A7	M			27.49761
SLC6A15	IC/M			30.19182
SLC6A8	IC/M			27.81127
SLC7A11	M			26.8739
SLC7A2	M			28.23259
SLC7A5	M		25.22144	31.02608
SLC7A6	IC/M			26.77516
SLC9A1	M			30.62636
SLC9A3R2	IC			27.55541
SLITRK6	M			27.29312
SLK	IC			28.16278
SMAD1	IC			26.74425
SMAD3	IC			26.40895
SMS	IC			27.40994
SMURF2	IC			28.92193
SNAP29	IC			27.97128
SNTB1	S			27.14639
SNTB2	IC/S			29.2629
SNX1	IC			26.11813
SNX12	IC			26.51647
SNX18	IC			25.74141
SNX2	IC			25.70431
SNX3	IC			29.54729
SNX6	IC			26.65283
SNX8	IC			24.89714
SNX9	IC			28.70827
SOD2	IC	27.68439		
SPARC	IC/S	33.04401	33.29606	29.09241
SPG20	IC			25.25945
SPINK6	S		27.65162	
SPON2	IC/S	31.83777	29.15317	27.46104
SPRED1	IC/M			25.46456
SPRY4	IC/M			29.75602
SQSTM1	IC			29.41323
SRI	IC			29.14304
SRM	IC			28.21769
SRPX	S	26.77399		26.57449
SSC5D	IC/S		27.42494	27.91464
STAM	IC			28.3395
STAMBP	IC			25.59631
STAT1	IC			26.62911
STAT3	IC			24.592
STC1	IC/S	33.90657	30.39974	30.8288
STC2	IC/S	30.68887	26.90369	27.23099
STEAP3	M			29.40799
STK10	IC			29.16569

STK24	IC			29.35902
STOM	M		27.66963	33.22626
STRAP	IC			28.27549
STX12	IC/M			27.0022
STX1B	IC/M			26.46746
STX2	M			27.33289
STX3	IC/M			28.62357
STX4	IC/M			31.71933
STX7	IC/M			28.86139
STXBP1	IC			30.63117
STXBP3	IC			30.75911
SUGT1	IC			27.05028
SWAP70	IC			25.69716
TALDO1	IC	27.14988		
TANC1	IC			26.13097
TAOK1	IC			29.44247
TAOK3	IC			29.35522
TAX1BP3	IC			27.06298
TBC1D10A	IC			24.61668
TBC1D10B	IC			26.30486
TBC1D24	IC			26.90921
TCEB1	IC			30.14599
TCEB2	IC			28.30707
TENM3	IC/M			28.00556
TENM4	IC/M			27.94677
TFPI	S		28.31768	27.09493
TFPI2	IC/S	31.08841	29.37049	28.62438
TFRC	IC/M	26.17429		29.32796
TGFBI	IC/S	33.4858	33.57981	33.05596
TGFBR2	M			28.52543
TGM2	IC	29.69313	29.89197	32.62613
TGOLN2	M			25.43608
THBD	M			29.35791
THBS1	S	28.46822	30.83725	27.42927
THBS3	IC/S		27.4583	
THBS4	IC/S		28.78571	
THOP1	IC			24.89549
THSD4	M/S			26.62123
THY1	M/S	27.45928		31.45987
TIGAR	IC			27.57929
TIMP1	IC/S	34.69346	33.77536	31.34348
TIMP2	IC/S	30.0822	30.43477	30.62524
TIMP3	S			26.71011
TIPRL	IC			26.3464
TLN2	IC			25.24303
TMBIM1	IC/M			25.41109

TMEM132A	IC/M	26.3662	25.97524	28.50434
TMEM2	IC/M			29.70256
TMEM200A	M			26.19149
TMEM237	M			24.73294
TMEM30A	IC/M			26.97923
TMEM51	M			29.14249
TMSB10	IC		31.38119	33.02569
TMSB4X	IC	28.41096	31.21314	33.6013
TNC	IC/S	31.30153	32.09578	33.71857
TNFAIP2	IC			25.40051
TNFRSF10B	M			29.6686
TNFRSF10C	IC/M			26.54047
TNFRSF10D	M			28.96876
TNFRSF11B	S	29.10577	28.27824	27.62111
TNFRSF12A	M/S	27.38242	26.84709	27.63399
TNFSF15	IC/S	27.12834		
TNIK	IC/S			26.547
TNKS1BP1	IC			28.49444
TNPO1;TNPO2	IC			26.76284
TNS1	IC			28.30429
TOLLIP	IC			27.84703
TOM1	IC			28.52424
TOMM34	IC			26.13038
TP53I3	IC			27.51487
TPBG	M			31.56175
TPD52L2	IC		26.03844	29.05898
TPPP3	IC			27.31166
TRAFD1	IC			24.71594
TRHDE	IC/M			27.37809
TRIM25	IC			27.64602
TRIO	IC/S			26.58948
TRIOBP	IC			27.60303
TRIP10	IC			27.58512
TRMT112	IC			24.96111
TRPA1	M			30.33752
TRPV2	IC/M			26.28234
TSG101	IC			28.79487
TSPAN14	M		28.95794	29.47107
TSPAN4	M			26.06594
TSPAN5	M			28.06747
TSPAN6	IC/M			27.55766
TSPAN9	M			28.63957
TSTA3	IC			26.16704
TTC9C	IC			25.63504
TTYH3	M			29.878
TUBB3	IC	27.97021	27.9849	30.39515

TWF2	IC	28.1489		28.1049
TWSG1	S	27.99457		
TXNDC17	IC		28.66179	30.59118
TXNDC5	IC/S			27.64334
TXNL1	IC			28.49805
TXNRD1	IC	29.11404		29.45654
UBA6	IC			26.62518
UBASH3B	IC			25.59314
UBE2D3;UBE2D2	IC			27.18207
UBE2Z	IC			25.54217
UBFD1	IC			25.81768
UBTD1	IC			29.73152
UCHL3	IC			27.18223
UFM1	IC			28.02705
UGDH	IC	26.72845		28.80932
UGP2	IC	27.29395	25.58408	28.19581
ULBP1	M			26.66503
ULBP3	S			26.04796
USO1	IC			26.41639
UTRN	IC			28.02263
VAMP3	M			28.2984
VANGL1	M			25.86647
VASN	M	28.55059		
VASP	IC			30.82736
VAT1L	IC			27.38023
VBP1	IC			27.38192
VCAN	IC/S	25.07668	28.20725	32.27998
VEGFA	IC/S	28.15244		
VEGFA	IC/S		25.64606	25.31255
VNN1	S	29.50603		
VNN2	IC/M/S			
VPS26A	IC			26.21141
VPS28	IC			28.67883
VPS29	IC			26.81575
VPS35	IC	27.61675		27.43072
VPS37B	IC			27.78124
VPS45	IC			24.79123
VPS4A	IC			28.15415
VPS4B	IC			28.7188
VTA1	IC			27.09741
VWA5A	IC			28.19843
WASF2	IC			28.61473
WDR48	IC			27.57496
WLS	IC/M			27.75981
WNT5A	S	29.76394	28.8759	31.56367
WNT5B	S	25.71335		

XPNPEP1	IC			26.84565
YKT6	IC			28.78298
ZDHHC20	M			26.75799
ZDHHC5	IC/M			30.98719

8.3 Mass Spectrometry 3: Proteomic assessment of Conditioned Media and EVs isolated by SEC from vector and OIS IMR90s

This data forms the basis of section 4.8 and is referred to throughout as MS3. Conditioned media (CM) and SEC fractions 8 (F8) and 20 (F20) were collected in triplicate from vector and OIS IMR90s. These were analysed by mass spectrometry through collaboration with the CECAD proteomic facility (University of Cologne). Gene lists detailing the label-free quantitation intensities (LFQ) for each sample were produced and analysed according to section 2.13.2. Mean LFQ intensity values (Mean LFQ) from OIS CM (blue), OIS F20 (orange), OIS F8 (yellow), vector CM (green), vector F20 (grey) and vector F8 (dark grey) replicates are detailed.

	Mean LFQ Intensity					
Gene names	**OIS CM Mean LFQ (Log2)**	**OIS F20 Mean LFQ (Log2)**	**OIS F8 Mean LFQ (Log2)**	**Vector CM Mean LFQ (Log2)**	**Vector F20 Mean LFQ (Log2)**	**Vector F8 Mean LFQ (Log2)**
AARS	24.99	25.76	26.03	23.79	25.60	26.92
ABCA1	24.61	24.90	29.06	24.66	24.98	24.35
ABCC4	23.74	25.08	26.61	24.16	24.74	24.48
ABI2	24.12	25.46	25.13	24.33	25.68	24.08
ACE	25.06	25.15	27.67	24.29	25.38	24.95
ACLY	27.66	26.54	28.65	25.07	25.16	28.13
ACOT7	24.16	25.08	26.29	24.55	25.05	25.00
ACSL4	24.15	24.98	29.00	24.17	25.10	24.43
ACTC1;ACTA1	31.03	25.28	30.14	30.35	28.15	31.13
ACTG1	35.15	34.50	35.81	35.09	34.59	36.22
ACTN4	30.44	29.43	29.52	31.00	28.13	30.11
ACTR2	27.93	27.83	29.00	27.32	28.58	27.69
ADAM10	29.03	28.03	32.05	28.22	28.69	29.39
ADAMTS7	25.70	24.50	24.28	24.77	24.47	25.34
ADSS	24.20	24.73	26.46	24.92	25.11	24.09
AGRN	32.33	32.86	32.74	31.49	32.33	33.91
AHCYL1;AHCYL2	23.59	25.16	27.06	24.61	25.28	25.07
AHNAK	29.43	26.52	31.18	29.46	27.54	32.09
AIMP2	24.14	24.87	26.51	24.16	25.14	24.28
AKAP12	24.78	24.75	25.86	24.66	24.59	24.79
ALCAM	28.88	26.85	31.25	28.45	29.87	30.14
ANGPTL2	26.45	25.97	25.24	27.98	25.17	29.14
ANKFY1	24.83	25.32	25.66	24.37	24.86	24.35

ANO6	24.06	24.62	27.39	24.38	25.21	26.68
ANPEP	26.32	25.71	32.63	24.65	27.61	29.77
ANTXR2	24.03	24.54	28.55	24.87	24.56	26.22
ANXA2;ANXA2P2	29.37	31.62	33.62	28.62	32.30	34.53
ANXA5	26.41	31.80	32.30	24.28	32.00	33.96
ANXA7	24.08	24.60	26.58	24.38	25.17	25.02
AP1G1	24.30	24.49	25.24	23.36	25.15	24.12
AP2B1	27.18	24.09	27.14	26.76	24.89	24.65
AP2M1	25.03	25.09	26.64	24.47	24.89	24.82
APOE	26.75	23.99	26.27	24.03	25.40	24.03
ARG1	24.13	25.26	23.52	24.53	24.53	25.52
ARHGAP1	24.62	24.55	23.74	25.18	24.79	25.55
ARPC1B	29.49	27.70	29.27	27.89	26.95	27.94
ARPC3	25.45	24.10	26.53	26.61	24.55	24.70
ARPC4;ARPC4-TTLL3	24.16	27.13	27.65	24.27	27.24	27.10
ATP1A1	26.10	29.67	33.09	24.68	31.76	31.17
ATP1B1	24.17	24.44	27.03	24.29	24.96	24.53
ATP2A2	24.78	25.28	27.15	24.32	24.81	27.96
ATP5A1	26.23	25.95	27.12	27.02	26.75	28.33
ATP6V1G1	26.55	25.09	27.38	24.20	25.92	24.43
B4GAT1	27.21	25.45	23.79	26.77	25.28	26.41
BLVRB	24.95	25.14	25.27	25.08	25.35	24.80
BMP1	28.30	27.48	27.87	28.40	27.48	24.41
BMP2	30.51	24.79	26.70	24.68	25.23	24.43
BSG	23.61	26.78	31.16	24.78	31.03	29.33
BTN2A1	24.80	24.77	29.05	24.31	25.06	24.85
C1QBP	25.21	24.93	24.78	25.89	24.80	23.86
C1R	31.25	31.26	24.57	33.04	30.23	28.75
C1S	31.69	31.57	24.35	33.03	30.21	27.87
CAB39	24.26	24.65	26.70	24.04	24.83	24.64
CACNA2D1	26.58	24.08	31.39	24.65	27.70	29.32
CAMK2D	24.57	25.04	24.58	24.77	25.26	26.00
CAP1	30.95	24.64	30.14	28.75	24.92	29.15
CAPN1	24.19	25.17	23.99	24.15	24.57	26.08
CARS	23.79	24.68	26.06	23.35	24.92	25.29
CAT	24.30	26.27	23.81	24.25	25.10	25.66
CAV1	24.06	25.19	27.15	24.46	24.91	29.07
CBR1	26.84	24.34	27.05	25.34	25.79	26.21
CCBE1	24.17	24.69	24.48	23.61	25.07	26.70
CCDC80	25.03	25.14	24.01	28.70	25.05	27.85
CCT2	27.97	25.27	29.75	27.67	27.26	27.72
CCT3	26.02	27.22	29.78	25.88	26.69	28.37
CCT6A	27.87	24.04	29.37	27.89	25.19	28.21
CCT8	28.21	26.50	30.12	26.83	27.49	28.51
CD109	25.08	24.58	25.71	24.53	25.82	24.98

CD151	27.21	27.45	33.29	24.18	28.27	30.07
CD276	24.03	24.62	28.53	24.14	25.79	24.26
CD44	32.88	32.36	35.17	31.16	32.96	34.21
CD46	24.43	25.71	27.70	24.38	25.44	26.49
CD47	24.19	24.73	27.40	24.77	25.05	25.35
CD59	31.45	30.92	34.82	28.95	31.69	32.59
CD81	28.27	31.80	32.20	25.74	33.60	31.38
CD82	25.07	25.34	29.58	24.01	26.36	26.70
CD9	29.17	25.18	33.46	28.18	28.46	30.36
CD97	23.82	24.57	28.40	23.87	24.74	24.55
CD99	24.09	23.84	31.08	24.56	28.44	30.12
CDC37	25.79	24.79	25.85	24.62	24.82	24.19
CDC42BPB	23.86	25.31	27.19	24.34	25.01	26.53
CDC42SE1	24.65	24.21	26.00	24.47	25.36	24.00
CDCP1	25.85	25.10	31.49	24.28	25.17	24.86
CDH13	29.05	27.83	32.63	27.41	26.76	30.54
CDH6	28.26	24.87	28.17	28.26	25.03	26.69
CDK4	24.36	25.52	26.26	23.87	24.68	24.63
CEMIP	25.40	25.99	24.44	24.32	24.91	27.43
CHMP1B	23.88	25.97	24.03	24.28	24.93	27.41
CHMP2A	24.74	25.09	28.45	24.37	24.32	25.03
CKAP4	27.37	25.03	29.21	26.39	27.79	30.38
CLDN11	24.33	24.59	24.37	24.24	24.83	29.14
CLIC1	30.87	25.63	31.35	28.82	29.97	30.03
CLIC4	30.68	24.45	31.21	29.59	25.18	30.74
CLSTN1	31.38	27.35	23.99	30.87	24.87	27.24
COL12A1	34.51	32.13	30.86	35.21	30.10	32.62
COL15A1	25.21	24.56	23.86	27.22	24.98	27.55
COL1A1	34.84	35.81	32.26	36.69	35.56	34.03
COL1A2	34.44	34.84	31.44	37.21	34.69	33.46
COL3A1	31.82	31.13	24.03	34.52	30.20	29.64
COL6A1	35.94	36.27	38.52	35.55	37.05	35.61
COL6A2	35.30	35.83	38.37	34.47	36.68	35.19
COL6A3	24.77	24.40	30.76	24.02	24.91	24.36
COL6A3	37.03	38.11	40.20	36.17	39.14	37.26
COL7A1	28.26	24.35	28.86	25.48	25.41	25.00
COMT	23.78	24.70	25.06	23.88	24.79	25.40
COPB2	24.41	25.06	25.58	24.96	25.58	24.64
CORO1B	27.90	25.43	27.84	25.53	25.28	26.76
COTL1	29.12	28.45	29.36	29.32	24.59	28.44
CPNE3	24.01	24.86	28.00	24.38	24.54	26.69
CRIP2	27.95	25.06	29.35	25.07	25.41	28.07
CRISPLD2	27.71	26.19	26.95	24.10	25.29	24.19
CRK	25.72	25.53	27.97	24.55	24.88	24.61
CS	25.85	25.11	24.57	24.87	24.88	26.28
CSPG4	30.14	30.47	33.18	25.26	31.35	32.26

CTGF	31.42	28.01	28.70	28.49	25.98	24.90
CTSZ	29.67	27.73	23.67	27.81	26.05	27.33
CTTN	28.65	25.20	27.92	28.05	24.32	24.53
CUL2	24.79	24.17	25.94	24.08	25.55	24.88
CYB5R3	24.48	25.49	26.92	24.47	25.26	24.88
CYBRD1	25.08	25.42	23.89	24.41	24.54	28.01
DAP	28.76	27.82	27.66	26.84	25.68	26.57
DBN1	28.21	24.98	27.35	26.90	25.46	26.55
DBNL	26.29	25.12	26.92	24.55	24.64	26.28
DCBLD2	27.89	23.81	28.49	24.54	24.70	24.86
DCN	30.41	28.66	24.10	36.41	30.02	31.20
DCTN1;DKFZp686E0752	26.57	25.82	26.60	24.56	24.95	25.71
DDAH1	24.22	24.40	26.99	24.05	25.27	28.23
DDAH2	27.24	24.80	27.81	26.75	24.89	28.95
DDR2	24.94	25.00	26.55	23.68	25.09	24.16
DDX17	24.71	24.77	23.71	23.86	24.15	25.45
DDX3X;DDX3Y	23.97	25.06	26.68	24.54	25.15	24.25
DKFZp566H1924;NPTN	23.99	24.62	28.38	25.15	24.98	28.94
DLL4	25.15	24.84	26.68	23.74	24.19	25.01
DMBT1	25.34	27.45	25.90	23.84	27.46	26.95
DNAJA1	24.82	24.61	27.34	24.40	24.88	24.54
DNAJA2	23.59	24.96	26.63	23.74	25.01	24.55
DNAJC13	24.23	25.45	25.14	24.36	25.57	24.16
DNASE1L1	24.75	24.39	28.25	23.91	24.74	24.84
DOCK10	23.10	24.68	26.18	24.31	24.66	24.72
DPP4	24.45	24.35	28.57	25.27	27.93	27.87
DPYSL3	26.64	25.70	26.80	26.50	25.22	27.87
DSTN	29.50	25.41	29.85	27.90	24.97	29.22
DYNC1H1	27.54	28.50	30.97	25.72	27.35	29.80
DYNC1I2	27.27	26.42	27.72	25.83	26.94	26.99
ECE1	24.77	24.51	29.59	24.02	25.98	27.19
ECM1	34.13	32.51	28.87	33.20	31.11	30.37
EEF1G	27.93	27.03	27.21	26.39	24.79	28.08
EFEMP1	26.04	24.54	24.22	29.95	24.57	26.55
EFNB1	26.43	25.27	27.41	24.05	25.02	26.68
EGFR	25.36	25.41	32.92	25.21	26.63	30.23
EHD2	24.83	24.47	28.52	24.37	24.80	29.12
EIF2S3;EIF2S3L	25.67	24.83	26.64	23.60	25.05	24.60
EIF3E	23.67	24.28	25.92	24.75	25.42	24.57
EIF3I	27.18	25.28	27.52	24.97	24.78	24.01
EIF4A1;EIF4A2	29.49	25.79	29.61	27.58	27.00	28.56
EIF4B	25.60	26.12	26.16	24.10	25.42	24.51
EIF5A;EIF5AL1;EIF5A2	29.07	26.34	27.59	29.06	27.53	28.69

ELFN2	24.51	24.88	26.14	24.34	24.92	24.87
EMILIN1	31.37	31.48	32.78	28.77	31.97	30.78
ENG	26.65	24.83	31.85	23.80	26.22	27.84
ENPP1	24.60	24.89	28.69	24.18	24.36	24.88
EPB41L2	24.38	24.73	25.33	24.85	24.80	27.71
EPB41L2	26.29	24.11	29.87	27.80	26.72	32.05
EPB41L3	24.70	25.18	26.31	24.62	24.66	27.31
EPHA2	23.49	25.62	32.05	24.38	28.59	28.62
EPHB2	25.72	25.33	30.33	24.28	24.95	28.56
EPHB4	24.70	24.64	27.11	24.24	25.76	24.36
ERBB2IP	24.36	24.97	26.12	24.81	25.26	24.83
ESR1	27.27	24.79	30.04	24.40	24.48	24.53
ESYT1	24.77	25.47	23.77	25.06	24.87	27.12
EXT2	25.77	24.89	24.31	27.08	25.40	24.65
F2RL1	23.74	25.35	25.24	24.76	25.48	24.20
F3	27.35	29.02	32.69	24.28	30.74	30.73
FABP5	26.05	24.59	24.11	26.84	25.03	25.06
FAM129B	27.57	25.08	29.40	26.26	24.92	27.14
FAM171A2	24.16	25.04	24.25	23.85	25.07	26.23
FAM49B	24.62	25.96	23.83	24.63	24.51	26.14
FAP	24.61	25.13	28.11	24.67	25.63	25.54
FARP1	24.34	25.16	30.19	25.04	25.08	31.14
FARSB	23.74	24.60	25.93	24.39	24.99	24.43
FAS	24.09	25.36	29.71	24.33	24.87	28.01
FASN	27.78	28.33	30.05	24.52	24.88	27.95
FAT1	29.08	27.39	31.94	26.30	27.07	30.88
FAT4	24.26	25.23	24.25	24.34	24.54	26.66
FBLN1	28.50	25.16	30.23	31.04	24.82	28.66
FBN1	32.56	29.43	25.64	33.00	24.85	26.72
FBN2	30.82	27.52	23.33	32.98	27.59	26.53
FERMT2	24.17	25.77	25.94	24.16	25.15	26.89
FHL2	24.84	24.24	27.71	23.89	24.89	28.52
FHL3	24.65	24.75	25.69	24.41	24.55	24.60
FKBP10	26.49	24.64	26.79	26.56	25.71	24.86
FLNB	27.76	24.75	24.08	27.54	24.67	27.01
FLOT1	24.20	24.46	27.38	24.79	25.04	29.57
FLOT2	24.17	24.36	23.50	24.27	24.23	27.18
FLRT3	24.27	24.82	27.65	24.49	25.08	24.70
FLT1	29.49	25.93	27.74	23.82	25.05	24.27
FMNL3	24.46	25.03	26.52	24.30	25.25	24.49
FN3KRP	23.39	24.65	26.41	23.63	24.86	24.00
FSTL1	33.13	29.57	24.71	34.44	29.30	29.31
FTH1	24.22	25.85	23.40	24.78	25.12	24.70
FZD6	24.78	24.48	25.84	23.94	25.05	25.24
GAS6	27.80	27.30	26.72	30.32	26.85	28.42
GDF15	32.54	29.56	31.51	26.47	30.17	29.64

GDI1	28.03	24.78	27.72	27.09	27.14	24.82
GFPT1	23.87	24.59	25.86	24.56	24.52	24.62
GGT1;GGT3P;GGT2	23.89	25.10	26.85	24.55	25.39	24.74
GIPC1	23.74	25.44	26.65	25.62	25.39	25.13
GJA1	24.31	25.17	31.25	23.84	24.09	29.19
GLI2	23.91	24.50	24.08	24.58	25.27	25.46
GLIPR1	23.77	25.13	25.52	24.29	25.24	24.81
GLIPR2	24.92	25.19	28.55	24.66	25.86	29.88
GLO1	26.78	24.80	23.57	25.81	25.06	24.84
GNAI1	24.53	24.40	27.11	24.45	24.96	24.21
GNAI3	24.11	24.96	28.72	23.98	24.92	24.25
GNAQ	24.34	24.66	26.09	24.29	25.11	24.78
GNB1	26.89	27.06	31.78	24.20	28.93	30.77
GNB2	25.43	24.92	31.91	24.16	26.77	30.54
GNB2L1	26.64	26.12	26.80	25.85	25.38	24.66
GNB4	24.64	25.14	29.01	24.50	25.35	26.11
GNG5	24.30	25.40	29.43	23.96	25.12	27.62
GNS	26.46	25.93	23.90	25.37	25.03	26.52
GPC1	30.29	28.51	28.36	30.80	28.20	29.92
GPC6	23.92	24.07	24.77	24.32	24.32	28.80
GPRC5B	24.28	25.39	24.73	24.78	25.10	28.28
GPRIN1	24.66	24.48	25.98	23.95	24.82	24.82
GRB2	24.04	24.50	26.71	24.28	24.78	25.00
GRK5	24.28	24.84	26.31	24.97	25.30	24.29
GRN	29.08	28.42	24.16	28.04	27.07	27.86
GSK3B	24.32	25.27	25.68	24.25	24.86	24.33
GSTO1	30.20	25.92	28.54	28.01	24.63	24.87
GSTP1	29.22	25.20	28.51	28.70	25.48	29.47
H2AFV;H2AFZ	24.63	24.48	24.53	24.54	24.77	27.63
H2AFY	24.52	24.88	23.85	24.49	24.61	28.37
H3F3B;H3F3A	24.33	28.53	25.39	25.36	28.12	31.82
HAPLN3	23.39	24.19	29.52	24.47	25.35	24.60
HEG1	24.90	24.96	25.99	24.78	24.35	28.16
HGF	33.05	28.91	31.57	30.13	28.18	29.04
HGFAC	27.83	24.77	23.78	29.06	24.82	24.77
HGS	24.16	24.91	26.93	24.53	25.20	27.93
HIST1H1B	26.14	26.83	24.12	28.07	25.67	31.01
HIST1H1C;HIST1H1A	25.99	27.42	24.36	29.64	27.13	31.30
HIST1H2AC;HIST3H2A;HIST1H2AB;HIST1H2AA	24.69	25.56	23.79	24.50	25.04	29.16
HIST1H2BC	24.79	30.80	24.53	24.21	27.93	33.16
HIST1H2BD	27.19	29.95	28.37	30.10	29.83	35.68
HIST1H2BH;HIST2H2BF	25.06	24.12	23.78	24.32	24.97	31.14

HIST1H2BK; H2BFS	24.43	25.27	23.41	24.20	25.19	31.19
HIST1H4A	26.27	27.16	25.16	27.83	28.49	31.50
HIST2H2AC; HIST2H2AA3	25.21	28.24	26.12	29.49	29.15	33.75
HLA-A	30.00	29.12	33.30	27.04	29.89	31.66
HLA-B	24.03	24.74	29.19	24.79	25.67	24.23
HLA-B	23.85	25.06	30.11	24.21	25.76	27.44
HLA-B	28.61	28.63	31.57	24.22	28.28	29.04
HLA-B	26.11	25.43	29.56	23.99	25.39	27.59
HLA-C	24.91	24.82	28.95	24.65	25.60	24.76
HLA-C	24.59	24.32	26.87	24.06	25.22	24.80
HLA-C	29.72	24.22	30.04	27.58	24.96	24.73
HMGB1;HMGB1P1	29.13	25.33	23.66	29.34	25.51	27.44
HMGN4	23.62	29.60	24.36	27.35	25.69	29.55
HNRNPA1;HNRNPA1L2	28.34	28.53	27.10	29.15	27.73	28.50
HNRNPA2B1	29.53	27.82	26.65	30.53	28.20	28.13
HNRNPA3	26.92	25.73	24.74	27.71	26.75	27.62
HNRNPH1;HNRNPH2	25.24	25.02	24.28	24.12	24.66	26.10
HNRNPK	26.87	26.09	26.77	27.38	27.05	27.22
HNRNPM	25.85	24.56	23.88	24.43	25.16	26.02
HP1BP3	24.42	24.86	23.38	24.74	24.83	28.02
HPCA;HPCAL1;NCALD	24.06	25.21	25.88	23.87	24.38	24.32
HRAS	32.05	32.91	35.76	24.40	34.35	30.29
HSP90B1	29.29	27.02	29.70	29.11	27.15	30.45
HSPA1B;HSPA1A	27.84	27.29	27.88	27.96	24.69	29.15
HSPA4	28.38	25.45	28.54	27.25	25.85	27.27
HSPA8	23.72	25.36	26.70	24.76	24.78	24.05
HSPG2	30.12	30.12	29.88	32.25	30.62	35.38
HSPH1	27.05	24.88	27.17	24.20	25.24	24.97
ICAM1	30.76	29.79	34.76	24.39	32.32	28.83
ICAM5	28.11	25.80	28.24	25.02	24.85	24.74
IGFBP3	30.86	26.35	27.71	30.64	24.81	23.84
IGFBP4	34.37	32.37	27.12	34.41	30.73	29.68
IGFBP6	31.27	28.72	23.65	30.46	26.30	25.13
IGSF8	23.77	28.18	31.69	24.32	30.67	31.10
IL1RAP	24.38	25.08	26.73	24.85	24.16	24.47
IL6ST	24.45	24.94	30.44	23.82	25.17	24.87
ILK	24.72	24.90	28.30	24.16	24.93	27.49
IRGQ	25.13	25.39	26.63	24.30	24.70	24.41
ITCH	24.47	25.70	25.68	24.57	25.84	24.34
ITFG3	23.33	24.77	29.89	24.30	25.60	27.42
ITGA1	25.85	26.50	33.63	24.66	29.77	31.82
ITGA2	24.40	25.33	30.13	24.21	24.54	25.06
ITGA2	30.98	30.49	35.51	25.58	31.51	31.03

ITGA3	24.36	26.72	32.32	24.28	27.50	31.31
ITGA4	24.51	25.56	30.53	24.34	24.76	27.31
ITGA5	25.16	27.78	31.96	23.76	30.47	29.20
ITGA6	24.36	25.26	31.44	24.19	27.91	24.80
ITGA8	24.49	25.09	27.95	24.51	25.19	24.63
ITGAV	25.34	25.34	33.11	24.45	29.09	30.12
ITGB1	30.92	31.68	35.41	27.24	33.02	32.97
ITGB3	24.47	24.78	31.59	24.07	28.72	29.85
ITGB5	26.18	26.77	32.84	23.95	28.00	26.52
JAK1	24.57	25.64	27.17	24.74	24.58	24.32
JAM3	24.27	24.97	28.10	24.79	24.95	23.71
KHDRBS1	26.34	24.89	23.72	26.12	25.55	24.88
KIRREL	24.10	24.69	29.23	24.02	25.28	28.03
KLC1	24.64	25.34	26.32	23.69	24.42	24.68
LAMA2	25.04	26.87	24.40	26.53	26.69	25.88
LAMA4	29.70	30.55	30.40	32.61	30.64	33.78
LAMA5	28.58	29.75	30.90	28.24	29.08	32.21
LAMB1	31.94	31.83	31.76	32.76	31.20	33.85
LAMB2	23.84	24.64	24.25	23.33	25.31	29.94
LAMC1	32.49	33.25	32.73	33.14	32.47	34.54
LAMP1	23.84	25.58	27.73	24.44	25.36	29.18
LAP3	23.75	25.15	27.00	23.83	25.29	24.64
LEPRE1	27.09	26.92	26.60	26.96	25.55	24.87
LLGL1	24.67	24.93	26.69	24.82	25.34	24.46
LMAN1	23.37	25.24	25.51	23.79	25.57	24.18
LMNA	30.73	26.59	24.33	32.09	24.86	29.50
LOXL2	33.81	31.99	30.01	31.99	30.50	32.71
LPAR1	24.53	25.08	27.71	23.89	24.16	29.69
LRRC17	26.88	24.84	30.81	25.61	24.64	26.15
LRRC32	24.82	25.22	25.43	24.48	25.11	24.17
LRRC47	23.98	25.24	25.82	24.53	24.96	24.90
LRRC59	27.64	25.17	23.85	26.36	25.58	25.20
LTBP2	31.73	29.35	26.50	31.95	27.45	29.48
LUM	29.89	25.21	23.97	33.01	24.61	27.93
MAP1B	28.08	24.55	23.46	27.24	25.38	24.79
MAP4K4	25.49	25.08	29.37	24.55	25.62	27.80
MAPRE1	24.00	24.78	24.28	23.99	25.28	25.27
MARCKS	27.47	24.51	29.39	29.24	24.70	30.22
MARCKSL1	24.81	27.75	30.13	25.53	28.88	28.89
MDK	30.22	24.85	26.78	31.27	24.90	29.39
MFGE8	31.36	28.99	33.51	32.30	30.68	35.19
MICA	24.41	25.03	27.60	24.22	25.62	25.16
MME	24.75	26.14	31.00	24.38	28.45	24.52
MMP14	30.62	27.08	31.16	26.23	24.70	28.02
MPZL1	23.61	24.99	28.01	24.63	25.39	24.89
MRC2	27.80	27.02	28.81	26.94	25.34	27.30

MRGPRF	24.17	24.44	25.19	24.57	25.38	28.33
MT2A	28.63	27.27	30.34	24.78	24.66	26.55
MXRA8	24.29	25.02	24.39	24.09	25.78	27.23
MYOF	24.72	24.70	30.30	25.12	24.62	31.33
NAPA	24.96	24.67	27.35	24.50	25.31	25.04
NAPG	24.37	24.87	27.68	24.26	24.86	24.29
NARS	24.64	25.00	23.45	24.24	24.72	25.81
NCKAP1	24.77	24.61	27.57	24.83	25.17	25.60
NDRG1	24.55	25.13	28.41	24.34	25.28	25.09
NES	29.29	26.66	29.02	26.93	25.42	26.86
NID1	32.16	32.21	31.47	31.95	31.50	33.20
NID2	32.07	30.87	30.22	33.04	30.77	33.50
NOTCH1	24.51	24.79	29.15	24.22	25.26	23.58
NOTCH3	25.06	24.29	27.68	23.91	25.02	26.75
NPM1	30.58	25.12	23.96	30.67	25.25	28.53
NRG1	31.80	24.09	28.26	25.34	24.85	26.10
NRP2	23.91	24.67	27.13	23.84	25.12	25.10
NT5E	29.74	29.02	33.84	23.87	32.11	31.14
NTM	28.96	27.99	29.97	25.34	28.94	25.86
NTN4	24.70	25.54	24.46	28.78	24.98	29.61
NTSR1	23.81	25.07	28.29	25.17	24.62	25.18
NUMB	24.20	25.36	28.37	23.83	25.08	24.48
NUTF2	24.83	25.44	26.55	24.21	24.58	27.66
OTUB1	25.77	25.19	26.45	24.15	24.68	24.42
P4HA1	23.99	26.36	28.31	24.31	25.08	26.49
P4HA2	26.53	25.17	27.60	24.81	25.08	24.60
PABPC1;PABPC3	27.48	25.30	23.40	26.04	25.52	24.83
PACSIN2	24.97	24.55	26.22	24.46	25.35	24.70
PACSIN3	24.27	25.28	23.97	24.07	24.75	25.92
PALLD	24.58	25.22	26.84	24.46	24.66	27.65
PALM2-AKAP2;PALM2	24.81	25.16	26.20	24.43	25.53	24.69
PAM	25.38	25.63	23.72	26.16	24.72	24.54
PAMR1	30.94	28.23	28.93	28.93	25.75	26.01
PBXIP1	24.52	24.79	26.10	24.82	24.79	27.26
PCDH7	24.79	25.63	26.03	23.99	25.34	24.30
PCDHGB4	24.49	25.02	25.56	23.83	25.49	24.77
PCDHGB5	23.70	24.82	28.10	24.56	25.70	24.77
PCDHGC3	23.88	24.52	28.35	24.38	25.54	26.58
PCMT1	26.70	24.55	27.50	24.69	25.05	24.06
PCOLCE	32.86	31.70	27.58	32.95	30.24	30.88
PDCD10	24.66	24.39	25.91	23.77	24.28	24.53
PDCD6IP	26.67	27.19	31.64	24.57	26.60	32.79
PDGFC	24.62	25.43	26.35	24.71	25.63	24.06
PDGFRA;FIP1L1	24.54	25.19	23.88	24.36	25.32	26.67

PDGFRB	25.85	25.69	31.36	24.47	28.09	30.69
PDLIM1	29.03	24.83	28.85	28.04	24.91	28.27
PDLIM4	27.80	24.37	28.31	23.21	24.75	24.66
PEBP1	28.42	25.03	27.29	28.39	24.14	28.12
PFDN1	24.68	25.00	26.42	23.76	25.33	25.80
PFDN2	27.07	24.87	26.84	24.03	24.63	25.07
PFKL	24.38	25.13	27.78	23.91	25.50	24.11
PGRMC1	23.98	24.72	24.26	24.06	25.27	27.00
PHB	24.92	25.01	25.90	23.96	25.03	24.68
PHGDH	24.86	25.00	27.17	23.77	25.60	30.23
PHLDA1	24.75	25.79	28.68	23.78	25.56	25.84
PHLDA3	24.67	24.77	24.41	24.27	24.61	24.85
PHLDB1	24.18	25.06	29.04	24.45	24.56	23.94
PI4KA	24.18	24.43	25.77	24.07	25.20	24.45
PLAT	33.94	30.35	31.31	30.15	27.49	28.82
PLAUR	24.97	25.91	32.58	24.18	27.62	25.73
PLIN3	28.95	24.58	28.01	27.45	24.50	27.26
PLOD2	26.97	24.48	26.41	25.34	24.34	25.03
PLS3	27.79	25.07	27.83	27.05	25.48	27.01
PLXNA1	24.68	25.21	29.44	24.90	27.50	26.82
PLXNB1	24.23	25.07	26.09	24.41	25.32	24.33
PLXNB2	27.08	24.78	31.40	26.46	27.47	29.24
PLXND1	24.09	24.76	26.32	24.28	24.70	24.82
POSTN	30.76	27.53	27.98	29.22	25.02	25.04
PPP1CA;PPP1CC	24.77	24.47	27.82	24.37	25.17	27.03
PRDX4	25.25	26.05	23.93	24.40	25.76	25.47
PRDX6	29.26	27.71	29.44	28.39	29.00	30.17
PRKAR2A	24.01	24.75	26.16	24.31	24.71	24.47
PRKCA	24.18	25.16	26.31	23.95	24.22	25.25
PRSS23	28.74	26.75	30.26	27.64	27.86	27.19
PSAT1	24.40	25.48	23.77	23.83	25.25	25.31
PSMA2	23.57	27.69	23.86	24.48	26.48	24.67
PSMA7;PSMA8	24.42	29.00	26.77	24.10	28.03	24.15
PSMB5	24.15	27.39	24.14	24.81	24.96	24.83
PSMC1	24.45	24.55	26.51	23.65	24.53	25.10
PSMC3	23.99	24.67	26.72	24.17	24.27	24.94
PSMC4	24.13	24.95	26.41	23.60	25.04	24.75
PSMC5	25.03	25.20	26.16	24.86	25.41	25.74
PSMD1	24.44	25.01	25.84	24.60	25.61	24.54
PSMD3	24.77	25.21	23.89	24.55	24.85	25.45
PSMD4	23.88	24.67	26.67	24.49	25.96	24.18
PSMD6	24.46	24.48	27.55	24.39	24.60	24.42
PSME2	27.62	24.26	26.62	24.87	24.99	24.19
PTGFRN	24.80	25.07	28.29	24.06	25.68	24.22
PTK7	28.72	25.27	30.21	28.02	28.44	31.06

PTMA	26.20	24.45	23.67	25.46	24.60	25.39
PTN	30.26	24.12	23.11	31.69	25.79	28.54
PTPRG	24.02	24.53	26.57	23.75	25.11	24.39
PTPRJ	24.37	24.92	25.23	25.02	25.09	24.40
PTPRK	28.01	25.15	28.74	26.28	25.41	27.80
PTRF	28.85	25.11	28.28	28.60	25.49	29.58
PTTG1IP	24.79	25.25	24.70	24.77	24.78	26.35
PTX3	32.06	33.43	37.21	30.69	34.75	33.64
PVR	28.13	25.46	29.58	28.42	26.99	28.25
PVRL2	24.51	24.84	28.72	24.79	24.95	27.56
PVRL3	24.44	24.33	28.10	23.92	24.70	25.12
PXDN	34.26	34.15	35.44	33.10	34.22	33.58
PXN	24.60	25.24	26.15	24.10	24.68	25.41
PYGB	26.81	25.16	27.70	25.78	24.69	26.34
QSOX1	30.72	30.56	27.76	32.96	30.25	29.59
RAB10	24.47	25.26	28.14	24.02	24.92	26.67
RAB13	23.94	25.06	29.38	24.36	25.00	28.45
RAB14	24.37	25.45	27.42	24.09	24.86	28.10
RAB1A	26.55	25.58	29.23	25.62	24.68	28.54
RAB1B;RAB 1C	24.22	24.54	28.47	23.60	25.97	24.50
RAB34	24.08	25.44	26.39	24.38	24.97	24.36
RAB35	24.56	25.61	29.10	25.13	24.82	27.55
RAB5B	24.36	24.04	26.70	24.56	24.93	24.58
RAB6A	24.41	24.61	26.45	24.88	24.68	24.23
RAB8A	24.27	25.07	27.28	24.02	24.81	24.88
RAC1	26.45	25.25	30.91	25.14	26.67	29.76
RAC2	24.07	25.40	28.05	24.55	25.10	24.14
RALB	23.81	25.03	29.84	24.17	24.73	28.90
RAP1A	24.40	24.92	26.56	24.30	25.05	24.68
RBP4	29.74	29.00	27.11	29.06	24.50	28.81
RELN	23.95	25.08	23.41	24.35	24.77	27.39
RFTN2	25.17	24.62	25.91	23.43	24.98	24.28
RHOA	23.85	25.02	29.81	24.36	27.53	28.43
RHOB	24.48	24.52	28.39	24.36	24.48	26.64
RHOC	28.00	25.61	29.74	26.98	26.04	28.03
RPL10A	29.34	25.07	26.06	28.14	24.98	27.41
RPL18	24.06	25.09	27.95	24.25	25.11	24.86
RPL23A	23.79	24.63	26.61	23.89	24.80	27.34
RPL26	23.90	24.92	27.71	23.98	24.72	26.29
RPL31	23.79	25.72	26.45	24.29	24.79	24.22
RPL32	26.45	24.62	24.43	23.69	25.25	27.50
RPL35A	24.47	25.17	26.76	24.16	24.58	24.02
RPL9	24.12	23.92	25.72	24.40	25.37	24.75
RPS12	28.82	23.85	26.92	27.16	25.02	25.15
RPS27;RPS2 7L	24.15	25.02	23.92	23.55	25.14	26.08

RPS27A;UBB;UBC;UBA52	27.35	30.19	30.49	28.03	29.75	32.47
RPS7	24.94	24.48	27.08	24.45	25.19	24.91
RRAS	25.04	25.10	26.46	23.80	24.72	23.96
RTN4	26.81	25.20	26.71	24.31	24.67	25.70
RUVBL1	25.38	24.93	26.92	24.04	25.29	24.20
S100A10	27.49	24.59	27.81	27.96	24.90	28.67
S100A13	24.21	24.86	28.53	25.24	24.69	27.20
S100A16	24.55	24.82	30.12	23.51	24.94	28.50
S100A6	28.94	28.88	30.06	29.14	29.89	31.01
SCARB2	25.39	25.53	24.28	24.43	24.76	27.63
SCRIB	23.82	25.47	27.56	23.93	24.85	25.00
SCUBE3	29.94	25.81	29.83	25.06	26.02	25.05
SDCBP	24.45	28.73	29.97	23.88	28.82	31.66
SEC13	24.53	25.44	26.63	24.60	25.25	25.59
SEC22B	24.66	24.84	26.20	23.67	24.90	27.20
SEC23A	23.92	25.44	27.97	24.45	25.34	25.88
SEMA5A	28.03	27.71	23.76	24.34	25.89	24.93
SERBP1	26.78	26.38	26.37	26.02	25.50	25.01
SERPINB2	25.79	24.78	29.02	23.86	25.03	25.44
SERPINE1	29.61	28.94	28.65	28.91	27.97	24.22
SERPINH1	29.01	27.68	29.08	30.55	25.19	30.04
SFPQ	25.20	25.16	23.44	25.68	25.36	25.38
SGCB	24.46	24.92	23.53	24.69	25.87	26.37
SGCD	24.72	25.54	27.30	24.98	25.48	28.22
SH3BGRL3	31.95	31.24	31.37	31.69	30.84	30.98
SHMT2	24.22	24.96	24.56	23.80	25.51	27.39
SIRPA;SIRPB1	24.25	24.78	27.30	24.69	25.20	24.00
SLC12A2	24.17	24.89	26.54	23.75	25.31	25.91
SLC16A3	23.50	24.86	30.96	25.14	25.69	29.20
SLC16A6	24.13	26.03	30.49	24.84	27.53	24.96
SLC20A1	23.71	24.71	29.86	24.24	24.69	24.50
SLC25A3	24.41	25.33	23.75	23.91	25.66	26.68
SLC2A3;SLC2A14	24.38	24.63	28.10	24.81	24.96	24.97
SLC35F6	25.12	24.52	24.39	23.81	24.34	26.13
SLC39A14	24.64	24.43	27.44	23.67	25.02	24.90
SLC3A2	26.30	25.15	30.99	24.48	26.70	29.53
SLC44A1	24.40	25.04	26.75	24.22	25.26	25.16
SLC4A7	24.23	25.12	26.58	24.17	24.93	24.50
SLC4A7	24.04	25.37	26.79	23.70	25.04	24.30
SLC5A3	23.80	25.01	25.62	23.16	24.41	24.38
SLC6A15	24.41	25.01	26.12	24.16	24.79	24.85
SLC6A6	24.10	24.77	25.72	24.62	25.02	24.11
SLC7A2	23.96	25.19	27.40	24.51	25.23	23.85
SLC9A1	24.29	24.03	28.18	24.07	25.52	26.02

SMURF2	23.93	24.33	26.36	24.25	25.50	25.12
SNAP29	24.20	24.74	26.23	23.75	25.27	24.28
SNTB2	24.64	25.17	25.77	23.97	24.67	24.49
SNX18	24.16	24.70	25.09	23.95	24.87	24.68
SOD1	30.44	28.77	28.53	29.00	28.33	29.53
SPARC	34.87	32.34	29.31	33.56	32.41	32.50
SPRY2	24.46	25.24	26.02	24.60	24.80	24.40
SPRY4	24.91	25.01	27.97	24.17	24.94	24.26
SPTBN1	24.72	25.28	23.70	24.51	24.43	26.31
SRGAP1	24.94	24.37	25.51	23.95	24.89	24.97
SRGAP2;SRGAP2B	25.05	25.15	27.68	24.28	25.66	26.51
SRI	24.10	24.76	26.15	24.66	25.26	24.54
SRPX	30.97	25.86	29.75	28.05	25.62	28.39
SRPX2	30.08	26.72	29.14	25.27	25.95	25.28
SRSF2	24.97	24.68	24.12	24.86	24.96	26.93
SRSF3	24.07	25.11	23.65	24.89	25.06	26.97
STC2	29.78	24.11	23.98	30.49	24.63	28.79
STEAP3	24.92	24.61	26.65	24.71	24.72	24.38
STIP1	30.58	25.55	29.21	27.79	25.71	27.68
STK10	23.96	25.00	25.50	23.92	24.89	25.06
STMN1	29.39	27.73	27.17	30.34	26.70	28.34
STOM	25.09	25.24	31.19	24.20	28.84	33.84
STUB1	24.61	24.96	28.15	24.33	25.94	24.44
STXBP1	24.30	23.65	27.72	24.38	24.93	27.08
STXBP3	24.46	24.16	27.72	25.36	24.72	24.76
SUSD2	25.37	25.33	29.76	24.31	29.45	24.07
SVEP1	26.09	25.11	23.40	33.20	24.85	30.20
TAGLN	24.52	24.48	23.96	24.29	25.10	27.33
TAOK1	24.22	24.61	26.08	24.30	24.83	24.38
TCEB1	27.54	24.71	26.62	25.78	25.40	24.20
TCP1	27.48	24.52	29.30	26.84	24.83	27.75
TENM3	24.45	25.25	27.66	24.10	25.25	24.03
TFPI	29.45	28.07	28.76	29.15	25.38	27.75
TGFB1	27.55	25.76	27.18	23.78	24.46	24.71
TGFBI	34.43	33.16	35.38	34.59	33.72	33.24
TGM2	28.02	26.67	29.93	25.56	27.80	28.36
THBD	25.13	24.75	27.72	23.68	25.48	25.03
THBS1	34.16	32.81	31.48	32.17	31.10	30.43
TIMP1	34.97	32.44	30.67	32.99	31.71	33.58
TIMP2	32.55	32.13	31.03	32.95	31.28	29.20
TJP1	24.19	25.38	29.21	24.83	25.42	25.07
TMED10	23.92	24.79	26.02	24.16	25.48	26.77
TMEM119	24.66	25.52	28.06	24.10	24.81	29.75
TMEM132A	27.85	25.05	28.07	24.77	24.71	25.30
TMEM2	25.42	26.11	28.78	24.82	25.33	24.53

TMEM30A	24.32	25.51	26.46	24.35	25.25	25.17
TMEM51	24.96	25.22	27.05	24.32	25.02	25.09
TMEM59	25.05	24.96	26.02	24.17	24.85	24.80
TNC	31.86	30.15	31.94	31.05	30.51	30.63
TNFRSF10B	25.12	25.18	29.01	24.75	25.83	24.01
TNFRSF10D	28.07	24.97	27.11	23.99	24.92	23.87
TNFRSF12A	29.36	27.62	27.76	27.21	26.83	25.67
TOLLIP	24.65	24.98	27.03	24.53	25.54	23.48
TPBG	24.78	24.91	30.98	24.46	25.45	26.20
TPD52L2	28.06	25.00	27.88	26.39	25.72	24.63
TRPA1	24.54	24.61	28.06	24.23	24.79	26.31
TSG101	24.89	24.72	23.65	24.15	25.64	28.04
TSPAN14	25.03	24.45	29.86	24.28	23.96	25.37
TSPAN4	24.65	24.70	27.36	24.76	24.77	24.72
TSPAN5	24.54	25.41	29.92	24.42	25.08	27.10
TSPAN9	23.90	25.12	27.79	24.33	25.22	24.19
TTYH3	23.35	25.21	29.04	24.59	27.49	30.23
TUBA1A;TUBA3C;TUBA3E	31.77	32.87	32.33	31.47	32.65	33.06
TUBA1B	24.81	24.68	27.59	23.95	25.26	24.31
TUBA4A	24.62	25.40	25.89	24.86	24.42	25.00
TUBB	28.55	30.55	30.71	27.91	30.83	31.68
TUBB2A	25.59	28.55	27.11	25.77	27.02	28.31
TUBB6	24.15	24.00	27.56	24.24	24.87	29.00
TXN	30.05	25.52	24.25	31.78	25.84	28.91
TXNL1	26.17	24.81	23.85	25.48	25.44	26.27
UACA	24.62	25.23	26.56	23.69	24.94	25.00
UBTD1	24.75	24.71	27.23	24.24	24.45	25.62
USP14	23.86	24.79	25.22	24.12	24.95	23.73
USP5	23.99	24.01	26.56	25.09	24.89	24.56
UTRN	24.12	25.27	23.62	24.58	25.39	26.79
VAPA	26.90	25.54	23.94	25.72	25.16	25.14
VASN	28.67	25.21	26.26	28.02	24.76	24.70
VASP	27.58	25.06	28.16	26.92	25.09	27.52
VAT1	28.35	24.97	28.73	27.34	25.00	30.30
VCAN	31.65	32.70	35.94	31.46	34.60	34.27
VCL	29.91	28.32	30.13	30.25	28.50	31.14
VDAC2	24.30	24.91	24.17	24.35	24.79	26.29
VPS35	24.79	25.59	26.95	23.80	25.41	24.40
VPS37B	23.83	24.74	23.57	24.21	25.39	27.21
VWA5A	24.38	25.48	26.08	24.37	25.66	24.48
WARS	27.41	26.27	26.95	27.04	25.11	28.33
WDR64	23.85	25.36	30.33	24.57	24.82	24.98
WLS	24.24	24.13	27.55	24.36	25.26	24.97
WNT5A	30.18	28.66	32.20	26.60	26.55	30.37
WNT5B	24.04	25.41	29.09	24.14	25.09	27.25

XRCC5	24.15	25.20	24.02	24.55	24.82	26.32
XRCC6	24.87	26.22	24.51	23.56	24.13	28.35
YWHAB	30.46	28.42	30.71	29.07	28.89	29.97
ZC3HAV1	23.63	25.05	27.72	23.40	24.07	24.75
ZDHHC20	24.65	24.64	28.04	23.93	24.94	24.68
A2M	24.02	27.97	23.88	26.63	27.55	24.67
AAMDC	25.05	25.24	24.79	24.62	24.74	24.91
ABCC1	23.65	25.35	26.61	24.44	25.53	26.99
ABI1	24.79	25.30	27.60	23.62	25.07	27.47
ABLIM3	24.36	24.91	24.90	25.10	25.09	24.47
ACAT2	24.41	24.47	24.34	25.61	25.16	24.25
ACTB	24.46	30.96	30.08	23.84	31.35	30.99
ACTN1	29.35	28.22	29.19	29.91	27.29	29.44
ACTR1A	25.06	25.70	27.25	24.71	25.66	26.65
ACTR3	28.51	28.32	29.67	27.27	27.71	29.10
ADAM17	24.85	24.14	27.98	23.84	25.65	27.36
ADAM19	28.57	25.06	24.56	26.28	24.90	24.13
ADAM9	29.23	24.89	29.74	29.82	24.95	29.86
ADAMTS1	28.67	24.93	26.43	27.07	25.16	27.34
ADAMTS12	28.17	25.63	25.86	25.51	25.08	24.98
ADD1	24.89	25.48	28.47	24.34	25.42	27.95
ADD3	24.91	24.44	27.41	23.46	25.16	27.30
ADH5	25.53	26.48	27.99	23.68	24.51	27.96
ADM	25.99	26.15	24.27	29.43	29.31	24.70
AEBP1	28.78	24.71	27.73	28.94	24.84	27.27
AFP	27.54	25.47	24.38	28.20	24.64	24.99
AHCY	26.78	24.44	26.76	28.05	24.70	27.01
AKR1A1	26.24	25.68	25.55	24.62	24.44	24.63
AKR1B1	30.17	25.51	28.61	28.26	25.74	27.94
AKR7A2	24.42	24.17	25.83	24.57	25.53	25.72
ALDH9A1	25.08	25.22	24.81	24.76	25.17	24.66
ALDOA	32.90	33.40	33.04	32.41	32.64	32.59
ANXA1	25.70	29.54	32.26	24.68	29.51	32.85
ANXA11	24.78	25.50	30.61	24.61	26.68	30.11
ANXA4	24.85	27.11	28.14	23.69	27.02	29.02
ANXA6	27.23	29.10	33.42	24.61	30.88	33.03
AP2A1	24.55	25.10	27.84	24.47	25.80	27.34
APEX1	25.32	25.22	24.98	25.47	24.88	24.78
APLP2	27.17	24.90	24.31	25.15	25.19	24.37
APOM	26.55	24.24	24.61	26.61	25.70	26.54
APP	31.85	27.88	24.98	30.80	25.44	25.22
AREG	31.63	27.66	28.36	24.76	27.07	28.85
ARHGDIA	29.80	25.84	29.06	29.07	26.05	29.15
ARL3	24.60	24.97	25.35	24.00	24.76	25.03
ARPC2	27.04	24.83	25.02	26.83	25.02	24.37
ARPC5	24.87	24.70	27.75	23.99	27.22	25.32

ATIC	24.93	25.35	27.70	23.66	24.75	27.77
ATP1B3	24.68	25.60	27.86	24.53	25.89	25.68
ATP2B1	24.38	24.37	31.15	24.49	28.02	30.56
ATP2B4	24.07	27.06	29.83	24.76	28.73	30.12
ATP5B	28.38	27.13	28.98	27.63	27.39	28.90
ATP6AP1	26.09	25.08	24.33	24.76	25.15	24.75
ATP6AP2	28.16	24.22	24.57	26.48	25.22	24.65
ATP6V1A	25.56	26.17	27.73	24.63	26.01	27.64
ATP6V1B2	25.40	24.02	28.01	24.70	24.58	26.99
ATP6V1E1	23.87	25.00	26.60	24.28	24.25	24.99
ATRN	25.26	24.50	25.17	26.35	25.22	24.76
AXL	27.25	25.25	24.11	27.20	25.40	23.79
B2M	34.39	32.61	32.67	34.36	32.11	32.14
BANF1	25.35	24.99	23.48	24.22	25.39	24.11
BASP1	28.44	27.07	32.06	28.82	25.96	32.24
BAX	25.07	25.24	24.95	24.72	24.80	24.80
BCAM	24.26	25.40	27.63	24.86	26.72	27.30
BDKRB2	24.83	24.61	28.47	24.22	24.79	28.16
BGN	32.58	29.35	27.38	31.80	27.54	27.17
BRK1	24.80	25.17	26.73	23.75	25.34	27.26
C12orf75;OCC1	24.22	24.28	27.40	24.02	24.11	27.16
C1QTNF3-AMACR;C1QTNF3	26.38	26.71	23.89	28.00	25.87	24.31
C8B	26.04	25.51	24.09	25.99	25.23	24.73
CAD	25.37	25.18	26.11	24.26	25.12	25.85
CADM1	24.55	25.44	28.42	24.07	26.85	28.01
CALD1	25.63	25.32	24.78	28.71	25.44	24.71
CALD1	29.76	28.61	28.41	30.07	27.68	29.24
CALM2;CALM1	24.44	28.76	30.71	25.74	29.76	30.88
CALR	29.64	27.50	28.10	28.98	26.41	28.29
CALU	30.71	27.16	23.55	30.88	25.76	25.43
CAND1	26.44	25.65	27.36	26.69	26.06	27.54
CANX	24.18	24.15	28.16	24.53	25.81	28.26
CAPG	24.58	24.51	25.19	23.77	25.30	25.40
CAPN2	27.28	25.29	27.15	24.98	25.22	27.47
CAPN5	24.46	25.22	28.52	23.30	24.56	26.49
CAPNS1	25.97	25.30	27.36	25.64	25.36	25.93
CAPZA1	29.93	26.93	28.84	28.76	29.24	29.26
CAPZA2	26.31	25.18	26.84	24.64	25.19	26.25
CAPZB	28.47	26.24	29.39	27.46	24.76	29.27
CASK	24.35	25.31	26.53	24.26	24.74	27.53
CAST	25.93	24.58	24.29	25.93	25.21	24.58
CCDC50	23.93	25.59	28.57	24.72	24.73	29.01
CCL2	27.64	24.81	23.51	25.85	25.19	25.04
CCNY	24.69	24.60	24.44	23.99	24.82	25.09

CCT4	29.03	29.04	30.30	27.41	28.22	29.74
CCT5	28.27	27.48	28.93	27.87	29.22	28.41
CCT7	27.88	26.21	29.26	25.10	26.55	28.56
CD248	30.34	29.66	29.66	29.32	28.81	29.57
CD55	24.60	24.70	26.09	23.27	25.14	24.40
CDC42	26.77	25.62	30.84	25.69	26.69	30.05
CDH11	27.69	25.86	29.46	28.15	24.53	28.88
CDH2	24.11	25.85	28.08	23.91	24.92	27.71
CFH	29.12	27.41	24.00	29.61	24.99	24.55
CFL1	33.03	31.32	32.61	32.10	31.93	33.06
CFL2	28.44	24.97	27.21	27.57	25.19	28.37
CHID1	26.39	25.25	24.82	26.16	25.21	24.79
CHMP4B	23.94	24.87	27.03	24.72	25.08	27.71
CHMP6	24.52	25.24	24.99	24.00	25.25	25.36
CHP1	25.36	25.36	26.34	24.76	25.34	24.85
CKB	26.73	26.58	27.35	26.25	26.67	27.45
CLEC11A	30.96	26.81	26.28	27.91	25.17	25.98
CLMP	24.12	24.69	27.44	24.61	25.23	25.97
CLTA	25.13	25.49	29.97	24.54	24.81	30.01
CLTB	23.97	24.88	27.19	24.70	25.08	26.15
CLTC	29.66	29.33	32.44	29.12	30.08	32.65
CLU	32.40	31.10	30.34	33.67	29.72	31.27
CNKSR3	25.98	25.22	24.11	27.27	25.24	24.40
CNP	24.59	24.90	29.44	23.87	25.50	29.29
COL11A1	27.87	26.26	24.91	28.42	24.78	24.85
COL16A1	27.50	25.31	23.49	27.50	24.90	24.54
COL18A1	29.99	26.62	28.74	28.04	27.75	27.50
COL4A1	31.10	26.65	29.28	31.18	24.87	28.00
COL4A2	32.40	29.13	27.65	32.64	26.89	27.51
COL5A1	31.69	29.13	26.86	31.48	28.58	27.91
COL5A2	30.49	29.87	24.36	33.32	29.75	26.20
COL8A1	24.75	24.82	24.29	27.55	24.75	24.99
COLEC10	28.85	25.34	23.64	27.49	24.95	24.55
COLGALT1	24.36	24.85	25.81	24.37	24.62	25.54
COMP	27.80	24.81	24.39	28.54	24.70	24.60
COPA	24.50	25.46	27.51	24.34	24.93	27.70
COPE	24.66	24.84	24.84	24.69	24.54	24.35
COPG1	24.69	24.90	26.74	24.03	25.21	26.05
COPS3	24.61	25.22	24.92	24.39	24.85	24.59
CORO1C	30.73	25.63	30.00	29.52	25.96	29.55
CORO2B	24.78	24.39	25.55	24.51	24.44	24.90
CPA4	26.50	24.36	25.02	29.10	24.99	24.72
CPE	24.98	24.66	23.84	27.16	24.66	24.89
CPNE1	23.41	25.79	26.89	24.26	24.94	27.50
CSF3	28.17	24.71	24.83	24.82	24.80	24.80
CSRP1	28.76	24.80	28.64	28.93	28.27	29.21

CST3	34.05	31.71	27.88	31.01	30.33	31.24
CTHRC1	29.09	25.06	24.36	28.45	25.25	24.27
CTNNA1	24.45	25.04	30.42	23.69	27.93	30.19
CTNNB1	24.29	25.07	28.47	24.21	25.12	29.21
CTNND1	24.65	24.33	30.38	24.52	25.08	30.19
CTSA	26.51	24.13	24.05	26.06	25.17	24.89
CTSB	33.77	31.28	29.22	30.54	28.95	31.65
CTSC	26.08	24.72	24.24	27.50	25.46	24.93
CTSD	29.12	24.99	24.14	26.32	25.52	24.47
CTSL	29.78	26.81	24.06	26.57	25.60	24.40
CXCL8	34.78	29.64	28.42	25.69	26.97	30.28
CYFIP1	24.97	24.57	27.87	24.32	25.59	28.11
CYR61	30.68	28.11	29.11	28.01	25.42	29.16
DAG1	27.82	24.72	24.17	28.17	24.78	24.48
DCD	24.48	27.25	26.41	24.91	27.78	26.42
DCHS1	24.95	25.30	25.72	24.19	25.38	25.86
DCTN2	27.31	25.03	23.81	25.46	24.62	24.66
DDX1	26.60	25.42	24.32	25.58	24.41	25.01
DIP2B	23.78	25.24	27.19	24.95	24.80	27.77
DKFZp686J1372	28.43	25.32	24.41	27.08	25.72	24.77
DKK3	31.18	29.22	26.91	29.71	26.61	28.26
DLG1	24.81	25.41	25.58	24.29	25.52	25.66
DNM2	23.93	24.94	26.52	24.41	25.28	26.05
DPYSL2	26.89	27.83	28.72	26.32	27.44	29.63
DSG1	24.41	24.62	25.30	23.97	25.21	25.32
DSP	26.55	24.68	24.27	28.37	24.96	24.30
DYNC1LI2	25.04	24.32	24.92	24.45	25.03	25.51
EDIL3	29.42	29.08	34.28	28.76	31.44	33.56
EEA1	25.87	25.04	23.78	25.95	24.98	23.57
EEF1A1;EEF1A1P5	32.39	31.26	31.93	31.27	31.40	31.98
EEF1B2	24.69	25.01	26.49	24.71	25.68	26.44
EEF1D	27.25	25.30	27.11	26.09	24.35	27.69
EEF2	30.69	28.86	30.83	29.64	29.11	30.17
EFEMP2	29.27	29.67	27.57	29.90	25.98	28.10
EHD1	25.53	25.55	31.00	24.43	24.14	30.64
EHD3	23.98	24.51	26.73	24.41	24.65	26.98
EHD4	24.27	24.84	28.21	24.26	24.90	27.96
EIF1	26.29	24.85	24.12	25.05	24.67	24.42
EIF3A	24.80	25.65	25.02	23.61	24.82	25.04
EIF3B	24.98	24.55	24.56	24.29	25.39	25.47
EIF3C;EIF3CL	24.48	24.75	25.38	24.21	25.08	25.30
EIF3D	23.65	25.74	25.98	24.11	24.61	26.37
EIF4H	24.77	24.95	26.67	24.53	24.65	25.00
EIF6	25.88	25.28	25.43	24.19	25.67	25.02
ENAH	25.28	24.86	24.05	25.10	25.32	23.73

ENO1	33.23	31.94	32.53	32.39	32.58	32.63
ENPP2	24.30	24.81	23.50	26.32	25.48	24.28
EPRS	26.72	25.28	26.91	26.56	25.22	26.35
ERAP1	26.54	24.43	23.73	24.49	24.84	24.87
ERP29	24.62	24.71	23.66	24.36	25.50	24.54
ESD	24.18	24.17	26.32	24.93	25.03	25.73
EVA1A	24.30	24.58	27.04	24.50	24.74	27.59
EVA1B	24.43	28.05	30.12	24.21	27.22	30.22
EXT1	25.32	26.86	24.29	26.36	26.01	25.15
EZR	27.56	25.35	28.33	28.41	24.86	28.99
F10	25.75	24.96	23.95	27.36	26.06	24.10
F11	24.93	25.24	24.05	29.15	24.30	24.52
F2R	23.96	25.05	27.76	24.89	25.02	27.18
FAM20C	24.68	25.27	23.96	25.22	25.50	24.28
FAM3C	29.15	24.84	23.54	27.36	25.22	24.07
FAU	24.52	25.08	26.32	24.84	25.60	25.13
FBLN1	31.67	31.40	33.19	32.73	31.76	32.61
FBLN5	26.15	25.00	23.44	28.66	25.73	24.37
FDPS	24.45	25.84	26.21	24.89	24.51	25.01
FGL2	26.72	24.50	23.85	24.96	25.17	24.73
FKBP1A	28.94	28.46	28.10	27.77	27.06	28.09
FLII	24.14	25.28	25.08	24.19	24.99	24.53
FLNA	32.33	30.31	31.30	32.42	29.05	31.93
FLNC	30.51	28.14	29.15	30.03	28.51	29.35
FN1	36.35	36.45	34.54	36.19	35.59	35.19
FSCN1	30.19	29.29	30.58	29.17	29.28	30.53
FST	28.78	27.89	23.71	30.06	27.31	24.81
FSTL3	27.02	25.45	23.61	27.44	25.33	24.54
FZD2	24.32	24.87	27.00	24.49	24.89	27.48
G6PD	27.86	24.91	28.81	27.08	26.78	28.49
GALK1	25.13	25.04	26.33	24.49	24.40	26.57
GALNT2	28.17	25.15	24.17	28.35	25.61	24.71
GALNT5	28.32	24.94	24.00	29.04	24.30	24.76
GANAB	28.56	25.21	28.43	27.70	25.01	28.50
GAPDH	33.06	31.94	33.59	31.19	31.23	33.29
GARS	24.19	25.83	26.97	24.74	24.72	27.59
GBE1	25.14	24.58	25.62	24.10	26.02	26.28
GCN1L1	25.15	24.99	25.41	24.05	24.30	24.30
GDI2	30.44	28.61	30.44	29.92	28.41	30.38
GLG1	29.02	25.04	24.95	24.82	25.22	24.66
GNA11;GNA 14	24.28	24.66	27.39	23.39	25.13	27.27
GNA13	24.24	24.90	26.91	24.86	25.10	25.12
GNAI2	25.68	27.33	31.94	23.37	30.55	31.31
GNAS	25.07	25.08	30.08	24.15	24.96	30.19
GNG12	23.95	25.09	29.86	24.29	27.82	29.77

GNG2	24.06	25.62	28.95	24.32	25.25	28.34
GNPTG	26.08	25.07	23.83	25.97	24.93	24.65
GOLM1	26.74	24.71	24.01	29.14	24.93	25.18
GPI	30.10	27.24	28.46	28.46	26.32	27.87
GPR124	24.02	24.75	25.23	24.19	24.42	26.16
GREM1	27.90	26.11	29.60	29.06	24.70	29.58
GRHPR	24.64	24.57	24.55	24.44	26.22	25.68
GSN	31.11	30.93	31.35	31.98	30.35	31.32
HEL-S-109;NUCB2;Nucb2	29.34	25.22	24.04	28.98	25.09	25.47
HEXB	28.05	25.07	24.08	27.84	24.87	24.75
HINT1	29.02	25.86	29.06	28.57	26.99	28.79
HMGA1	31.24	29.89	28.59	29.48	28.80	28.15
HMGA2	26.61	25.01	23.72	25.63	25.04	24.64
HMOX2	24.26	24.65	25.39	24.64	25.25	24.93
HN1	26.84	25.72	26.26	25.96	24.67	26.39
HNRNPC	28.53	25.18	24.10	29.23	24.93	26.33
HNRNPD	26.20	24.34	25.11	25.52	24.98	24.77
HNRNPDL	25.68	24.63	23.90	25.90	25.50	24.46
HNRNPL	25.53	25.63	24.62	25.91	25.57	24.63
HNRNPU	27.28	25.87	23.97	27.77	24.61	24.71
HSP90AA1	30.29	28.52	29.34	29.60	28.12	28.87
HSP90AB1	31.65	29.48	31.00	31.16	30.36	31.10
HSPA5	31.40	31.02	30.58	30.30	29.27	30.98
HSPA6;HSPA7	24.95	24.93	26.69	23.83	25.12	26.02
HSPA8	23.54	24.31	26.25	24.07	25.01	26.00
HSPA8	33.22	31.71	33.02	31.98	31.75	33.15
HSPA9	27.71	24.27	27.79	26.41	24.51	28.28
HSPB1	29.41	26.50	29.73	29.85	28.87	30.82
HSPD1	28.87	29.74	29.46	27.97	29.08	29.88
HSPE1;HSPE1-MOB4	29.82	24.74	26.99	28.30	25.24	27.17
HTRA1	30.41	26.01	29.08	29.59	24.93	29.29
HYOU1	24.18	24.82	25.07	24.09	24.99	25.16
IDH1	26.53	24.79	25.08	25.99	25.38	25.58
IFT74	24.32	24.88	24.10	25.27	26.15	25.10
IGF2	30.80	28.89	24.02	30.22	24.46	23.98
IGF2BP1	24.35	24.53	26.64	24.60	25.23	25.24
IGF2R	27.38	27.72	27.23	27.48	25.97	27.41
IGFBP2	32.08	27.24	23.98	31.03	24.30	26.58
IGFBP5	35.70	33.49	31.60	35.98	33.23	32.12
IGFBP7	33.45	32.13	28.73	33.37	31.01	29.64
ILF3	26.61	24.14	24.72	26.81	25.27	25.07
IMPDH2	24.60	24.68	25.34	24.12	25.23	25.61
INHBA	33.12	28.32	27.76	24.10	26.70	27.50
IPO5	25.17	24.93	25.94	24.05	24.89	25.46

IQGAP1	28.10	25.08	28.29	26.58	24.75	27.93
IST1	25.21	24.64	26.99	23.77	25.10	27.46
ITGA11	24.00	25.14	27.82	24.84	24.32	27.84
JUP	23.17	27.87	27.71	24.70	27.41	28.17
KIF5B	28.42	24.66	28.28	26.40	24.33	27.66
KPNB1	28.47	25.68	28.95	27.41	24.93	28.76
KPRP	24.32	27.20	26.58	24.52	26.98	26.95
KRAS	24.38	25.26	27.72	24.50	24.83	28.09
L1CAM	23.69	25.29	25.07	23.65	25.64	24.34
LAMA1	26.62	28.38	29.39	27.13	26.79	30.01
LASP1	29.34	24.03	28.66	30.01	24.91	28.72
LDHA	30.91	29.21	29.67	30.18	26.90	29.79
LDHB	30.77	29.07	30.19	29.57	27.60	29.61
LGALS1	33.49	31.24	33.55	33.58	33.18	33.34
LGALS3	27.32	25.09	23.66	26.96	25.22	24.52
LGALS3BP	29.50	32.91	30.52	29.35	31.87	30.22
LHFPL2	23.77	25.60	25.68	24.48	24.63	25.28
LIMS1;LIMS 2	24.30	25.36	24.87	23.72	25.01	24.74
LIN7C	24.12	25.09	27.46	23.78	24.14	27.71
LMAN2	27.69	24.87	24.56	27.42	24.46	24.40
LOX	28.76	28.68	24.48	28.83	25.54	26.65
LOXL1	26.41	24.93	23.77	27.72	24.38	24.03
LPP	24.59	24.69	26.15	23.52	25.17	26.44
LPXN	25.41	24.93	25.09	24.26	25.63	24.79
LRP1	29.33	30.91	30.15	28.89	29.97	30.49
LTBP1	33.24	29.14	30.76	31.94	27.11	29.66
LTBP3	29.65	25.63	25.27	26.67	25.11	24.69
LTBP4	28.35	26.81	24.17	30.16	24.53	24.94
LTF	27.84	25.09	24.08	28.68	25.56	24.07
LUC7L2	24.34	25.39	24.26	24.04	24.67	24.18
MAMDC2	23.83	25.57	25.95	24.32	24.91	26.22
MAN1A1	25.09	24.63	24.40	25.80	25.15	24.08
MAN2A1	27.56	24.78	24.70	24.78	25.37	25.47
MAP1LC3B; MAP1LC3B2	24.46	24.85	25.80	23.81	25.10	24.76
MAP4	28.87	25.53	24.14	29.37	25.66	24.55
MAPK3	24.24	25.24	24.15	24.26	25.55	23.92
MARK3	24.48	25.28	25.96	23.50	25.48	25.51
MASP1	24.21	25.10	23.49	29.93	24.71	24.89
MCAM	24.74	25.82	29.65	24.64	27.47	29.86
MDH1	29.34	27.79	27.98	28.46	25.22	27.54
MDH2	29.70	25.35	27.75	28.66	25.41	27.55
MEMO1	23.94	25.25	23.63	25.25	25.28	24.35
MFAP2	27.38	24.26	24.44	26.82	25.16	23.68
MGAT5	27.36	25.32	24.23	26.98	24.57	24.62
MIF	28.80	27.22	28.74	27.24	27.17	29.00

MINK1	24.38	25.67	27.69	24.41	25.19	27.22
MMP1	36.68	34.36	31.99	30.95	32.78	33.54
MMP2	32.62	31.92	30.06	33.41	31.40	30.15
MOXD1	24.56	25.26	26.16	23.93	24.90	26.36
MSN	33.02	31.16	33.78	32.07	30.21	33.14
MST1	25.60	24.34	25.01	25.89	25.00	24.75
MT1E;MT1L	24.78	24.63	25.59	24.05	25.00	24.80
MTAP	25.58	25.23	25.07	24.86	24.67	24.47
MTHFD1	24.26	24.55	27.66	24.59	24.69	27.04
MTPN	29.04	25.89	27.14	27.62	25.12	27.89
MVP	28.29	25.67	31.62	26.45	29.26	31.67
MYDGF	25.58	26.53	25.53	25.27	25.08	25.92
MYH9	33.23	29.85	33.04	33.28	30.20	33.18
MYL12A;MYL12B	27.74	24.88	26.42	27.13	25.22	27.71
MYL6	31.00	28.96	30.52	30.07	27.76	30.72
MYO1B	24.07	24.89	28.97	24.21	24.52	28.65
MYO1C	24.51	24.58	30.84	24.70	25.58	30.66
MYO6	23.93	24.65	25.99	24.59	25.11	24.69
NANS	24.40	25.28	25.29	24.27	24.95	24.88
NAP1L1	24.82	25.72	26.77	23.70	24.17	26.45
NCAM1	26.83	25.06	24.87	27.73	24.60	24.52
NCL	29.19	25.41	24.19	29.61	25.05	27.15
NEDD8;NEDD8-MDP1	27.05	24.99	27.36	26.23	25.07	27.18
NEO1	27.20	24.57	27.19	27.84	24.95	27.62
NME1	26.77	25.11	24.30	27.90	25.98	24.78
NME1-NME2;NME2;NME1;NME2P1	29.67	27.26	29.12	29.14	26.61	27.77
NOTCH2	24.41	25.31	29.53	24.60	24.90	28.88
NPC2	29.29	24.81	23.89	29.42	24.71	25.05
NPEPPS	24.69	25.03	26.87	24.09	25.34	26.67
NPTX1	30.30	27.68	23.80	27.64	25.45	25.14
NRAS	25.16	24.43	27.18	24.76	24.86	27.34
NRP1	27.08	25.99	29.65	24.68	24.98	29.21
NUCB1	32.95	28.34	26.04	32.16	24.56	27.91
OAF	28.08	25.29	24.02	26.96	25.39	24.68
OLFML2A	25.27	25.49	24.50	26.69	25.02	24.50
OLFML3	27.74	24.84	23.80	30.46	24.84	25.28
OMD	26.37	24.67	24.15	26.88	24.44	25.16
OS9	26.26	25.34	23.61	25.36	24.68	24.55
P4HB	31.22	30.60	30.33	30.77	30.47	30.17
PA2G4	28.07	24.54	23.50	26.35	25.34	24.43
PAICS	24.31	24.85	26.66	24.47	24.63	26.42
PAK2	24.71	25.07	26.25	24.78	25.35	25.91
PAPPA	28.71	27.28	26.38	26.72	25.65	24.92

PARK7	29.81	25.76	28.05	28.95	25.63	28.08
PCBP1	27.37	26.23	28.72	26.78	24.64	28.21
PCBP2	24.23	25.00	26.18	25.23	25.54	25.92
PCDH18	25.19	24.96	26.93	26.07	24.68	26.70
PDAP1	25.56	25.16	24.23	25.16	24.81	24.88
PDCD5	26.07	25.19	24.12	25.81	25.31	24.19
PDCD6	24.72	25.05	24.42	24.02	24.89	23.98
PDGFD	24.19	24.73	26.65	25.21	24.64	27.14
PDIA3	30.64	30.22	29.62	30.05	28.47	30.20
PDIA4	28.13	27.62	26.57	27.66	26.84	27.45
PDIA6	26.69	25.09	26.43	26.82	24.85	27.02
PDLIM7	25.58	25.39	25.87	26.88	24.99	26.70
PFDN6	24.42	24.50	25.99	24.51	24.68	25.84
PFKP	24.08	25.21	27.90	24.81	25.22	27.68
PFN1	32.70	30.36	32.01	32.22	30.29	31.61
PFN2	27.40	24.99	26.93	27.44	25.37	27.27
PGAM1;PGAM4	30.30	29.32	31.13	29.02	28.94	30.44
PGD	29.28	26.30	28.67	28.16	24.98	29.13
PGK1	32.18	28.86	30.35	30.23	28.27	30.60
PHPT1	27.44	25.55	26.89	27.42	24.65	27.12
PI4K2A	24.68	24.38	24.52	24.24	25.31	23.77
PKM	33.15	32.61	33.90	31.62	32.83	33.53
PLAU	36.38	32.55	33.03	31.63	31.95	32.76
PLD3	24.37	24.37	26.63	25.23	24.93	25.91
PLEC	31.43	28.80	30.19	29.89	27.48	29.75
PLEKHO2	24.29	24.96	25.36	24.20	25.22	24.84
PLOD1	30.74	30.27	29.68	29.26	29.33	28.75
PLOD3	28.29	27.27	27.25	26.00	27.32	26.68
PLTP	28.15	25.35	24.97	27.83	25.03	26.12
PLXNA3	23.79	25.32	25.84	23.61	25.15	24.91
POSTN	34.54	30.34	31.45	32.15	29.26	31.12
PPIA	32.97	30.70	32.07	32.19	30.82	32.07
PPIB	28.40	25.09	27.24	27.42	25.13	26.53
PPP1CB	24.64	25.47	24.43	24.66	25.07	25.06
PPP1R12A	24.90	25.11	24.13	25.03	24.98	24.63
PPP2CA	27.24	25.40	27.70	27.44	24.92	27.57
PPP2R1A	27.41	24.28	27.72	25.69	25.48	28.01
PRDX1	31.22	29.62	30.73	30.62	30.44	31.18
PRDX2	26.96	24.94	27.53	27.80	25.21	27.53
PRDX3	24.79	24.55	24.61	26.44	25.06	24.36
PRDX5	26.84	25.00	23.54	25.62	24.67	24.54
PRKAR1A	26.63	24.93	26.43	24.99	25.27	26.94
PRKCDBP	24.99	24.73	26.70	23.77	25.81	27.33
PRKCSH	27.22	27.62	27.26	26.35	26.28	27.67
PROS1	27.33	25.59	23.23	27.49	24.89	24.42

PSAP	32.11	27.13	26.65	29.70	25.51	27.96
PSG4	26.00	24.97	24.30	27.95	25.04	24.16
PSMA1	24.82	31.54	27.12	24.18	30.34	27.10
PSMA3	24.31	27.46	24.10	23.78	25.47	24.40
PSMA5	24.60	29.24	27.21	24.16	28.23	27.31
PSMA6	24.81	28.62	25.82	24.58	26.81	24.06
PSMB2	24.03	27.11	23.76	24.82	26.10	24.05
PSMB7	24.20	28.51	23.74	24.27	26.70	24.83
PSMC2	25.63	25.40	27.32	24.12	24.89	27.39
PSMC6	24.74	24.97	26.07	24.13	25.09	24.42
PSMD11	24.72	25.02	26.36	23.39	25.22	26.09
PSMD2	24.30	26.55	27.50	24.74	24.78	27.63
PTGDS	27.38	24.72	23.81	29.56	24.97	24.68
PTGES3	27.18	25.02	26.99	25.15	24.71	27.23
PTMS	25.99	24.98	23.80	27.61	24.67	24.39
QPCT	28.10	24.52	24.01	25.50	25.21	24.27
RAB11B;RAB11A	27.90	24.84	28.55	25.62	24.93	28.16
RAB21	24.31	25.15	25.48	24.91	25.83	25.10
RAB2A	25.62	25.22	25.85	24.19	24.41	26.72
RAB5C	24.27	24.89	28.40	24.49	23.86	27.68
RAB7A	23.85	24.41	28.09	24.25	25.36	28.81
RAB8B	24.24	25.30	27.37	24.47	24.75	26.04
RAD23B	25.72	24.75	24.16	26.61	24.67	25.01
RAF1	24.80	24.96	25.36	23.25	25.32	24.63
RALA	24.30	24.41	28.12	24.03	25.27	27.16
RAN	28.51	25.66	28.64	28.52	25.28	28.49
RANBP1	24.62	24.21	26.55	23.78	25.15	26.57
RAP1B	24.45	24.84	30.42	24.51	28.53	29.54
RAP1GDS1	25.43	24.67	24.26	24.46	25.63	25.21
RAP2C	24.83	24.83	26.28	24.21	25.12	24.97
RARRES2	25.24	26.04	24.16	28.23	25.37	24.93
RARS	25.00	25.27	25.33	24.15	25.50	24.94
RASA2	23.90	24.84	24.76	24.57	25.39	25.25
RASA3	23.94	24.83	25.60	23.98	24.49	26.05
RBMX;RBMXL2	26.80	25.14	24.42	27.21	25.11	24.43
RCN1	28.45	24.81	24.54	29.13	24.59	24.87
RCN3	26.89	25.35	24.03	27.58	24.86	24.45
RDX	24.37	24.57	27.82	23.36	24.40	28.02
RECK	24.87	25.50	28.40	24.16	24.74	29.18
RFTN1	23.82	24.79	30.63	24.93	25.46	31.08
RHBDF1	24.95	24.07	27.08	24.60	25.35	26.99
RHOG	24.17	26.22	29.33	24.00	24.93	29.11
RIN1	24.31	25.06	25.84	24.54	26.08	25.02
RNASE4	27.38	24.91	24.51	28.22	24.58	24.15
RNASET2	25.10	24.29	23.92	25.47	25.06	25.04

RND3	24.11	25.20	26.18	24.42	24.94	26.60
RNH1	27.16	25.00	27.03	24.69	25.08	27.00
ROCK2	24.20	25.01	26.67	24.14	25.06	26.17
RP2	23.70	25.08	28.13	24.15	25.08	27.80
RPL10	24.71	24.88	26.98	24.66	25.05	26.37
RPL11	30.20	30.16	31.65	29.18	25.08	31.52
RPL12	27.11	27.70	28.45	25.91	25.04	28.12
RPL13	27.07	26.66	28.42	27.66	25.88	28.79
RPL14	24.25	25.20	27.03	23.44	24.85	27.22
RPL15	24.65	25.64	28.61	24.77	24.85	28.27
RPL17;RPL17-C18orf32	24.18	25.20	27.63	24.40	28.48	28.05
RPL18A	24.40	25.11	27.13	25.43	24.92	26.43
RPL19	27.56	26.96	27.89	27.94	25.06	28.31
RPL21	24.25	25.42	26.13	24.24	24.83	24.96
RPL23	24.34	25.01	25.37	23.62	25.25	24.00
RPL24	24.42	24.90	25.81	25.26	25.44	26.14
RPL27A	24.40	25.76	27.24	24.60	25.75	27.67
RPL28	24.71	24.33	27.11	23.79	25.23	27.23
RPL29	24.78	24.59	26.97	24.48	25.51	27.57
RPL3	27.34	26.36	28.33	25.90	25.46	27.95
RPL30	27.03	24.74	27.09	24.82	25.33	27.02
RPL34	23.85	25.51	25.79	24.87	25.16	26.20
RPL36AL;RPL36A;RPL36A-HNRNPH2	23.83	24.95	25.16	24.43	24.59	24.63
RPL4	28.10	26.58	28.67	28.62	27.51	28.81
RPL5	28.40	24.75	28.07	27.42	25.00	28.16
RPL6	28.83	26.14	29.09	26.51	26.46	28.86
RPL7	24.30	25.13	28.84	24.78	24.92	28.61
RPL7A	25.90	25.34	27.40	25.03	25.14	27.44
RPL8	25.86	25.95	28.62	25.88	24.89	28.86
RPLP0;RPLP0P6	26.16	25.10	26.13	26.38	25.67	25.21
RPLP1	25.95	25.08	26.96	24.37	26.98	26.49
RPLP2	27.51	24.99	25.31	26.66	25.08	26.13
RPN1	27.04	24.97	27.29	23.95	24.93	27.65
RPS11	26.16	25.91	28.22	24.48	26.36	28.58
RPS14	24.37	26.05	28.63	24.61	24.54	28.71
RPS15	25.06	25.61	25.57	24.04	24.72	25.11
RPS16;ZNF90	23.82	25.02	27.30	23.84	25.02	27.38
RPS17	24.60	24.51	27.10	24.97	24.70	26.86
RPS18	24.42	24.43	27.37	24.12	24.37	26.63
RPS19	27.06	24.59	26.70	25.20	24.43	25.20
RPS2	26.15	24.27	28.61	24.12	25.25	28.39
RPS20	27.16	24.99	28.41	26.71	25.76	28.36
RPS21	27.19	29.48	26.76	26.57	28.36	26.82

RPS23	26.63	25.12	27.56	24.01	24.84	27.98
RPS25	24.08	24.86	27.38	24.60	24.99	27.56
RPS26;RPS26P11	24.12	24.82	25.69	24.20	25.04	26.88
RPS28	26.60	25.38	24.42	26.07	24.75	24.67
RPS29	24.57	24.86	24.06	25.14	25.40	24.66
RPS3	25.60	24.22	25.99	26.20	24.53	25.17
RPS3A	26.47	26.91	28.69	27.86	26.07	28.77
RPS4X	26.23	26.33	29.09	25.48	24.75	29.09
RPS5	27.32	24.98	27.97	25.63	23.79	27.40
RPS6	27.10	24.47	28.79	24.91	24.89	28.58
RPS8	26.34	26.35	28.73	24.32	24.57	29.02
RPS9	24.07	25.70	25.90	24.44	25.12	25.55
RPSA	27.34	27.66	27.95	24.53	24.59	27.40
RRAS2	25.00	25.08	25.94	23.99	25.12	26.35
RRBP1	29.21	24.81	24.72	28.96	24.41	25.69
RSU1	26.02	25.16	24.37	25.25	25.23	24.83
RTCB	24.53	25.12	27.42	24.03	25.54	26.90
RUVBL2	24.33	24.35	26.26	25.06	24.55	25.84
S100A11	27.02	24.94	31.13	28.35	25.83	30.65
SARS	24.42	25.03	24.25	24.36	24.82	25.57
SCAMP3	24.27	24.86	27.37	24.51	25.34	26.51
SCRN1	26.91	25.59	27.16	25.99	24.95	27.59
SDC4	29.23	28.81	26.87	29.59	25.90	27.98
SDF4	31.08	25.57	24.51	29.89	25.15	27.25
SEC31A	24.19	25.42	26.91	24.31	24.80	25.78
SEMA7A	33.40	29.41	27.53	26.59	27.19	28.99
SEPT11	28.25	25.35	28.15	27.10	24.93	27.40
SEPT2	26.47	25.27	28.55	24.50	24.95	27.58
SEPT7	28.08	25.11	28.65	27.67	25.35	28.12
SEPT9	27.39	24.98	28.34	27.19	24.80	27.75
SERPINF1	31.38	24.84	24.87	30.49	25.57	25.63
SH3BGRL	24.64	25.16	24.19	26.43	24.62	24.39
SH3GL1	26.54	24.99	27.17	25.02	24.92	27.27
SLC14A1	24.07	25.22	25.49	24.23	24.38	24.38
SLC16A1	24.47	25.48	28.54	24.28	24.66	28.09
SLC1A5	24.08	25.24	30.87	24.42	25.78	31.51
SLC2A1	24.34	24.74	27.61	24.51	24.07	27.95
SLC38A2	24.83	25.25	27.76	24.45	25.16	26.96
SLC39A10	24.74	24.67	28.50	23.90	24.50	27.94
SLC39A6	24.27	24.62	26.85	23.34	25.62	26.60
SLC7A5	24.41	25.00	28.91	24.63	25.48	29.95
SLC9A3R2	24.89	24.26	25.81	24.46	25.24	26.55
SLK	24.43	24.01	24.91	24.44	25.39	24.13
SMAD5;SMAD1;SMAD2;SMAD9	25.29	25.36	24.96	24.33	25.35	24.65

SNAP23	24.57	25.06	28.38	23.39	24.79	28.70
SND1	28.05	24.65	28.08	26.52	25.38	27.49
SNX6	23.96	24.50	25.50	24.91	25.05	25.85
SNX9	24.57	25.24	26.44	24.97	25.08	25.54
SPCS2	23.45	25.04	24.32	24.56	25.11	24.44
SPINK6	26.05	24.63	24.31	26.36	24.44	23.92
SPON2	32.63	26.87	27.54	30.60	29.32	29.08
SPTAN1	24.41	25.14	24.41	25.79	24.43	24.05
SQSTM1	23.98	24.95	28.10	24.49	24.20	28.34
SRM	24.72	24.30	23.93	23.57	24.11	24.04
SRSF1	24.86	24.53	24.65	25.67	25.94	24.80
SSC5D	28.29	28.38	30.74	27.00	28.04	30.29
ST13;ST13P5 ;ST13P4	25.57	24.38	23.71	25.89	24.06	25.19
STC1	36.01	30.87	31.55	28.47	31.20	32.30
STPG2	27.12	24.71	24.53	27.64	25.03	25.20
STRAP	26.34	24.65	26.49	24.84	25.99	25.12
STX4	24.64	24.99	29.53	24.29	25.25	29.22
STX7	24.80	25.36	25.53	24.82	24.62	26.88
SUMO2	24.67	24.99	23.85	26.23	25.41	24.16
SYNCRIP	25.29	25.05	25.21	24.80	24.69	25.71
TAGLN2	27.57	24.73	26.60	28.05	24.90	27.52
TALDO1	28.33	26.19	27.10	28.67	25.68	27.76
TARS	26.78	24.15	25.78	24.78	25.27	26.23
TBCA	29.57	27.45	26.98	27.24	25.38	27.63
TEK	23.98	25.23	27.72	24.99	24.89	27.12
TENM4	24.39	24.93	25.47	24.23	24.28	24.71
TFPI2	30.65	27.56	28.65	23.77	26.54	27.96
TFRC	24.85	25.07	28.38	23.87	25.91	28.16
TGFBR2	24.50	24.93	23.97	24.09	25.90	25.21
TGOLN2	23.97	24.87	24.42	26.21	25.19	25.03
THBS4	24.61	25.05	24.08	26.08	24.49	24.63
THY1	23.89	26.10	31.44	24.17	26.91	30.15
TIMP3	24.36	24.50	26.06	23.91	24.61	24.74
TKT	29.60	29.84	30.03	29.36	28.96	30.58
TLDC1	23.76	24.56	28.44	24.63	24.77	27.85
TLN1	31.94	28.68	32.55	30.97	30.70	32.45
TLN2	24.46	25.02	25.01	24.35	25.82	24.63
TMSB10	32.88	32.27	31.46	32.47	31.62	31.64
TMSB4X	32.06	31.25	30.77	32.70	30.84	31.43
TNFAIP3	24.86	25.39	25.68	24.52	24.49	24.72
TNFRSF11B	30.58	25.50	25.11	25.53	24.70	24.60
TNPO1	25.12	25.75	24.84	24.61	24.68	24.69
TPI1	31.53	30.00	31.35	30.78	28.52	31.12
TPM1	26.39	25.35	24.67	28.65	24.23	25.55
TPM2	29.43	26.71	27.79	29.18	24.31	26.60

TPM3	31.13	29.55	30.28	29.83	28.80	29.67
TPM4	31.71	30.81	31.49	32.39	30.27	31.38
TPP1	27.38	25.21	25.56	24.10	25.04	26.51
TPP2	23.77	28.95	27.98	24.27	28.29	27.45
TPT1	31.81	25.80	28.46	30.59	25.32	28.62
TRHDE	24.52	24.83	24.33	24.03	24.94	26.42
TSPAN6	24.77	25.43	26.25	24.30	24.92	26.47
TUBB3	28.29	28.73	29.78	26.83	28.84	29.00
TUBB4B	31.47	31.43	32.13	31.42	31.50	32.28
TUBB8	24.66	24.66	26.66	24.32	28.82	24.96
TUFM	24.83	25.43	26.42	24.46	25.67	26.63
TWF1	24.47	24.88	26.74	24.20	24.38	26.25
TWF2	24.50	24.50	26.21	25.73	25.28	24.55
TWSG1	29.85	27.86	24.45	29.88	24.64	24.97
TXNDC17	27.82	25.45	26.34	26.34	25.54	26.39
TXNDC5	26.80	25.43	26.69	27.30	26.90	26.71
TXNRD1	26.42	25.11	26.30	26.40	24.18	26.89
UBA1	28.19	24.79	29.07	26.96	25.29	29.40
UBE2L3	28.07	24.45	23.58	26.75	25.58	24.70
UBE2NL;UBE 2N	27.80	24.59	28.06	27.23	25.17	27.95
UBE4B	27.20	25.23	24.71	25.90	24.92	24.35
UBR4	23.63	24.26	24.36	24.57	25.29	24.48
UCHL1	31.81	27.95	30.52	30.74	28.21	31.17
UGDH	26.08	25.21	27.16	24.13	24.28	27.51
UGP2	25.29	24.78	25.36	23.77	24.91	25.23
VAMP3	23.96	24.75	27.26	24.17	25.66	27.39
VAMP5	24.56	25.02	25.31	24.14	25.53	27.85
VARS	24.44	24.00	26.98	24.36	25.36	26.50
VBP1	24.25	25.09	24.80	24.72	25.30	24.60
VCP	29.81	31.29	29.87	28.62	30.64	30.35
VEGFC	29.97	24.78	24.26	28.44	24.48	24.99
VIM	35.66	33.57	34.22	34.55	32.98	34.35
VPS28	23.51	25.46	27.23	23.62	24.63	27.99
VPS37C	24.26	25.13	25.59	24.29	24.64	25.82
VPS4A	24.48	24.94	26.65	24.67	24.84	27.03
WDR1	31.12	28.86	30.93	30.24	30.30	31.20
WFDC1	24.84	24.92	24.59	26.45	25.40	24.94
YARS	24.77	24.95	26.51	24.08	25.54	26.38
YBX1	25.15	26.66	24.06	24.32	25.48	25.74
YES1;FYN	24.64	25.59	26.99	24.26	25.59	26.36
YWHAE	29.95	29.80	30.74	30.83	29.72	30.81
YWHAG	30.56	29.33	31.42	30.03	29.44	30.95
YWHAH	27.89	28.09	29.01	27.75	28.09	29.70
YWHAQ	29.15	29.07	30.52	28.81	28.95	30.88
YWHAZ	31.57	31.64	32.64	31.68	31.05	32.50

ZDHHC5	23.33	25.59	28.58	23.84	25.13	28.56
ZYX	27.51	25.21	28.57	26.78	25.01	28.51

8.4 Genes Uniquely Present at Increased Levels in OIS Fraction 8 (MS3)

This data describes genes identified in MS3 that are uniquely present at increased levels in OIS Fraction 8 compared to the vector condition (see Figure 4.23). The fold change (FC) in mean label free quantitation intensities (LFQ) are detailed. Unpaired Student's t-tests were also performed with the p-value described in the final column (-Log10 p-value).

Gene Names	FC Mean LFQ (Log2)	-Log10 p-value
PLAUR	7.6796	2.55668
COL6A3	6.68073	3.91471
MME	6.47649	3.37821
ITGA6	6.24975	2.13407
SLC16A6	5.73359	4.54713
IL6ST	5.44257	3.44419
NOTCH1	5.44209	2.18692
SLC20A1	5.18488	2.19877
TNFRSF10B	5.18328	2.56654
ABCA1	5.12311	2.59873
WDR64	5.08365	3.23384
PHLDB1	5.06077	4.17423
TSPAN14	4.98351	4.29193
TPBG	4.94208	2.67139
GNAI3	4.85355	3.6341
TMEM2	4.78101	2.64556
CD276	4.65514	4.76923
BTN2A1	4.58885	2.35384
HAPLN3	4.50395	3.75333
SERPINE1	4.29867	2.64861
ACSL4	4.27189	2.96307
TJP1	4.20534	2.96967
ZC3HAV1	4.14844	3.69103
JAM3	4.13358	2.95375
PTGFRN	4.11049	3.61435
SPRY4	4.10961	2.74152
NDRG1	4.07997	2.54307
RAB1B;RAB1C	3.94292	3.77417
NUMB	3.88735	2.62617
CD97	3.86316	2.28264
RAC2	3.82144	2.29388
PFKL	3.7465	2.32777
ENPP1	3.73056	2.25033
BMP1	3.66694	2.68924
TSPAN9	3.62629	2.37894

NAPG	3.61952	3.66181
CTTN	3.6054	3.05456
EPHA2	3.51458	4.02505
ITGA4	3.48856	2.31438
STUB1	3.4845	2.14515
GNB4	3.47477	0.902115
TENM3	3.4554	3.15951
PCDHGB5	3.42782	2.26536
TOLLIP	3.41366	3.4679
SLC7A2	3.39634	2.60314
ZDHHC20	3.37914	3.15789
TSPAN5	3.35236	1.17905
TUBA1B	3.32676	2.12674
FAP	3.26517	3.22314
DNASE1L1	3.25913	4.03387
FLRT3	3.21466	3.12342
SIRPA;SIRPB1	3.21077	2.13076
ITGA8	3.20778	1.92631
TSPAN4	3.1748	2.40633
COL6A2	3.15788	3.11707
GDI1	3.14982	2.54865
RPL18	3.13923	2.24503
CHMP2A	3.13665	2.73555
PVRL3	3.05107	3.50906
ITGAV	3.0411	5.11119
RPL35A	3.01795	2.41491
CD9	3.01167	3.74771
PSMD6	3.0116	2.14091
SCRIB	2.87608	3.37354
SLC2A3;SLC2A14	2.86767	1.82592
COL6A1	2.85609	3.10533
MPZL1	2.84544	2.3047
PHLDA1	2.82451	1.70019
NTSR1	2.81992	3.5321
ACE	2.78342	2.08311
ADAM10	2.71384	2.2816
ADSS	2.68018	1.25487
DNAJA1	2.67708	2.43995
STXBP3	2.66525	3.50934
SEC23A	2.66452	0.815143
EGFR	2.64836	3.16499
RAB6A	2.62549	3.02636
ATP1B1	2.61197	3.07656
PLXNA1	2.60759	2.24137
GNAI1	2.60092	2.43566
SLC9A1	2.5432	1.57151

EPHB4	2.53763	1.11309
LLGL1	2.53646	1.73707
SLC4A7	2.52244	2.26717
MICA	2.52186	1.86503
IL1RAP	2.51204	1.78571
GNB2L1	2.46013	1.91351
VPS35	2.43916	2.50103
CCT2	2.43419	1.35335
ABCC4	2.43253	3.11678
WLS	2.42312	1.90593
PSMA7;PSMA8	2.41712	2.16082
PTPRG	2.40755	2.68977
GRK5	2.38766	2.60299
STEAP3	2.36968	2.26696
PSMD4	2.36763	1.37465
ECE1	2.35283	1.57568
RAB5B	2.31844	1.43067
SLC6A6	2.31229	1.31949
GJA1	2.29579	2.38953
ERBB2IP	2.28741	1.96108
VCAN	2.28056	1.39945
RPL31	2.27152	1.17849
PDGFC	2.25882	1.9385
ANTXR2	2.25609	2.66749
FN3KRP	2.25392	1.73616
RHOB	2.25003	0.990751
AP2B1	2.23767	2.42289
SLC39A14	2.22836	1.0092
LAP3	2.19396	1.76322
ARPC5	2.1862	0.567269
DDX3X;DDX3Y	2.17222	3.60387
RAB8A	2.16456	2.18382
DNAJA2	2.16182	1.23935
ITFG3	2.15813	1.50676
NRP2	2.12714	2.34148
ATP1A1	2.11211	1.97527
FMNL3	2.11001	3.62628
AIMP2	2.09155	1.27184
IRGQ	2.09077	1.69763
FBLN1	2.08506	1.02505
NAPA	2.05218	2.97395
VWA5A	2.05159	2.0003
RAP1A	2.0474	2.92753
USP5	2.03383	1.64219
PLXNB2	2.01075	1.82948
SNAP29	2.00953	1.81389

TGFBI	2.00163	2.65473
PSMC4	1.95624	2.25435
VASN	1.95312	1.04699
PRKAR2A	1.94531	1.65253
CDC42SE1	1.93943	2.35904
AP2M1	1.93367	4.61808
CD47	1.87813	1.41043
ITGB3	1.87526	2.60301
RPS7	1.87456	1.29156
BSG	1.87375	2.97944
CLMP	1.86995	0.830849
FKBP10	1.86835	1.01497
CYB5R3	1.86549	3.46359
KLC1	1.85554	1.37981
PLXND1	1.83354	3.11717
AHCYL1;AHCYL2	1.82073	2.29318
PSMC3	1.80164	1.47158
WNT5B	1.76577	1.47224
GGT1;GGT3P;GGT2	1.76363	2.00666
TMEM51	1.75379	1.62402
SERBP1	1.7407	1.69608
SLC16A3	1.74033	1.84086
CAB39	1.73775	1.42601
PCDHGC3	1.73653	2.06266
ANXA7	1.73301	3.03918
GNG5	1.73292	2.33973
CDH6	1.7252	0.946123
FAS	1.71904	2.31658
MRC2	1.71884	1.79488
RAB34	1.69932	2.10225
PLXNB1	1.69311	1.80324
TRPA1	1.67866	1.10524
TIMP2	1.67653	1.86387
RAB8B	1.67582	0.82785
UACA	1.67176	2.43022
RPL23	1.60843	0.738344
UBTD1	1.60343	1.35182
CHP1	1.59725	0.647464
PCDH7	1.5838	1.16672
TCP1	1.57169	1.68061
SCAMP3	1.55414	0.537675
MAP4K4	1.54029	2.53706
SRGAP2;SRGAP2B	1.51	2.60919
PSMC6	1.49591	0.586429
CDK4	1.49422	2.15823
PI4KA	1.48227	1.09335

RAB10	1.47144	2.56314
PVR	1.46146	1.85576
TWF2	1.45752	0.815344
DOCK10	1.44564	1.37543
SEC31A	1.43601	0.855749
PDCD10	1.43336	1.46114
KIRREL	1.43132	2.44106
GRB2	1.42724	2.08198
HPCA;HPCAL1;NCALD	1.42145	0.920769
RAB35	1.41979	2.47248
TAOK1	1.40958	1.93306
PSMD1	1.40841	1.01377
GIPC1	1.40534	1.63444
GNA13	1.40525	0.886101
CLTB	1.40359	0.898419
SRI	1.40201	1.52057
LRRC32	1.39978	2.55451
FARSB	1.39716	1.36658
CCT3	1.38705	1.32099
SMURF2	1.37768	1.1602
GSK3B	1.36992	1.5521
STK10	1.36789	2.50896
PYGB	1.36677	1.03747
SEC13	1.35857	1.8437
ATP1B3	1.34978	0.514662
CCT6A	1.34959	1.46888
CPNE3	1.34335	2.28665
GPRIN1	1.33938	1.24623
ARPC3	1.33055	1.43437
PACSIN2	1.33005	2.37013
LRRC47	1.32921	1.71494
GFPT1	1.32172	1.97383
ANKFY1	1.31703	2.54787
PVRL2	1.30703	2.52715
IGF2BP1	1.29961	0.91818
ACTR2	1.29668	1.76523
FAU	1.29117	0.553239
ITCH	1.29057	2.13185
PSMC1	1.28701	3.1405
SLC44A1	1.28419	1.64
RPL21	1.27289	0.861075
PHB	1.27264	1.463
SNTB2	1.27083	1.35238
SPRY2	1.24954	1.76841
S100A13	1.24878	2.12282
NCKAP1	1.24653	2.31313

GNAQ	1.24471	1.52943
ATP6V1E1	1.23178	0.808747
ABI2	1.22631	2.08991
CUL2	1.22187	0.954673
ALCAM	1.21272	2.13899
EIF3E	1.20523	4.13211
PALM2-AKAP2;PALM2	1.19488	2.70462
ESD	1.18923	0.629283
LMAN1	1.18353	1.28796
MARCKSL1	1.18266	1.72357
ELFN2	1.18246	1.75968
MYO6	1.17885	0.795197
EIF4H	1.17583	0.938533
ACOT7	1.17069	1.04149
SLC5A3	1.15463	1.60193
PSMC5	1.14733	1.10291
SLC6A15	1.1413	1.04577
RHOA	1.13762	1.4499
RAP2C	1.13596	0.555552
TNC	1.13123	1.97589
TMEM30A	1.11866	1.18861
AP1G1	1.11528	1.39952
CD46	1.10855	1.76414
CD99	1.10554	1.75064
PFDN1	1.09018	1.08421
COPG1	1.0874	0.816108
RPL36AL;RPL36A;RPL36A-HNRNPH2	1.08523	0.616868
ATP6V1B2	1.08295	0.954361
RPL26	1.07784	1.66214
ITGA3	1.06872	1.99092
CD109	1.0459	1.83189
DNAJC13	1.03705	1.12784
CAPNS1	1.02416	0.627633
PRKCA	1.02354	1.11611
F2RL1	1.02096	2.05256
SLC14A1	1.00803	0.939625
PXN	1.00606	1.71754